

Les informations que la scapula, l'atlas, et l'axis peuvent apporter à la compréhension de la bipédie

Auteur : Van Oostende, Florence

Promoteur(s) : Noiret, Pierre

Faculté : Faculté de Philosophie et Lettres

Diplôme : Master en histoire de l'art et archéologie, orientation archéométrie, à finalité approfondie

Année académique : 2018-2019

URI/URL : <http://hdl.handle.net/2268.2/6656>

Avertissement à l'attention des usagers :

Tous les documents placés en accès ouvert sur le site le site MatheO sont protégés par le droit d'auteur. Conformément aux principes énoncés par la "Budapest Open Access Initiative"(BOAI, 2002), l'utilisateur du site peut lire, télécharger, copier, transmettre, imprimer, chercher ou faire un lien vers le texte intégral de ces documents, les disséquer pour les indexer, s'en servir de données pour un logiciel, ou s'en servir à toute autre fin légale (ou prévue par la réglementation relative au droit d'auteur). Toute utilisation du document à des fins commerciales est strictement interdite.

Par ailleurs, l'utilisateur s'engage à respecter les droits moraux de l'auteur, principalement le droit à l'intégrité de l'oeuvre et le droit de paternité et ce dans toute utilisation que l'utilisateur entreprend. Ainsi, à titre d'exemple, lorsqu'il reproduira un document par extrait ou dans son intégralité, l'utilisateur citera de manière complète les sources telles que mentionnées ci-dessus. Toute utilisation non explicitement autorisée ci-avant (telle que par exemple, la modification du document ou son résumé) nécessite l'autorisation préalable et expresse des auteurs ou de leurs ayants droit.

Corpus d'images

Mémoire de Van Oostende Florence. *Les informations que l'atlas, l'axis et la scapula peuvent apporter à la compréhension de la bipédie.*

Mémoire de master, année 2018 – 2019.

Promoteurs : Noiret P. (ULiège) et Maureille B. (Université de Bordeaux)

Lectrice : Rots V. (ULiège)



Table des matières

Données anatomiques.....	3
Description de l'atlas, l'axis et la scapula chez l'homme moderne	4
Atlas	4
Axis	6
Scapula	8
Description de l'atlas, l'axis et la scapula chez un représentant du <i>knuckle-walking</i> , exemple du chimpanzé	10
Atlas	10
Axis	12
Scapula	14
Description de l'atlas, l'axis et la scapula chez le quadrupède, exemple du bovin.....	18
Atlas	18
Axis	20
Scapula	22
Comparaison des ossements entre ceux du bovin, du chimpanzé et de l'homme moderne....	23
Comparaison de l'atlas	23
Comparaison de l'axis	27
Comparaison de la scapula	31
Hypothèses de Dernier Ancêtre Commun (D.A.C.) pour la locomotion	35
D.A.C. possibles entre les humains et les grands singes	35
Le cas d' <i>Ardipithecus ramidus</i>	53
D.A.C. possibles entre les taxons humains	54
Données sur les représentants de la lignée humaine, qui ne sont pas modernes.....	55
Australopithèques	56
<i>Australopithecus afarensis</i>	56
<i>Australopithecus africanus</i>	62
<i>Australopithecus incertae sedis</i>	65
<i>Australopithecus sediba</i>	70
Paranthropes	82
<i>Homo</i>	83
<i>Homo naledi</i>	83
<i>Homo georgicus</i>	88
<i>Homo floresiensis</i>	89

<i>Homo erectus</i>	91
<i>Homo antecessor</i>	93
<i>Homo heidelbergensis</i>	94
<i>Homo neandertaliensis</i>	105
<i>Homo sapiens</i> ou les hommes anatomiques modernes	132
Différents types d'architecture de l'épaule à partir de 0,78 Ma.....	142

Données anatomiques

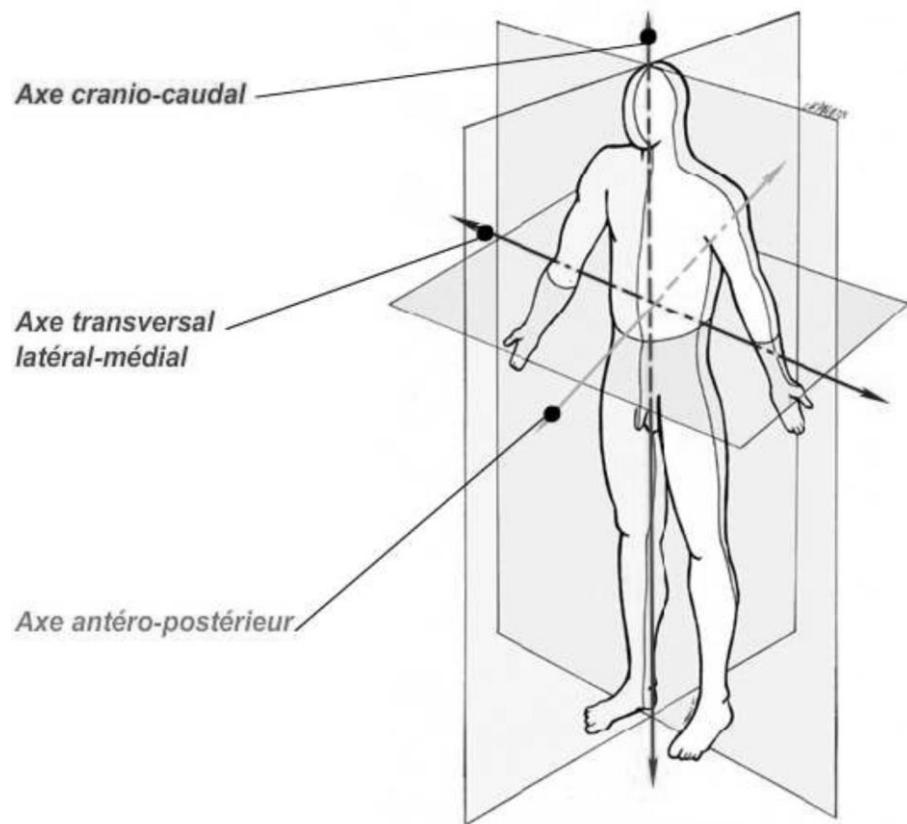


Figure 1. Plans et axes de référence. Image tirée du syllabus d'Ostéologie, Anatomie générale, de l'UVT (Université Virtuelle de Tunis), p. 13.

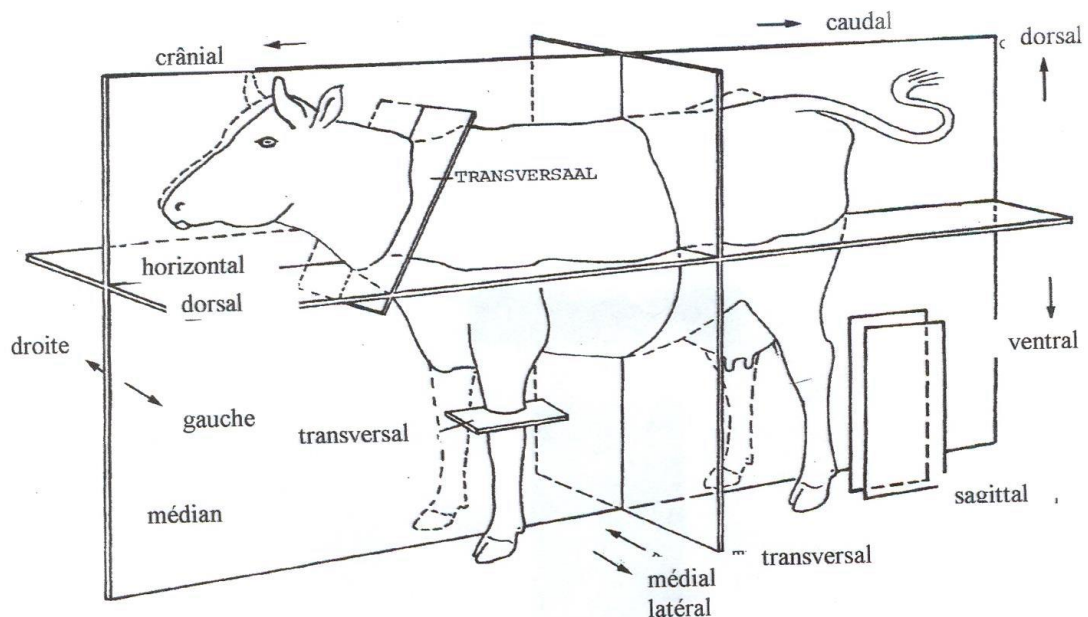


Figure 2. Plans et axes de référence sur un bovin. Image tirée du BARONE R., 1976. *Anatomie comparée des mammifères domestiques. Tome 1. Ostéologie*, t.1, fascicule 1, Paris.

Description de l'atlas, l'axis et la scapula chez l'homme moderne

Atlas

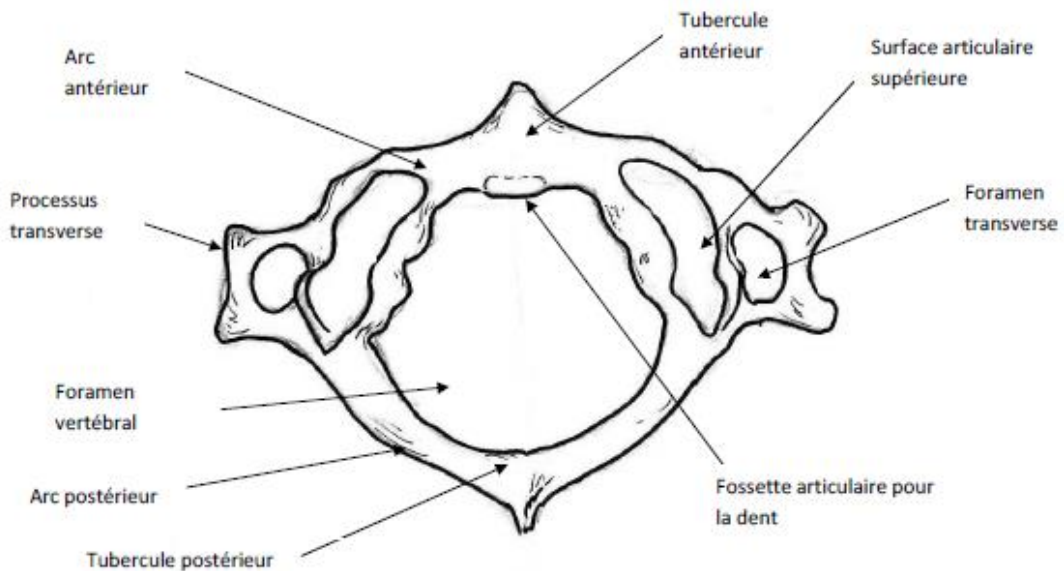


Fig. 3. Atlas, vue supérieure. Image tirée du syllabus d'*Ostéologie, Colonne vertébrale*, de l'UVT (Université Virtuelle de Tunis), <https://www.fichier-pdf.fr/2012/09/04/04-cv/04-cv.pdf>, p. 11.

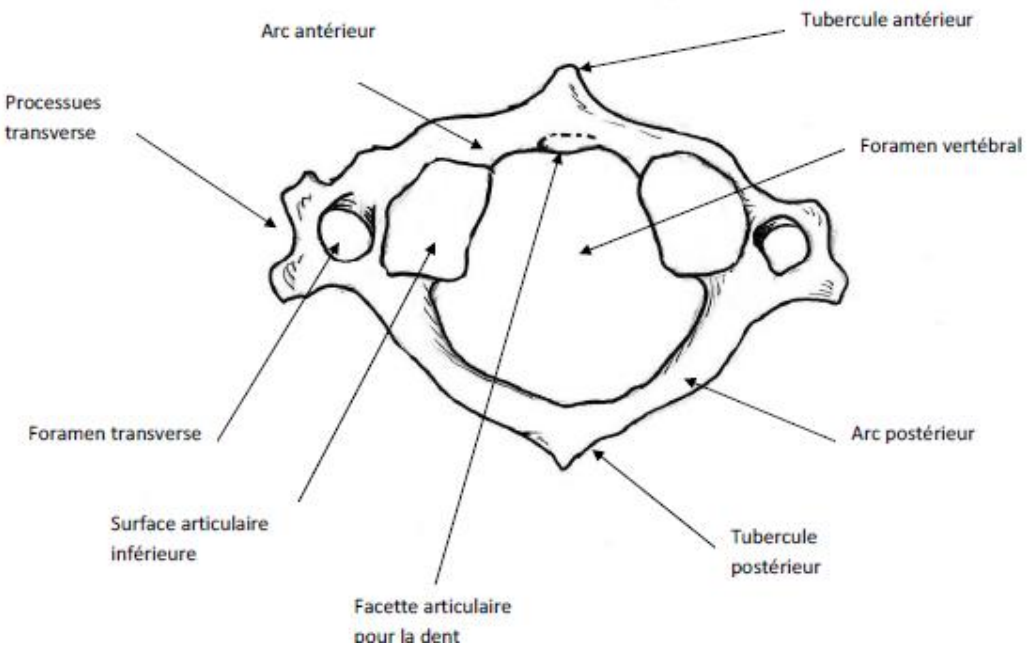


Fig. 4. Atlas, vue inférieure. Image tirée du syllabus d'*Ostéologie, Colonne vertébrale*, de l'UVT, <https://www.fichier-pdf.fr/2012/09/04/04-cv/04-cv.pdf>, p. 12.

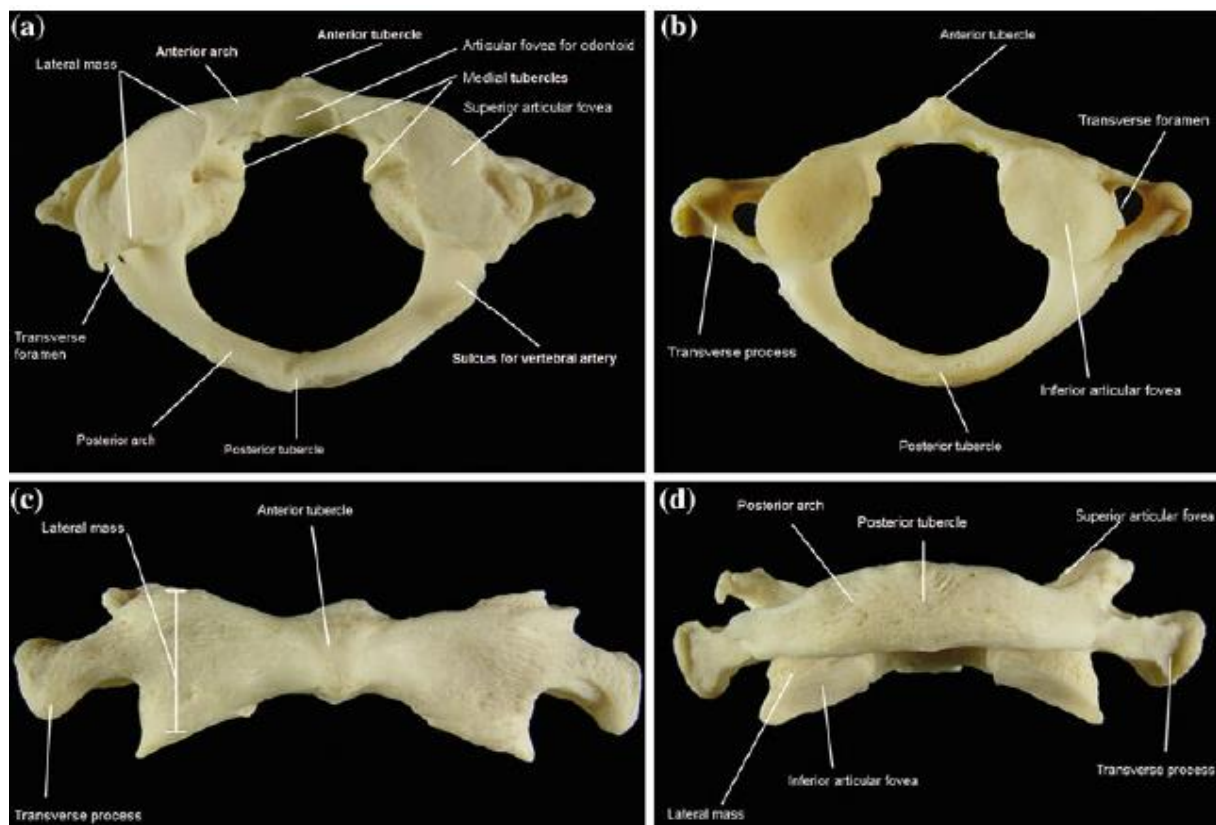


Fig. 5. Atlas, vue supérieure (a), inférieure (b), antérieure (c) et postérieure (d). Photo tirée de KORRES D. S. (ed.), 2013. *Axis vertebrae*, Milan, p. 8.

Axis

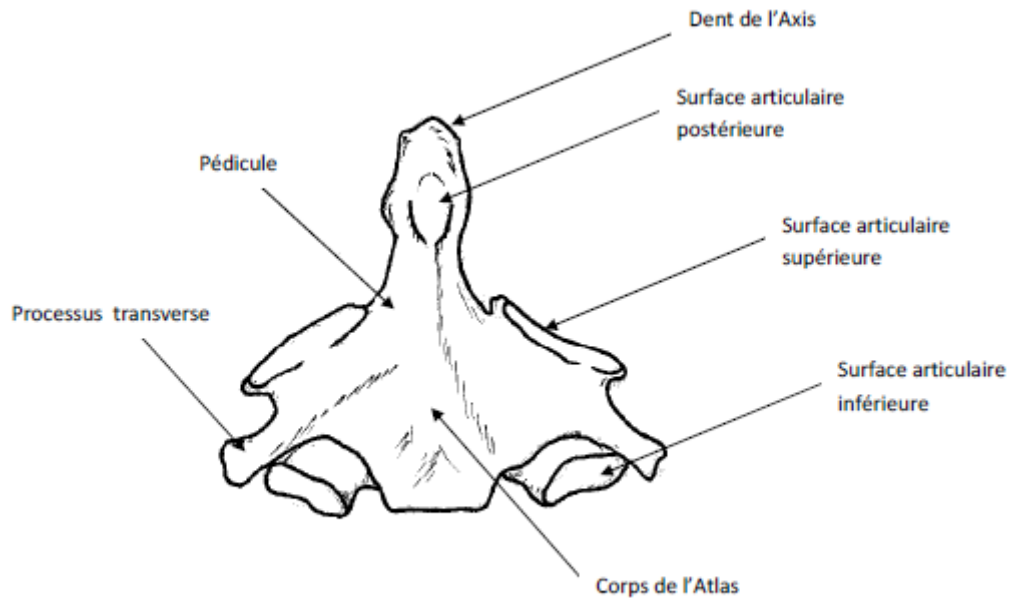


Fig. 6. Axis, vue antérieure. Image tirée du syllabus d'Ostéologie, Colonne vertébrale, de l'UVT, <https://www.fichier-pdf.fr/2012/09/04/04-cv/04-cv.pdf>, p. 13.

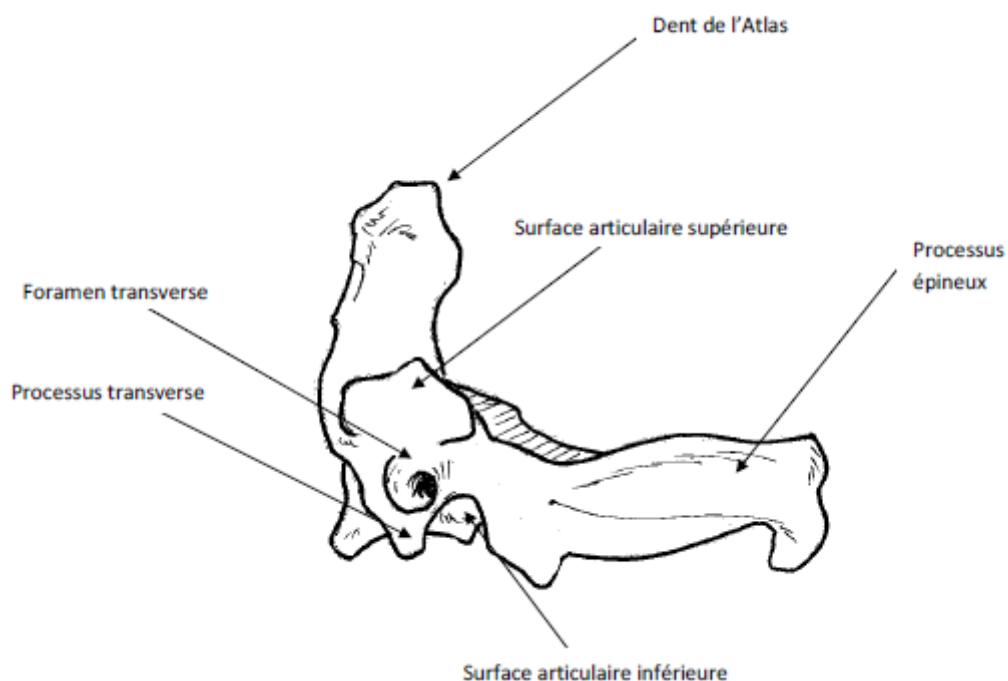


Fig. 7. Axis, vue latérale. Image tirée du syllabus d'Ostéologie, Colonne vertébrale, de l'UVT, <https://www.fichier-pdf.fr/2012/09/04/04-cv/04-cv.pdf>, p. 14.

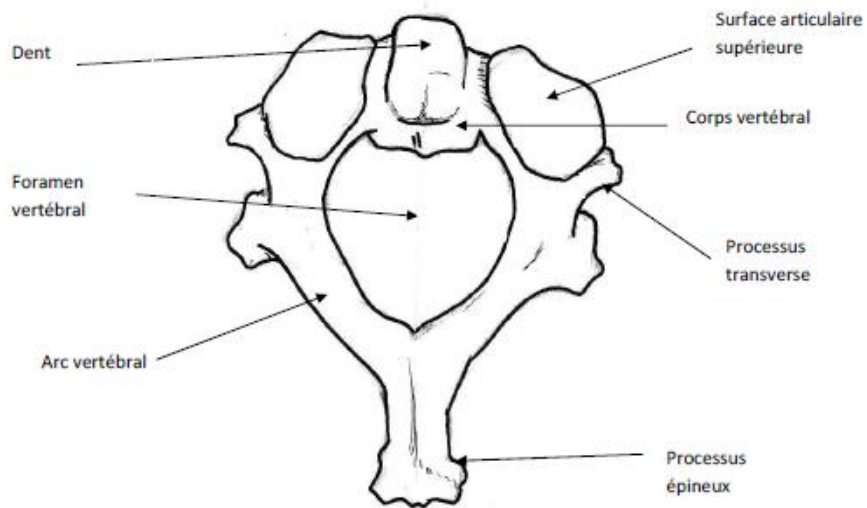


Fig. 8. Axis, vue supérieure. Image tirée du syllabus d'Ostéologie, Colonne vertébrale, de l'UVT, <https://www.fichier-pdf.fr/2012/09/04/04-cv/04-cv.pdf>, p. 15.

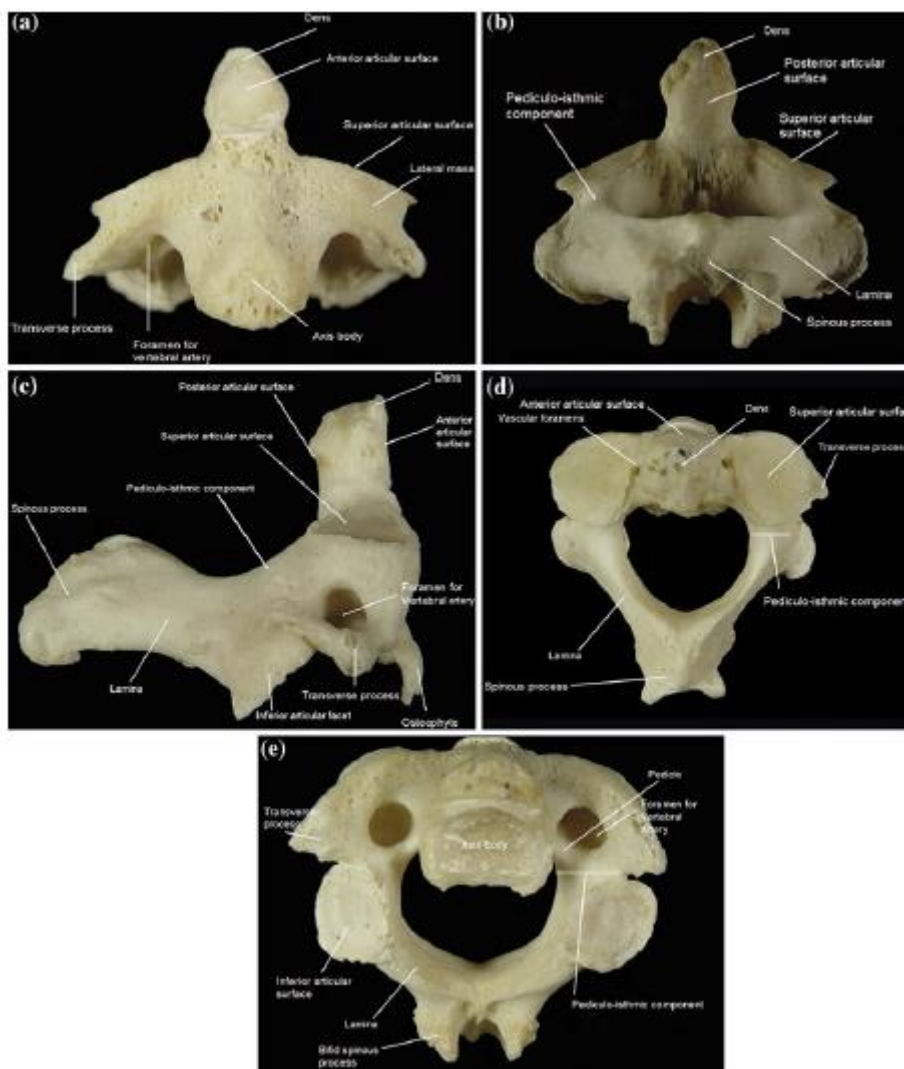


Fig. 9. Axis, vue antérieur (a), postérieure (b), latérale (c), supérieure (d), et inférieure (e). Photo tirée de KORRES D. S. (ed.), 2013. *Axis vertebrae*, Milan, p. 9.

Scapula

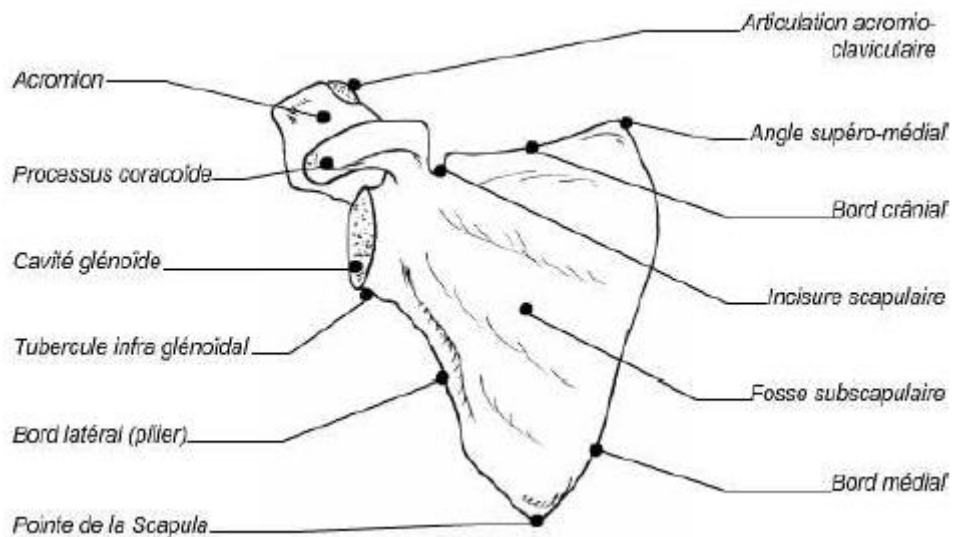


Fig. 10. Scapula droite, vue antérieure. Image tirée du syllabus d'Ostéologie, Membre thoracique, de l'UVT, <https://www.fichier-pdf.fr/2012/09/04/02-mth/02-mth.pdf>, p. 3.

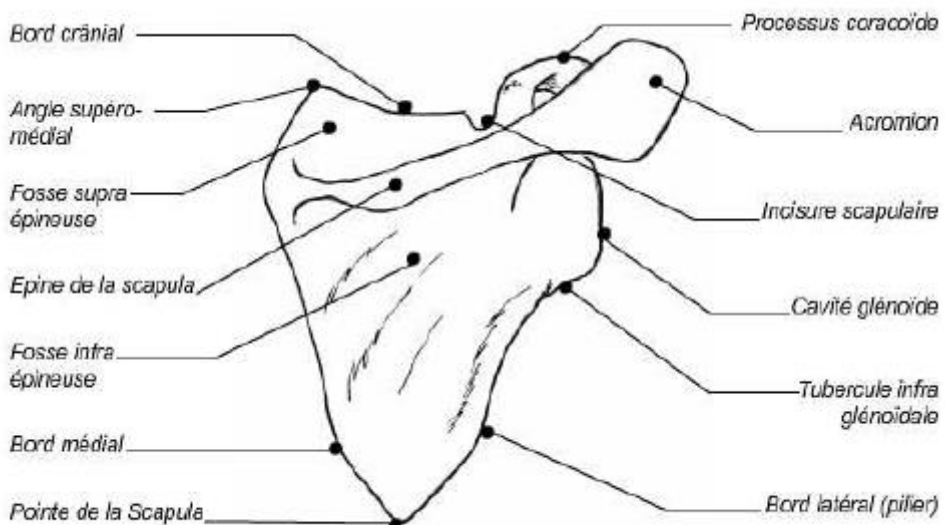


Fig. 11. Scapula droite, vue postérieure. Image tirée du syllabus d'Ostéologie, Membre thoracique, de l'UVT, <https://www.fichier-pdf.fr/2012/09/04/02-mth/02-mth.pdf>, p. 4.

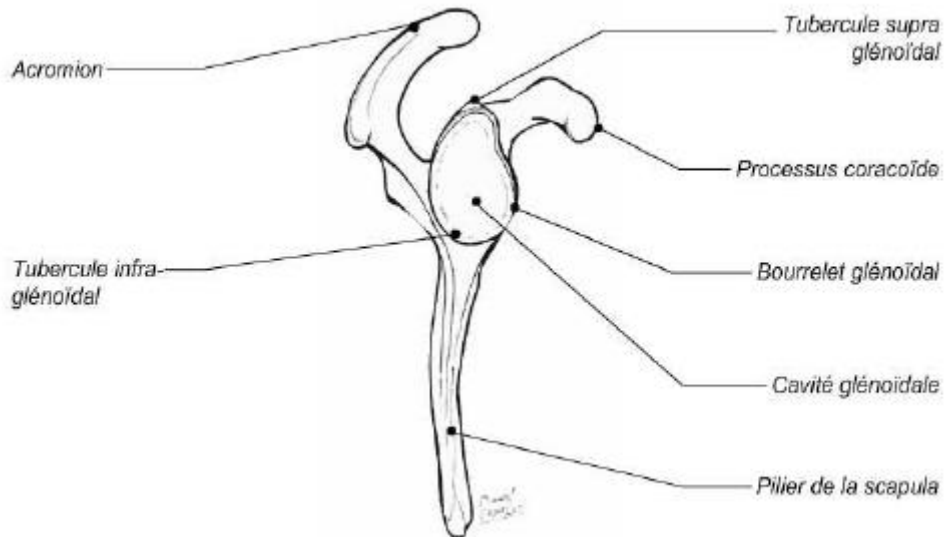


Fig. 12. Scapula droite, vue latérale. Image tirée du syllabus d'Ostéologie, Membre thoracique, de l'UVT, <https://www.fichier-pdf.fr/2012/09/04/02-mth/02-mth.pdf>, p. 6.

Description de l'atlas, l'axis et la scapula chez un représentant du knuckle-walking, exemple du chimpanzé

Atlas

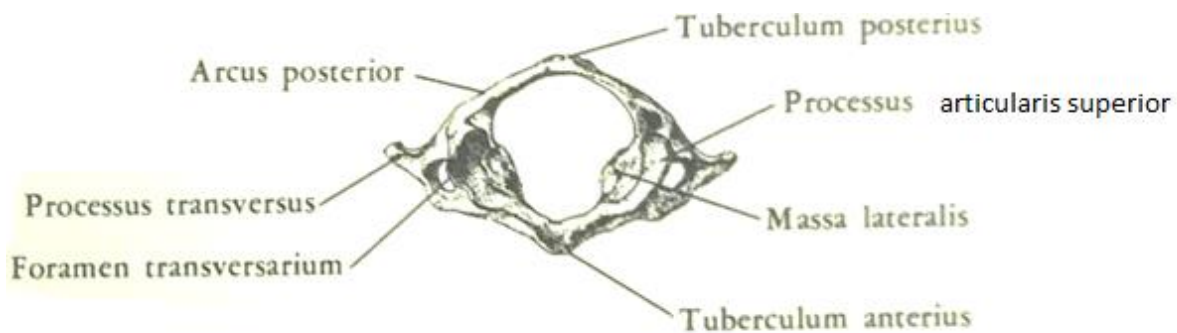


Fig. 13. Atlas de chimpanzé, vue supérieure. Photo tirée de SWINDLER D.R. et WOOD. C. D., 1982. *Atlas of Primate Gross Anatomy: Baboon, Chimpanzee, and Man*, Seattle, p. 15.

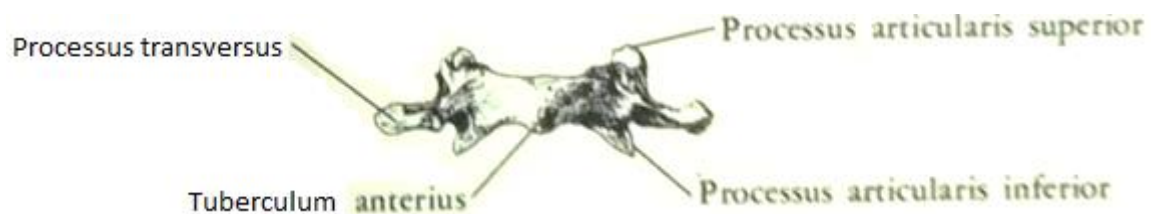


Fig. 14. Atlas de chimpanzé, vue antérieure. Photo tirée de SWINDLER D.R. et WOOD. C. D., 1982. *Atlas of Primate Gross Anatomy: Baboon, Chimpanzee, and Man*, Seattle, p. 15.

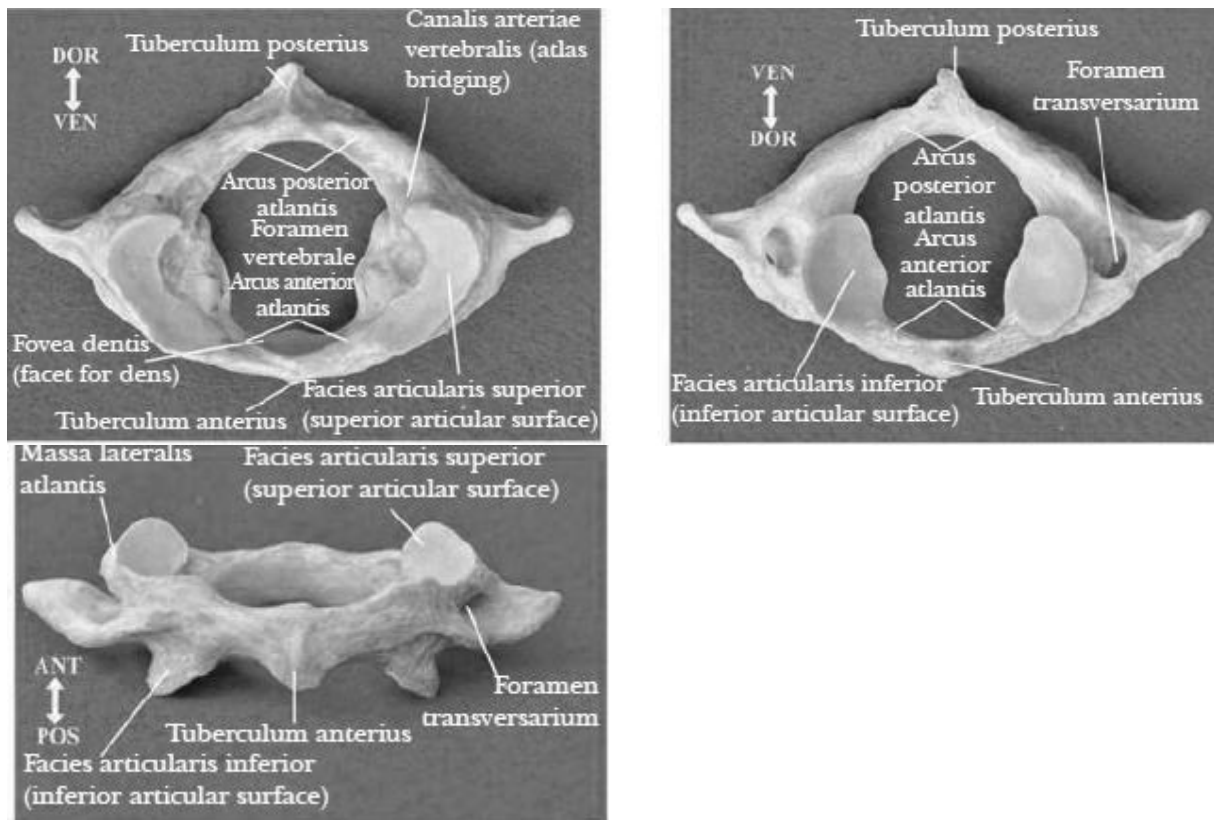


Fig. 15. Atlas de chimpanzé, vue supérieure (a), inférieure (b), ventrale (c). Photos tirées de DIOGO R., POTAU J. M., et PASTOR J. F. (et al.), 2013. *Photographic and Descriptive Musculoskeletal Atlas of Chimpanzees. With notes on the attachements, variations, innervation, function and synonymy and weight of the muscles*, Boca Raton, p. 146.

Axis

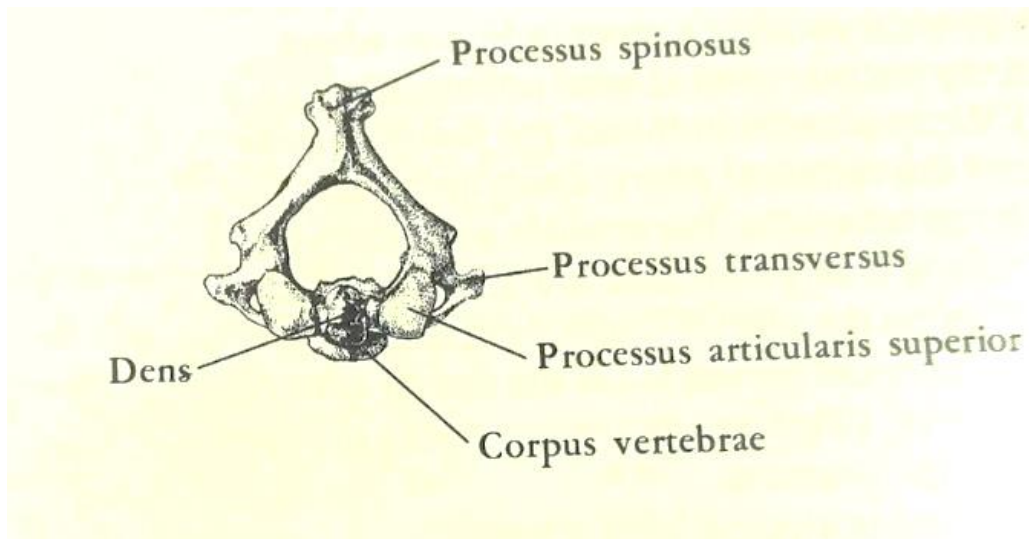


Fig. 16. Axis de chimpanzé, vue supérieure. Photo tirée de SWINDLER D.R. et WOOD. C. D., 1982. *Atlas of Primate Gross Anatomy: Baboon, Chimpanzee, and Man*, Seattle, p. 17.

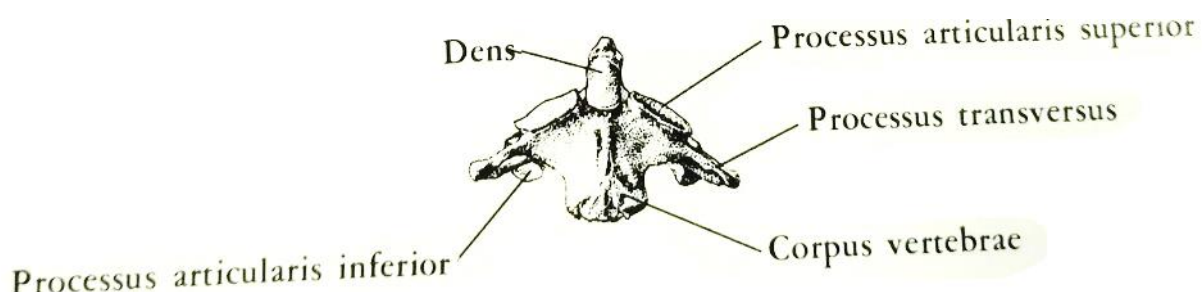


Fig. 17. Axis de chimpanzé, vue antérieure. Photo tirée de SWINDLER D.R. et WOOD. C. D., 1982. *Atlas of Primate Gross Anatomy: Baboon, Chimpanzee, and Man*, Seattle, p. 17.

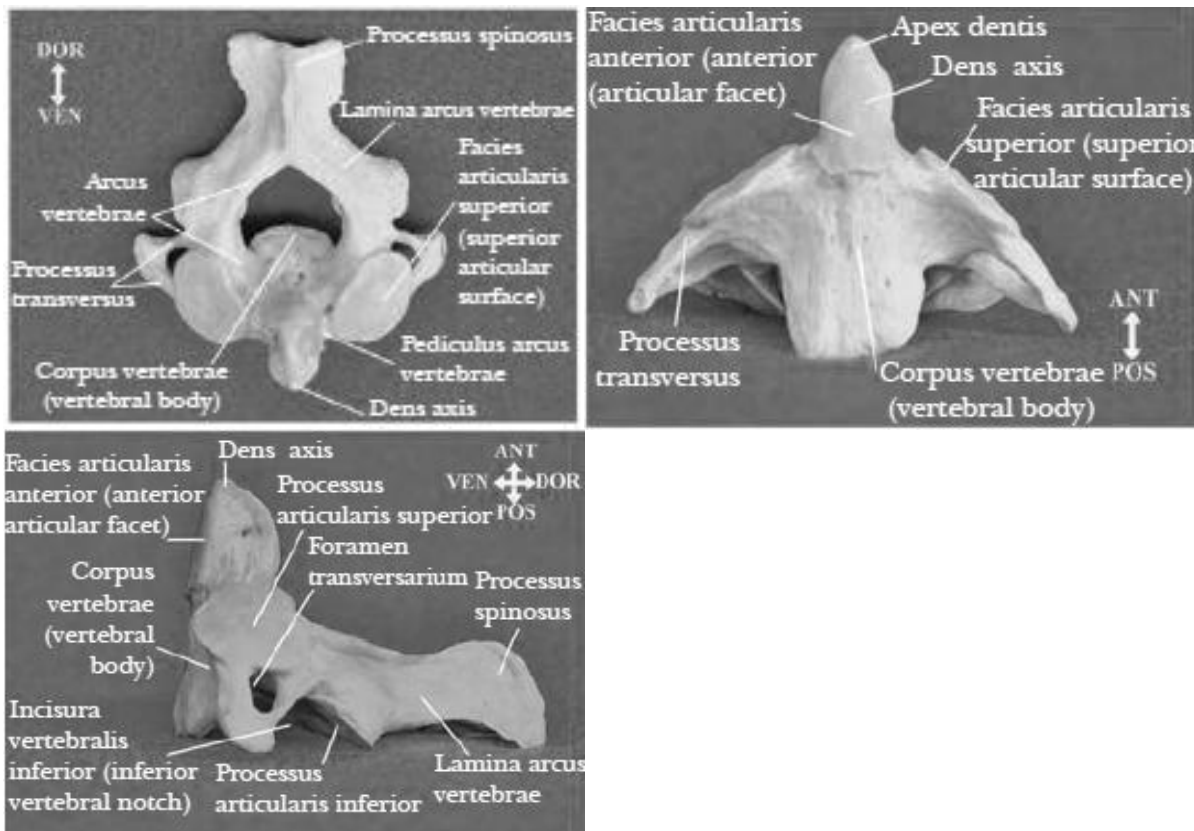


Fig. 18. Axis de chimpanzé (*Pan troglodytes*), vue supérieure (a), antérieure (b), et latérale (c). Photos tirées de DIOGO R., POTAU J. M., et PASTOR J. F. (et al.), 2013. *Photographic and Descriptive Musculoskeletal Atlas of Chimpanzees. With notes on the attachements, variations, innervation, function and synonymy and weight of the muscles*, Boca Raton, pp. 146 - 147.

Scapula



Fig. 19. Scapula droite de chimpanzé, vue antérieure. Photo tirée de SWINDLER D.R. et WOOD. C. D., 1982. *Atlas of Primate Gross Anatomy: Baboon, Chimpanzee, and Man*, Seattle, p. 29.



Fig. 20. Scapula gauche de chimpanzé, vue antérieure. Image tirée de PÜSCHEL T. et SELLERS W., 2016. Standing on the Shoulders of Apes : Analyzing the Form and Function of the Hominoid Scapula Using Geometric Morphometrics and Finite Element Analysis, *American Journal of Physical Anthropology*, 159, p. 330.

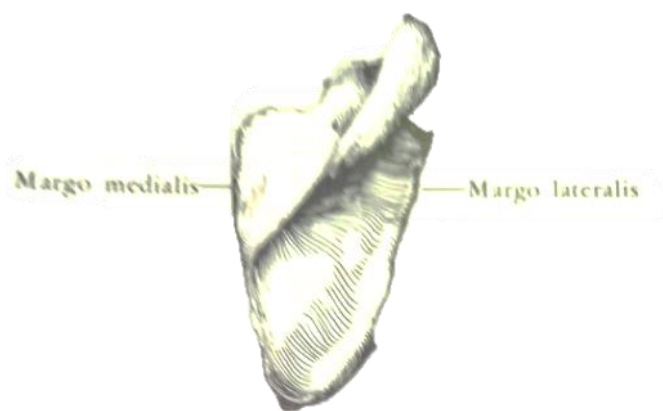


Fig. 21. Scapula droite de chimpanzé, vue postérieure. Photo tirée de SWINDLER D. R. et WOOD. C. D., 1982. *Atlas of Primate Gross Anatomy: Baboon, Chimpanzee, and Man*, Seattle, p. 29.



Fig. 22. Scapula gauche de chimpanzé, vue postérieure. Image tirée de PÜSCHEL T. et SELLERS W., 2016. Standing on the Shoulders of Apes : Analyzing the Form and Function of the Hominoid Scapula Using Geometric Morphometrics and Finite Element Analysis, *American Journal of Physical Anthropology*, 159, p. 330.



Fig. 23. Scapula droite de chimpanzé, vue médiale/latérale. Photo tirée de SWINDLER D.R. et WOOD. C. D., 1982. *Atlas of Primate Gross Anatomy: Baboon, Chimpanzee, and Man*, Seattle, p. 29.



Fig. 24. Scapula gauche de chimpanzé, vue latérale/médiale. Image tirée de PÜSCHEL T. et SELLERS W., 2016. Standing on the Shoulders of Apes : Analyzing the Form and Function of the Hominoid Scapula Using Geometric Morphometrics and Finite Element Analysis, *American Journal of Physical Anthropology*, 159, p. 330.

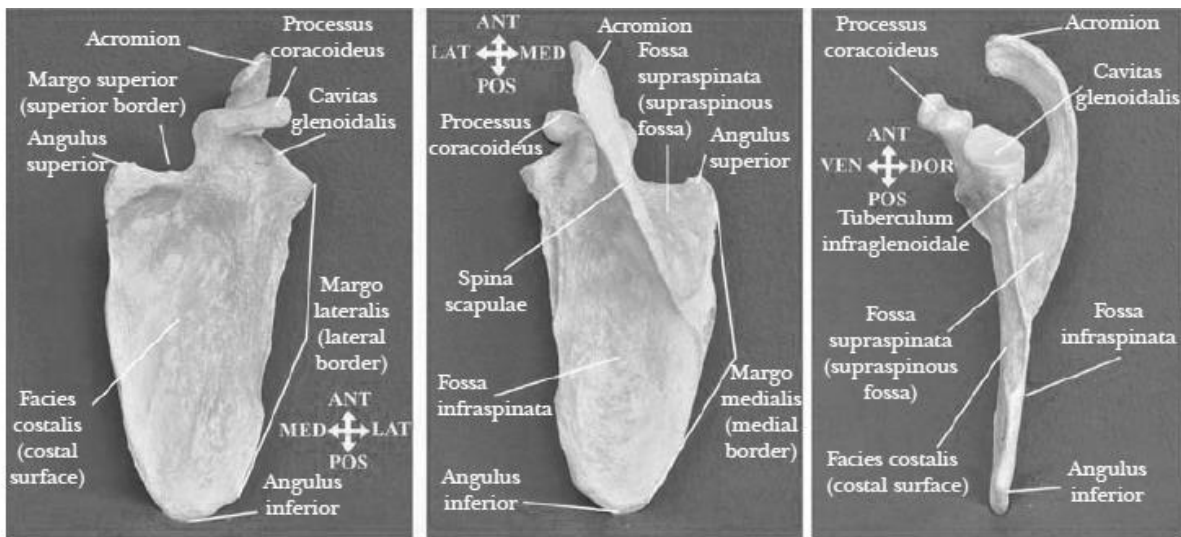


Fig. 25. Scapula gauche de chimpanzé (*Pan troglodytes*), vue antérieure (a), postérieure (b), et latérale (c). Photos tirées de DIOGO R., POTAU J. M., et PASTOR J. F. (et al.), 2013. *Photographic and Descriptive Musculoskeletal Atlas of Chimpanzees. With notes on the attachements, variations, innervation, function and synonymy and weight of the muscles*, Boca Raton, p. 153.

Description de l'atlas, l'axis et la scapula chez le quadrupède, exemple du bovin

Atlas

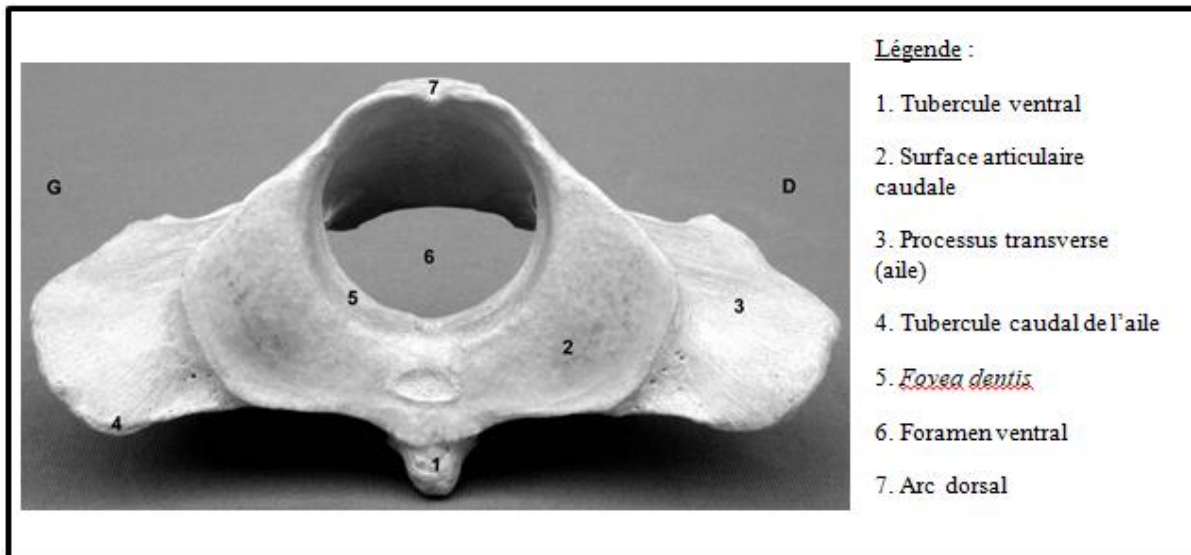


Fig. 26. Atlas de bovin, vue caudale. Photo et légende tirées du site de l'Unité d'Anatomie de l'E.N.V.A., http://theses.vet-alfort.fr/Th_multimedia/mraffaelli/SCRIPT/form.php?action=1&rank=5&id=7.

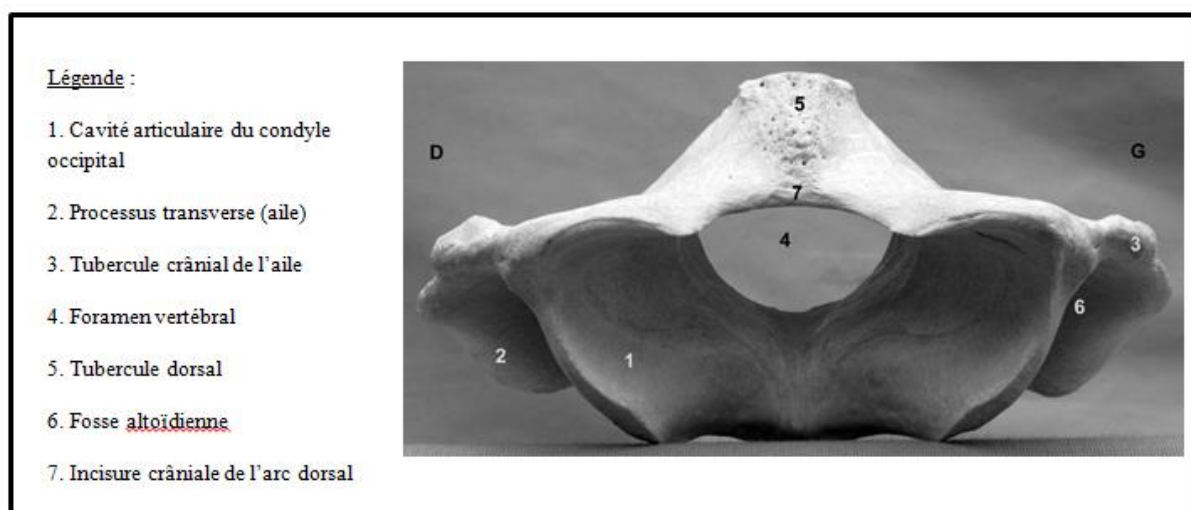


Fig. 27. Atlas de bovin, vue crâniale. Photo et légende tirées du site de l'Unité d'Anatomie de l'E.N.V.A, http://theses.vet-alfort.fr/Th_multimedia/mraffaelli/SCRIPT/form.php?action=2&id=8.

Légende :

1. Incisure crâniale de l'arc dorsal
2. Tubercule dorsal
3. Foramen vertébral latéral
4. Foramen alaire
5. Processus transverse
6. *Fovea dentis*
7. Surface articulaire caudale

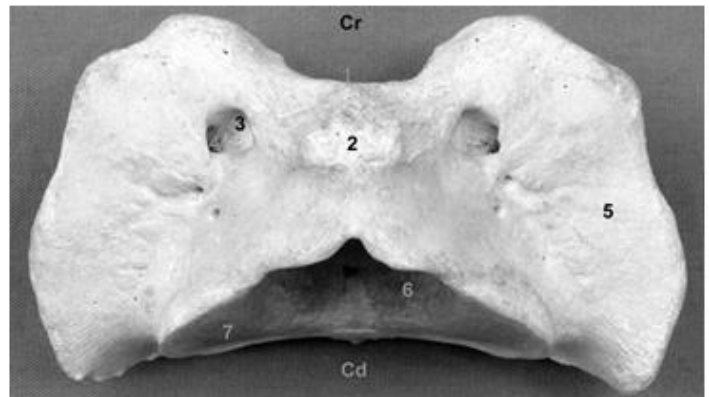


Fig. 28. Atlas de bovin, vue dorsale. Photo et légende tirées du site de l'Unité d'Anatomie de l'E.N.V.A, http://theses.vet-alfort.fr/Th_multimedia/mraffaelli/SCRIPT/form.php?action=1&rank=5&id=9.

Axis

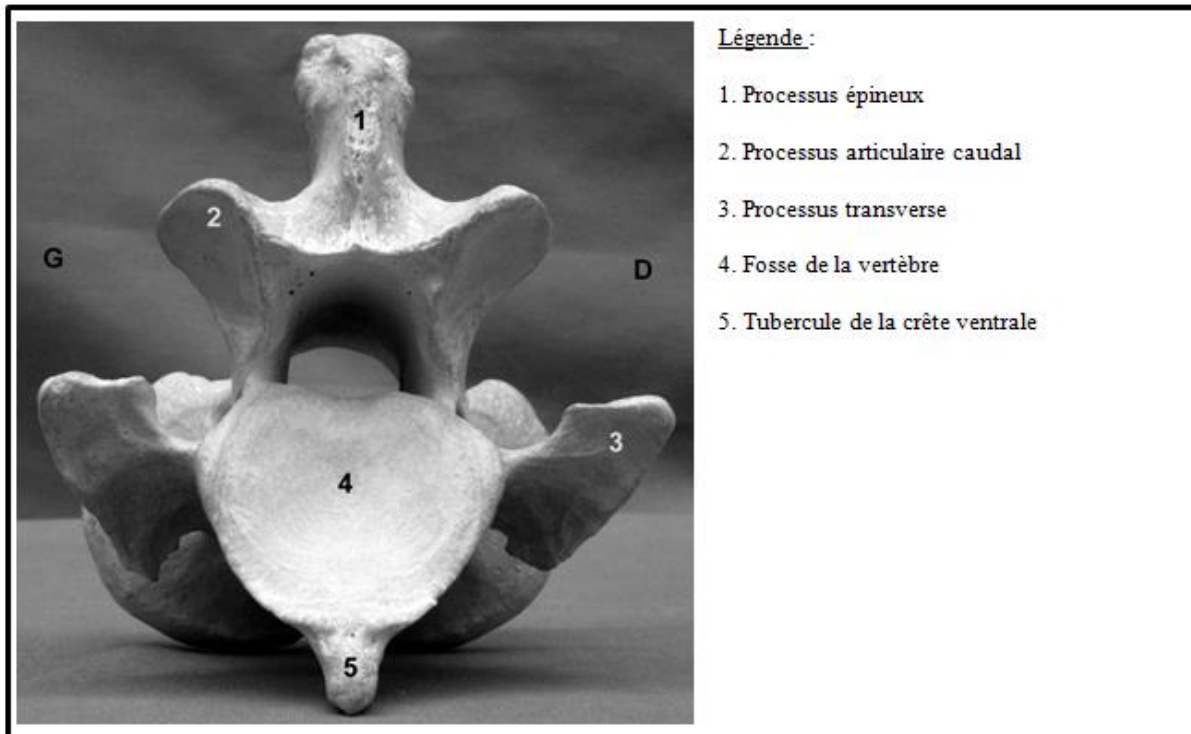


Fig. 29. Axis de bovin, vue caudale. Photo et légende tirées du site de l'Unité d'Anatomie de l'E.N.V.A, http://theses.vet-alfort.fr/Th_multimedia/mraffaelli/SCRIPT/form.php?action=1&rank=5&id=14.

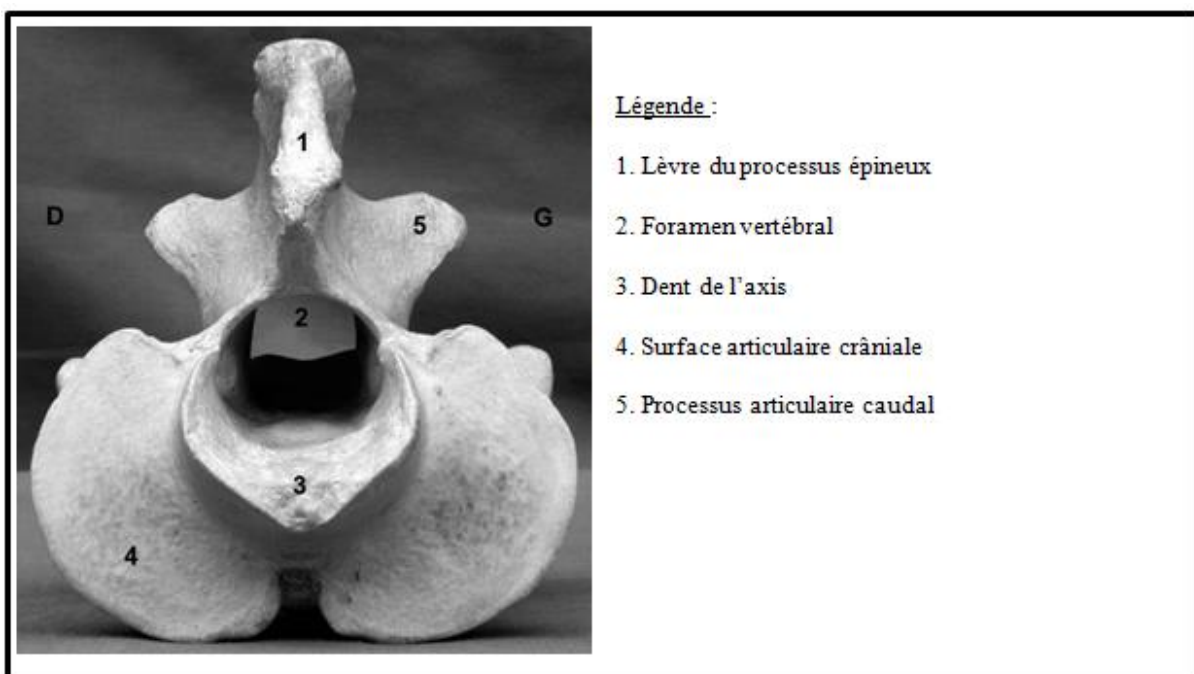


Fig. 30. Axis de bovin, vue crâniale. Photo et légende tirées du site de l'Unité d'Anatomie de l'E.N.V.A, http://theses.vet-alfort.fr/Th_multimedia/mraffaelli/SCRIPT/form.php?action=2&id=15.

Légende :

1. Lèvre du processus épineux
2. Dent de l'axis
3. Surface articulaire crâniale
4. Foramen vertébral latéral
5. Processus articulaire caudal
6. Processus transverse
7. Tubercule de la crête ventrale



Fig. 31. Axis de bovin, vue dorsale. Photo et légende tirées du site de l'Unité d'Anatomie de l'E.N.V.A, http://theses.vet-alfort.fr/Th_multimedia/mraffaelli/SCRIPT/form.php?action=1&rank=5&id=16.

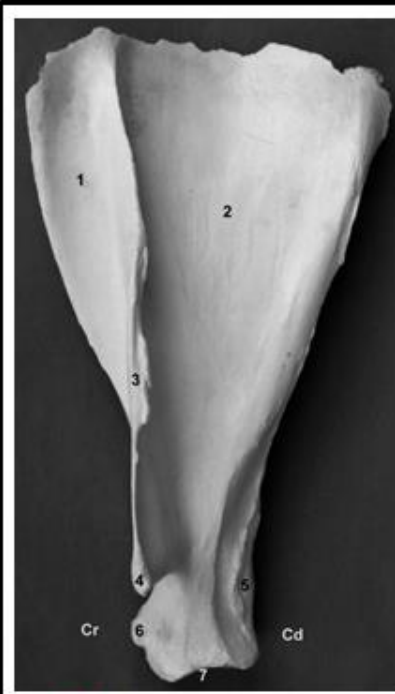
Légende :

1. Dent de l'axis
2. Processus épineux
3. Foramen vertébral latéral
4. Processus articulaire caudal
5. Processus transverse
6. Crête ventrale du corps
7. Tubercule de la crête ventrale



Fig. 32. Axis de bovin, vue latérale. Photo et légende tirées du site de l'Unité d'Anatomie de l'E.N.V.A, http://theses.vet-alfort.fr/Th_multimedia/mraffaelli/SCRIPT/form.php?action=1&rank=5&id=17.

Scapula



Légende :

1. Fosse supra-épineuse
2. Fosse infra-épineuse
3. Épine scapulaire
4. Acromion
5. Col
6. Tubercule supraglénoidal
7. Cavité glénoïdale

Fig. 33. Scapula gauche du bovin, vue latérale. Photo et légende tirées du site de l'Unité d'Anatomie de l'E.N.V.A, http://theses.vet-alfort.fr/Th_multimedia/mraffaelli/SCRIPT/form.php?action=1&rank=5&id=124.



Légende :

1. Surface dentelée
2. Fosse subscapulaire
3. Incisure scapulaire
4. Acromion
5. Tubercule infraglénoidal
6. Tubercule supraglénoidal
7. Processus caracoïde
8. Cavité glénoïdale

Fig. 34. Scapula gauche du bovin, vue médiale. Photo et légende tirées du site de l'Unité d'Anatomie de l'E.N.V.A, http://theses.vet-alfort.fr/Th_multimedia/mraffaelli/SCRIPT/form.php?action=1&rank=5&id=125.

Comparaison des ossements entre ceux du bovin, du chimpanzé et de l'homme moderne

Comparaison de l'atlas

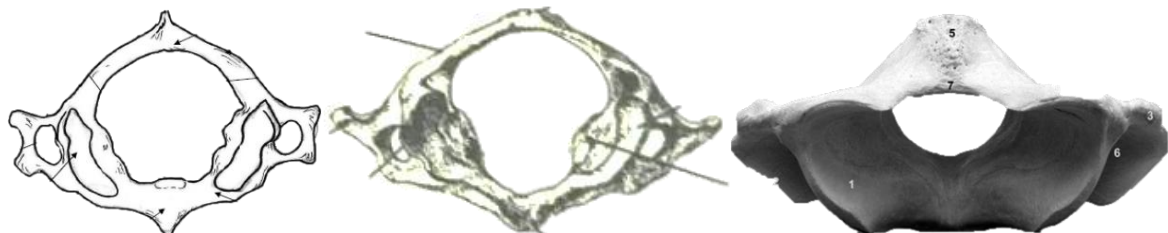


Fig. 35. Atlas, vue supérieure. Humain, chimpanzé, bovin. Images tirées du syllabus d'Ostéologie, Colonne vertébrale, de l'UVT (Université Virtuelle de Tunis), <https://www.fichier-pdf.fr/2012/09/04/04-cv/04-cv.pdf>, p. 11. (humain) ; de SWINDLER D.R. et WOOD. C. D., 1982. *Atlas of Primate Gross Anatomy: Baboon, Chimpanzee, and Man*, Seattle, p. 15. (chimpanzé) ; du site de l'Unité d'Anatomie de l'E.N.V.A, http://theses.vet-alfort.fr/Th_multimedia/mraffaelli/SCRIPT/form.php?action=2&id=8 (bovin).



Fig. 36. Atlas, vue ventrale (a et b), et dorsale (c et d). Humain, chimpanzé, bovin. Images tirées de KORRES D. S. (ed.), 2013. *Axis vertebrae*, Milan, p. 8 (humain) ; DIOGO R., POTAU J. M., et PASTOR J. F. (et al.), 2013. *Photographic and Descriptive Musculoskeletal Atlas of Chimpanzees. With notes on the attachements, variations, innervation, function and synonymy and weight of the muscles*, Boca Raton, p. 146 (chimpanzé); site de l'Unité d'Anatomie de l'E.N.V.A, http://theses.vet-alfort.fr/Th_multimedia/mraffaelli/SCRIPT/form.php?action=1&rank=5&id=9. (bovin).



Fig. 37. Atlas, vue inférieure. Humain, bovin. Images tirées du syllabus d'Ostéologie, Colonne vertébrale, de l'UVT (Université Virtuelle de Tunis), <https://www.fichier-pdf.fr/2012/09/04/04-cv/04-cv.pdf>, p. 12. (humain) ; du site de l'Unité d'Anatomie de l'E.N.V.A, http://theses.vet-alfort.fr/Th_multimedia/mraffaelli/SCRIPT/form.php?action=1&rank=5&id=7. (bovin).



Fig. 38. Atlas, vue supérieure. Humain, bovin. Images tirées Images tirées du syllabus d'Ostéologie, Colonne vertébrale, de l'UVT (Université Virtuelle de Tunis), <https://www.fichier-pdf.fr/2012/09/04/04-cv/04-cv.pdf>, p. 12. (humain) ; site de l'Unité d'Anatomie de l'E.N.V.A, http://theses.vet-alfort.fr/Th_multimedia/mraffaelli/SCRIPT/form.php?action=2&id=8.(bovin).



Fig. 39. Atlas, vue dorsale. Humain, bovin. Images tirées de KORRES D. S. (ed.), 2013. *Atlas vertebrae*, Milan, p. 8 (humain) ; site de l'Unité d'Anatomie de l'E.N.V.A, http://theses.vet-alfort.fr/Th_multimedia/mraffaelli/SCRIPT/form.php?action=1&rank=5&id=9. (bovin).

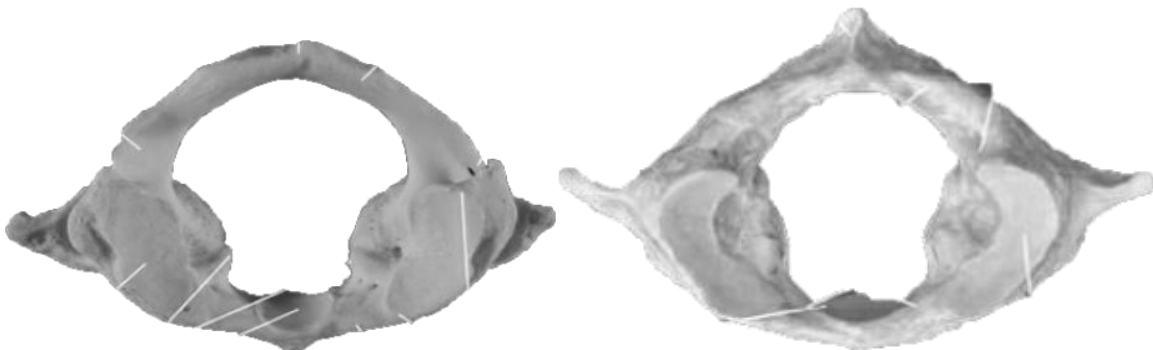


Fig. 40. Atlas, vue inférieure. Humain, chimpanzé. Images tirées de KORRES D. S. (ed.), 2013. *Atlas vertebrae*, Milan, p. 8 (humain) ; DIOGO R., POTAU J. M., et PASTOR J. F. (et al.), 2013. *Photographic and Descriptive Musculoskeletal Atlas of Chimpanzees. With notes on the attachements, variations, innervation, function and synonymy and weight of the muscles*, Boca Raton, p. 146 (chimpanzé)

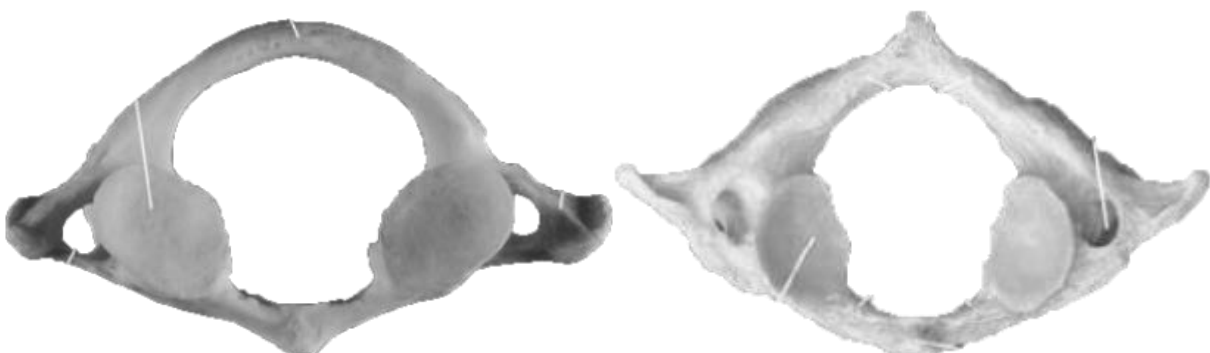


Fig. 41. Atlas, vue supérieure. Humain, chimpanzé. Images tirées de KORRES D. S. (ed.), 2013. *Atlas vertebrae*, Milan, p. 8 (humain) ; DIOGO R., POTAU J. M., et PASTOR J. F. (et al.), 2013. *Photographic and Descriptive Musculoskeletal Atlas of Chimpanzees. With notes on the attachements, variations, innervation, function and synonymy and weight of the muscles*, Boca Raton, p. 146 (chimpanzé)



Fig. 42. Atlas, vue ventrale. Humain, chimpanzé. Images tirées de KORRES D. S. (ed.), 2013. *Atlas vertebrae*, Milan, p. 8 (humain) ; DIOGO R., POTAU J. M., et PASTOR J. F. (et al.), 2013. *Photographic and Descriptive Musculoskeletal Atlas of Chimpanzees. With notes on the attachements, variations, innervation, function and synonymy and weight of the muscles*, Boca Raton, p. 146 (chimpanzé)

Comparaison de l'axis

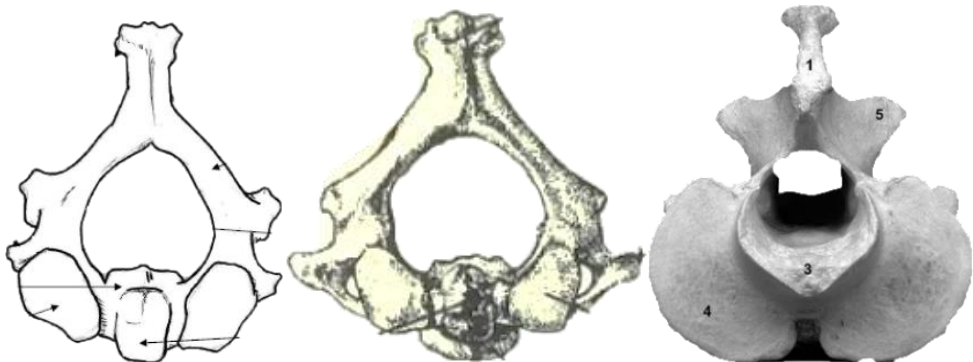


Fig. 43. Axis, vue supérieure. Humain, chimpanzé, bovin. Images tirées du syllabus d'Ostéologie, Colonne vertébrale, de l'UVT (Université Virtuelle de Tunis), <https://www.fichier-pdf.fr/2012/09/04/04-cv/04-cv.pdf>, p. 15. (humain) ; de SWINDLER D.R. et WOOD. C. D., 1982. *Atlas of Primate Gross Anatomy: Baboon, Chimpanzee, and Man*, Seattle, p. 17. (chimpanzé) ; du site de l'Unité d'Anatomie de l'E.N.V.A, http://theses.vet-alfort.fr/Th_multimedia/mraffaelli/SCRIPT/form.php?action=2&id=15. (bovin).

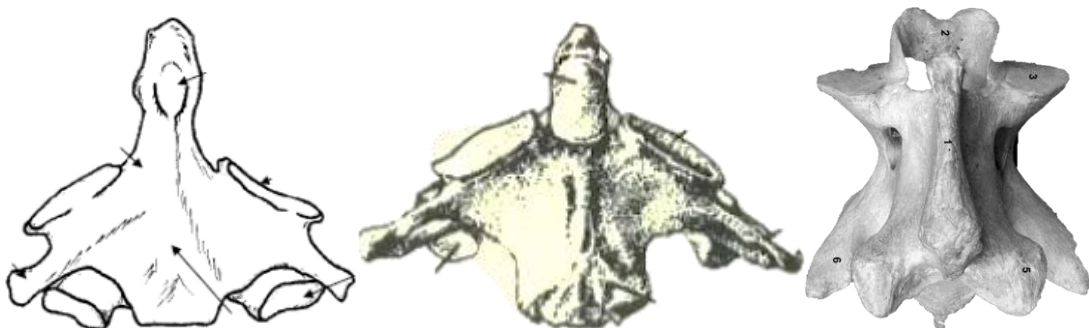


Fig. 44. Axis, vue dorsale. Humain, chimpanzé, bovin. Images tirées du syllabus d'Ostéologie, Colonne vertébrale, de l'UVT (Université Virtuelle de Tunis), <https://www.fichier-pdf.fr/2012/09/04/04-cv/04-cv.pdf>, p. 13. (humain) ; de SWINDLER D.R. et WOOD. C. D., 1982. *Atlas of Primate Gross Anatomy: Baboon, Chimpanzee, and Man*, Seattle, p. 17. (chimpanzé) ; du site de l'Unité d'Anatomie de l'E.N.V.A, http://theses.vet-alfort.fr/Th_multimedia/mraffaelli/SCRIPT/form.php?action=1&rank=5&id=14. (bovin).

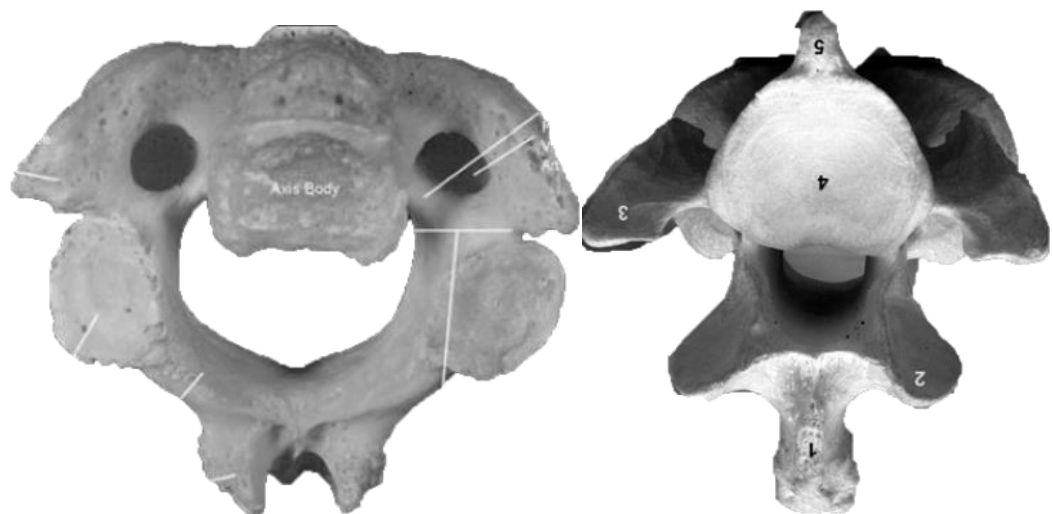


Fig. 45. Axis, vue inférieure. Humain, bovin. Images tirées de KORRES D. S. (ed.), 2013. *Axis vertebrae*, Milan, p. 9 (humain) ; site de l'Unité d'Anatomie de l'E.N.V.A, http://theses.vet-alfort.fr/Th_multimedia/mraffaelli/SCRIPT/form.php?action=1&rank=5&id=14.



Fig. 46. Axis, vue supérieure. Humain, bovin. Images tirées de KORRES D. S. (ed.), 2013. *Axis vertebrae*, Milan, p. 9 (humain) ; site de l'Unité d'Anatomie de l'E.N.V.A, http://theses.vet-alfort.fr/Th_multimedia/mraffaelli/SCRIPT/form.php?action=2&id=15.

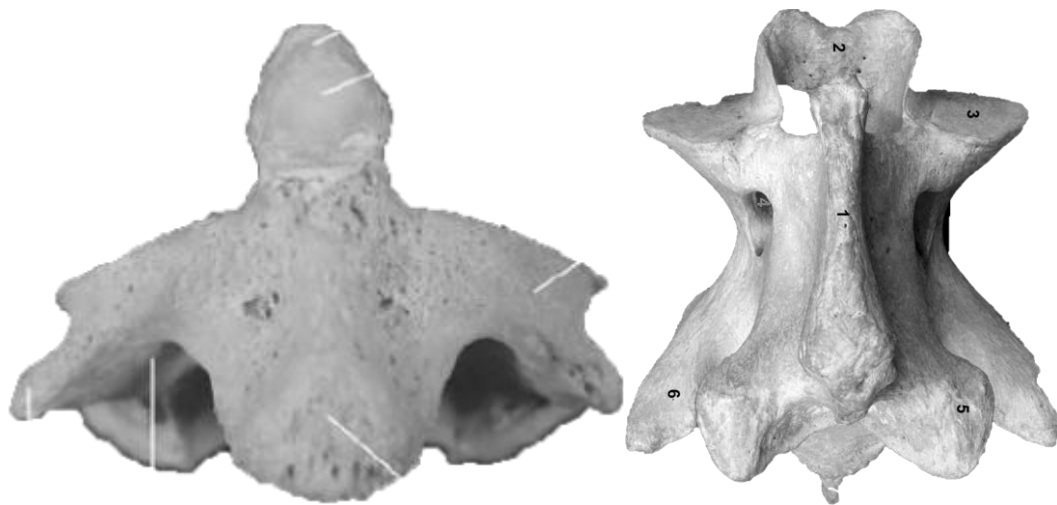


Fig. 47. Axis, vue dorsale. Humain, bovin. Images tirées de KORRES D. S. (ed.), 2013. *Axis vertebrae*, Milan, p. 9 (humain) ; site de l'Unité d'Anatomie de l'E.N.VA, http://theses.vet-alfort.fr/Th_multimedia/mraffaelli/SCRIPT/form.php?action=1&rank=5&id=16.

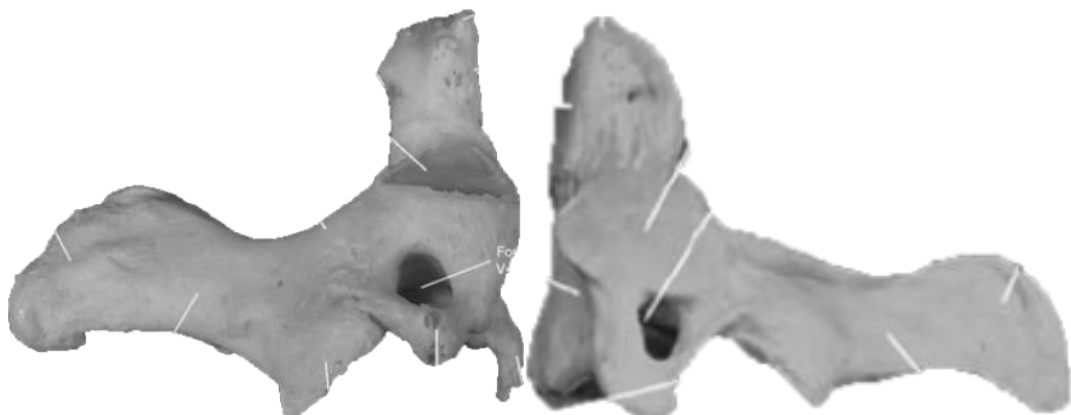


Fig. 48. Axis, vue latérale. Humain, chimpanzé. Images tirées de KORRES D. S. (ed.), 2013. *Axis vertebrae*, Milan, p. 9 (humain) ; DIOGO R., POTAU J. M., et PASTOR J. F. (et al.), 2013. *Photographic and Descriptive Musculoskeletal Atlas of Chimpanzees. With notes on the attachements, variations, innervation, function and synonymy and weight of the muscles*, Boca Raton, p. 147. (chimpanzé)



Fig. 49. Axis, vue supérieure. Humain, chimpanzé. Images tirées de KORRES D. S. (ed.), 2013. *Axis vertebrae*, Milan, p. 9 (humain) ; DIOGO R., POTAU J. M., et PASTOR J. F. (et al.), 2013. *Photographic and Descriptive Musculoskeletal Atlas of Chimpanzees. With notes on the attachements, variations, innervation, function and synonymy and weight of the muscles*, Boca Raton, p. 146. (chimpanzé)



Fig. 50. Axis, vue dorsale. Humain, chimpanzé. Images tirées de KORRES D. S. (ed.), 2013. *Axis vertebrae*, Milan, p. 9 (humain) ; DIOGO R., POTAU J. M., et PASTOR J. F. (et al.), 2013. *Photographic and Descriptive Musculoskeletal Atlas of Chimpanzees. With notes on the attachements, variations, innervation, function and synonymy and weight of the muscles*, Boca Raton, p. 147. (chimpanzé)

Comparaison de la scapula

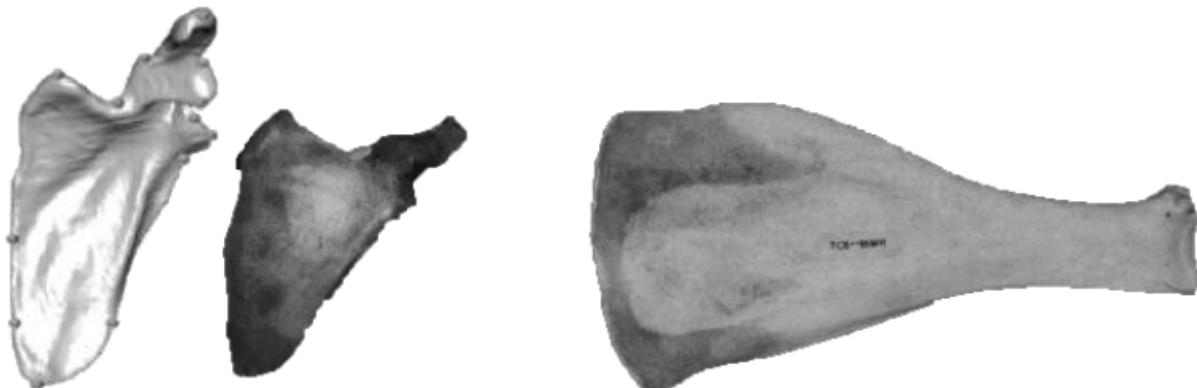


Fig. 51. Scapula gauche, vue antérieure. Chimpanzé, humain, bovin. Images tirées de PÜSCHEL T. et SELLERS W., 2016. Standing on the Shoulders of Apes : Analyzing the Form and Function of the Hominoid Scapula Using Geometric Morphometrics and Finite Element Analysis, *American Journal of Physical Anthropology*, 159, p. 330. (chimpanzé); ADAMS B.J. et CRABTREE P. J., 2008, p. 39. (humain et bovin)



Fig. 52. Scapula gauche, vue postérieure. Chimpanzé, humain, bovin. Images tirées de PÜSCHEL T. et SELLERS W., 2016. Standing on the Shoulders of Apes : Analyzing the Form and Function of the Hominoid Scapula Using Geometric Morphometrics and Finite Element Analysis, *American Journal of Physical Anthropology*, 159, p. 329. (chimpanzé et humain, à échelle); ADAMS B.J. et CRABTREE P. J., 2008, p. 40. (bovin)

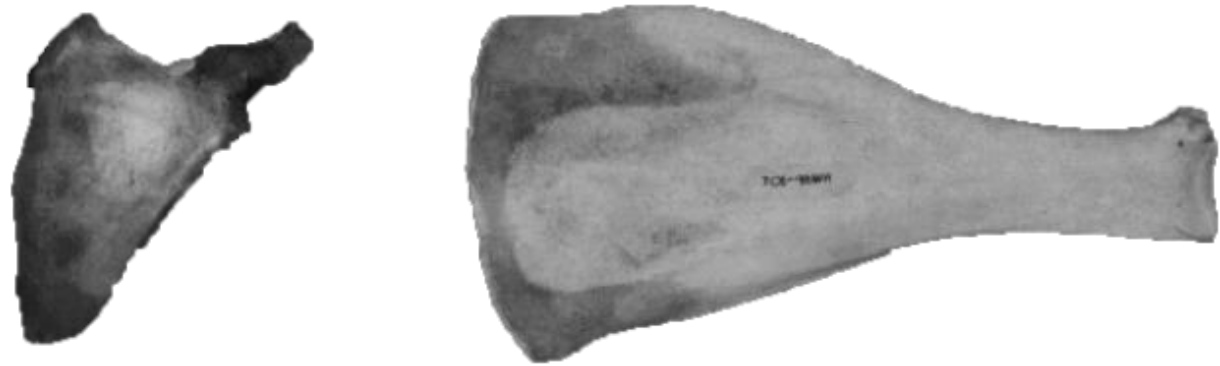


Fig. 53. Scapula gauche, vue antérieure. Humain et bovin, à échelle. Images tirées d'ADAMS B.J. et CRABTREE P. J., 2008, p. 39.



Fig. 54. Scapula gauche, vue postérieure. Humain et bovin, à échelle. Images tirées d' ADAMS B.J. et CRABTREE P. J., 2008, p. 40.

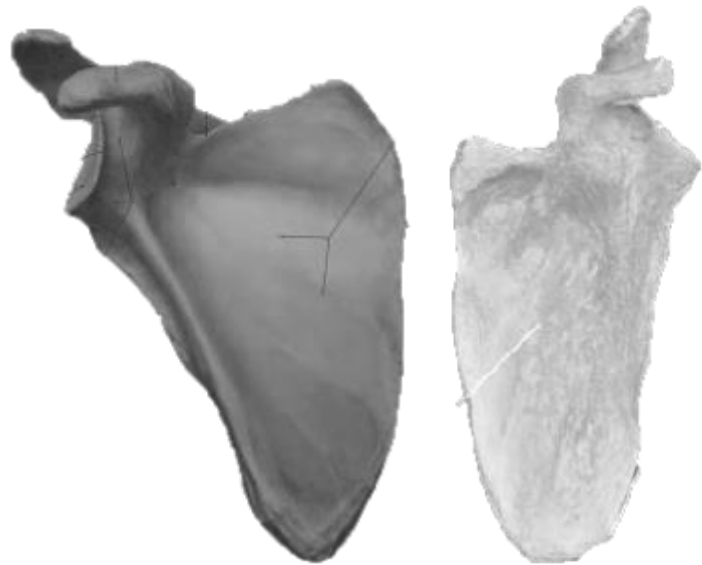


Fig. 55. Scapula, vue ventrale. Humain (droite), chimpanzé (gauche). Images tirées de SCHUENKE M., SCHULTE E., et SCHUMACHER U., 2010. *Atlas d'anatomie*, Paris, p. 255 (humain) ; DIOGO R., POTAU J. M., et PASTOR J. F. (et al.), 2013. *Photographic and Descriptive Musculoskeletal Atlas of Chimpanzees. With notes on the attachements, variations, innervation, function and synonymy and weight of the muscles*, Boca Raton, p. 153. (chimpanzé).

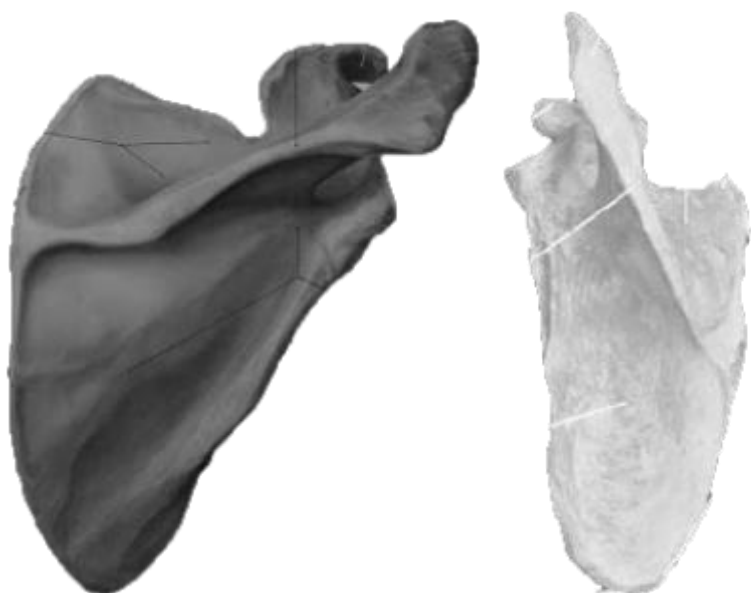


Fig. 56. Scapula, vue dorsale. Humain (droite), chimpanzé (gauche). Images tirées de SCHUENKE M., SCHULTE E., et SCHUMACHER U., 2010. *Atlas d'anatomie*, Paris, p. 255 (humain) ; DIOGO R., POTAU J. M., et PASTOR J. F. (et al.), 2013. *Photographic and Descriptive Musculoskeletal Atlas of Chimpanzees. With notes on the attachements, variations, innervation, function and synonymy and weight of the muscles*, Boca Raton, p. 153. (chimpanzé).



Fig. 57. Scapula, vue latérale. Humain (droite), chimpanzé (gauche). Images tirées de SCHUENKE M., SCHULTE E., et SCHUMACHER U., 2010. *Atlas d'anatomie*, Paris, p. 255 (humain) ; DIOGO R., POTAU J. M., et PASTOR J. F. (et al.), 2013. *Photographic and Descriptive Musculoskeletal Atlas of Chimpanzees. With notes on the attachements, variations, innervation, function and synonymy and weight of the muscles*, Boca Raton, p. 153. (chimpanzé).

Hypothèses de Dernier Ancêtre Commun (D.A.C.) pour la locomotion

D.A.C. possibles entre les humains et les grands singes

<i>P. troglodytes</i>	Cervical	Thoracic	Lumbar	Sacral	Trans.	N	Freq. (%)
Avg./total N	7.00	13.09	3.69	5.70	12.80	239	—
7	13	4	6	T13	69	28.87	
7	13	4	5	T13	35	14.64	
7	13	3	6	T13	18	7.53	
7	13	4	6	T12	17	7.11	
7	13	4	5	T12	12	5.02	

Only those formulae represented at ~5% frequency or higher are shown here (see SOM for full lists of formulae).

Tableau 1. Formules vertébrales chez les chimpanzés, classées par fréquence, avec nombre régional des vertèbres et situation de la vertèbre de transition. Tableau tiré de WILLIAMS S. A. (et al.), 2016. Vertebral Numbers and Human Evolution, *Yearbook of Physical Anthropology*, vol. 159, p. 26.

<i>H. sapiens</i>	Cervical	Thoracic	Lumbar	Sacral	Trans.	N	Freq. (%)
Avg./total N	7.00	12.00	5.00	5.18	11.79	1,159	—
7	12	5	5	T12	499	43.05	
7	12	5	5	T11	204	17.60	
7	12	5	6	T12	108	9.32	
7	12	5	5	T11/T12	62	5.35	

Only those formulae represented at ~5% frequency or higher are shown here (see SOM for full lists of formulae).

Tableau 2. Formules vertébrales chez les humains, classées par fréquence, avec nombre régional des vertèbres et situation de la vertèbre de transition. Tableau tiré de WILLIAMS S. A. (et al.), 2016. Vertebral Numbers and Human Evolution, *Yearbook of Physical Anthropology*, vol. 159, p. 26.

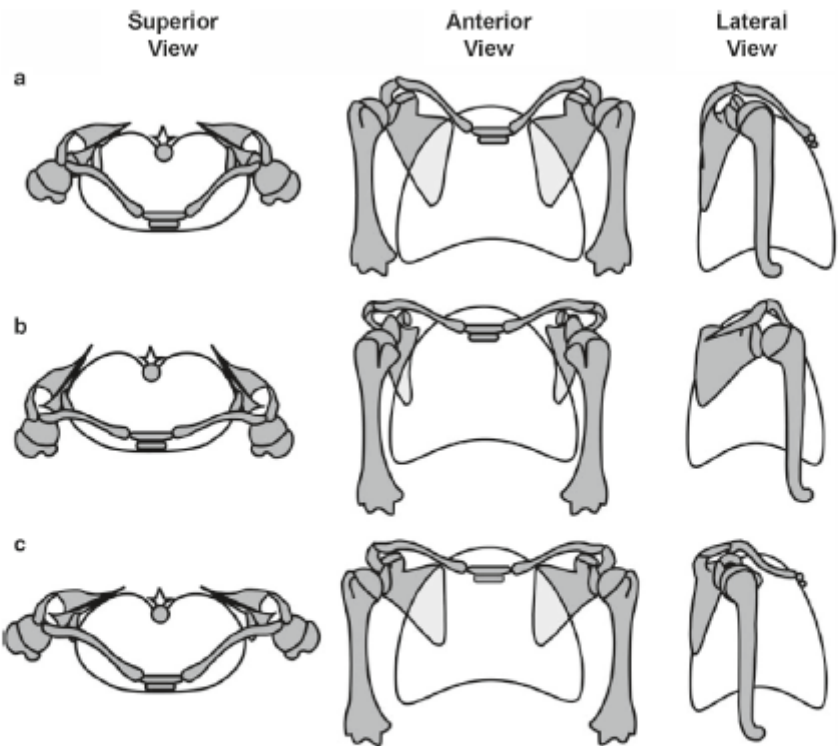


Fig. 7.4 Proposed course of hominin pectoral girdle evolution. (a) Superior, anterior and lateral schematic views of thorax showing pectoral girdle and shoulder of early hominin condition. Scapulae are dorsally positioned with a cranially facing glenoids, and clavicles are short and oriented obliquely resulting in a "hunched-shoulder" appearance. Humerus displays low to modest torsion. (b) Proposed transitional stage in hominin pectoral girdle evolution in which change from a cranially oriented glenoid fossa has been brought about in a way analogous to a downward rotation and translation of the scapula,

constrained by a relatively short clavicle. Scapulae are more laterally positioned, and glenoid fossae face anteriorly. Parasagittal functioning of the elbow joint is maintained without major increases in humeral torsion. Such a configuration would explain the low degree of humeral torsion and relatively short clavicles seen in early *H. erectus* (KNM-WT 15000). (c) Pectoral girdle and shoulder of a modern human with elongated clavicles, dorsally positioned scapulae and laterally facing glenoid fossae. The humerus displays marked torsion to maintain a parasagittal plane for elbow function.

Fig. 58. Proposition de l'évolution de la ceinture de l'épaule chez les hominoïdes. Vue supérieure, antérieure et latérale. Image et légende tirées de LARSON S., 2009. Evolution of the Hominin Shoulder : Early *Homo*, dans GRINE F.E., FLEAGLE J. G. , et LEAKY R. E. (éd.), 2009. *The First Humans: Origin and Early Evolution of the Genus Homo*, New York, p. 71.

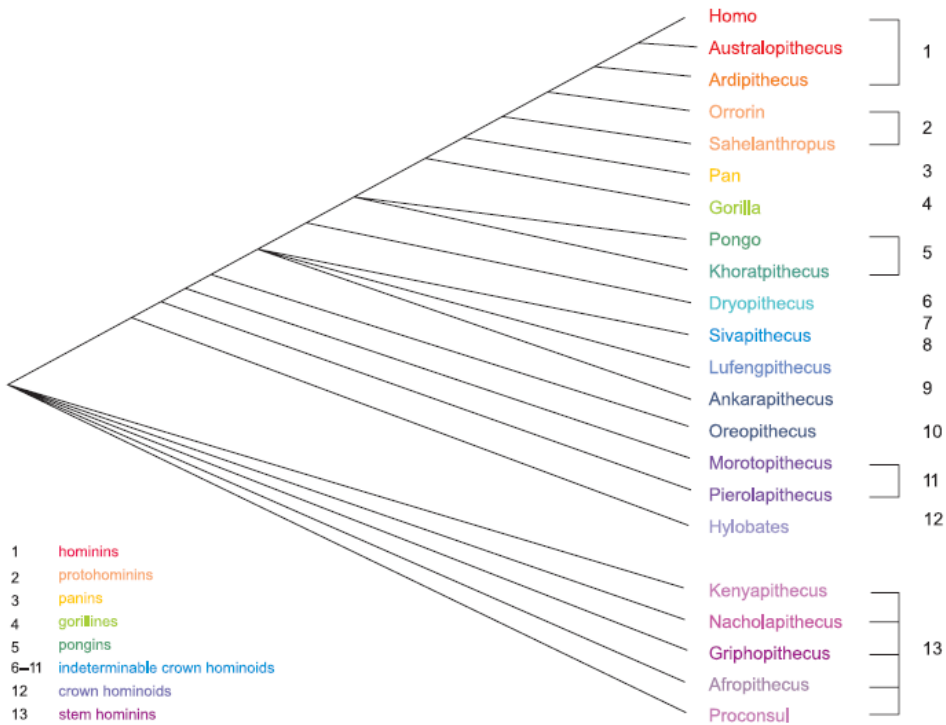


Fig. 59. Diagramme des relations possibles entre les différents taxons hominidés. Image tirée de CROMPTON R., VEREECKE E., et THORPE S., 2008. Locomotion and posture from the common hominoid ancestor to fully modern hominins, with special reference to the last common panin/hominin ancestor, *Journal of Anatomy*, 212, p. 502.

Landmark	Type ^a	Name/definition
1	II	Suprascapular notch
2	III	Superior angle of the scapula
3	I	Intersection between vertebral border and base of scapular spine
4	II	Spinoglenoid notch
5	I	Intersection point of the teres major fossa and the vertebral border of the scapula
6	III	Inferior angle of the scapula
7	III	Lateral expansion of the teres major fossa
8	I	Intersection point of the teres major fossa and the lateral border of the scapula
9	II	Infraglenoid tubercle

Tableau 3. Type et description des points utilisés pour l'analyse GM de Bello- Hellegouarch. Tableau tiré de BELLO-HELLEGOUARCH G., POTAU J.M., et ARIAS – MARTORELL J. (et al.), 2012. A Comparison of Qualitative and Quantitative Methodological Approaches to Characterizing the Dorsal Side of the Scapula in Hominoidea and Its Relationship to Locomotion, *International Journal of Primatology*, 34, p. 320.

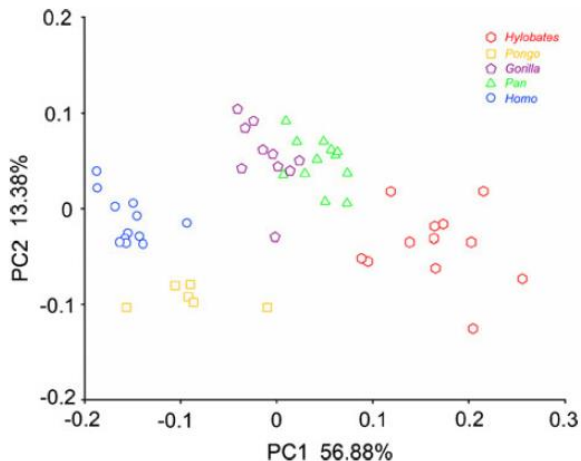


Fig. 60. Résultat des analyses des deux composants principaux (PC1 et PC2) dérivés de la PCA de l'analyse GM. Image tirée de BELLO-HELLEGOUARCH G., POTAU J.M., et ARIAS – MARTORELL J. (et al.), 2012. A Comparison of Qualitative and Quantitative Methodological Approaches to Characterizing the Dorsal Side of the Scapula in Hominoidea and Its Relationship to Locomotion, *International Journal of Primatology*, 34, p. 323.

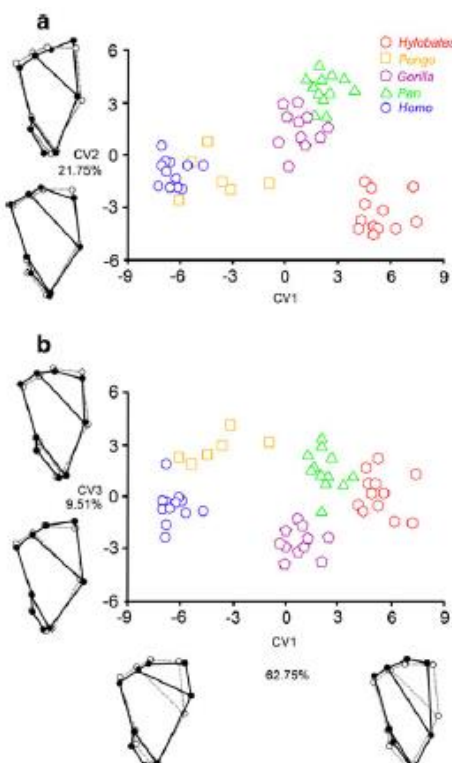


Fig. 61. Résultats démontrant la dispersion des groupes locomoteurs pour la CV1 contre la CV2 (a), et la CV1 contre la CV3(b). Les traits noirs reliés montrent la forme externe de chaque CV, et les traits gris reliés représentent la *mean shape* (coordonées 0,0) Image tirée de BELLO-HELLEGOUARCH G., POTAU J.M., et ARIAS – MARTORELL J. (et al.), 2012. A Comparison of Qualitative and Quantitative Methodological Approaches to Characterizing the Dorsal Side of the Scapula in Hominoidea and Its Relationship to Locomotion, *International Journal of Primatology*, 34, p. 324.

Species	Mahalanobis distance (<i>P</i> value)			
	Procrustes distance (<i>P</i> value)			
	<i>Gorilla</i>	<i>Homo</i>	<i>Pan</i>	<i>Pongo</i>
<i>Homo</i>	18.43 (<0.0001) 0.18 (<0.0001)			
<i>Pan</i>	7.44 (0.0023) 0.11 (<0.0001)	17.82 (0.0001) 0.22 (<0.0001)		
<i>Pongo</i>	37.33 (0.0192) 0.18 (<0.0001)	20.22 (0.0135) 0.13 (<0.0001)	14.48 (0.0351) 0.20 (<0.0001)	
<i>Hylobates</i>	12.75 (<0.0001) 0.21 (<0.0001)	25.48 (<0.0001) 0.32 (<0.0001)	13.74 (<0.0001) 0.17 (<0.0001)	11.92 (0.0601) 0.27 (<0.0001)

Tableau 4. Résultats des distances Mahalanobis et Procrustes (en italique) entre les groupes aves les valeurs *P* (entre parenthèses), basé sur 1000 permutations. Tableau tiré de BELLO-HELLEGOUARCH G., POTAU J.M., et ARIAS – MARTORELL J. (et al.), 2012. A Comparison of Qualitative and Quantitative Methodological Approaches to Characterizing the Dorsal Side of the Scapula in Hominoidea and Its Relationship to Locomotion, *International Journal of Primatology*, 34, p. 325.

Table IV Percentages of *post hoc* correct classification probabilities derived from the discriminant functions after leave-one out cross-validations for the canonical variate shape analysis (CVA) and the discriminant quantitative analysis (DA)

	CVA	DA
<i>Pongo–Hylobates</i>	66.7	100
<i>Pongo–Pan</i>	77.8	79.2
<i>Pongo–Homo</i>	88.9	58.4
<i>Pongo–Gorilla</i>	88.2	100
<i>Hylobates–Pan</i>	100	75.0
<i>Hylobates–Homo</i>	100	100
<i>Hylobates–Gorilla</i>	91.3	83.4
<i>Pan–Homo</i>	95.8	100
<i>Pan–Gorilla</i>	91.3	86.4
<i>Homo–Gorilla</i>	100	100

Tableau 5. Pourcentage de probabilités de classification *posthoc* correctes dérivées des fonctions discriminantes après la validation croisée d'un *leave-one out* pour la CVA et la DA. Tableau et légende tirés de BELLO-HELLEGOUARCH G., POTAU J.M., et ARIAS – MARTORELL J. (et al.), 2012. A Comparison of Qualitative and Quantitative Methodological Approaches to Characterizing the Dorsal Side of the Scapula in Hominoidea and Its Relationship to Locomotion, *International Journal of Primatology*, 34, p. 325.

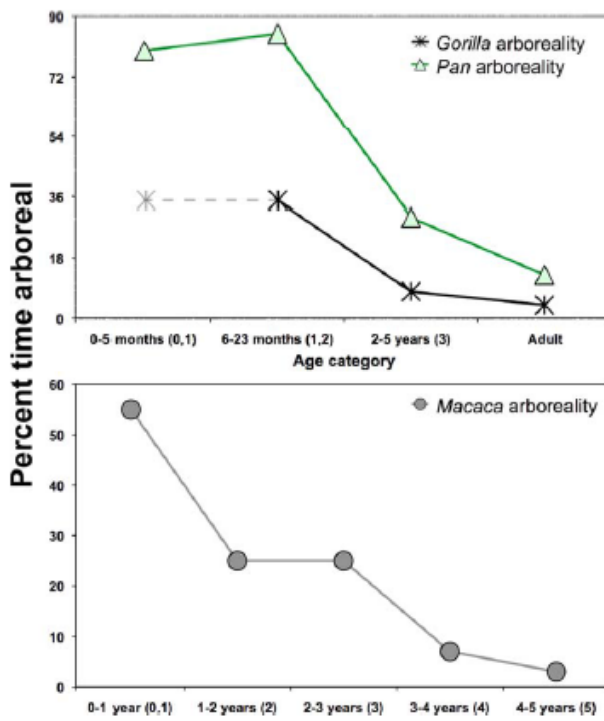


Fig. 62. Graphiques démontrant les changements de comportements locomoteurs durant l'ontogénèse de *Gorilla* et *Pan*. Image et légende tirées de GREEN D., 2013. Ontogeny of the Hominoid Scapula. The Influence of Locomotion on Morphology, *American Journal of Physical Anthropology*, 152, p. 242.

TABLE 4. List of measurements used in this study

Measurement name	Description
Glenoid size	The square root of the product of glenoid height (landmarks 7–10) and width (8–9)
Axillary/medial border (AMB) angle	The angle formed by the medial (between landmarks 2 and 4) and axillary (between landmarks 4 and 5) borders
Axillary/infraspinous medial border (AIM) angle	The angle formed by the medial border and infraspinous breadth line (see below)
Ventral bar/glenoid (VBG) angle	The angle formed by the “bar” of bone on the subscapularis fossa and glenoid height line
Total length	The distance between landmarks 3 and 10
Total breadth	The distance between landmarks 2 and 4 (also used as the line for “medial border”)
Medial border/spine (MBS) angle	The angle formed by the medial border and the base of the spine (between landmarks 3 and 6)
Axillary border/spine (ABS) angle	The angle formed by the axillary border and the base of the spine
Spine length	The distance between landmarks 3 and 15
Superior border length	The distance between landmarks 2 and 15
Infraspinous breadth	The distance between landmarks 3 and 4
Infraspinous length	The distance between landmarks 4 and 6
Infraspinous length (transv.)	The distance between landmarks 3 and 5
Infraspinous neck width	The distance between landmarks 5 and 6
Supraspinous breadth	The distance between landmarks 2 and 3
Supraspinous length	The distance between landmarks 1 and 3
Supraspinous length (transv.)	The distance between landmarks 3 and 6
Lateral expansion of subscapularis fossa	The perpendicular distance from landmark 5 to the ventral bar
Subscapularis insertion facet height	The total height of the subscapularis insertion facet on the lesser tubercle of the proximal humerus
Subscapularis insertion facet width	The total width of the insertion facet, perpendicular to the height

Tableau 6. Listes des mesures utilisées pour l'étude de GREEN. Tableau tiré de GREEN D., 2013. Ontogeny of the Hominoid Scapula. The Influence of Locomotion on Morphology, *American Journal of Physical Anthropology*, 152, p. 243.

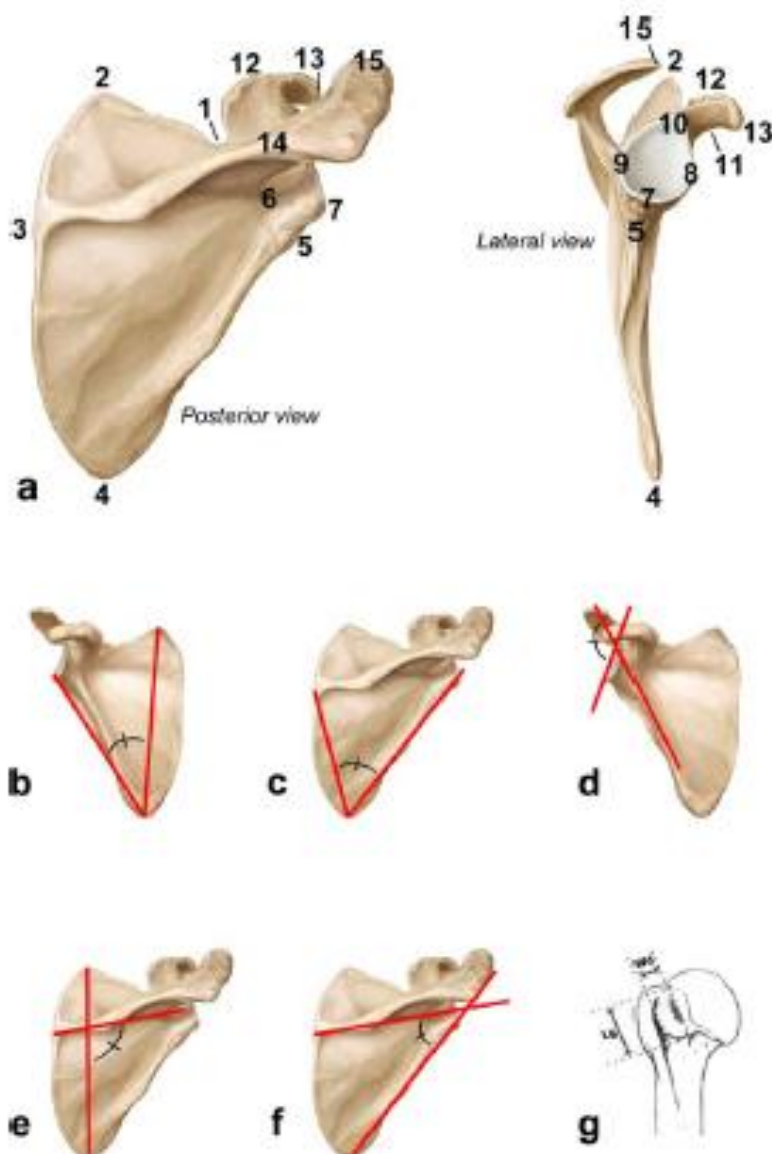


Fig. 1. Plots showing behavioral shifts throughout ontogeny in *Gorilla* and *Pan* (top plot) and *Macaca* based on data presented by Doran (1997) and Rawlins (1993), respectively. Percentage of time spent arboreal is plotted against chronological age and corresponding age stages (in parentheses) based on dental eruption sequences outlined by Smith et al. (1994). No data are presented for 0- to 5-month-old gorillas as they primarily use their mother as a substrate and these behaviors are not considered “arboreal”. [Color figure can be viewed in the online issue, which is available at wileyonlinelibrary.com.]

Fig. 63. Marquage des points et angles utilisés pour l'étude de GREEN. Image et légende tirées de GREEN D., 2013. Ontogeny of the Hominoid Scapula. The Influence of Locomotion on Morphology, *American Journal of Physical Anthropology*, 152, p. 242.

TABLE 3. Scapular landmarks

- | |
|--|
| 1. Suprascapular notch—the inferior-most point of this notch |
| 2. Superior angle—the superior-most point of the scapula with the superior and inferior angles in line with imaginary vertebral column |
| 3. Point of spine that meets vertebral border (a straight line from the spinoglenoid notch to the medial edge of the spine was this point if the spine diminished before intersecting with the vertebral border) |
| 4. Inferior angle—the inferior-most point of the scapula with the superior and inferior angles in line with imaginary vertebral column |
| 5. Infraglenoid tubercle—inferomedial to point 7 (below); attachment site of triceps brachii muscle |
| 6. Spinoglenoid notch—the point where the base of the spine meets the blade inferior to the junction of the spine and the acromion |
| 7. Inferior-most point of glenoid fossa |
| 8. Coracoid side of maximum glenoid width—anterior-most point of fossa |
| 9. Acromion side of maximum glenoid width—posterior-most point of fossa |
| 10. Superior-most point of glenoid fossa |
| 11. Inferior “elbow” of coracoid—point directly below point 12 (below) |
| 12. Superior “elbow” of coracoid—superior point where coracoid turns laterally |
| 13. Most distal point of coracoid |
| 14. Point of spine above spinoglenoid notch—the union of the spine and the acromion |
| <u>15. Distal most point on the acromion</u> |

Tableau 7. Marquage scapulaire pour l'étude de GREEN. Tableau tiré de GREEN D., 2013. Ontogeny of the Hominoid Scapula. The Influence of Locomotion on Morphology, *American Journal of Physical Anthropology*, 152, pp. 239 – 260.

TABLE 8. Scapular shape characteristics for each age-stage within species; angle or ratio value (SD)

	Scapular shape characteristics				
	Stages 0,1	Stage 2	Stage 3	Stage 4	Stages 5-7
Axillary/medial border (AMB) angle (°)					
<i>Pan troglodytes</i>	32.2 (1.7)	31.9 (2.6)	30.5 (2.1)	30.2 (2.3)	29.2 (2.2) ^a
<i>Gorilla gorilla</i>	38.2 (2.6)	36.4 (3.4)	37.1 (2.7)	36.4 (2.3)	34.4 (3.2) ^b
<i>Pongo pygmaeus</i>	49.1 (6.1)	43.1 (2.7)	42.8 (2.7)	42.3 (2.2)	39.1 (4.0) ^c
<i>Hylobates</i> sp.	—	36.6 (2.7)	35.5 (3.6)	35.1 (3.6)	32.7 (3.3) ^c
<i>Homo sapiens</i>	42.1 (5.3)	39.6 (3.4)	40.3 (3.3)	37.8 (3.4)	38.1 (3.6) ^c
<i>Macaca mulatta</i>	45.2 (5.1)	43.8 (3.6)	42.4 (3.1)	44.3 (3.3)	42.9 (2.8) ^c
Axillary/infraspinous medial border (AIM) angle (°)	Stages 0,1	Stage 2	Stage 3	Stage 4	Stages 5-7
<i>Pan troglodytes</i>	50.2 (5.2)	51.6 (5.2)	49.7 (5.2)	47.4 (4.7)	42.9 (4.1) ^a
<i>Gorilla gorilla</i>	67.3 (3.6)	63.1 (6.5)	60.9 (3.9)	58.4 (4.2)	54.9 (4.3) ^b
<i>Pongo pygmaeus</i>	65.0 (3.8)	53.1 (2.5)	53.9 (2.6)	51.9 (2.4)	48.9 (4.5) ^c
<i>Hylobates</i> sp.	—	68.9 (4.1)	65.7 (5.4)	63.1 (7.3)	58.1 (6.4) ^c
<i>Homo sapiens</i>	61.3 (4.1)	56.7 (3.0)	54.8 (3.5)	52.8 (3.3)	51.5 (3.3) ^c
<i>Macaca mulatta</i>	73.0 (4.0)	70.4 (1.9)	67.8 (2.5)	68.7 (2.9)	67.9 (2.9) ^c
Ventral bar/glenoid (VBG) angle (°)	Stages 0,1	Stage 2	Stage 3	Stage 4	Stages 5-7
<i>Pan troglodytes</i>	131.0 (6.5)	127.9 (4.8)	126.1 (4.8)	127.1 (5.1)	127.9 (4.5) ^a
<i>Gorilla gorilla</i>	132.6 (6.5)	131.6 (5.7)	128.0 (5.0)	129.8 (5.1)	130.2 (5.5) ^b
<i>Pongo pygmaeus</i>	130.1 (1.7)	126.3 (5.9)	123.3 (4.4)	128.0 (6.3)	131.4 (6.4) ^b
<i>Hylobates</i> sp.	—	121.9 (6.0)	119.8 (5.6)	122.4 (4.1)	121.1 (5.2) ^c
<i>Homo sapiens</i>	155.7 (6.0)	144.9 (5.5)	139.4 (5.2)	140.7 (6.3)	142.4 (5.5) ^a
<i>Macaca mulatta</i>	133.5 (5.2)	132.5 (4.3)	133.0 (4.8)	138.0 (3.8)	135.1 (4.1) ^c
Total breadth/glenoid size	Stages 0,1	Stage 2	Stage 3	Stage 4	Stages 5-7
<i>Pan troglodytes</i>	4.85 (0.2)	4.78 (0.3)	5.09 (0.3)	5.21 (0.3)	5.71 (0.3) ^a
<i>Gorilla gorilla</i>	4.85 (0.2)	4.87 (0.2)	5.02 (0.2)	5.12 (0.3)	5.32 (0.4) ^b
<i>Pongo pygmaeus</i>	3.70 (0.7)	3.95 (0.2)	4.00 (0.4)	4.11 (0.4)	4.45 (0.4) ^c
<i>Hylobates</i> sp.	—	3.70 (0.2)	4.07 (0.3)	4.39 (0.3)	5.15 (0.4) ^c
<i>Homo sapiens</i>	4.34 (0.4)	4.46 (0.4)	4.64 (0.3)	4.96 (0.4)	5.07 (0.3) ^c
<i>Macaca mulatta</i>	3.86 (0.3)	4.10 (0.2)	4.30 (0.2)	4.36 (0.2)	4.79 (0.3) ^c
Total length/glenoid size	Stages 0,1	Stage 2	Stage 3	Stage 4	Stages 5-7
<i>Pan troglodytes</i>	3.65 (0.3)	3.74 (0.4)	3.86 (0.3)	3.83 (0.3)	3.87 (0.2) ^a
<i>Gorilla gorilla</i>	3.98 (0.3)	3.89 (0.2)	3.84 (0.2)	3.80 (0.2)	4.02 (0.2) ^b
<i>Pongo pygmaeus</i>	3.33 (0.2)	3.37 (0.2)	3.28 (0.2)	3.35 (0.4)	3.46 (0.3) ^c
<i>Hylobates</i> sp.	—	4.66 (0.3)	4.86 (0.6)	4.92 (0.5)	5.33 (0.5) ^c
<i>Homo sapiens</i>	3.38 (0.3)	3.12 (0.3)	3.24 (0.2)	3.39 (0.2)	3.50 (0.2) ^c
<i>Macaca mulatta</i>	5.02 (0.4)	5.31 (0.3)	5.22 (0.3)	5.47 (0.3)	5.81 (0.3) ^c
Total breadth/length	Stages 0,1	Stage 2	Stage 3	Stage 4	Stages 5-7
<i>Pan troglodytes</i>	1.34 (0.1)	1.28 (0.1)	1.32 (0.1)	1.37 (0.1)	1.44 (0.1) ^a
<i>Gorilla gorilla</i>	1.23 (0.1)	1.26 (0.1)	1.31 (0.1)	1.35 (0.1)	1.38 (0.1) ^b
<i>Pongo pygmaeus</i>	1.11 (0.1)	1.17 (0.1)	1.22 (0.1)	1.24 (0.1)	1.29 (0.1) ^c
<i>Hylobates</i> sp.	—	0.80 (0.1)	0.85 (0.1)	0.90 (0.1)	0.97 (0.1) ^c
<i>Homo sapiens</i>	1.29 (0.1)	1.42 (0.1)	1.44 (0.1)	1.46 (0.1)	1.45 (0.1) ^c
<i>Macaca mulatta</i>	0.77 (0.1)	0.79 (0.04)	0.82 (0.05)	0.80 (0.04)	0.83 (0.05)

Tableau 8. Caractéristiques morphologiques de la scapula pour l'étude de GREEN. Tableau tiré de GREEN D., 2013. Ontogeny of the Hominoid Scapula. The Influence of Locomotion on Morphology, *American Journal of Physical Anthropology*, 152, p. 246.

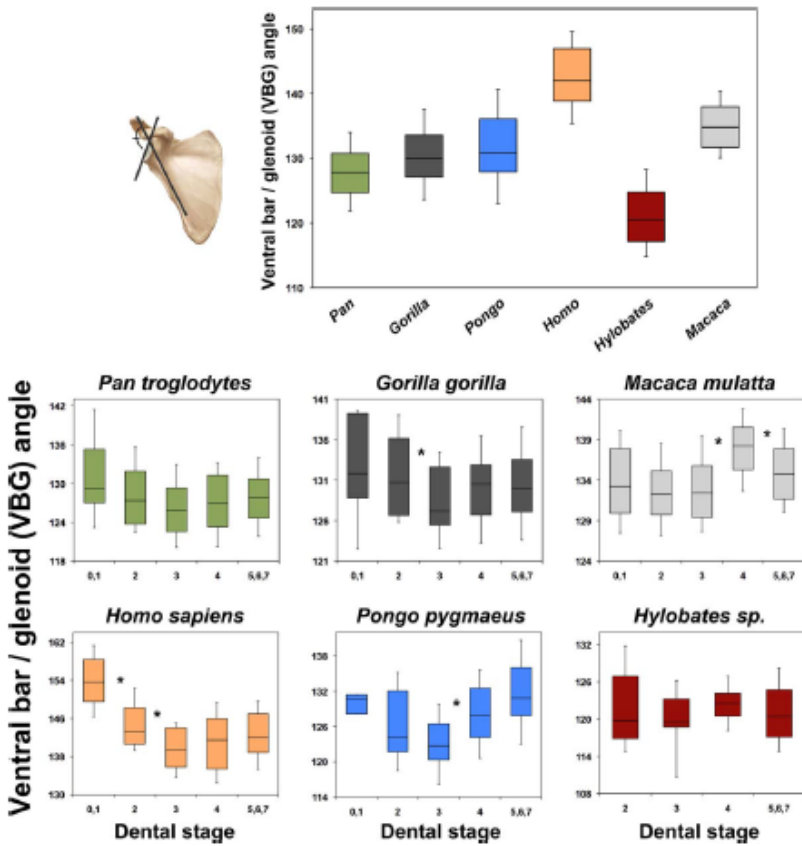


Fig. 5. Ventral bar/glenoid angle. Top chart is of adult individuals only and bottom plots show ontogenetic shifts within the six taxa. Asterisks represent a significant difference between two stages ($\alpha \leq 0.05$; see also Table 8). [Color figure can be viewed in the online issue, which is available at wileyonlinelibrary.com.]

Fig. 64. Angle barre ventral/cavité glénoïde. Image et légende tirée de GREEN D., 2013. Ontogeny of the Hominoid Scapula. The Influence of Locomotion on Morphology, *American Journal of Physical Anthropology*, 152, p. 247.

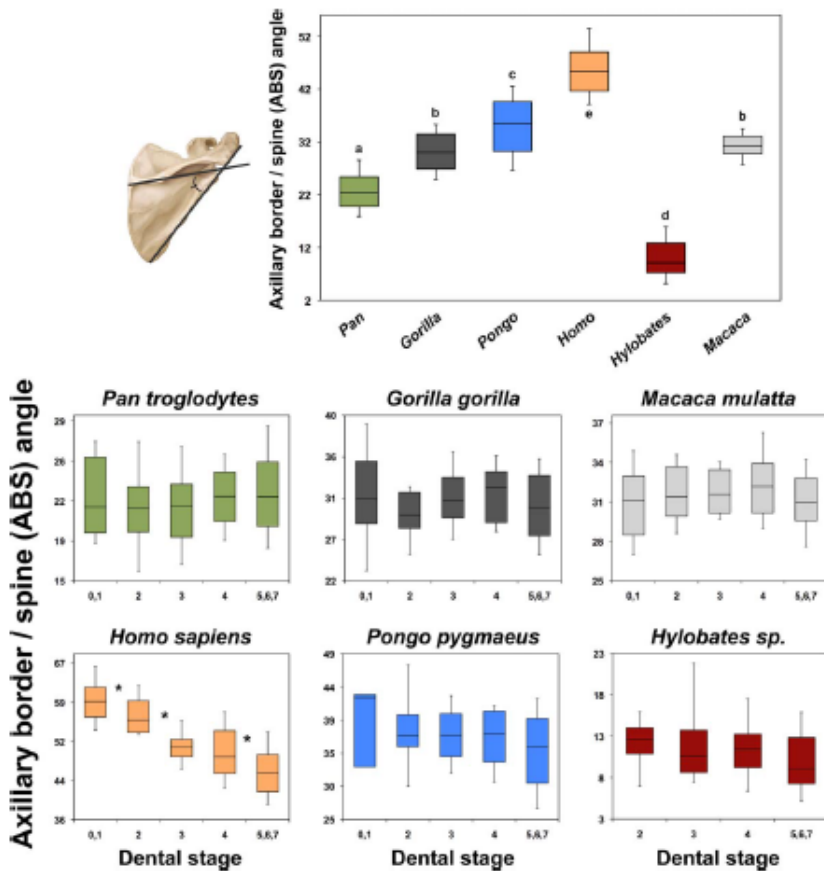


Fig. 6. Axillary border/spine angle. Top chart is of adult individuals only and bottom plots show ontogenetic shifts within the six taxa. Asterisks represent a significant difference between two stages ($\alpha \leq 0.05$; see also Table 9). [Color figure can be viewed in the online issue, which is available at wileyonlinelibrary.com.]

Fig. 65. Angle entre le bord axillaire et l'angle épineux. Image et légende tirée de GREEN D., 2013. Ontogeny of the Hominoid Scapula. The Influence of Locomotion on Morphology, *American Journal of Physical Anthropology*, 152, p. 248.

TABLE 9. Scapular spine and superior border characteristics for each age-stage within species; angle or ratio value (SD)

	Scapular spine and superior border characteristics				
	Stages 0,1	Stage 2	Stage 3	Stage 4	Stages 5-7
Medial border/spine (MBS) angle (°)					
<i>Pan troglodytes</i>	125.5 (3.2)	126.7 (4.7)	128.2 (4.3)	127.4 (3.9)	127.9 (4.8) ^a
<i>Gorilla gorilla</i>	110.6 (5.4)	114.1 (5.7)	112.0 (4.2)	112.3 (4.0)	115.5 (5.3) ^b
<i>Pongo pygmaeus</i>	91.5 (8.9)	99.2 (7.5)	99.7 (4.2)	101.0 (6.0)	105.9 (7.0) ^c
<i>Hylobates</i> sp.	—	130.9 (4.3)	132.3 (7.0)	133.6 (5.4)	137.3 (5.3) ^c
<i>Homo sapiens</i>	78.2 (6.0)	83.5 (5.7)	89.1 (3.7)	92.3 (5.6)	96.3 (5.0) ^c
<i>Macaca mulatta</i>	103.5 (5.2)	104.3 (4.5)	105.7 (3.4)	103.2 (4.5)	105.8 (4.0) ^c
Axillary border/spine (ABS) angle (°)	Stages 0,1	Stage 2	Stage 3	Stage 4	Stages 5-7
<i>Pan troglodytes</i>	22.3 (3.6)	21.5 (3.6)	21.3 (3.8)	22.4 (3.1)	22.8 (4.3) ^a
<i>Gorilla gorilla</i>	31.1 (5.2)	29.5 (3.8)	30.8 (3.5)	31.3 (3.4)	30.1 (4.2) ^b
<i>Pongo pygmaeus</i>	39.5 (5.9)	37.6 (5.3)	37.5 (4.2)	36.6 (5.4)	35.0 (5.9) ^c
<i>Hylobates</i> sp.	—	12.4 (2.7)	12.2 (5.1)	11.3 (4.0)	10.1 (4.2) ^c
<i>Homo sapiens</i>	59.7 (4.8)	57.0 (5.0)	50.6 (3.4)	49.8 (6.6)	45.6 (5.3) ^c
<i>Macaca mulatta</i>	31.2 (2.9)	31.8 (2.5)	31.9 (1.9)	32.5 (2.9)	31.3 (2.9) ^c
Spine length/glenoid size	Stages 0,1	Stage 2	Stage 3	Stage 4	Stages 5-7
<i>Pan troglodytes</i>	4.24 (0.3)	4.37 (0.4)	4.61 (0.4)	4.62 (0.4)	4.96 (0.3) ^a
<i>Gorilla gorilla</i>	4.52 (0.3)	4.46 (0.3)	4.45 (0.3)	4.49 (0.3)	4.92 (0.3) ^c
<i>Pongo pygmaeus</i>	3.71 (0.5)	3.97 (0.3)	3.97 (0.3)	4.06 (0.5)	4.16 (0.4) ^c
<i>Hylobates</i> sp.	—	5.30 (0.4)	5.68 (0.7)	5.81 (0.6)	6.50 (0.6) ^c
<i>Homo sapiens</i>	3.85 (0.3)	3.78 (0.3)	3.96 (0.2)	4.20 (0.4)	4.39 (0.3) ^c
<i>Macaca mulatta</i>	5.51 (0.4)	5.85 (0.3)	5.86 (0.2)	5.79 (0.2)	6.19 (0.3) ^c
Spine length/total length	Stages 0,1	Stage 2	Stage 3	Stage 4	Stages 5-7
<i>Pan troglodytes</i>	1.16 (0.03)	1.17 (0.03)	1.19 (0.04)	1.21 (0.04)	1.25 (0.04) ^a
<i>Gorilla gorilla</i>	1.14 (0.04)	1.15 (0.04)	1.16 (0.04)	1.18 (0.04)	1.22 (0.05) ^c
<i>Pongo pygmaeus</i>	1.11 (0.1)	1.18 (0.1)	1.21 (0.04)	1.21 (0.04)	1.20 (0.06) ^c
<i>Hylobates</i> sp.	—	1.14 (0.04)	1.17 (0.04)	1.18 (0.04)	1.22 (0.03) ^c
<i>Homo sapiens</i>	1.15 (0.04)	1.21 (0.04)	1.22 (0.03)	1.24 (0.05)	1.25 (0.04) ^a
<i>Macaca mulatta</i>	1.10 (0.04)	1.12 (0.03)	1.12 (0.04)	1.06 (0.02)	1.07 (0.03) ^c
Superior border length/glenoid size	Stages 0,1	Stage 2	Stage 3	Stage 4	Stages 5-7
<i>Pan troglodytes</i>	2.45 (0.2)	2.42 (0.2)	2.45 (0.2)	2.49 (0.2)	2.68 (0.2) ^a
<i>Gorilla gorilla</i>	2.64 (0.3)	2.67 (0.3)	2.71 (0.2)	2.74 (0.3)	2.88 (0.3) ^c
<i>Pongo pygmaeus</i>	2.79 (0.3)	3.05 (0.3)	3.15 (0.3)	3.19 (0.4)	3.23 (0.3) ^c
<i>Hylobates</i> sp.	—	3.34 (0.3)	3.48 (0.4)	3.41 (0.4)	3.63 (0.4) ^c
<i>Homo sapiens</i>	3.11 (0.4)	2.97 (0.3)	3.16 (0.2)	3.17 (0.3)	3.31 (0.3) ^c
<i>Macaca mulatta</i>	3.95 (0.4)	4.17 (0.3)	4.12 (0.2)	4.11 (0.3)	4.31 (0.3) ^c
Superior border length/total length	Stages 0,1	Stage 2	Stage 3	Stage 4	Stages 5-7
<i>Pan troglodytes</i>	0.68 (0.1)	0.65 (0.1)	0.63 (0.05)	0.65 (0.1)	0.68 (0.1) ^a
<i>Gorilla gorilla</i>	0.66 (0.1)	0.69 (0.1)	0.71 (0.1)	0.72 (0.05)	0.72 (0.1) ^c
<i>Pongo pygmaeus</i>	0.84 (0.04)	0.91 (0.1)	0.96 (0.1)	0.98 (0.05)	0.93 (0.1) ^c
<i>Hylobates</i> sp.	—	0.72 (0.04)	0.72 (0.05)	0.69 (0.05)	0.68 (0.1) ^a
<i>Homo sapiens</i>	0.92 (0.1)	0.94 (0.1)	0.98 (0.1)	0.93 (0.1)	0.95 (0.1) ^c
<i>Macaca mulatta</i>	0.78 (0.05)	0.80 (0.04)	0.79 (0.04)	0.75 (0.04)	0.74 (0.04) ^b

Tableau 9. Caractérisation de l'épine scapulaire et du bord supérieure pour chaque stade parmi les espèces, angle ou valeurs de ratio (SD). Tableau et légende tirés de GREEN D., 2013. Ontogeny of the Hominoid Scapula. The Influence of Locomotion on Morphology, *American Journal of Physical Anthropology*, 152, p. 249.

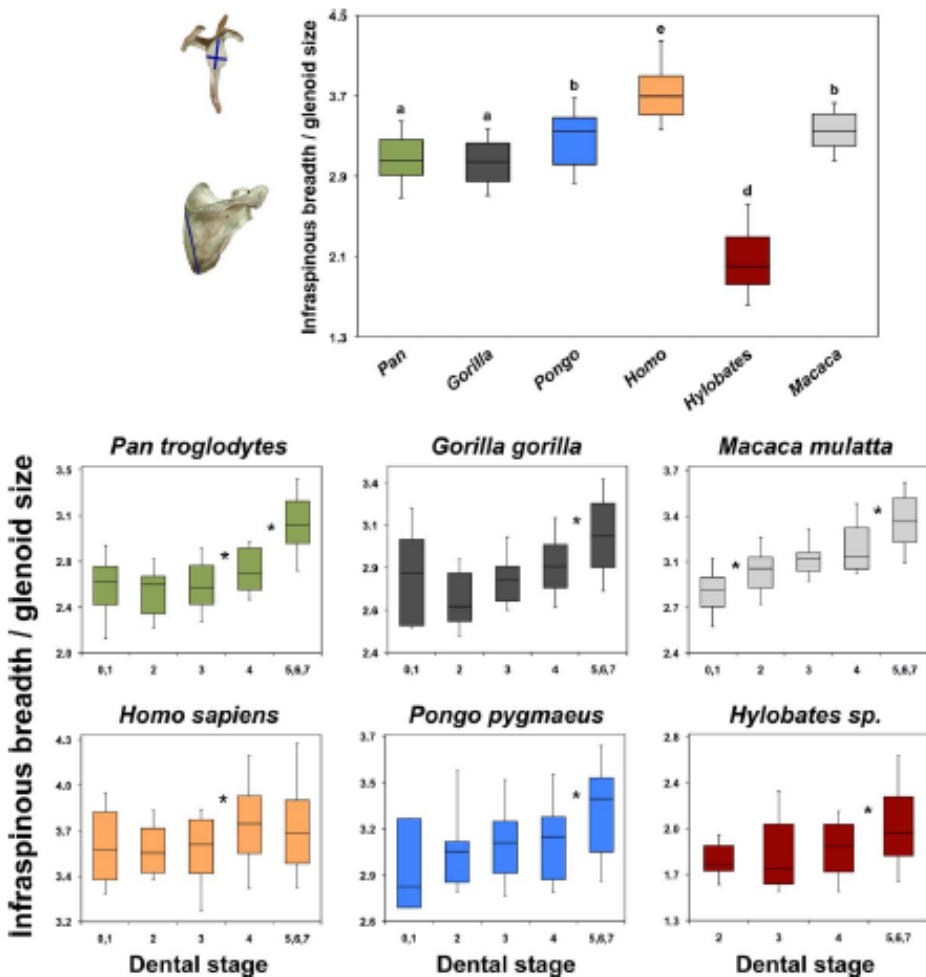


Fig. 7. Infraspinous breadth/glenoid size. Top chart is of adult individuals only and bottom plots show ontogenetic shifts within the six taxa. Asterisks represent a significant difference between two stages ($\alpha \leq 0.05$; see also Table 10). [Color figure can be viewed in the online issue, which is available at wileyonlinelibrary.com.]

Fig. 66. Ratio de taille entre la largeur de la fosse infra – épineuse et de la cavité glénoïde. Image et légende tirées de GREEN D., 2013. Ontogeny of the Hominoid Scapula. The Influence of Locomotion on Morphology, *American Journal of Physical Anthropology*, 152, p. 250.

TABLE 10. Infraspinous fossa shape characteristics for each age-stage within species; ratio value (SD)

	Infraspinous fossa shape characteristics				
	Stages 0,1	Stage 2	Stage 3	Stage 4	Stages 5-7
Breadth/glenoid size					
<i>Pan troglodytes</i>	2.55 (0.2)	2.49 (0.2)	2.55 (0.2)	2.70 (0.2)	3.07 (0.3)^a
<i>Gorilla gorilla</i>	2.79 (0.3)	2.65 (0.2)	2.78 (0.2)	2.86 (0.2)	3.05 (0.3)^a
<i>Pongo pygmaeus</i>	2.90 (0.3)	3.02 (0.2)	3.07 (0.2)	3.10 (0.3)	3.28 (0.3)^b
<i>Hylobates</i> sp.	—	1.79 (0.1)	1.86 (0.3)	1.90 (0.3)	2.08 (0.4)^d
<i>Homo sapiens</i>	3.63 (0.3)	3.62 (0.2)	3.60 (0.2)	3.77 (0.3)	3.72 (0.3)^c
<i>Macaca mulatta</i>	2.86 (0.2)	2.99 (0.2)	3.08 (0.1)	3.17 (0.2)	3.36 (0.2)^b
Length/glenoid size	Stages 0,1	Stage 2	Stage 3	Stage 4	Stages 5-7
<i>Pan troglodytes</i>	4.42 (0.2)	4.50 (0.3)	4.68 (0.3)	4.79 (0.3)	5.30 (0.3)^a
<i>Gorilla gorilla</i>	4.03 (0.2)	4.05 (0.3)	4.15 (0.2)	4.24 (0.3)	4.66 (0.4)^b
<i>Pongo pygmaeus</i>	3.51 (0.4)	3.96 (0.2)	4.07 (0.3)	4.15 (0.3)	4.60 (0.4)^{ab}
<i>Hylobates</i> sp.	—	4.34 (0.2)	4.61 (0.4)	4.79 (0.3)	5.53 (0.4)^c
<i>Homo sapiens</i>	3.33 (0.3)	3.61 (0.3)	3.93 (0.2)	4.20 (0.3)	4.43 (0.3)^d
<i>Macaca mulatta</i>	4.74 (0.3)	5.00 (0.3)	5.14 (0.2)	5.19 (0.3)	5.69 (0.3)^e
Breadth/length	Stages 0,1	Stage 2	Stage 3	Stage 4	Stages 5-7
<i>Pan troglodytes</i>	0.58 (0.05)	0.56 (0.04)	0.54 (0.05)	0.56 (0.04)	0.58 (0.05) ^a
<i>Gorilla gorilla</i>	0.69 (0.1)	0.65 (0.1)	0.67 (0.05)	0.68 (0.05)	0.66 (0.05)^b
<i>Pongo pygmaeus</i>	0.83 (0.1)	0.76 (0.1)	0.76 (0.05)	0.75 (0.1)	0.71 (0.1)^f
<i>Hylobates</i> sp.	—	0.41 (0.03)	0.41 (0.1)	0.40 (0.1)	0.38 (0.1)^d
<i>Homo sapiens</i>	1.09 (0.1)	1.01 (0.1)	0.92 (0.04)	0.90 (0.1)	0.84 (0.05)^e
<i>Macaca mulatta</i>	0.60 (0.04)	0.60 (0.04)	0.60 (0.03)	0.61 (0.04)	0.59 (0.04) ^a
Neck/glenoid size	Stages 0,1	Stage 2	Stage 3	Stage 4	Stages 5-7
<i>Pan troglodytes</i>	0.87 (0.1)	0.82 (0.1)	0.78 (0.1)	0.77 (0.1)	0.78 (0.1)^a
<i>Gorilla gorilla</i>	0.90 (0.1)	0.84 (0.1)	0.84 (0.1)	0.84 (0.1)	0.86 (0.1) ^b
<i>Pongo pygmaeus</i>	0.86 (0.03)	0.84 (0.1)	0.83 (0.1)	0.86 (0.1)	0.82 (0.1) ^{ab}
<i>Hylobates</i> sp.	—	0.84 (0.1)	0.84 (0.1)	0.87 (0.1)	0.95 (0.1)^c
<i>Homo sapiens</i>	0.94 (0.1)	0.93 (0.1)	0.94 (0.1)	0.92 (0.1)	0.90 (0.1)^d
<i>Macaca mulatta</i>	0.60 (0.1)	0.50 (0.1)	0.50 (0.1)	0.46 (0.05)	0.48 (0.05)^e

Tableau 10. Caractéristiques de la forme de la fosse infraépineuse pour chaque stade parmi les espèces ; valeurs ratio (SD). Tableau et légende tirés de GREEN D., 2013. Ontogeny of the Hominoid Scapula. The Influence of Locomotion on Morphology, *American Journal of Physical Anthropology*, 152, p. 251.

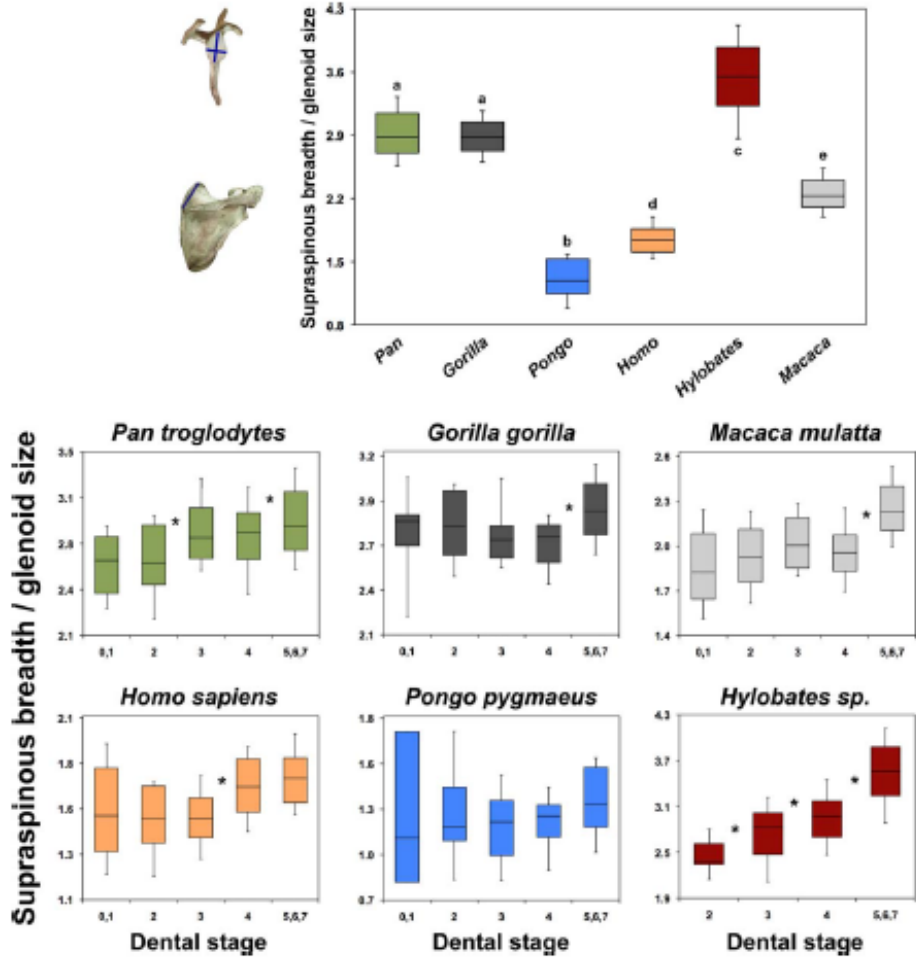


Fig. 8. Supraspinous breadth/glenoid size. Top chart is of adult individuals only and bottom plots show ontogenetic shifts within the six taxa. Asterisks represent a significant difference between two stages ($\alpha \leq 0.05$; see also Table 11). [Color figure can be viewed in the online issue, which is available at wileyonlinelibrary.com.]

Fig. 67. Ratio de taille entre la largeur de la fosse supra – épineuse et la cavité glénoïde. Image et légende tirées de GREEN D., 2013. Ontogeny of the Hominoid Scapula. The Influence of Locomotion on Morphology, *American Journal of Physical Anthropology*, 152, p. 252.

TABLE 11. Supraspinous fossa shape characteristics for each age-stage within species; ratio value (SD)

	Supraspinous fossa shape characteristics				
	Stages 0,1	Stage 2	Stage 3	Stage 4	Stages 5–7
Breadth/glenoid size					
<i>Pan troglodytes</i>	2.59 (0.2)	2.60 (0.3)	2.85 (0.3)	2.80 (0.3)	2.92 (0.3)^a
<i>Gorilla gorilla</i>	2.74 (0.3)	2.77 (0.2)	2.72 (0.2)	2.70 (0.2)	2.89 (0.2)^b
<i>Pongo pygmaeus</i>	1.21 (0.5)	1.21 (0.3)	1.14 (0.2)	1.18 (0.2)	1.32 (0.3) ^b
<i>Hylobates</i> sp.	—	2.44 (0.2)	2.69 (0.4)	2.94 (0.3)	3.51 (0.5)^c
<i>Homo sapiens</i>	1.56 (0.3)	1.51 (0.3)	1.51 (0.2)	1.70 (0.2)	1.74 (0.2)^d
<i>Macaca mulatta</i>	1.86 (0.3)	1.95 (0.2)	2.01 (0.2)	1.95 (0.2)	2.24 (0.2)^e
Length/glenoid size	Stages 0,1	Stage 2	Stage 3	Stage 4	Stages 5–7
<i>Pan troglodytes</i>	2.74 (0.3)	2.81 (0.3)	2.96 (0.3)	2.91 (0.3)	2.97 (0.2)^a
<i>Gorilla gorilla</i>	3.06 (0.3)	2.93 (0.2)	2.88 (0.2)	2.85 (0.2)	2.99 (0.2)^a
<i>Pongo pygmaeus</i>	2.52 (0.3)	2.29 (0.3)	2.22 (0.3)	2.25 (0.3)	2.36 (0.3) ^b
<i>Hylobates</i> sp.	—	3.14 (0.3)	3.50 (0.4)	3.70 (0.4)	4.21 (0.5)^c
<i>Homo sapiens</i>	2.42 (0.2)	2.22 (0.2)	2.31 (0.2)	2.35 (0.1)	2.43 (0.2)^d
<i>Macaca mulatta</i>	3.97 (0.3)	4.02 (0.2)	3.99 (0.2)	4.07 (0.2)	4.45 (0.3)^d
Breadth/length	Stages 0,1	Stage 2	Stage 3	Stage 4	Stages 5–7
<i>Pan troglodytes</i>	0.95 (0.04)	0.93 (0.05)	0.96 (0.05)	0.96 (0.05)	0.98 (0.05) ^a
<i>Gorilla gorilla</i>	0.90 (0.1)	0.95 (0.05)	0.94 (0.05)	0.95 (0.1)	0.97 (0.05) ^a
<i>Pongo pygmaeus</i>	0.47 (0.1)	0.53 (0.1)	0.52 (0.1)	0.53 (0.1)	0.56 (0.1)^b
<i>Hylobates</i> sp.	—	0.78 (0.05)	0.77 (0.05)	0.80 (0.05)	0.83 (0.1)^c
<i>Homo sapiens</i>	0.65 (0.1)	0.67 (0.1)	0.66 (0.1)	0.72 (0.1)	0.72 (0.1)^d
<i>Macaca mulatta</i>	0.47 (0.1)	0.48 (0.05)	0.50 (0.05)	0.48 (0.05)	0.50 (0.04)^b
Supraspinous breadth/infraspinous breadth	Stages 0,1	Stage 2	Stage 3	Stage 4	Stages 5–7
<i>Pan troglodytes</i>	1.03 (0.2)	1.04 (0.1)	1.13 (0.2)	1.05 (0.2)	0.96 (0.1)^a
<i>Gorilla gorilla</i>	0.99 (0.2)	1.05 (0.1)	0.98 (0.1)	0.95 (0.1)	0.95 (0.1) ^a
<i>Pongo pygmaeus</i>	0.41 (0.1)	0.41 (0.1)	0.37 (0.1)	0.38 (0.1)	0.40 (0.1) ^b
<i>Hylobates</i> sp.	—	1.37 (0.2)	1.51 (0.4)	1.59 (0.4)	1.76 (0.5)^c
<i>Homo sapiens</i>	0.43 (0.1)	0.41 (0.1)	0.42 (0.1)	0.45 (0.1)	0.47 (0.1) ^b
<i>Macaca mulatta</i>	0.65 (0.1)	0.65 (0.1)	0.65 (0.1)	0.62 (0.1)	0.67 (0.1) ^d

Tableau 11. Caractéristiques de la forme de la fosse supraépineuse pour chaque stade parmi les espèces ; valeurs de ratio (SD). Tableau et légende tirés de GREEN D., 2013. Ontogeny of the Hominoid Scapula. The Influence of Locomotion on Morphology, *American Journal of Physical Anthropology*, 152, p. 253.

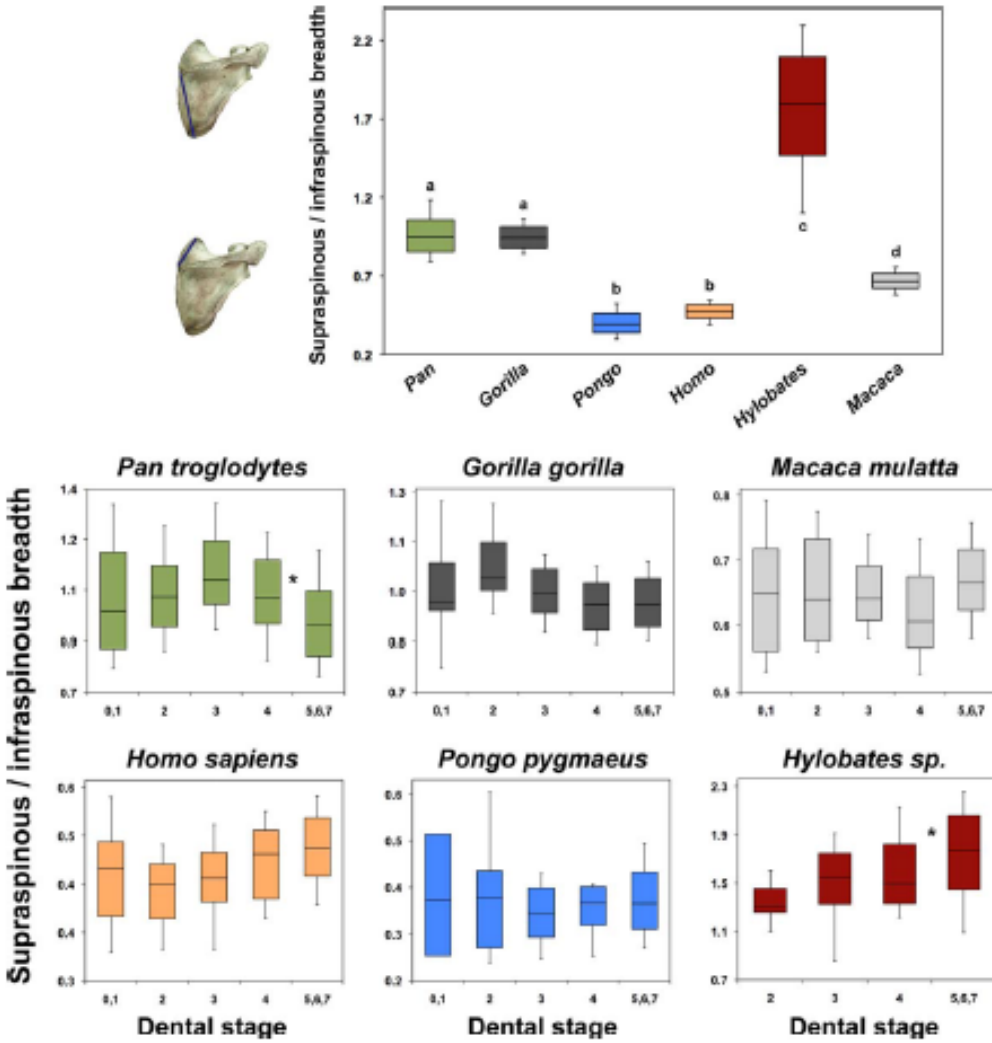


Fig. 9. Supraspinous/infraspinous breadth. Top chart is of adult individuals only and bottom plots show ontogenetic shift within the six taxa. Asterisks represent a significant difference between two stages ($\alpha \leq 0.05$; see also Table 11). [Color figure can be viewed in the online issue, which is available at wileyonlinelibrary.com.]

Fig. 68. Ratio de largeur entre les fosses infra- et supra – épineuses. Image et légende tirées de GREEN D., 2013. Ontogeny of the Hominoid Scapula. The Influence of Locomotion on Morphology, *American Journal of Physical Anthropology*, 152, p. 254.

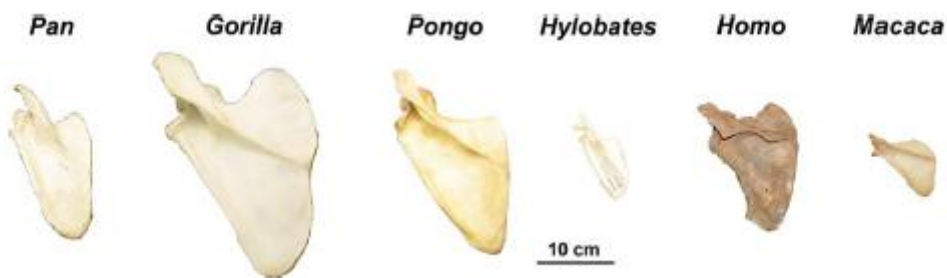


Fig. 69. Vues dorsales de scapulas adultes de six taxons représentés dans l'étude de GREEN. Image tirée de GREEN D., 2013. Ontogeny of the Hominoid Scapula. The Influence of Locomotion on Morphology, *American Journal of Physical Anthropology*, 152, p. 244.

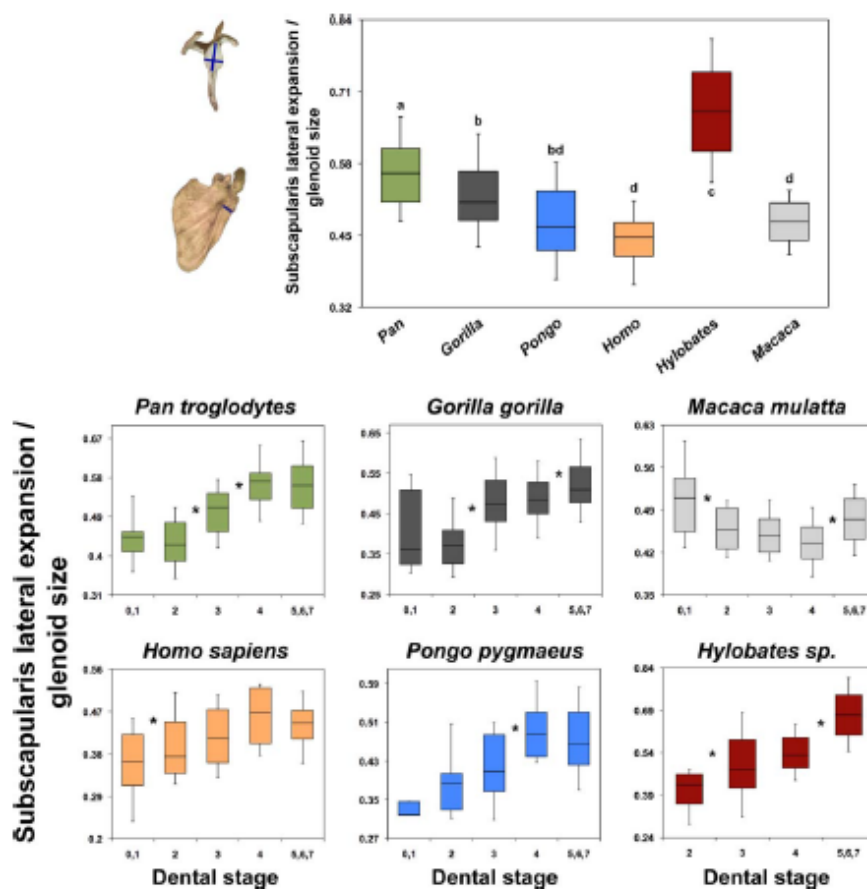


Fig. 10. Subscapularis lateral expansion/glenoid size. Top chart is of adult individuals only and bottom plots show ontogenetic shifts within the six taxa. Asterisks represent a significant difference between two stages ($\alpha \leq 0.05$; see also Table 12). [Color figure can be viewed in the online issue, which is available at wileyonlinelibrary.com.]

Fig. 70. Ratio de l'expansion latérale subscapulaire et de la taille de la cavité glénoïde. Image et légende tirées de GREEN. Image tirée de GREEN D., 2013. Ontogeny of the Hominoid Scapula. The Influence of Locomotion on Morphology, *American Journal of Physical Anthropology*, 152, p. 255.

TABLE 12. Subscapularis fossa shape characteristics for each age-stage within species; ratio value (SD)

	Subscapularis fossa shape and insertion facet characteristics				
Lateral expansion of fossa/glenoid size	Stages 0,1	Stage 2	Stage 3	Stage 4	Stages 5–7
Pan troglodytes	0.44 (0.05)	0.43 (0.1)	<u>0.50 (0.1)</u>	<u>0.56 (0.1)</u>	<u>0.56 (0.1)</u> ^a
Gorilla gorilla	0.41 (0.1)	0.38 (0.1)	<u>0.48 (0.1)</u>	<u>0.48 (0.1)</u>	<u>0.52 (0.1)</u> ^b
Pongo pygmaeus	0.33 (0.02)	0.38 (0.1)	0.42 (0.1)	<u>0.50 (0.1)</u>	<u>0.47 (0.1)</u> ^{bd}
Hylobates sp.	–	0.41 (0.1)	<u>0.49 (0.1)</u>	<u>0.54 (0.1)</u>	<u>0.68 (0.1)</u> ^c
Homo sapiens	0.36 (0.1)	<u>0.40 (0.1)</u>	0.42 (0.1)	<u>0.45 (0.1)</u>	0.44 (0.1) ^d
Macaca mulatta	0.51 (0.1)	<u>0.46 (0.04)</u>	0.45 (0.04)	<u>0.44 (0.04)</u>	<u>0.47 (0.05)</u> ^d
Insertion facet height/glenoid size	–	–	Stages 2, 3	Stage 4	Stages 5–7
Pan troglodytes	–	–	0.81 (0.1)	<u>0.77 (0.1)</u>	<u>0.84 (0.1)</u> ^a
Gorilla gorilla	–	–	0.80 (0.1)	0.76 (0.1)	<u>0.80 (0.1)</u> ^b
Pongo pygmaeus	–	–	0.74 (0.1)	0.71 (0.1)	0.70 (0.1) ^c
Hylobates sp.	–	–	0.83 (0.1)	0.82 (0.07)	0.84 (0.1) ^a
Homo sapiens	–	–	0.60 (0.1)	0.67 (0.1)	<u>0.71 (0.1)</u> ^c
Macaca mulatta	–	–	0.72 (0.05)	0.75 (0.03)	<u>0.77 (0.04)</u> ^b
Insertion facet width/glenoid size	–	–	Stages 2, 3	Stage 4	Stages 5–7
Pan troglodytes	–	–	0.44 (0.1)	0.42 (0.04)	0.43 (0.05) ^{ac}
Gorilla gorilla	–	–	0.42 (0.05)	<u>0.38 (0.05)</u>	0.40 (0.05) ^b
Pongo pygmaeus	–	–	0.46 (0.1)	0.46 (0.1)	0.43 (0.1) ^{ac}
Hylobates sp.	–	–	0.41 (0.1)	0.41 (0.05)	<u>0.44 (0.04)</u> ^c
Homo sapiens	–	–	0.34 (0.04)	<u>0.41 (0.04)</u>	<u>0.42 (0.05)</u> ^{ab}
Macaca mulatta	–	–	0.47 (0.05)	<u>0.42 (0.04)</u>	<u>0.45 (0.03)</u> ^c
Insertion facet height/width	–	–	Stages 2, 3	Stage 4	Stages 5–7
Pan troglodytes	–	–	1.87 (0.2)	1.84 (0.1)	<u>1.95 (0.2)</u> ^{abd}
Gorilla gorilla	–	–	1.93 (0.2)	2.01 (0.2)	1.99 (0.3) ^b
Pongo pygmaeus	–	–	1.60 (0.1)	1.58 (0.1)	1.65 (0.3) ^c
Hylobates sp.	–	–	2.04 (0.2)	1.98 (0.2)	<u>1.91 (0.2)</u> ^d
Homo sapiens	–	–	1.77 (0.2)	1.61 (0.2)	<u>1.70 (0.2)</u> ^c
Macaca mulatta	–	–	1.56 (0.1)	<u>1.79 (0.2)</u>	1.73 (0.1) ^c

Tableau 12. Caractéristiques de la forme de la fosse subscapulaire pour chaque stade parmi les espèces; valeurs de ratio (SD). Tableau et légende tirés de GREEN D., 2013. Ontogeny of the Hominoid Scapula. The Influence of Locomotion on Morphology, *American Journal of Physical Anthropology*, 152, p. 256.

Le cas d'*Ardipithecus ramidus*

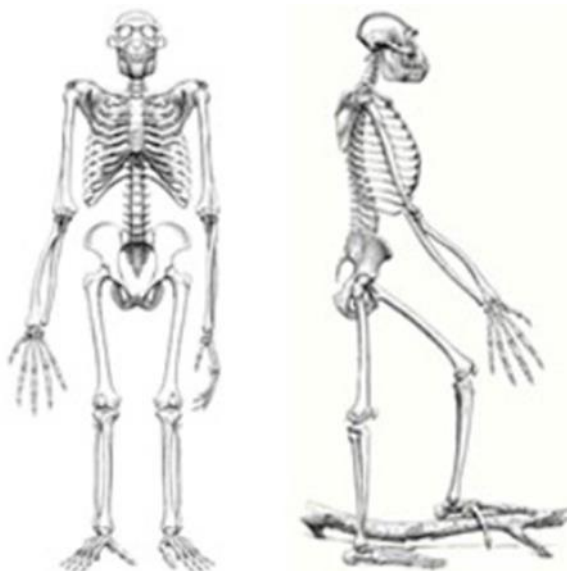


Fig. 71. *Ardipithecus ramidus*, squelette ARA – VP – 6/500, vue frontale et latérale reconstituées. Image tirée de LOVEJOY C. O., SUWA G., et WHITE T. (et al.), 2009. The Great Divides : *Ardipithecus ramidus* reveals the Postcrania of Our Last Common Ancestors, *Science*, 326, p. 101.

D.A.C. possibles entre les taxons humains

Table 6

Comparison of linear atlas measurements (mm) between the SH specimens, Neandertals, and fossil and recent *H. sapiens*

	Sima de los Huesos			Neandertals ¹			Burgos males			H-T males	
	n	Mean	SD	n	Mean	SD	n	Mean	SD	Mean	SD
MDvD	2	47.8	0.5	2	50.9	3.3	35	44.8	2.8	46.6	3.3
MTRD	1	80.0					32	78.3	3.9	78.1	5.3
STrD	3	49.6	2.0	5	49.1	2.6	35	48.6	2.4	50.0	3.6
ITrD	3	49.1	1.1	5	47.5	2.0	36	45.5	2.5	46.4	2.7
M10	3	33.5	1.2	3	35.2	1.6	35	30.2	1.9	31.5	2.4
M11	3	31.0	2.4	5	30.1	2.2	36	29.0	2.1	28.5	2.4
DTub	3	18.5	1.9	2	17.3	1.5	36	16.0	2.0		
AAH	2	11.4	1.2	3	11.0	1.9	37	11.0	1.1	11.1	8.5
AATh	2	6.4	0.2	5	5.7	1.8	38	6.3	0.8	10.1	6.6
TrDFA	2	11.8	0.0	3	13.0	1.2	38	10.1	1.4		
MHLM	2/2	21.1/21.3	2.2/1.8	1/2	19.3/20.5	—/1.5	38/36	21.5/21.6	1.9/1.8		
PAH	3	9.1	0.5	2	8.2	2.5	35	9.9	2.0		
PATh	3	7.0	1.0	2	3.6	0.6	35	7.8	2.1		
HPAG	2/3	4.2/5.2	0.1/0.3	0/2	—/5.2	—/0.1	35/33	4.2/4.0	0.9/0.6		
UAFMAD	2/2	22.9/23.4	0.3/1.8	6/6	23.6/24.1	2.2/2.2	37/36	23.7/23.5	1.8/1.7		
UAFTrD	2/2	11.6/11.5	0.4/0.0	6/5	12.2/11.4	1.4/0.7	38/37	10.4/10.5	1.2/1.0		
LAFDvD	3/2	18.6/18.2	0.8/0.3	5/5	18.1/18.2	0.9/1.4	37/37	16.3/16.2	1.3/1.2		
LAFTrD	3/2	16.0/16.0	0.1/0.8	4/5	14.3/15.6	1.2/1.6	37/38	15.5/15.8	1.0/1.2		

Cells that contain two entries are for the right and left sides (right/left).

¹ Neandertal sample (*n* = 9; MNI = 8) includes: Kebara 2 (Arensburg, 1991); Krapina 98, 99, and 100; La Chapelle-aux-Saints; La Ferrassie 1; Shanidar 2; Subalyuk 1 (Pap et al., 1996); and Tabun C1 (McCown and Keith, 1939).

Tableau 13. Comparaison des mesures de l'atlas entre les spécimens de Sima de los Huesos, les *H. neandertaliensis*, et les *H. sapiens*. Tableau et légende tirés de GOMEZ-OLIVENCIA A., CARRETERO J.M., et ARSUAGA J.L. (et al.), 2007. Metric and Morphological Study of The Upper Cervical Spine from the Sima de los Huesos Site (Sierra de Atapuerca, Burgos, Spain), *Journal of Human Evolution*, 53, p. 15.

Données sur les représentants de la lignée humaine, qui ne sont pas modernes

Species	Location	Age (Ma)
<i>Proconsul heseloni</i>	Rusinga Island, Kenya	17.9–17.0
<i>Proconsul nyerzae</i>	Mfangano, Kenya	17.9
<i>Morotopithecus bishopi</i>	Moroto, Uganda	20.6–15.0
<i>Pierolapithecus catalaunicus</i>	Barcelona, Spain	13.0–12.5
<i>Nachoapithecus kerioi</i>	Nakola, Kenya	15.0–14.0
<i>Kenya pithecius/Equatorius africanus</i>	Maboko Island and Tugen Hills, Kenya	16.0–14.5
<i>Kenya pithecius wickeri</i>	Fort Ternan, Kenya	14.0–114.5
<i>Hispanopithecus (Dryopithecus) laietanus</i>	Can Ullabateres, Spain	9.5
<i>Paidopithecus rhenanus</i>	Eppelsheim, Germany	
<i>Griphopithecus darwini</i>	Devinska Nova Ves, Slovakia	16.0–14.0
<i>Austriacopithecus/Griphopithecus</i>	Klein Hadendorf, Austria	14.5–14.0
<i>Dryopithecus brancoi</i>	Rudabanya, Hungary	10.0
<i>Sivapithecus</i>	Siwaliks, Pakistan	11.0–9.0
<i>Oreopithecus bambolii</i>	Tuscany and Sardinia, Italy	9.0–7.0
<i>Sahelanthropus tchadensis</i>	Toros, Chad	7.0–6.0
<i>Orrorin tugenensis</i>	Tugen Hills, Kenya	6.2–5.6
<i>Ardipithecus kadabba</i>	Middle Awash, Ethiopia	5.8–5.2
<i>Ardipithecus ramidus</i>	Aramis, Middle Awash, Ethiopia	4.4–3.9
<i>Australopithecus anamensis</i>	Allia Bay and Kanapoi, Kenya	4.2–3.9
<i>Australopithecus afarensis</i>	Asa Issie, Ethiopia	4.2–4.1
<i>Australopithecus incertae sedis cf. afarensis</i>	Laetoli, Tanzania	3.6
	Hadar, Ethiopia	3.4–3.0
	Maka, Middle Awash, Ethiopia	3.5
	Allia Bay, Kenya	3.9
	South Turkwel, Kenya	3.6–3.2
<i>Australopithecus incertae sedis</i>	Bouri Hata, Middle Awash, Ethiopia	2.5
<i>Australopithecus incertae sedis cf. africanus</i>	Omo Shungura, Ethiopia	2.4–2.2
<i>Australopithecus africanus</i>	Sterkfontein Member 2, South Africa	3.5
<i>Paranthropus robustus</i>	Sterkfontein Member 1 and 4, S Africa	3.0–2.4
	Swartkrans Member 1, S Africa	1.9–1.4
	Kromdraai, S Africa	1.8
<i>Paranthropus boisei</i>	Koobi Fora, Kenya	2.5–1.3
	Olduvai, Tanzania	2.6–1.4
<i>Homo incertae sedis</i>	East Turkana, Kenya	c. 2.4–1.6
<i>Homo habilis incertae sedis cf Paranthropus</i>	Olduvai Bed I, Tanzania	1.9–1.6
<i>Homo habilis</i>	Olduvai Bed I, Tanzania	1.9–1.6
	East Turkana, Kenya	
<i>Homo rudolfensis</i>	East Turkana, Kenya	2.4–1.6
<i>Homo erectus</i>	East Turkana, Kenya	1.6
	West Turkana, Kenya	
<i>Homo antecessor</i>	Dmanisi, Georgia	1.75
<i>Homo heidelbergensis</i>	Perning, Java	1.81
	Gran Dolina, Sierra de Atapuerca, Spain	c. 0.8
	Bodo and Broken Hill, Africa	0.6–0.3
<i>Homo neanderthalensis</i>	Mauer, Boxgrove, Arago, Steinheim and Swanscombe, Europe	0.25–0.5
<i>Homo sapiens</i>		c. 0.3–
		c. 0.3–

Tableau 14. Tableau des espèces humaines découvertes jusqu'en 2008, de *Proconsul heseloni* à *Homo sapiens*. Tableau tiré de CROMPTON R., VEREECKE E., et THORPE S., 2008. Locomotion and posture from the common hominoid ancestor to fully modern hominins, with special reference to the last common panin/hominin ancestor, *Journal of Anatomy*, 212, p. 512.

Australopithèques

Australopithecus afarensis

Assigned Accession Number	Element
KSD-VP-1/1a	right ulna
KSD-VP-1/1b	right humerus
KSD-VP-1/1c	left distal femur
KSD-VP-1/1d	right innominate
KSD-VP-1/1e	left tibia
KSD-VP-1/1f	left clavicle
KSD-VP-1/1g	right scapula
KSD-VP-1/1h	cervical vertebra
KSD-VP-1/1i	cervical vertebra
KSD-VP-1/1j	cervical vertebra
KSD-VP-1/1k	cervical vertebra
KSD-VP-1/1l	cervical vertebra
KSD-VP-1/1m	vertebral body
KSD-VP-1/1n	left second rib
KSD-VP-1/1o	right lower rib (7th or 8th)
KSD-VP-1/1p	right lower rib (8th or 9th)
KSD-VP-1/1q	right upper rib (5th, 6th or 7th)
KSD-VP-1/1r	left 11 th rib
KSD-VP-1/1s	middle rib fragment
KSD-VP-1/1t	superior sacral body and ala
KSD-VP-1/1u	Posterior sacral spine fragment
KSD-VP-1/1v	Sacral spine fragment
KSD-VP-1/1w	coccygeal body?
KSD-VP-1/1x	R. Spinous process with Sup. and Inf. facets
KSD-VP-1/1y	R. Spinous process and Sup. with Inf. facets
KSD-VP-1/1z	R. Spinous process and Sup. with Inf. facets
KSD-VP-1/1aa	L. Spinous process and Sup. with Inf. facets
KSD-VP-1/1ab	L. Spinous process and Sup. with Inf. facets
KSD-VP-1/1ac	L. Spinous process and Sup. with Inf. facets
KSD-VP-1/1ad	vertebral body fragment
KSD-VP-1/1ae	left superior facet of vertebra
KSD-VP-1/1af	left superior facet of vertebra

Tableau 15. Inventaire des découvertes de Woranso-Mille, Éthiopie. Tableau tiré de HAILE-SELASSIE Y., LATIMER B. M., et ALENE M. (et al.), 2010. An early *Australopithecus afarensis* postcranium from Woranso-Mille, Ethiopia, *Proceedings of the National Academy of Sciences of the United States of America*, 107, annexe, p. 33.

Figure S23. Definitions of Angles Used to Evaluate

Geometry of Hominoid

Scapulas. A human scapula is shown here with the five angles used in the PCA described in the text. CD-EF = axillary-vertebral angle; GH-AB = glenoid-spinal angle; AB-IJ = bar-glenoid angle; AB-CD = glenoid-axillary angle; GH-CD = spinal-axillary angle. For discussion see text.

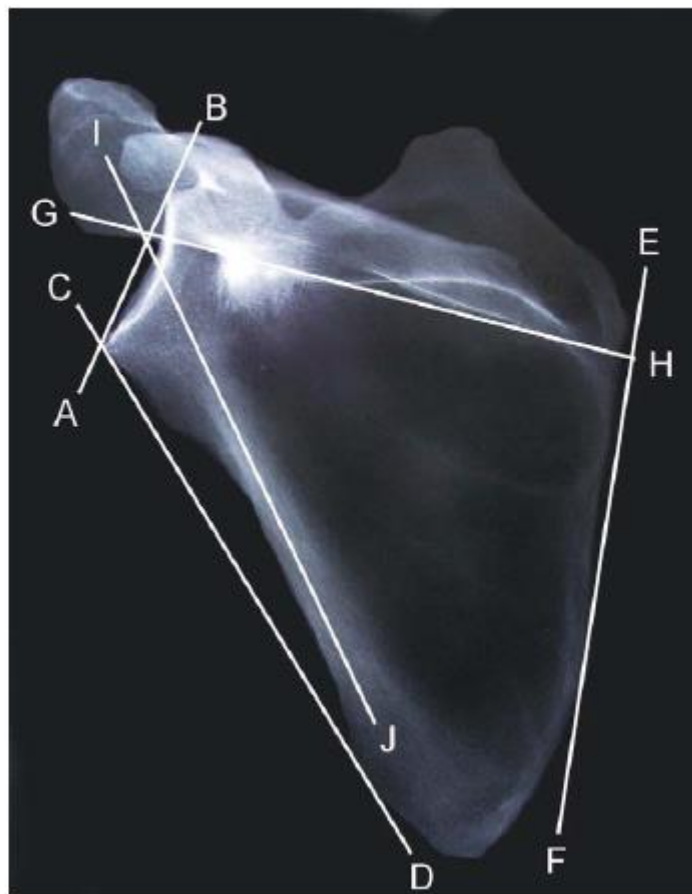


Fig. 72. Définitions des angles utilisés pour évoluer la géométrie des scapulas hominoïdes.

Photo et légende tirées de HAILE-SELASSIE Y., LATIMER B. M., et ALENE M. (et al.), 2010. An early Australopithecus afarensis postcranium from Woranso-Mille, Ethiopia, *Proceedings of the National Academy of Sciences of the United States of America*, 107, annexe, p. 25.

Table 1. Angular data for the scapular angles in hominoids*

Taxon	N	Axillary-vertebral	Glenoid-spine	Axillary-spine	Axillary-glenoid	Bar-glenoid
<i>H. sapiens</i>	11	39.2 (3.0)	98.2 (5.4)	53.4 (6.5)	137.4 (5.5)	140.1 (4.4)
<i>P. troglodytes</i>	10	29.0 (8.6)	88.2 (5.3)	28.0 (4.4)	118.4 (5.2)	124.4 (6.1)
<i>G. gorilla</i>	10	31.2 (8.9)	88.9 (7.0)	29.9 (5.0)	123.4 (4.9)	129.3 (6.1)
KSD-VP-1/1	31		104	50	128	134

*For a definition of each angle, see SI Appendix, Fig. S13.

Tableau 16. Données angulaires pour les angles scapulaires des hominoïdes. Tableau tiré de HAILE-SELASSIE Y., LATIMER B. M., et ALENE M. (et al.), 2010. An early Australopithecus afarensis postcranium from Woranso-Mille, Ethiopia, *Proceedings of the National Academy of Sciences of the United States of America*, 107, p. 12123.

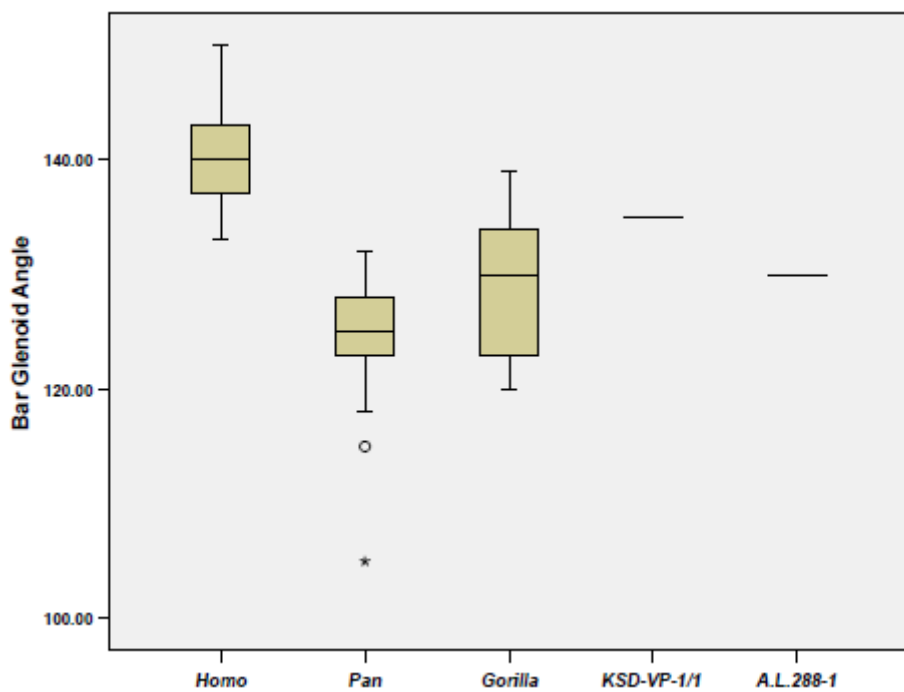


Fig. 73. Angle barre ventral/ cavité glénoïde chez KSD – VP – 1/1g et A.L. – 288 – 1, *Pan*, *Gorilla*, et *Homo*. Image tirée de HAILE-SELASSIE Y., LATIMER B. M., et ALENE M. (et al.), 2010. An early Australopithecus afarensis postcranium from Woranso-Mille, Ethiopia, *Proceedings of the National Academy of Sciences of the United States of America*, 107, annexe, p. 26.

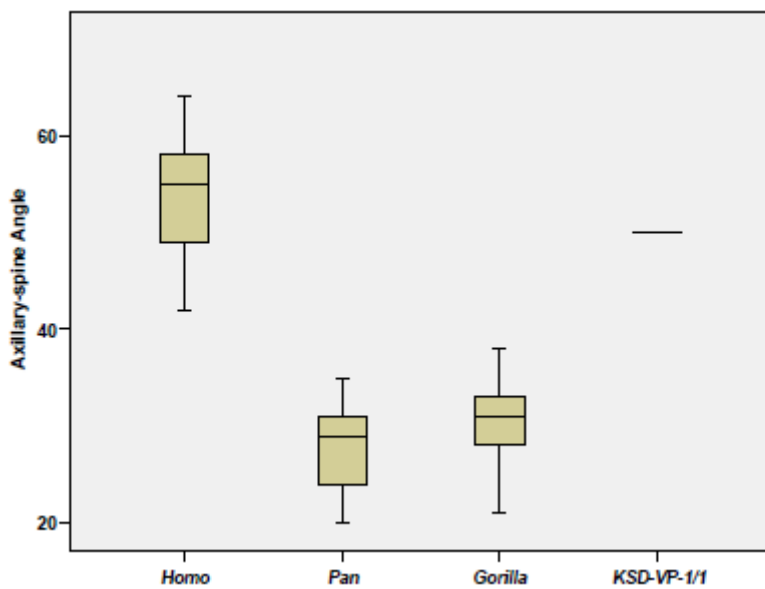


Fig. 74. Angle axillo – épineux de KSD – VP – 1/1g, *Pan*, *Gorilla* et *Homo*. Image tirée de HAILE-SELASSIE Y., LATIMER B. M., et ALENE M. (et al.), 2010. An early Australopithecus afarensis postcranium from Woranso-Mille, Ethiopia, *Proceedings of the National Academy of Sciences of the United States of America*, 107, annexe, p. 27.

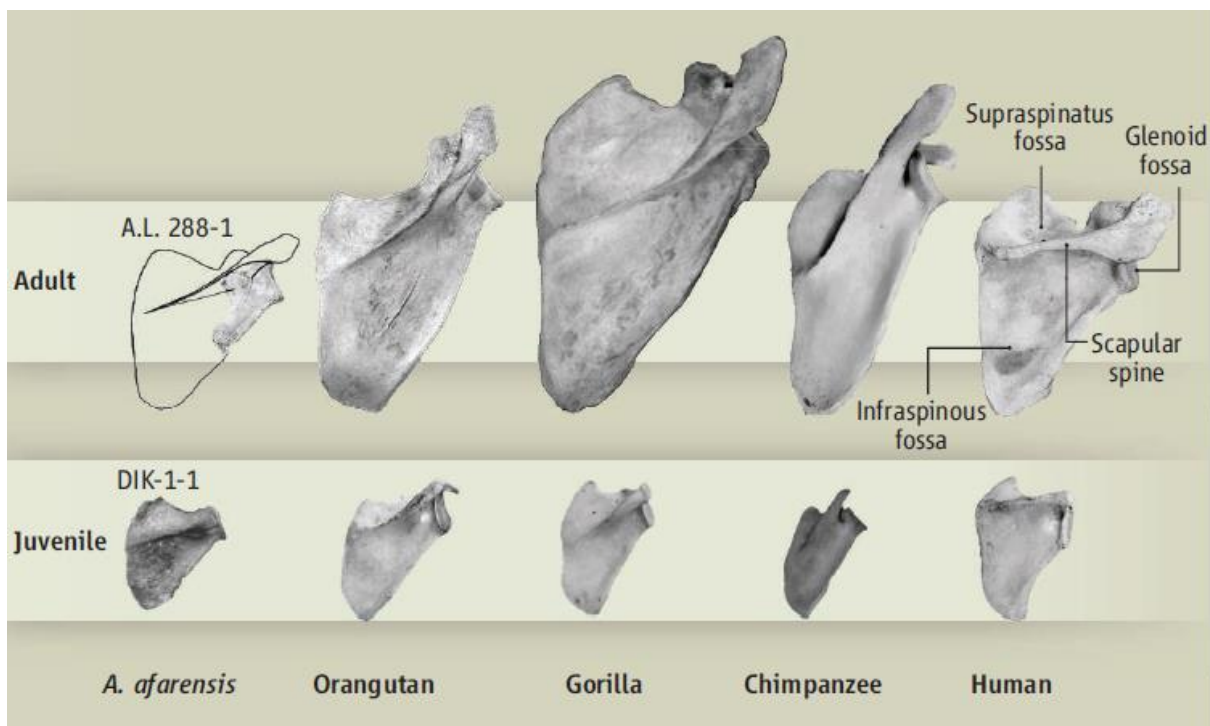


Fig. 75. Changements de croissance des scapulas des grands singes et des humains. Image tirée de LARSON S., 2012. Did Australopiths Climb Trees?, *Science*, vol. 338, p. 478. Cette image est également visible dans GREEN D.J. et ALEMSEGED Z., 2012. *Australopithecus afarensis Scapular Ontogeny, Function, and the Role of Climbing in Human Evolution*, *Science*, vol. 338, p. 515.

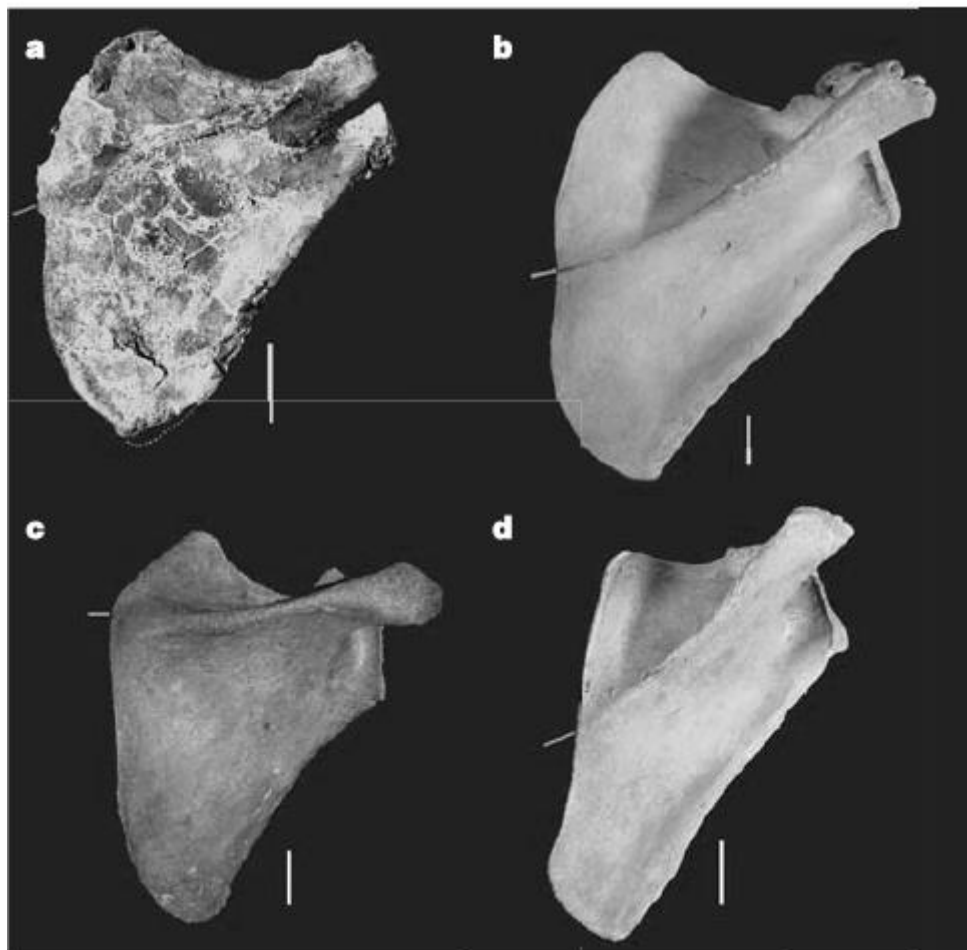


Fig. 76. Scapula de DIK – 1 – 1 (a), comparée à celles d'un gorille (b), de *Homo sapiens* (c) et d'un chimpanzé (d). Image tirée de ALEMSEGED Z., SPOOR F., et KIMBEL W. H., (et al.), 2006. A juvenile early hominin skeleton from Dikika, Ethiopi, *Nature*, 443, p. 300.

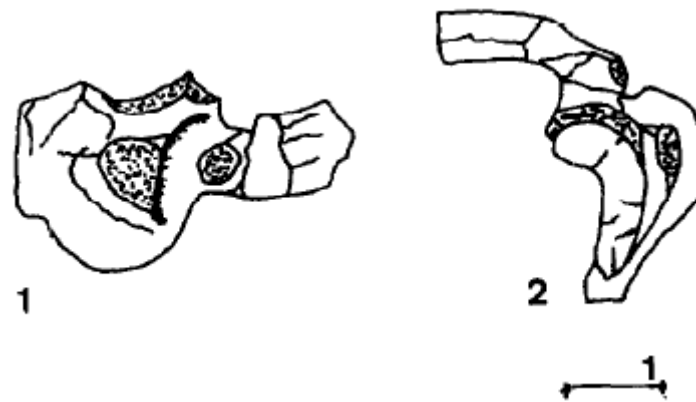


Fig. 77. Atlas AL 333 – 83, Hadar. Vue latérale gauche (1) et supérieure (2). Image tirée de GOMMERY D., 1997. Les atlas et les axis des Hominidés du Plio-Pléistocène : morphologie et systématique, *C. R. Acad. Sci. Paris, Sciences de la terre et des planètes*, vol. 325, p. 640.

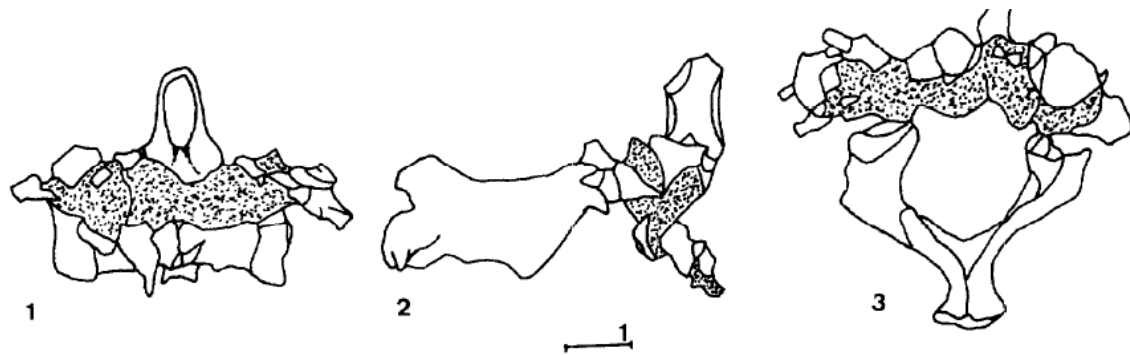


Fig. 78. Axis AL 333 – 101, Hadar. Vue ventrale (1), latérale droite (2) et supérieure (3). Image tirée de GOMMERY D., 1997. Les atlas et les axis des Hominidés du Plio-Pléistocène : morphologie et systématique, *C. R. Acad. Sci. Paris, Sciences de la terre et des planètes*, vol. 325, p. 641.

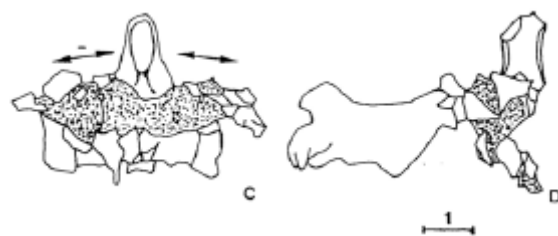


Fig. 79. Orientation et morphologie de l'axis AL 333 – 101, Hadar. Vue ventrale (C) et latérale (D). Image tirée de GOMMERY D., 2003. Evolution of the Vertebral Column in Miocene Hominoids and Plio-Pleistocene Hominids, dans ISHIDA H., TUTTLE R. et PICKFORD M. (et al.), 2003. *Human Origins and Environmental Backgrounds*, p. 36. Cette image n'est pas l'originale, elle a été modifiée par Van Oostende Florence.

Australopithecus africanus



Fig. 80. Scapula droite de STS 7, Sterkfontein. Vue dorsale. Photo tirée de VRBA E. S., 1979. A New Study of the Scapula of *Australopithecus africanus* from Sterkfontein, *American Journal of Physical Anthropology*, 51, p. 118.

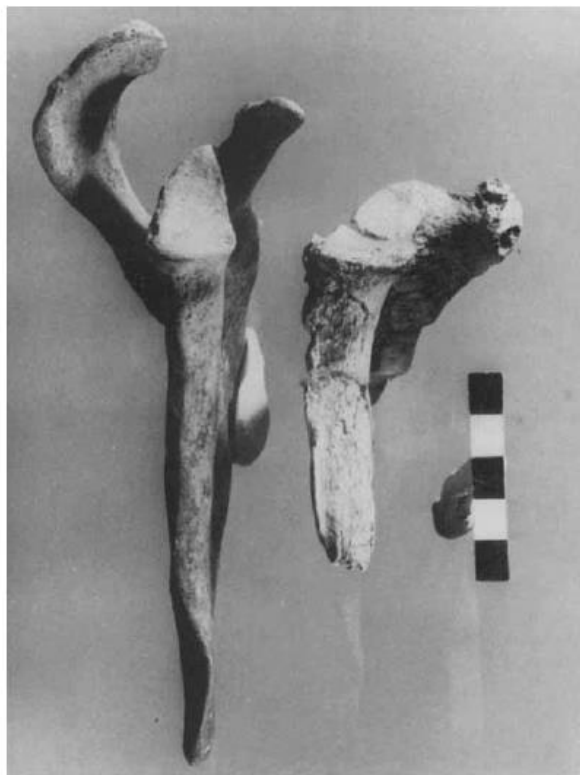


Fig. 81. Scapula droite de STS 7, Sterkfontein. Vue latérale. Photo tirée de VRBA E. S., 1979. A New Study of the Scapula of *Australopithecus africanus* from Sterkfontein, *American Journal of Physical Anthropology*, 51, p. 121.

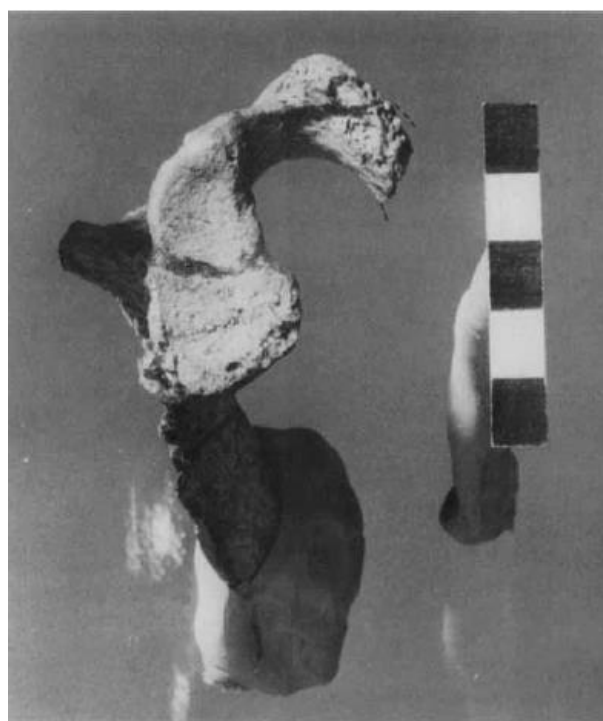


Fig. 82. Scapula gauche de STS 7, Sterkfontein. Cavité glénoïde. Photo tirée de VRBA E. S., 1979. A New Study of the Scapula of *Australopithecus africanus* from Sterkfontein, *American Journal of Physical Anthropology*, 51, p. 119.

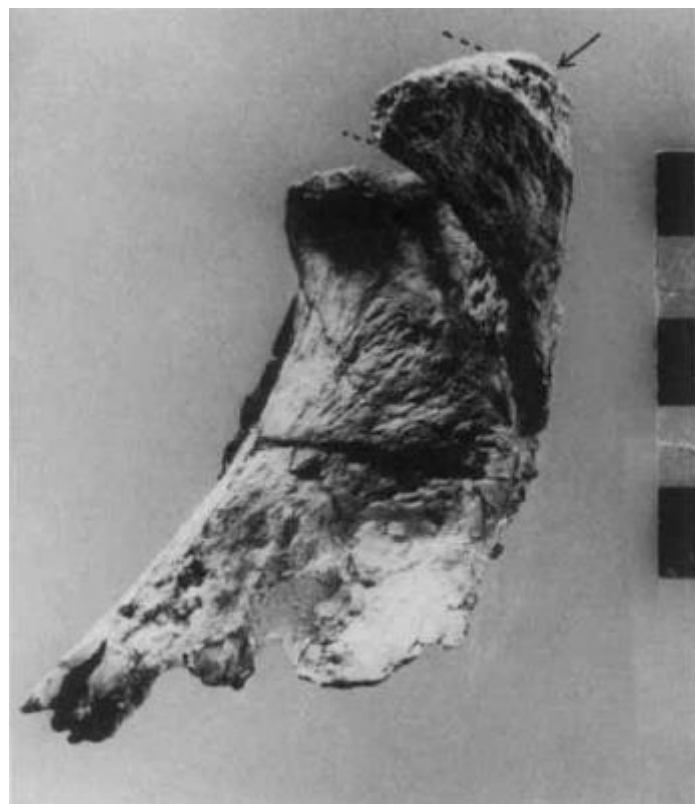


Fig. 83. Scapula gauche de STS 7, Sterkfontein. Processus coracoïde. Photo tirée de VRBA E. S., 1979. A New Study of the Scapula of *Australopithecus africanus* from Sterkfontein, *American Journal of Physical Anthropology*, 51, p. 123.

Australopithecus incertae sedis

Table 7.1 *Australopithecus* postcranial fossils from Sterkfontein Member 4

Skeletal part	Catalog number(s)	Details/notes
Partial skeleton	Sts 14	9 thoracic and 6 lumbar vertebrae, complete pelvis, proximal left femur minus head
	StW 431	4 thoracic and 5 lumbar vertebrae, partial pelvis with partial sacrum and parts of both ilia, lateral half of right clavicle shaft, lateral margin of left scapula, distal half of right humerus and proximal halves of right radius and ulna
Vertebra	Sts 73	Partial vertebra
	StW 8/41	2 thoracic and 4 lumbar vertebrae conjoined
	StW 642	Partial column of 12 thoracic and lumbar and 1 cervical vertebrae
Clavicle	StW 616	Left shaft fragment
	StW 582	Right shaft
Scapula	StW 162	Left proximal portion
	StW 366	Left spine of scapula
	StW 612	Left spine of scapula
	Sts 7	Right proximal portion

Tableau 17. Restes postcrâniaux des *Australopithecus* de Sterkfontein, Member 4. Tableau (partiel) tiré de REED K. E., FLEAGLE J. G., et LEAKY R. E. (éd.), 2013. The Paleobiology of *Australopithecus*, *Vertebrate Paleobiology and Paleoanthropology Series*, Dordrecht, p. 113.



Fig. 84. Scapula droite de StW 573, *Little Foot* (centre droit), en vue ventrale (l'arrière du crâne se situe en haut à gauche). Photo tirée de CLARKE R.J., 2008. Latest information on Sterkfontein's *Australopithecus* skeleton and a new look at *Australopithecus*, *South African Journal of Science*, 104, p. 444.

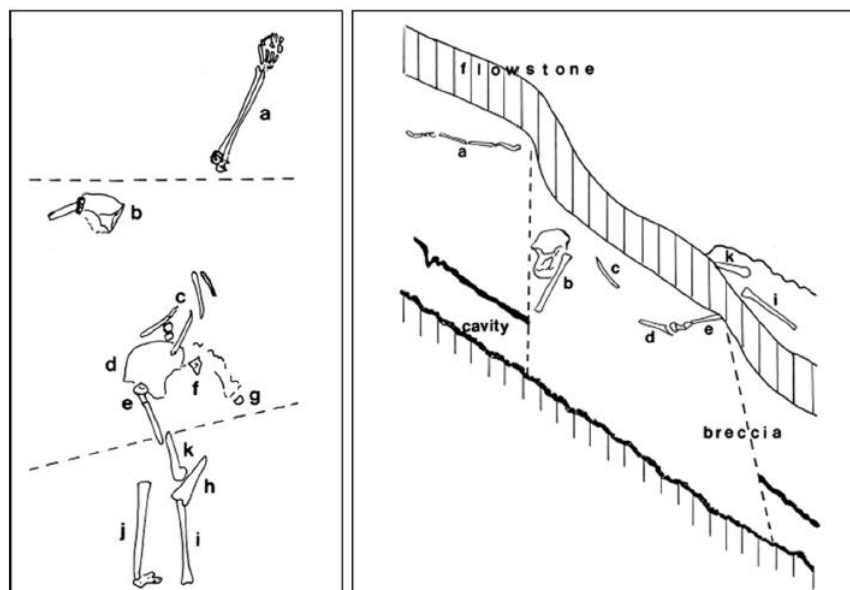


Fig. 85. Position de StW 573 au moment de la découverte. Image tirée de CLARKE R.J., 2019. Excavation, reconstruction and taphonomy of the StW 573 *Australopithecus Prometheus* skeleton form Sterkfontein Caves, South Africa, *Journal of Human Evolution*, 127, p. 49.



Fig. 86. Squelette de StW 573, en cours de nettoyage. Photo tirée de CLARKE R.J., 2019. Excavation, reconstruction and taphonomy of the StW 573 *Australopithecus Prometheus* skeleton form Sterkfontein Caves, South Africa, *Journal of Human Evolution*, 127, p. 51.



Fig. 87. Squelette de StW 573, nettoyé. Photo tirée de CLARKE R.J., 2019. Excavation, reconstruction and taphonomy of the StW 573 *Australopithecus Prometheus* skeleton from Sterkfontein Caves, South Africa, *Journal of Human Evolution*, 127, p. 52.

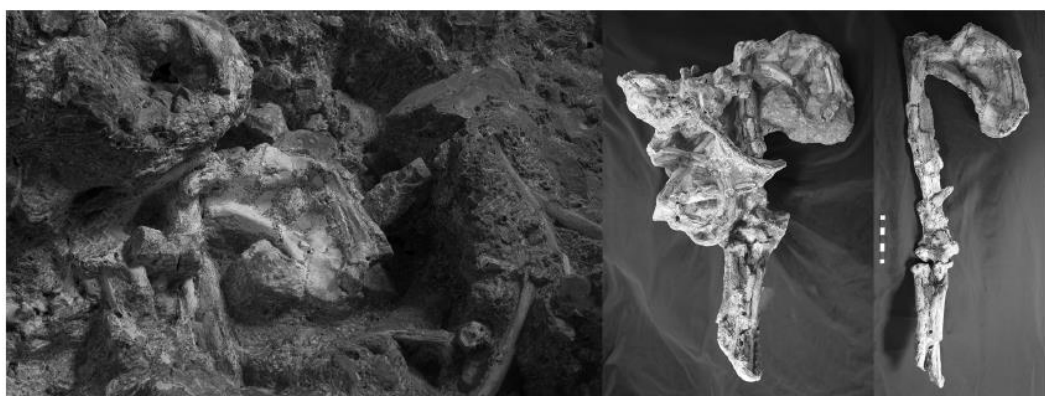


Fig. 88. Scapula droite *in situ*, toujours en articulation avec l'humérus (gauche), la scapula en nettoyage (milieu), et la scapula articulée avec l'humérus, dégagée (droite). Photos tirées de CLARKE R.J., 2019. Excavation, reconstruction and taphonomy of the StW 573 *Australopithecus Prometheus* skeleton form Sterkfontein Caves, South Africa, *Journal of Human Evolution*, 127, p. 44.

Australopithecus sediba

Measurement	Abbreviation	Description
Variables used in the first PCA (following 3)		
Supraspinous Fossa Breadth	SSFB	Superior angle to the intersection of the scapular spine and vertebral border.
Infraspinous Fossa Breadth	ISFB	Inferior angle to the intersection of the scapular spine and vertebral border.
Perpendicular Supraspinous Fossa Breadth	PSFB	Perpendicular distance from the spine to the superomedial margin of the supraspinous fossa (taken from the superoinferior midpoint of the spine).
Perpendicular Infraspinous Fossa Breadth	PIFB	Perpendicular distance from the spine to the inferolateral margin of the infraspinous fossa (taken from the superoinferior midpoint of the spine).
Scapular Length	LENGTH	Vertebral border at the spine to the superoinferior center of the glenoid fossa on the posterior rim.
Spinoacromial Length	SAL	Vertebral border at the spine to the most lateral point on the acromion process.
Scapular Breadth	BREADTH	Inferior angle to superior angle.
Glenoid-Medial Angle	GMA	Angle between line comprising scapular breadth (BREADTH) and a line through the most cranial and caudal points of the glenoid fossa.
Spinal-Medial Angle	SMA	Angle between the line comprising scapular breadth (BREADTH) and the line comprising the spinoacromial length (SAL).
Glenoid Fossa Size	GFS	Square root of (glenoid fossa maximum superoinferior length * glenoid fossa maximum dorsoventral breadth)
Variables used in the second PCA (following 6)		
Axillary-Vertebral Angle	AVA	Angle between the line from the most caudal point on the glenoid fossa to the most lateral projection of the teres major flange and the line running from the inferior angle to the point where the spine meets the vertebral border.
Glenoid-Spinal Angle	GSA	Angle between the line running through the most cranial and caudal points of the glenoid fossa and the line comprising the spinoacromial length (SAL).
Spinal-Axillary Angle	SAA	Angle between the line running from the most caudal point of the glenoid fossa to the most lateral projection of the teres major flange and the line comprising the spinoacromial length (SAL).
Glenoid-Axillary Angle	GAA	Angle between the line running from the most caudal point of the glenoid fossa to the most lateral projection of the teres major flange and the line running through the most cranial and caudal points of the glenoid fossa.

Tableau 18. Ostéométrie employée dans les PCAs scapulaires. Tableau tiré de CHURCHILL S.E., HOLLIDAY T. W., et CARLSON K.J. (et al.), 2013. The Upper Limb of *Australopithecus sediba*, *Science*, 340, p. 9. Les termes “following 3” désignent les analyses faites sur DIK – 1 – 1.

	GAA	GSA	GMA	SMA	SAA	AVA
<i>Au. sediba</i> (MH2)	123.4†	82.9	28.8	56.2	28.2	42.1
Modern <i>Homo</i> (n = 47)	137.8 4.6	102.4 3.5	7.1 9.1	70.4 3.9	52.6 3.9	45.5 3.0
<i>Pan</i> (n = 14)	119.0 4.9	76.7 3.7	43.9 7.4	38.8 6.5	17.7 3.3	32.7 3.6
<i>Gorilla</i> (n = 20)	122.4 4.3	77.8 4.3	31.5 3.4	49.4 4.2	21.4 3.8	42.9 3.1
<i>Pongo</i> (n = 8)	124.1 3.5	79.7 5.7	26.2 3.5	54.8 5.6	24.4 3.7	38.7 3.3
<i>Hylobates</i> (n = 33)	115.3 5.2	64.1 4.7	36.6 6.3	34.7 2.9	11.1 3.0	38.1 6.0

Angles as defined in table S2:
GAA: Glenoid-axillary angle.
GSA: Glenoid-spinal angle.
GMA: Glenoid-medial angle.
SMA: Spinal-medial angle.
SAA: Spinal-axillary angle.
AVA: Axillary-vertebral angle.

† Mixed-sex samples from the A.H. Schultz collection (University of Zurich).
‡ Previously (7) we reported an axilloglenoid angle of 114° for MH2. That value was based on the angle between the glenoid fossa and the proximal half of the lateral edge of the axillary border (rather than the lateral extent of the teres major origin as was used here), so as to be consistent with reported values from fragmentary australopith and early *Homo* remains.

Tableau 19. Angles scapulaires, en degré, de MH2 et des échantillons comparatifs. Tableau tiré de CHURCHILL S.E., HOLLIDAY T. W., et CARLSON K.J. (et al.), 2013. The Upper Limb of *Australopithecus sediba*, *Science*, 340, p. 10.

	LENGTH	BREADTH	Scap. Index	GFS	GF Index	SAL
<i>Au. sediba</i> (MH2)	80.0	121.9	65.6	22.4	55.6	100.2
<i>Homo</i> (n = 47)	96.8 6.5	143.6 11.1	67.6 4.7	27.9 2.4	68.3 5.2	127.6 9.1
<i>Pan</i> (n = 14)	99.6 5.6	147.4 8.4	67.6 3.3	25.9 2.1	71.2 4.7	131.7 8.5
<i>Gorilla</i> (n = 20)	151.8 20.4	219.8 33.2	69.4 4.5	38.4 5.2	62.9 5.7	199.9 25.5
<i>Pongo</i> (n = 8)	95.8 11.1	135.9 14.4	70.5 2.3	28.8 2.6	62.1 4.3	123.9 13.3
<i>Hylobates</i> (n = 33)	67.3 3.6	60.8 3.2	111.0 6.2	12.3 0.8	77.8 7.5	86.2 4.6

Table S4 continued

	SSFB	ISFB	SSFB/GFS	SSFB/ISFB	PSFB	PIFB
<i>Au. sediba</i> (MH2)	49.4	89.2	2.21	0.55	19.7	88.2
<i>Homo</i> (n = 47)	47.2 6.4	108.3 8.24	1.69 0.16	0.44 0.05	31.9 5.3	107.2 8.4
<i>Pan</i> (n = 14)	74.5 6.6	78.5 6.8	2.88 0.21	0.96 0.12	33.8 6.2	59.9 7.5
<i>Gorilla</i> (n = 20)	111.3 18.9	121.4 19.2	2.88 0.25	0.91 0.08	58.9 12.5	112.9 21.0
<i>Pongo</i> (n = 8)	39.1 9.6	102.3 7.4	1.35 0.25	0.38 0.07	25.8 7.1	93.1 11.1
<i>Hylobates</i> (n = 33)	44.6 3.6	20.2 3.2	3.62 0.33	2.27 0.46	17.3 2.5	17.0 2.7

Table S4 continued

LENGTH: Scapular length from midpoint of the dorsal margin of the glenoid cavity to the midpoint of the end of the scapular spine at the vertebral border (mm).

BREADTH: Scapular breadth from caudal-most point on inferior angle to cranial-most point on superior angle (mm).

Scap. Index: $100 \times \text{LENGTH} / \text{BREADTH}$.

GFS: Glenoid fossa size, taken as $(\text{glenoid fossa length} * \text{breadth})^{0.5}$ (3).

GF Index: Glenoid fossa index, taken as $100 * \text{glenoid fossa breadth} / \text{length}$.

SAL: Spinoacromial length (from the most lateral point on the acromion process to the midpoint of the end of the scapular spine at the vertebral border) (mm).

SSFB: Supraspinatus fossa breadth (following 3) (mm).

ISFB: Infraspinatus fossa breadth (following 3) (mm).

PSFB: Perpendicular supraspinatus fossa breadth (following 3) (mm).

PIFB: Perpendicular infraspinatus fossa breadth (following 3) (mm).

† Mixed-sex samples from the A.H. Schultz collection (University of Zurich).

Tableau 20. Dimensions scapulaires de MH2 et des échantillons comparatifs. Tableau tiré de CHURCHILL S.E., HOLLIDAY T. W., et CARLSON K.J. (et al.), 2013. The Upper Limb of *Australopithecus sediba*, *Science*, 340, p. 11.

	PC1 (62.4%)	PC2 (16.5%)	PC3 (14.2%)
SSFB	0.94389	-0.22788	0.02142
ISFB	-0.98152	-0.06581	0.13060
PSFB	0.61821	-0.54705	-0.45674
PIFB	-0.99070	-0.02843	-0.05026
LENGTH	0.90659	0.38162	-0.04063
SAL	0.91612	0.34495	-0.03522
BREADTH	-0.40333	-0.33853	0.77490
GMA	0.65131	-0.30838	0.56950
SMA	-0.87703	0.12186	-0.41099
GFS	-0.03376	0.89674	0.31230

Variables as defined in table S2. PCs 4-10 are not reported here since each accounted for $\leq 1.4\%$ of the total variance.

Tableau 21. Tableau récapitulatif des valeurs obtenues pour la première PCA, basée sur les variables linéaires et angulaires obtenues pour DIK – 1 – 1. Tableau tiré de CHURCHILL S.E., HOLLIDAY T. W., et CARLSON K.J. (et al.), 2013. The Upper Limb of *Australopithecus sediba*, *Science*, 340, p. 12.

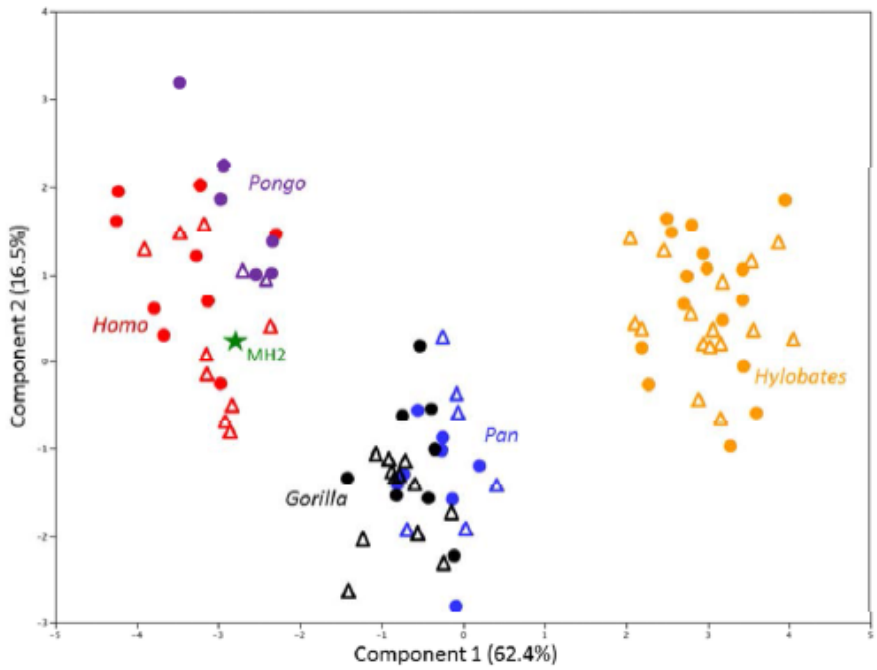


Fig. S2: PCA of 10 angles and size-adjusted linear scapular measurements using the variable set from (3). Individual scores on PC2 (accounting for 16.5% of the total variance) are plotted against scores on PC1 (62.4% of the variance); component loadings are provided in table S5. Green star: *Au. sediba* (MH2). Closed circles represent females and open triangles represent males. Red: *Homo sapiens*; purple: *Pongo pygmaeus/abelii*; black: *Gorilla gorilla*; blue: *Pan troglodytes*; orange: *Hylobates lar*.

Fig. 89. Illustration des résultats obtenus pour la première et seconde composantes de la première PCA. Image tirée de CHURCHILL S.E., HOLLIDAY T. W., et CARLSON K.J. (et al.), 2013. The Upper Limb of *Australopithecus sediba*, *Science*, 340, p. 20.

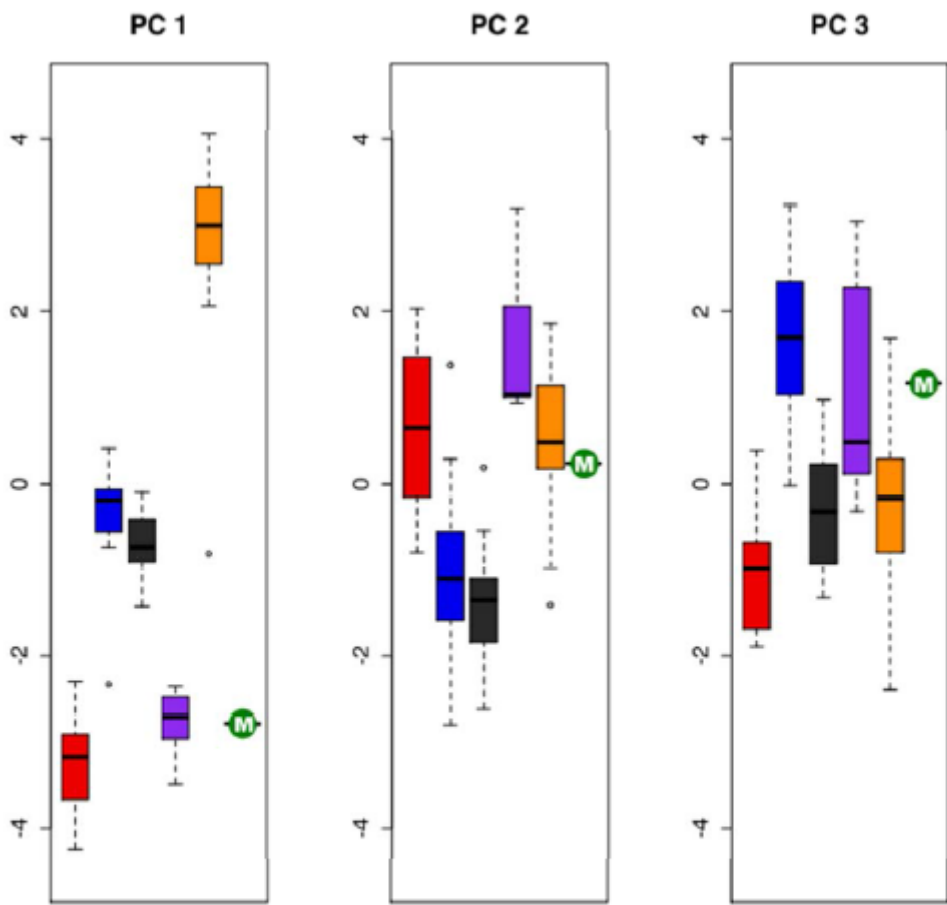


Fig. S4: Box plots showing the position of MH2 (green circles marked M) relative to the distribution of PC scores of the comparative samples on PC1 (left), PC2 (middle) and PC3 (right) from the first PCA (using variables from 3). Box and whisker plots show the median (thick horizontal line), upper and lower quartiles (box), range (whiskers) and outliers (circles) for each group. Red: *Homo sapiens*; purple: *Pongo pygmaeus/abelii*; black: *Gorilla gorilla*; blue: *Pan troglodytes*; orange: *Hylobates lar*.

Fig. 90. Illustration exposant la position de MH2 suite aux trois composantes de la première PCA. Image tirée de CHURCHILL S.E., HOLLIDAY T. W., et CARLSON K.J. (et al.), 2013. The Upper Limb of *Australopithecus sediba*, *Science*, 340, p. 22.

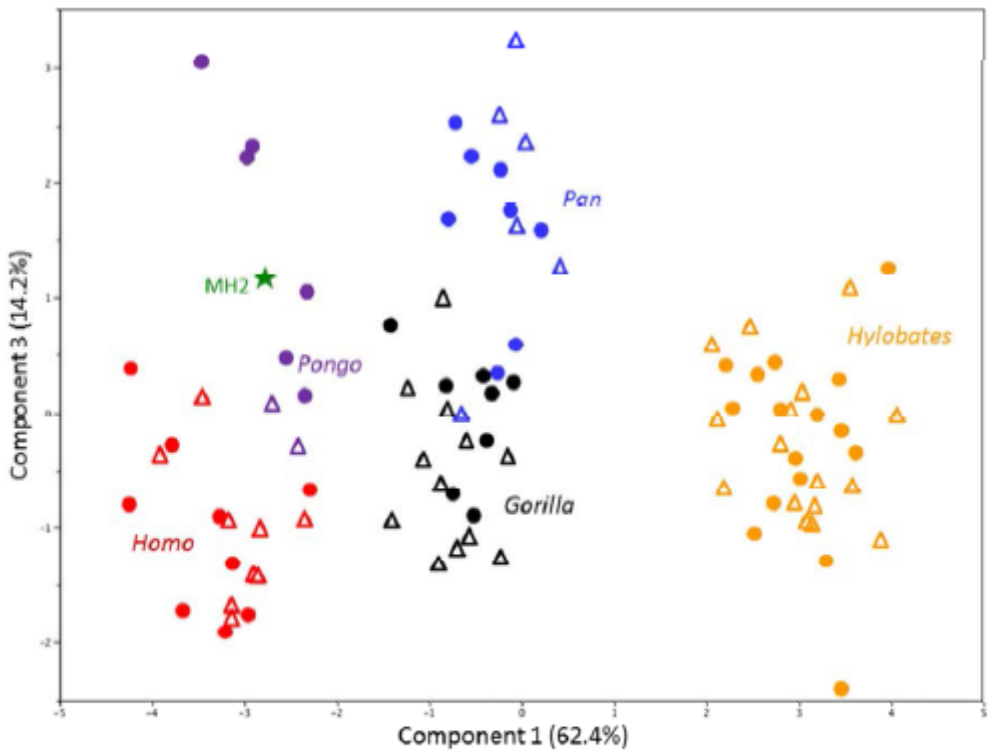


Fig. S3: PCA of 10 angles and size-adjusted linear scapular measurements using the variable set from (3). Individual scores on PC3 (accounting for 14.2% of the total variance) are plotted against scores on PC1 (62.4% of the variance); component loadings are provided in table S5. Green star: *Au. sediba* (MH2). Closed circles represent females and open triangles represent males. Red: *Homo sapiens*; purple: *Pongo pygmaeus/abelii*; black: *Gorilla gorilla*; blue: *Pan troglodytes*; orange: *Hylobates lar*.

Fig. 91. Illustration des résultats obtenus pour la troisième composante de la première PCA. Image tirée de CHURCHILL S.E., HOLLIDAY T. W., et CARLSON K.J. (et al.), 2013. The Upper Limb of *Australopithecus sediba*, *Science*, 340, p. 21.

	PC1 (77.2%)	PC2 (17.1%)	PC3 (4.2%)
AVA	0.64109	0.76712	0.00689
GSA	0.94349	-0.22038	-0.18911
SAA	0.96627	-0.11418	-0.13980
GAA	0.92327	-0.18798	0.33476
Variables as defined in table S2. PC 4 accounted for only 1.5% of the total variance and is not reported here.			

Tableau 22. Tableau récapitulatif des valeurs obtenues pour la seconde PCA, basée sur les variables angulaires de KSD – VP – 1/1. Tableau tiré de CHURCHILL S.E., HOLLIDAY T. W., et CARLSON K.J. (et al.), 2013. The Upper Limb of *Australopithecus sediba*, *Science*, 340, p. 12.

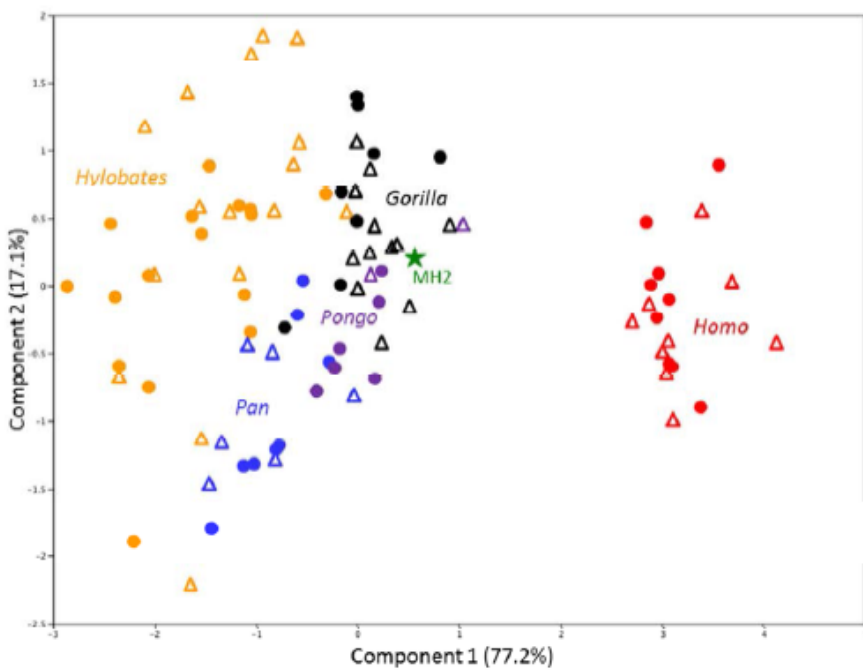


Fig. S5: PCA of four angles as used by (6). Individual scores on PC2 (accounting for 17.1% of the total variance) are plotted against scores on PC1 (77.2% of the variance); component loadings are provided in table S6. Green star: *Au. sediba* (MH2). Closed circles represent females and open triangles represent males. Red: *Homo sapiens*; purple: *Pongo pygmaeus/abelii*; black: *Gorilla gorilla*; blue: *Pan troglodytes*; orange: *Hylobates lar*.

Fig. 92. Illustration des résultats obtenus pour la première et seconde composantes de la seconde PCA. Image tirée de CHURCHILL S.E., HOLLIDAY T. W., et CARLSON K.J. (et al.), 2013. The Upper Limb of *Australopithecus sediba*, *Science*, 340, p. 23.

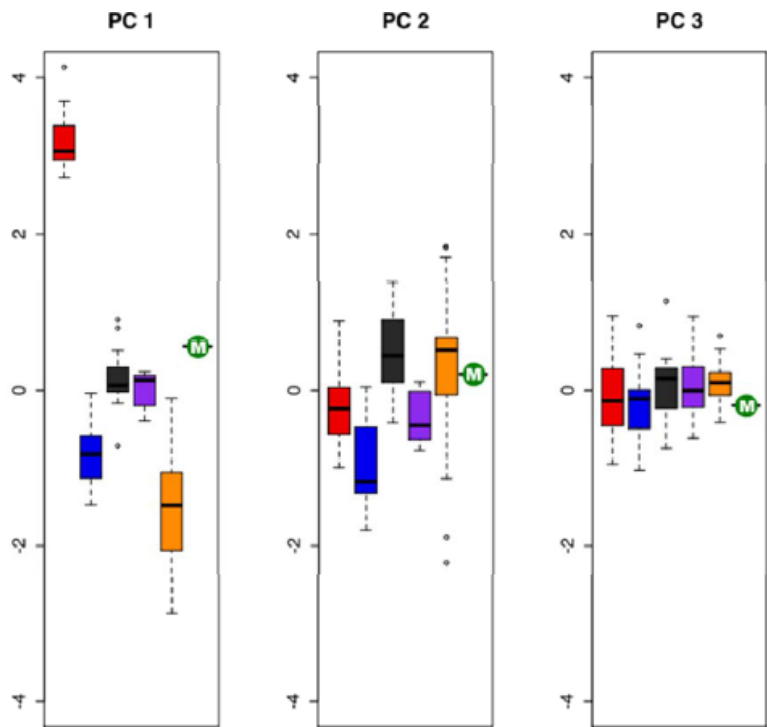


Fig. S7: Box plots showing the position of MH2 (green circle marked M) relative to the distribution of PC scores of the comparative samples on PC1 (left), PC2 (middle) and PC3 (right) from the second PCA (using variables from 6). Box and whisker plots show the median (thick horizontal line), upper and lower quartiles (box), range (whiskers) and outliers (circles) for each group. Red: *Homo sapiens*; purple: *Pongo pygmaeus/abelii*; black: *Gorilla gorilla*; blue: *Pan troglodytes*; orange: *Hylobates lar*.

Fig. 93. Illustration exposant la position de MH2 suite aux trois composantes de la seconde PCA. Image tirée de CHURCHILL S.E., HOLLIDAY T. W., et CARLSON K.J. (et al.), 2013. The Upper Limb of *Australopithecus sediba*, *Science*, 340, p. 25.

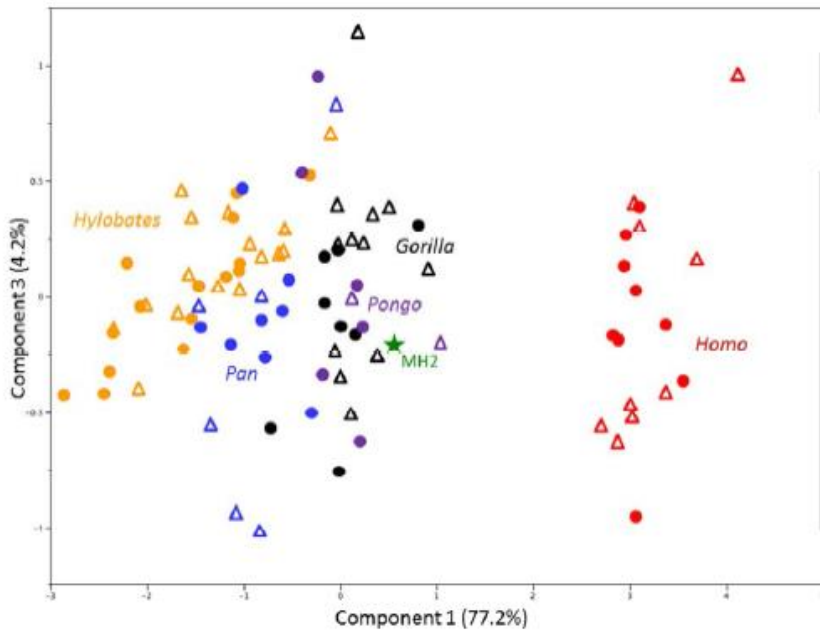


Fig. S6: PCA of four angles as used by (6). Individual scores on PC3 (accounting for 4.2% of the total variance) are plotted against scores on PC1 (77.2% of the variance); component loadings are provided in table S6. Green star: *Au. sediba* (MH2). Closed circles represent females and open triangles represent males. Red: *Homo sapiens*; purple: *Pongo pygmaeus/abelii*; black: *Gorilla gorilla*; blue: *Pan troglodytes*; orange: *Hylobates lar*.

Fig. 94. Illustration des résultats obtenus pour la troisième composante de la seconde PCA. Image tirée de CHURCHILL S.E., HOLLIDAY T. W., et CARLSON K.J. (et al.), 2013. The Upper Limb of *Australopithecus sediba*, *Science*, 340, p. 24.

	PC1 (61.8%)	PC2 (13.8%)	PC3 (11.7%)
SSFB	-0.92415	0.09975	-0.23597
ISFB	0.93175	-0.32662	0.00803
PSFB	-0.56158	0.30567	-0.67348
PIFB	0.96868	-0.15180	-0.01657
LENGTH	-0.86279	0.33927	0.32011
SAL	-0.87190	0.32565	0.28664
BREADTH	0.28980	-0.83403	-0.06358
GMA	-0.76045	-0.52621	-0.11236
SMA	0.93599	0.26202	-0.00057
GFS	0.00713	-0.01465	0.95409
AVA	0.47584	0.49272	-0.09586
GSA	0.92055	0.14169	-0.04730
SAA	0.90809	0.29052	0.00984
GAA	0.85573	0.30333	-0.06389

Variables as defined in table S2. PCs 4-14 are not reported here since each accounted for $\leq 1.5\%$ of the total variance.

Tableau 23. Tableau récapitulatif des valeurs obtenues pour la troisième PCA, basée sur les variables linéaires et angulaires combinées de DIK – 1 – 1 et de KSD – VP – 1/1. Tableau tiré de CHURCHILL S.E., HOLLIDAY T. W., et CARLSON K.J. (et al.), 2013. The Upper Limb of *Australopithecus sediba*, *Science*, 340, p. 13.

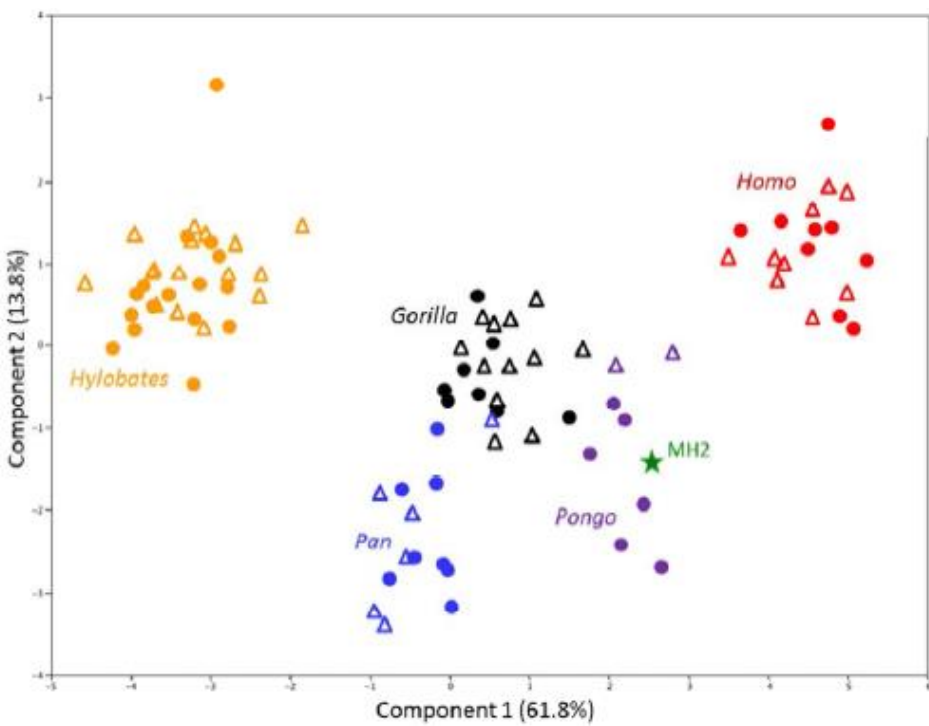


Fig. S8: PCA of the complete variable set (eight linear and six angular dimensions) of (6) and (3). Individual scores on PC2 (accounting for 13.8% of the total variance) are plotted against scores on PC1 (61.8% of the variance); component loadings are provided in table S7. Green star: *Au. sediba* (MH2). Closed circles represent females and open triangles represent males. Red: *Homo sapiens*; purple: *Pongo pygmaeus/abelii*; black: *Gorilla gorilla*; blue: *Pan troglodytes*; orange: *Hylobates lar*.

Fig. 95. Illustration des résultats obtenus pour le premier et second composants de la troisième PCA. Image tirée de CHURCHILL S.E., HOLLIDAY T. W., et CARLSON K.J. (et al.), 2013. The Upper Limb of *Australopithecus sediba*, *Science*, 340, p. 26.

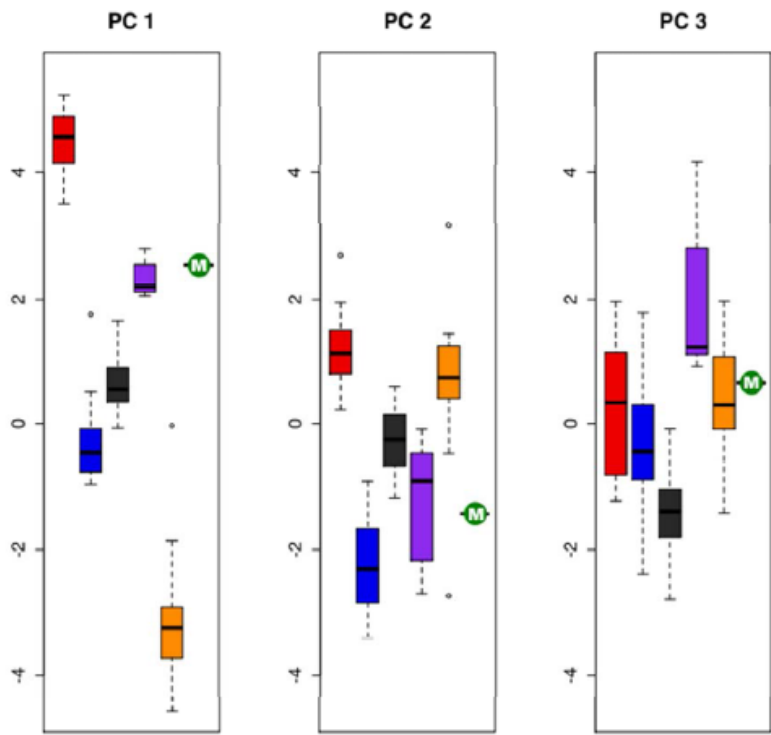


Fig. S10: Box plots showing the position of MH2 (green circle marked M) relative to the distribution of PC scores of the comparative samples on PC1 (left), PC2 (middle) and PC3 (right) from the third PCA (using variables from both δ and β). Box and whisker plots show the median (thick horizontal line), upper and lower quartiles (box), range (whiskers) and outliers (circles) for each group. Red: *Homo sapiens*; purple: *Pongo pygmaeus/abelii*; black: *Gorilla gorilla*; blue: *Pan troglodytes*; orange: *Hylobates lar*.

Fig. 96. Illustration exposant la position de MH2 suite aux trois composants de la troisième PCA. Image tirée de CHURCHILL S.E., HOLLIDAY T. W., et CARLSON K.J. (et al.), 2013. The Upper Limb of *Australopithecus sediba*, *Science*, 340, p. 28.

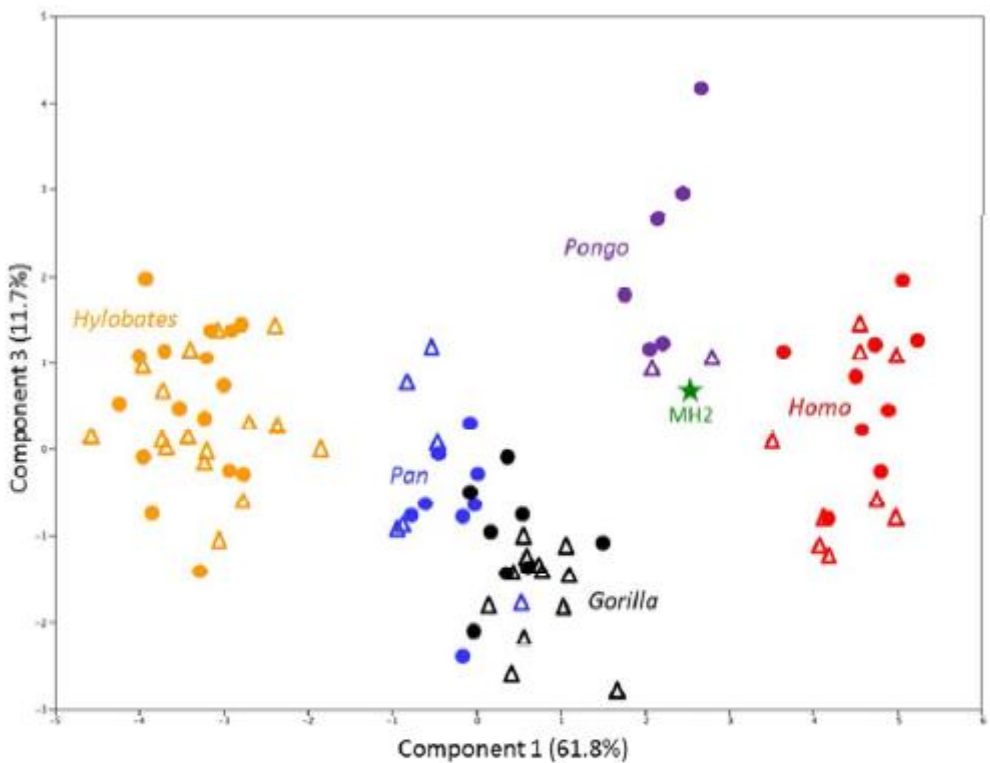


Fig. S9: PCA of the complete variable set (eight linear and six angular dimensions) of (6) and (3). Individual scores on PC3 (accounting for 11.7% of the total variance) are plotted against scores on PC1 (61.8% of the variance); component loadings are provided in table S7. Green star: *Au. sediba* (MH2). Closed circles represent females and open triangles represent males. Red: *Homo sapiens*; purple: *Pongo pygmaeus/abelii*; black: *Gorilla gorilla*; blue: *Pan troglodytes*; orange: *Hylobates lar*.

Fig. 97. Illustration des résultats obtenus pour le troisième composants de la troisième PCA. Image tirée de CHURCHILL S.E., HOLLIDAY T. W., et CARLSON K.J. (et al.), 2013. The Upper Limb of *Australopithecus sediba*, *Science*, 340, p. 27.

Paranthropes



Fig. 98. Orientation et morphologie de l'axis SK 854, Swartkrans. Vue ventrale (A) et latérale (B). Image tirée de GOMMERY D., 2003. Evolution of the Vertebral Column in Miocene Hominoids and Plio-Pleistocene Hominids, dans ISHIDA H., TUTTLE R. et PICKFORD M. (et al.), 2003. *Human Origins and Environmental Backgrounds*, p. 36. Cette image n'est pas l'originale, elle a été modifiée par Van Oostende Florence.

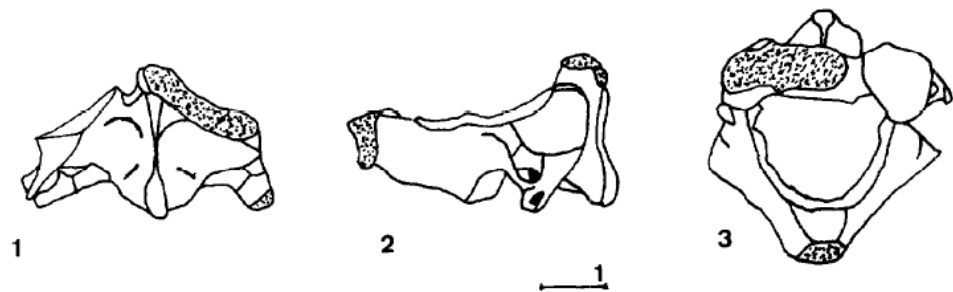


Fig. 99. Axis de SK 854, Swartkrans. Vue ventrale (1), latérale droite (2) et supérieure (3). Image tirée de GOMMERY D., 1997. Les atlas et les axis des Hominidés du Plio-Pléistocène : morphologie et systématique, *C. R. Acad. Sci. Paris, Sciences de la terre et des planètes*, vol. 325, p. 641.

Homo

Homo naledi

Table 1

Available measurements (in mm) on the *H. naledi* atlas (C1), axis (C2), and comparative data.^a

	<i>H. naledi</i> ^g AL 333 ^h	<i>A. afarensis</i> SK854	<i>P. robustus</i> KNM-ER 1825 ⁱ	<i>P. boisei?</i> Dmanisi	<i>H. erectus</i> Gran Dolina ^j	Neandertals ^k	Modern humans	<i>Pan troglodytes</i>
C1 SAF dorsoventral diameter ^b	14.1	23.1	—	20.0	—	19.5	24.1 (2.3, N = 6)	21.7 (2.4, N = 20)
C1 SAF transverse diameter ^c	7.9	10.8	—	10.0	—	13.5	11.3 (0.4, N = 6)	10.7 (1.2, N = 19)
C2 Body inferior transverse diameter (M8) ^d	13.8	—	14.8	—	14.7	—	19.8 (1.6, N = 5)	18.2 (1.6, N = 49)
C2 Body inferior dorsoventral diameter (M5) ^e	10.4	—	11.2	—	13.7	—	17.4 (1.6, N = 4)	15.1 (1.4, N = 49)
C2 Maximum height (axis with dens) (M1a) ^f	27.1 ⁱ	—	—	—	29.9	—	36.2 (1.4, N = 5)	35.2 (2.8, N = 49)
								30.1 (2.0, N = 18)

^a Taxa with more than one individual are shown as means, with standard deviation and sample size in parentheses. Original fossil specimens were studied except when indicated. M = Martin number.

^b Superior articular facet (SAF) dorsoventral diameter: the dorsal-most point of the facet measured along its midline to the ventral-most point.

^c Superior articular facet transverse diameter: measured at the maximum facet width orthogonal to the dorsoventral measurement.

^d Defined in Bräuer (1988) as the inferior vertebral body transverse diameter at the most laterally projecting points.

^e Defined in Bräuer (1988) as the inferior vertebral body dorsoventral diameter measured at the sagittal midline.

^f Defined in Bräuer (1988) as the maximal height of the axis at the sagittal midline, including the odontoid process.

^g U.W. 101-651 (C1) and U.W. 101-1279 (C2) are included.

^h AL 333-83 (C1) and AL 333-101 (C2) are included.

ⁱ KNM-ER 1825 data from Leakey and Walker (1985).

^j ATD6-90 data from Carretero et al. (1999).

^k VC3 and VC7 (Sima de los Huesos) data from Gómez-Olivencia et al. (2007); Kebara 2, La Chapelle-aux-Saints, La Ferrassie, Regourdou, and Shanidar 2 data from Gómez-Olivencia et al. (2013a).

^l This measurement is based on a slight reconstruction.

Tableau 24. Dimensions des vertèbres de *H. naledi* et données comparatives. Tableau tiré de WILLIAMS S.A., GARCIA-MARTINEZ D. et BASTIR M. (et al.), 2016. The vertebrae and ribs of *Homo naledi*, *Journal of Human Evolution*, p. 6.

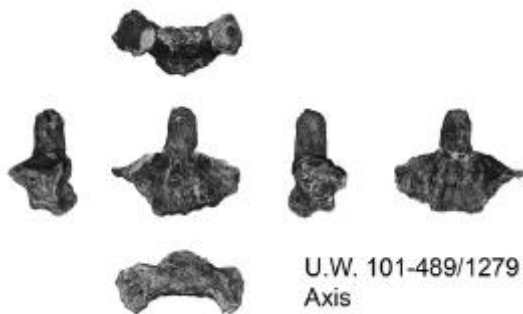


Fig. 100. Axis UW 101 – 1279, Dinaledi Chambre. Vue crâniale (en haut), caudale (en bas), latérale droite, ventrale, latérale gauche et dorsale (rangée du milieu, de gauche à droite). Photo tirée de WILLIAMS S.A., GARCIA-MARTINEZ D. et BASTIR M. (et al.), 2016. The vertebrae and ribs of *Homo naledi*, *Journal of Human Evolution*.

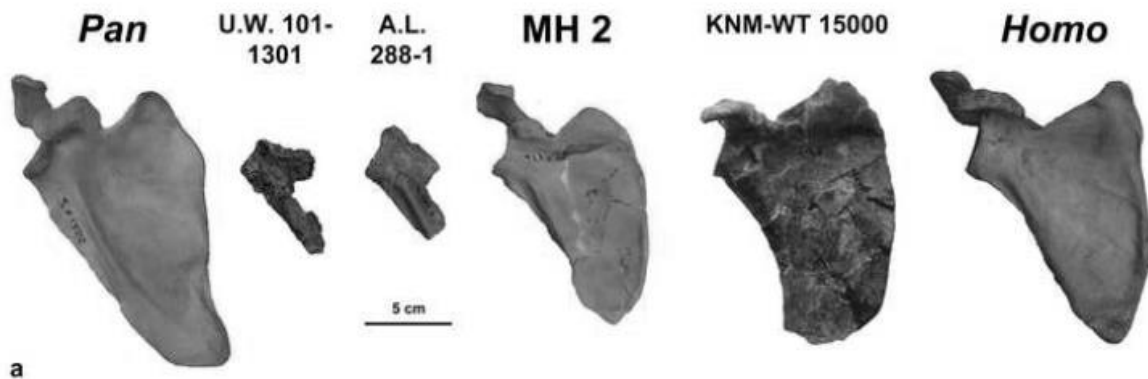


Fig. 101. Comparaison des scapulas droites de *Pan*, *H. naledi* (UW 101 – 1301), *Austra. afarensis* (AL 288 – 1), *Austra. sediba* (MH2), *H. erectus* (KNM – WT 15000), et *H. sapiens*. Photo tirée de FEUERRIEGEL E.M., GREEN D.J., et WALKER C.S. (et al.), 2016. *The upper limb of Homo naledi*.

Trait	<i>A. sediba</i> ^a	<i>A. africanus</i> ^b	<i>A. afarensis</i> ^c	<i>H. floresiensis</i> ^d	<i>H. habilis</i> ^e	<i>H. naledi</i>	<i>H. erectus</i> ^f	Additional references
Scapula								
Axillary border ventral bar	Strongly developed	Strongly developed	Strongly developed	Strongly developed	NA	Strongly developed	Moderately developed	Larson et al. (2007)
Axillary sulcus position	Ventral	Ventral	Ventral	Ventral	NA	Predominantly ventral (85.8%)	Ventral	Toussaint et al. (2003); Melillo (2016)
Axiloscapular angle (°)	44.4	29.8	43.1 (n = 2)	45.0	NA	26.8	69.6	
Ventral bar/glenoid angle (°)	131.2	126.2 (n = 2)	133.1 (n = 2)	157.0	NA	121.1	137.5	
Clavicle								
Relative length	Short	NA	NA	Short	Short	Short?	Short?	Larson et al. (2007)
Conoid tubercle morphology	Angular margin	Angular margin	Angular margin	Angular margin	Weak/absent	Prominent tubercle	Weak/absent	Drapeau et al. (2005); Larson (2007, 2013)
Mid-lateral shaft x-sectional shape	Dorsoventrally elongated oval	Dorsoventrally elongated oval	Dorsoventrally elongated oval	Rounded	Rounded	Rounded	Variably dorsoventrally elongated oval or rounded	Lovejoy et al. (1982)

^a As represented by MH1 and MH2.

^b As represented by Sts 7, Sts 14, StW 25, StW 88, StW 99, StW 102, StW 181, StW 311, StW 347, StW 358, StW 363, StW 389, StW 392, StW 403, StW 431, StW 443, StW 479, StW 486, StW 501, StW514, StW 522, StW 527, StW 573, and StW 598.

^c As represented by A.L. 288-1, A.L. 333-6, A.L. 333-9a, A.L. 333-9b, A.L. 333X-6/9, and KSD-VP-1/1.

^d As represented by LB1/5, LB1/50, LB1/51, LB1/52, LB2/1, LB3, LB4/1, LB6/2, and LB6/4.

^e As represented by OH 48 and OH 62.

^f Early *H. erectus* (*ergaster*) represented by KNM-WT 15000 and D4166, D4161, D4162, D4507, D2715, D2680, D3160, and D2724.

Tableau 25. Comparatif de la ceinture pectorale entre les *Australopithecus* et les *Homo*.

Tableau tiré de FEUERRIEGEL E.M., GREEN D.J., et WALKER C.S. (et al.), 2016. *The upper limb of Homo naledi*, annexe, p. 2.

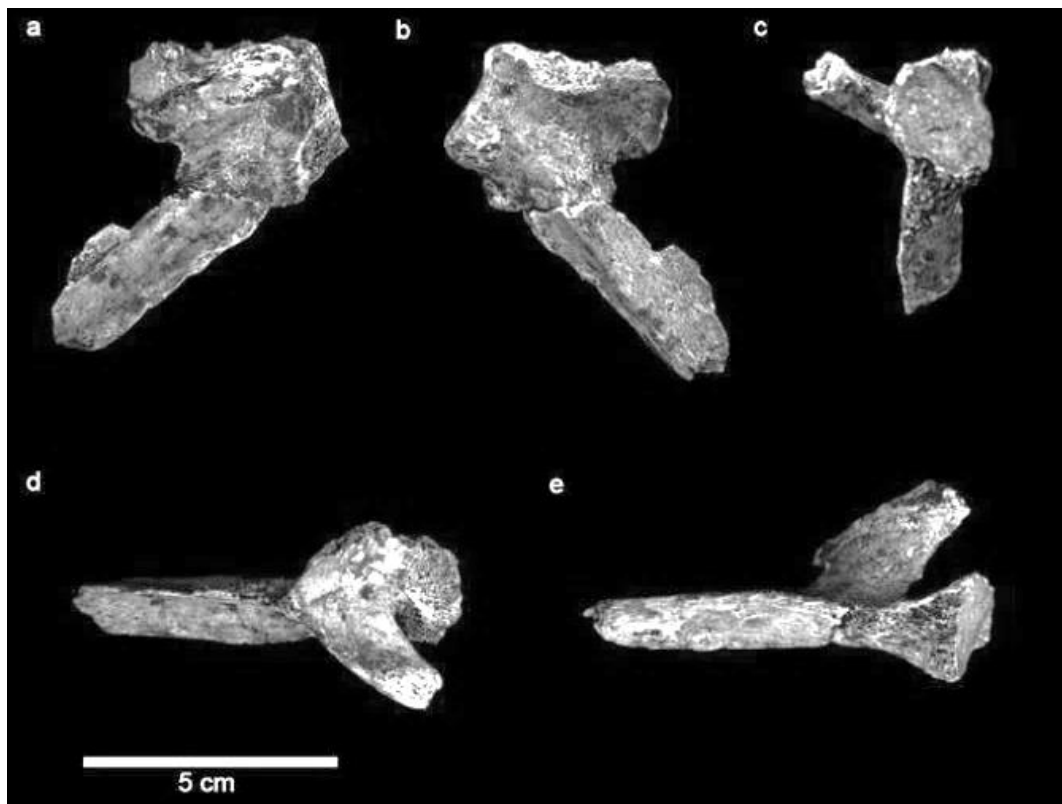


Fig. 102. Scapula partielle UW 101 – 1301, Dinaledi Chambre. Vue dorsale (a), ventrale (b), bord latéral (c), supérieure (d), et infériolatérale (e). Cavité glénoïde sur la droite de l'image. Photo tirée de FEUERRIEGEL E.M., GREEN D.J., et WALKER C.S. (et al.), 2016. *The upper limb of Homo naledi*.

Species	Ventral bar / glenoid angle	Axillospinal angle
<i>Homo naledi</i> (U.W. 101-1301)	121.1°	26.8°
<i>H. erectus</i> (KNM-WT 15000)	137.5°	69.6°
<i>H. floresiensis</i> (LB1) ^b	157.0°	45.0°
<i>A. sediba</i> (MH2) ^c	131.2°	44.4°
<i>A. afarensis</i> (A.L. 288-1)	132.2°	38.2°
<i>A. afarensis</i> (KSD VP-1/1) ^d	132.7°	48.0°
<i>A. africanus</i> (Sts 7)	128.0°	29.8°
<i>A. africanus</i> (StW 162)	124.3°	-
<i>H. sapiens</i> (n = 109)	142.4° (5.5°)	45.6° (5.3°)
<i>P. troglodytes</i> (n = 110)	127.9° (4.5°)	22.8° (4.3°)
<i>G. gorilla</i> (n = 140)	130.2° (5.5°)	30.1° (4.2°)
<i>P. pygmaeus/abelii</i> (n = 55)	131.4° (6.4°)	35.0° (5.9°)
<i>Hylobates</i> sp. (n = 194)	121.1° (5.2°)	10.1° (4.2°)

^a Standard deviation values are presented in parentheses for the extant groups.
^b Data from Larson et al. (2009).
^c Measured from a 3D digital printout of the MH2 scapula, following methods reported in Green and Alemseged (2012) and Green (2013), which slightly differs from the approach taken in Churchill et al. (2013).
^d Data from Melillo (2011). All other comparative and fossil data collected by D.J.G.

Tableau 26. Valeurs angulaires (barre ventrale/ cavité glénoïde et axilloépineux) de la scapula d'hominidés fossiles et hominoïdes existants. Tableau tiré de FEUERRIEGEL E.M., GREEN D.J., et WALKER C.S. (et al.), 2016. *The upper limb of Homo naledi*, annexe, p. 9.

Table 1. Hominin fossil material from the Lesedi Chamber. All diagnostic hominin specimens are listed, with attribution to element. Specimens that have been refitted are not listed separately. Most Locality 102a cranial fragments are presumed to be part of LES1 and are not listed separately.

Specimen number	Element	Notes
LOCALITY 102a		
LES1	cranium	constituted of 57 specimens, not listed separately
U.W. 102a-001	proximal right femur	
U.W. 102a-002	proximal right humerus	
U.W. 102a-003	proximal left femur	
U.W. 102a-004	distal left femur	
U.W. 102a-010	right scapula fragment	acromion
U.W. 102a-013	humeral head fragments	
U.W. 102a-015	right proximal ulna	
U.W. 102a-018	long bone fragment	immature

Table 1 continued

Specimen number	Element	Notes
U.W. 102a-279	left scapula fragment	partial glenoid fossa
U.W. 102a-280	rib fragment	
U.W. 102a-300	vertebral fragment	
U.W. 102a-306	L4 vertebra body	
U.W. 102a-322	L2 vertebra body	
U.W. 102a-337	vertebral fragment	neural arch
U.W. 102a-348	right pubic ramus fragment	
U.W. 102a-349	vertebral fragment	neural arch
U.W. 102a-358	rib fragments	
U.W. 102a-360	vertebral fragment	
U.W. 102a-455	ulna shaft fragment	
U.W. 102a-456	ulna shaft fragment	
U.W. 102a-470	rib fragments	
U.W. 102a-471	right distal radius fragment	
U.W. 102a-474	long bone fragment	immature
U.W. 102a-476	right capitate	
U.W. 102a-477	partial right lunate	
U.W. 102a-479	rib fragment	
LOCALITY 102b		
U.W. 102b-178	Li ₂	
U.W. 102b-437	rdm ₂	
U.W. 102b-438	right mandibular corpus fragment	immature, RP ₄ in crypt
U.W. 102b-502	cranial fragments	
U.W. 102b-503	RP ₄ crown	
U.W. 102b-506	cranial fragment	
U.W. 102b-507	cranial fragment	
U.W. 102b-509	cranial fragment	
U.W. 102b-511	LC ₁ crown	
U.W. 102b-514	cranial fragment	
U.W. 102b-515	Li ²	
U.W. 102b-516	cranial fragment	
LOCALITY 102c		
U.W. 102 c-589	left mandibular fragment	LM ₁ and LM ₂ in place

DOI: 10.7554/eLife.24232.004

Tableau 27. Inventaire des découvertes de la Lesedi Chamber, Rising Star Cave, Afrique du Sud. Tableau tiré de HAWKS J., ELLIOTT M., et SCHMID P. (et al.), 2017. New fossil remains of *Homo naledi* from the Lesedi Chamber, South Africa, eLIFE Research article, *Genomics and evolutionary biology*.

Homo georgicus



Fig. 103. Scapula D4166, scapula adulte droite provenant de Dmanisi, Géorgie. Photo tirée de LORDKIPANIDZE D., JASHASHVILI T., et VEKUA A. (et al.), 2007. Postcranial evidence from early *Homo* from Dmanisi, Georgia, *Nature*, 449, p. 306.

Table 1 | Postcranial dimensions of the Dmanisi hominins

Measurements	Australopiths	Earliest <i>Homo</i>	Dmanisi	KNM-WT15000	Modern humans
Shoulder girdle					
Olecranon orientation relative to midaxillary border (M17) (°)	115.0–116.0†	–	129.0	127.0	133.8–154.0
Glenocoracoid angle (°)	–	–	55.0	59.5	60.0–94.5
Clavicular length (M1) (mm)	–	149.4‡	137.3 (L), 135.6 (R), 123.2	130.5	113.0–159.0, 113.0–139.0
Humerus					
Length (M1) (mm)	226.0–235.0§	–	295.0, 282.2	319.0	263.0–341.0, 255.0–334.0
Mid-shaft a–p diameter (mm)	19.0	–	37.1, 17.1 (L), 16.8 (R)	19.9	16.5–36.0, 12.5–24.3
Mid-shaft m–l diameter (mm)	15.0	–	34.8, 14.3 (L), 14.7 (R)	16.7	11.5–24.5, 13.3–31.4
Torsion (M18) (°)	111.0–130.0	–	110.0, 104.0	126.0	134.9–180.0, 138.2–160.7
Vertebrae					
C2 anterior angle of superior articular process (°)	107.0–120.0¶	–	111.0	–	129.1–147.2
C2/C3 zygapophyseal joint angle (°)	–	–	62.5	–	62.0–85.0
Th10 centrum area (M4*M7) (mm ²)	–	–	692.2	–	601.1–958.6
L1 centrum area (M4*M7) (mm ²)	–	–	777.8	803.4	706.3–1,288.9
Femur					
Length (M1) (mm)	280.0#	401.0–396.0★ 386.0	432.0	337.0–434.0	
Head diameter (M19) (mm)	27.9–39.4**	40.0–42.0☆ 40.0	46.0	42.7–55.1	
Mid-shaft a–p diameter (M6) (mm)	22.0#	27.7–28.8☆ 26.5	24.5	29.1–34.7	
Mid-shaft m–l diameter (M7) (mm)	21.0#	26.4–25.6☆ 22.2	24.3	26.1–29.9	
Medial condylar breadth (M21c) (mm)	19.3–22.3††	20.7–21.☆ 24.2	–	27.6–40.3	
Lateral condylar breadth (M21e) (mm)	17.9–22.1††	19.2–25.5☆ 23.3	–	24.2–32.9	
Bicondylar angle (M30) (°)	75.0–81.0‡‡	77.0–80.0☆ 81.5	80.0	76.0–88.0	
Tibia					
Length (M1a) (mm)	–	–	306.0	380	290.0–374.0
Mid-shaft a–p diameter (M8) (mm)	–	22.5–31.0§§	27.0	24.5	25.8–42.3
Mid-shaft m–l diameter (M9) (mm)	–	14.6–23.6§§	18.0	20.4	15.5–24.6
Angle of inclination (M13) (°)	–	–	82.0	–	89.1–111.7
Foot					
Neck angle of talus (M16) (°)	32.3	33.5¶¶	26.0	–	12.0–31.0
Estimates*					
Stature (cm)	110.0–151.0 (ref. 50)	125.0–157.0 (ref. 50)	144.9–166.2	150.5–169.1 (ref. 42)	–
Body mass (kg)	29.0–49.0 (ref. 50)	32.0–52.0 (ref. 50)	40.0–50.0	45.5–70.6 (ref. 42)	–
Encephalization quotient	2.4–3.1 (ref. 50)	3.1 (ref. 50)	2.57–3.13	2.71–3.78	6.3

Measurement ranges were used for australopiths and modern humans. Data for subadults are in italic font. a–p, antero-posterior; m–l, mediolateral. For measurement codes (M1, M7, and so on) see ref. 69 of Supplementary Information.

*See Supplementary Table 6 for details on estimation procedures. †Sts7, AL288-1, OH48. §AL288-1, Bou-VP-12/1. || AL288-1, ER739, Sts7, Omo119. ¶AL333-101, SK-854. #AL288-1, KNM-ER1481, KNM-ER1472. **AL288-1, AL333-4. ††AL129, AL333-4, Sts34, TM1513. ‡‡AL288-1, AL129-1a, AL333-4, AL333w-56, Sts34, TM1513, ER993. §§OH35a, ER813a, ER741. |||| AL288-1, TM1517, ER1476a, ER813, ER1464, Stw573. ¶¶OH8.

Tableau 28. Dimensions des éléments découverts à Dmanisi, Géorgie. Tableau tiré de LORDKIPANIDZE D., JASHASHVILI T., et VEKUA A. (et al.), 2007. Postcranial evidence from early *Homo* from Dmanisi, Georgia, *Nature*, 449, p. 306.

Homo floresiensis

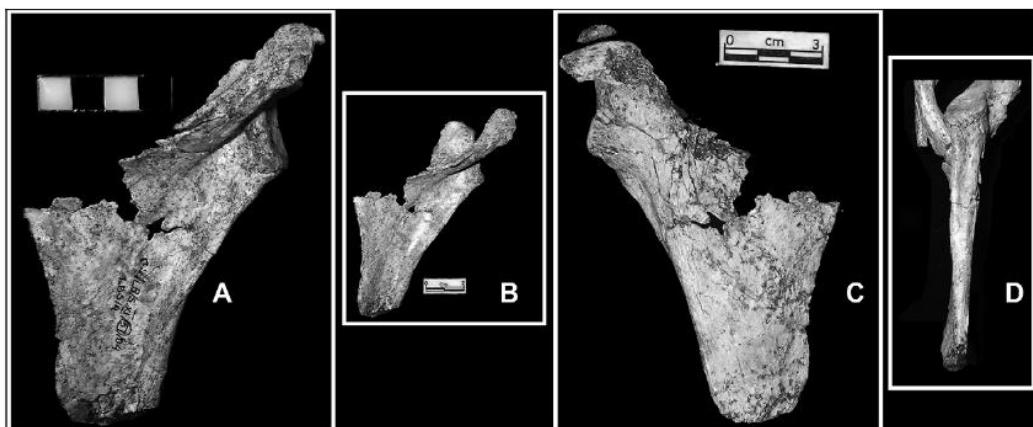


Fig. 104. Scapula droite LB6/4 en vue dorsale (A), vue dorsale avec effets possibles de la distorsion (B), vue ventrale (C), et vue latérale du bord axillaire (D). Photos tirées de LARSON S.G., JUNGERS W.L., et TOCHERI M.W. (et al.), 2009. Descriptions of the upper limb skeleton of *Homo floresiensis*, *Journal of Human Evolution*, 57, p. 566.

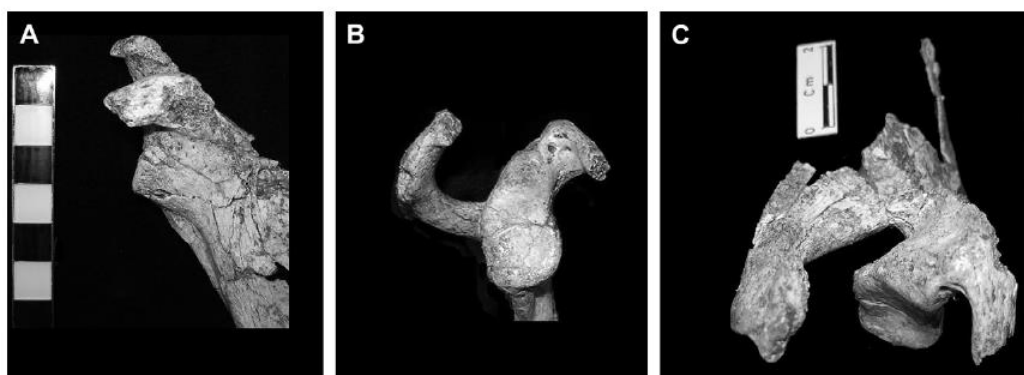


Fig. 105. Scapula droite LB6/4, vue ventrale du processus coracoïde (A), vue latérale de la cavité glénoïde (B), et vue supérieure de la région glénoïdale (C). Photos tirées de LARSON S.G., JUNGERS W.L., et TOCHERI M.W. (et al.), 2009. Descriptions of the upper limb skeleton of *Homo floresiensis*, *Journal of Human Evolution*, 57, p. 567.

Character number	Character and character states Intraspecific variation coded as 'intermediate' Dataset A	Character and character states Intraspecific variation coded as 'polymorphic' Dataset B	Reference for use of character in phylogenetic analyses or its importance for species differentiation C = used in previous cladistic analyses
101*	Infraglenoid tubercle (scapular) 1. broad 2. narrow	Infraglenoid tubercle (scapular) 1. broad 2. narrow	Finarelli and Clyde, 2004:642 (C) Brown and Maeda, 2009:578
102*	Axillary border (scapular) 1. pronounced and rounded 2. flattened 3. sharp ridge	Axillary border (scapular) 1. pronounced; rounded 2. flattened 3. sharp ridge	Begun et al., 1997:392 (C) Finarelli and Clyde, 2004:639 (C)
103*	Spinous process root (scapular) (Ordered) 1. robust 2. intermediate: robust and gracile 3. gracile	Spinous process root (scapular) 1. robust 2. gracile	Larson et al., 2009:566
104*	Orientation of scapular spine (Ordered) 1. 20°–40° 2. intermediate: 20°–40° and 41°–60° 3. 41°–60° 4. intermediate 41–60° and >60° 5. >60°	Orientation of scapular spine (Ordered) 1. 20°–40° 2. 41°–60° 3. >60°	Larson et al., 2007:723 Argue et al., 2009:Appendix 1 (C) Larson et al., 2009:566 Data source for <i>A. afarensis</i> , <i>A. africanus</i> , <i>H. ergaster</i> , <i>H. floresiensis</i> , <i>H. sapiens</i> , <i>Pan</i> , <i>Gorilla</i> , <i>Pongo</i> : Larson et al., 2007:725, Figure A
105*	Bar-glenoid angle (scapular) (Ordered) 1. 135° (superiorly directed glenoid fossa) 2. 136°–150° 3. >150°	Bar-glenoid angle (scapular) (Ordered) 1. 135° (superiorly directed glenoid fossa) 2. 136°–150° 3. >150°	Larson et al., 2007:725 Argue et al., 2009:Appendix 1 (C) Data source for <i>A. afarensis</i> , <i>A. africanus</i> , <i>H. ergaster</i> , <i>H. floresiensis</i> , <i>H. sapiens</i> , <i>Pan</i> , <i>Gorilla</i> , <i>Pongo</i> : Larson et al., 2007:725, Figure B
106*	Sub-scapula fossa 1. flat to convex 2. flat to concave	Subscapula fossa 1. flat to convex 2. flat to concave	Larson et al., 2009:566
107*	Infra spinous fossa (scapular) 1. convex with gentle curve to axillary border 2. flat or mild concavity with abrupt step to axillary border	Infra spinous fossa (scapular) 1. convex with gentle curve to axillary border 2. flat or mild concavity with abrupt step to axillary border	Larson et al., 2009:566–567

Tableau 29. Liste des caractéristiques prises en compte pour l'analyse bayesienne phylogénétique (incomplète). Tableau tiré de ARGUE D., GROVES C.P., et LEE M.S.Y. (et al.), 2017. The affinities of *Homo floresiensis* based on phylogenetic analyses of cranial, dental, and postcranial characters, *Journal of Human Evolution*, 107, p. 121.

Homo erectus



Fig. 106. Photo (incomplète) de KNM – WT 15 000, Nariokotome. Photo tirée de <https://www.nature.com/scitable/content/the-nariokotome-homo-erectus-skeleton-a-k-96680824>.

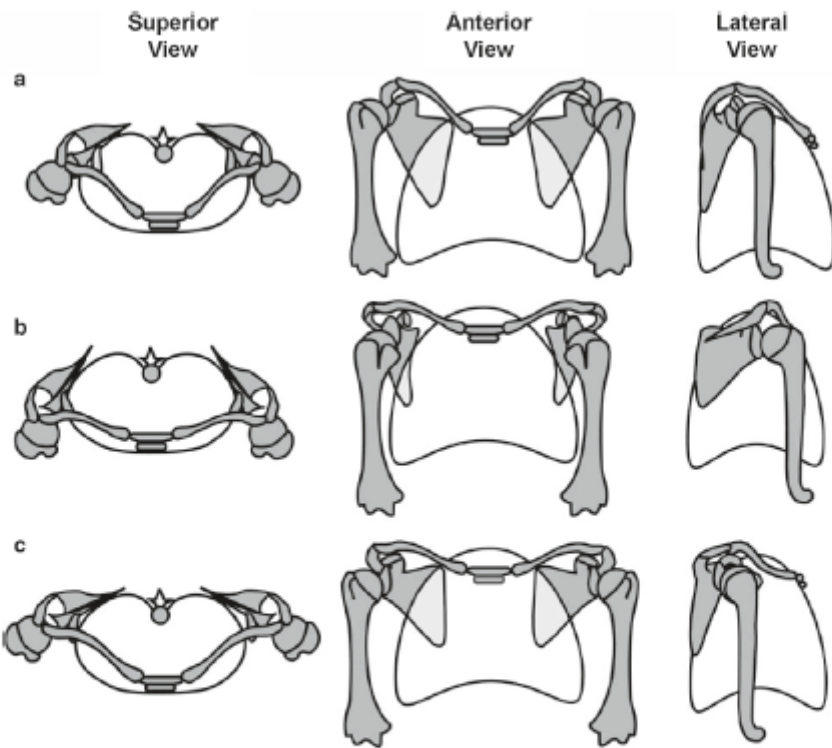


Fig. 7.4 Proposed course of hominin pectoral girdle evolution. (a) Superior, anterior and lateral schematic views of thorax showing pectoral girdle and shoulder of early hominin condition. Scapulae are dorsally positioned with a cranially facing glenoids, and clavicles are short and oriented obliquely resulting in a “hunched-shoulder” appearance. Humerus displays low to modest torsion. (b) Proposed transitional stage in hominin pectoral girdle evolution in which change from a cranially oriented glenoid fossa has been brought about in a way analogous to a downward rotation and translation of the scapula,

constrained by a relatively short clavicle. Scapulae are more laterally positioned, and glenoid fossae face anteriorly. Parasagittal functioning of the elbow joint is maintained without major increases in humeral torsion. Such a configuration would explain the low degree of humeral torsion and relatively short clavicles seen in early *H. erectus* (KNM-WT 15000). (c) Pectoral girdle and shoulder of a modern human with elongated clavicles, dorsally positioned scapulae and laterally facing glenoid fossae. The humerus displays marked torsion to maintain a parasagittal plane for elbow function.

Fig. 107. Proposition de l'évolution de la ceinture de l'épaule chez les hominoïdes. Vue supérieure, antérieure et latérale. Image et légende tirées de LARSON S., 2009. Evolution of the Hominin Shoulder : Early *Homo*, dans GRINE F.E., FLEAGLE J. G. , et LEAKEY R. E. (éd.), 2009. *The First Humans: Origin and Early Evolution of the Genus Homo*, New York, p. 71.

Homo antecessor

Specimen/sample	Species	Sex	Original/cast	Location
ATD6-90 (C1) Krapina (C1, n = 3; C2, n = 3)	<i>H. antecessor</i> <i>H. neanderthalensis</i>	Female ?	Original Original	Museo de Burgos, Burgos (Spain) Croatian Natural History Museum, Zagreb (Croatia)
La Chapelle-aux-Saints (C1 and C2)	<i>H. neanderthalensis</i>	Male	Original	Musée de l'Homme, Paris (France)
La Ferrassie 1 (C1 and C2)	<i>H. neanderthalensis</i>	Male	Original	Musée de l'Homme, Paris (France)
Shanidar 2 (C1 and C2)	<i>H. neanderthalensis</i>	Male	Cast	Musée de l'Homme, Paris (France)
Skhul V (C1 and C2)	<i>H. sapiens</i>	Male	Original	Peabody Museum of Archaeology and Ethnology, Cambridge (MA, USA)
Arcy-sur-Cure, Grotte des Fées (C1 and C2)	<i>H. sapiens</i> (?) ¹	?	Original (C1) Cast (C2)	Musée de l'Homme, Paris (France) (C1) Institut de Paléontologie Humaine, Paris (France) (C2)
Cro-Magnon (C1)	<i>H. sapiens</i>	Male	Original	Musée de l'Homme, Paris (France)
Carolingian ² (C2, n = 4)	<i>H. sapiens</i>	?	Original	Musée de l'Homme, Paris (France)
Neolithic ³ (C2, n = 2)	<i>H. sapiens</i>	?	Original	Musée de l'Homme, Paris (France)
Afalou-Bou-Rhummel ⁴ (C1, n = 12; C2, n = 10)	<i>H. sapiens</i>	?	Original	Institut de Paléontologie Humaine, Paris (France)
Taforalt ⁵ (C1, n = 8; C2, n = 9)	<i>H. sapiens</i>	?	Original	Institut de Paléontologie Humaine, Paris (France)
Burgos ⁶ (n = 40)	<i>H. sapiens</i>	Males	Original	Laboratorio de Evolución Humana-University of Burgos, Burgos (Spain)
Hamman-Todd ⁷ (n = 101)	<i>H. sapiens</i>	50 males/51 females	Original	Cleveland Museum of Natural History, Cleveland (OH, USA)

¹ The Arcy-sur-Cure atlas was found in 1860 in the lower level of the Grotte des Fées, (Yonne, France). The axis was found in 1898 in the clearings of older excavations (Leroi-Gourhan, 1958). Leroi-Gourhan (1958) identified both specimens as Neandertal. In the case of the axis, the taxonomic assignment was based on the surface color of the fossil; Leroi-Gourhan pointed out that this specimen is within the modern human range of variation but that it resembles Neandertals in its weak cervical curvature. In the case of the atlas, he did not find any trait to distinguish it from modern humans. Due to the problematic provenience of both specimens and the fact that these fossils are morphologically more similar to our modern human comparative samples than to Neandertals, they should be cautiously considered as representing *H. sapiens*.

² The Carolingian sample comes from the Saint-Germain-des-Prés cemetery (Paris, France).

³ The Neolithic sample comes from a cave site in the Petit Morin Valley (France).

⁴ The Afalou-Bou-Rhummel sample was recovered from the homonymous rock-shelter in Algeria. This sample and the Taforalt sample are dated to >10,000 BP (see Irish, 2000, and references therein).

⁵ The Taforalt sample was recovered from the homonymous cave site in Morocco.

⁶ The Burgos sample comprises 40 contemporary adult (estimated age at death is 20–45 years) male individuals from Burgos, Spain.

⁷ The Hamann-Todd sample comprises 100 North American adults (50 Euro-Americans and 50 Afro-Americans, with equal sexual representation) from the Hamann-Todd Osteological Collection.

Tableau 30. Atlas et axis utilisés pour les mesures de GOMEZ-OLIVENCIA et al. Tableau et légende tirés de GOMEZ-OLIVENCIA A., CARRETERO J.M., et ARSUAGA J.L. (et al.), 2007. Metric and Morphological Study of The Upper Cervical Spine from the Sima de los Huesos Site (Sierra de Atapuerca, Burgos, Spain), *Journal of Human Evolution*, 53, p. 8.

Homo heidelbergensis

Specimen	Year	Side	Region	Age	Figured in
(1) AT-246	1989	Right	Spine	J	Figure 12(a), (b)
(2) AT-316	1989	Left	Spine	J	Figure 12(c), (d)
(3) AT-320	1990	Left	gl+ax.b	Ad	Figure 13(d), (e) and Figure 15
(4) AT-342	1990	Left	Glenoid	Ad	Not figured
(5) AT-343	1990	Left	Glenoid	Ad	Figure 12(j)
(6) Scapula I	1991	Right	gl+spine+ax.b	Ad	Figure 13(a), (b), (c)
(7) AT-583	1992	Right	Glenoid	J	Figure 12(g), (h)
(8) AT-713	1992	Right	Spine	Ad	Figure 12(e)
(9) AT-749	1992	Left	Spine	Ad	Figure 12(f)
(10) AT-794	1993	Right	Glenoid	Ad	Figure 12(i)
(11) AT-801	1993	Right	gl+ax.b	J	Figure 12(f), (g)
(12) AT-1126	1994	Left	ax.b	Ad	Figure 12(k) and Figure 5
(13) AT-1127	1994	Left	Spine	Ad	Not figured
(14) AT-1152	1994	Left	Glenoid	J	Figure 12(l)
(15) AT-1154	1994	Right	Medial angle	Ad	Figure 12(m)
(16) AT-1253	1994	Left	Spine	Ad	Not figured
(17) AT-1256	1994	Right	Glenoid	Ad	Figure 13(h), (i) and Figure 5

The Scapula I is formed by AT-487 + AT-566.

Ad, adult; J, juvenile; gl, glenoid cavity; ax.b, axillary border.

Tableau 31. Inventaire des scapulas découvertes à Sima de los Huesos. Tableau tiré de CARRETERO J.M., ARSUAGA J.L., et LORENZO C., 1997. Clavicles, scapulae and humeri from the Sima de los Huesos Site (Sierra de Atapuerca, Spain), *Journal of Human Evolution*, 33, p. 368.

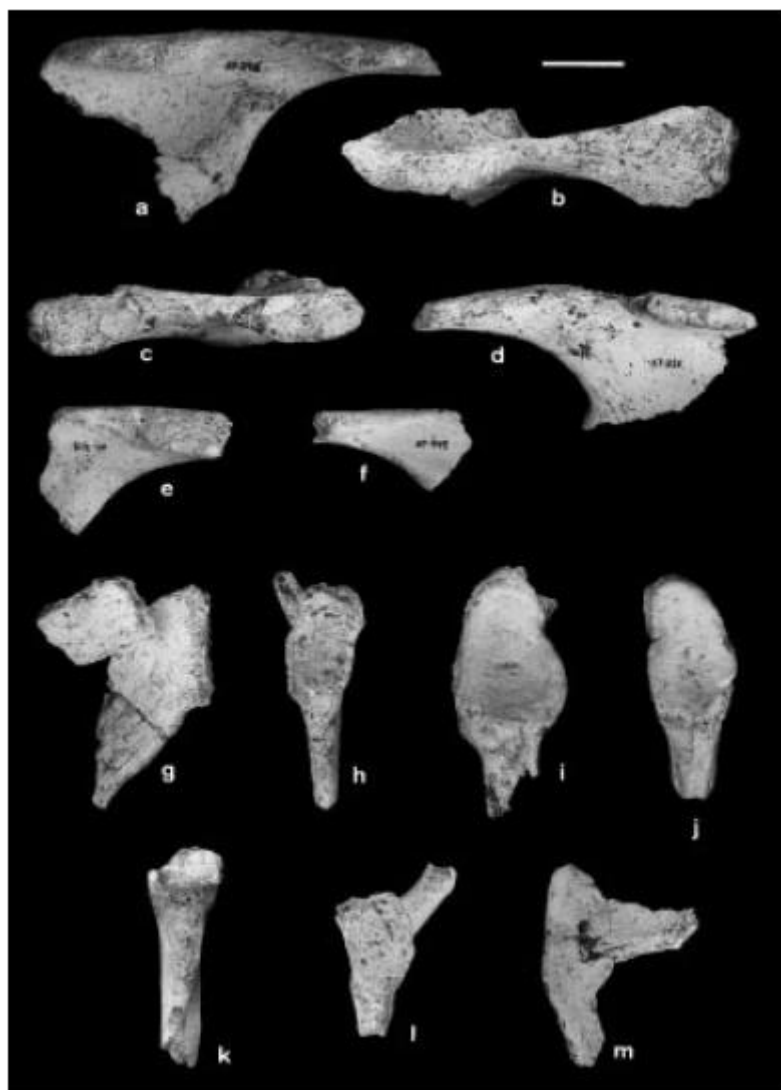


Fig. 108. Fragments scapulaires de Sima de los Huesos. Vues inférieure et postérieure des fragments épineux AT – 246 (a et b), AT – 316 (c et d). Vue inférieure d'AT – 713 (e) et AT – 749 (f). Vues postérieure et latérale d'AT – 583 (g et h). Vue latérale des cavités glénoïdales AT – 794 (i), AT – 343 (j), AT – 1126 (k) et AT – 1152 (l). Vue postérieure de l'angle médial d'AT – 1154 (m). L'échelle représente 2cm. Photo tirée de CARRETERO J.M., ARSUAGA J.L., et LORENZO C., 1997. Clavicles, scapulae and humeri from the Sima de los Huesos Site (Sierra de Atapuerca, Spain), *Journal of Human Evolution*, 33, p. 370.



Fig. 109. Fragments scapulaires de Sima de los Huesos. Vues postérieure, latérale et antérieure de la Scapula I (a,b et c). Vues postérieure et latérale d'AT – 320 (d et e) et AT – 801 (f et g). Vues antérieure et latérale d'AT – 1256 (h et i). L'échelle représente 2cm. Photo tirée de CARRETERO J.M., ARSUAGA J.L., et LORENZO C., 1997. Clavicles, scapulae and humeri from the Sima de los Huesos Site (Sierra de Atapuerca, Spain), *Journal of Human Evolution*, 33, p. 375.

Sample:	Dorsal	Bisulcate	Ventral
Chimpanzee (<i>n</i> =30)	—	—	100·0%
Gorilla (<i>n</i> =30)	—	—	100·0%
<i>Australopithecus</i> (<i>n</i> =2)	—	—	100·0%
WT-15000	—	—	X
ER-1808	X	—	—
Sima de los Huesos (<i>n</i> =4)	100·0%	—	—
Neandertals (<i>n</i> =25)	72·0%	28·0%	—
Skhul-Qafzeh (<i>n</i> =4)	—	100·0%	—
Upper Palaeolithic (<i>n</i> =8)	25·0%	62·5%	12·5%
Coimbra (<i>n</i> =248)	—	32·7%	67·3%
Recent Europeans (<i>n</i> =120)*	0·4%	23·8%	75·8%
Pecos Pueblo (<i>n</i> =119)*	—	13·4%	86·6%
Germans from Eppstein (<i>n</i> =265)†	6·4%	21·9%	56·4%
Muge (Portugal) (<i>n</i> =50)‡	26·7%	46·7%	26·6%

Australopithecus sample=AL-288-11 and Sts 7.

Skhul-Qafzeh sample=Qafzeh 8 (Vandermeersch, 1981) and Skhul IV, V and IX (McCown & Keith, 1939).

Upper Palaeolithic=Predmost III, X & XII, Combe-Capelle & Chancelade with sulcus axillaris bisulcata (Heim, 1982a), Obercassel and Predmost XIV with dorsal sulcus and Predmost IV with ventral sulcus (Endo & Kimura, 1970).

Neandertals=La Ferrassie 1 (r-l), La Ferrassie 2, Krapina 125, 127, 128, 129, 130, 131, 132, 133, 134, 135, 139, Neandertal 1 and Tabun C1 (by the authors), Amud 1 (Endo & Kimura, 1970), Shanidar 1, 2, 3 and 4 (Trinkaus, 1983), Spy 1, Spy 2 and St. Césaire (Frayer, 1992).

*Data from Trinkaus (1977).

†Data from Chambers (1992).

‡Data from Frayer (1992).

Coimbra=124 individuals both sides (248 scapulae).

Tableau 32. Fréquence de position du sulcus axillaire. Tableau tiré de CARRETERO J.M., ARSUAGA J.L., et LORENZO C., 1997. Clavicles, scapulae and humeri from the Sima de los Huesos Site (Sierra de Atapuerca, Spain), *Journal of Human Evolution*, 33, p. 377.

	Glenoid height (1)	Glenoid breadth (2)	Glenoid depth (3)	Glenoid index (4)	Depth index (5)
AL-288-11	27.0	18.1	2.7	67.0	10.0
Sts 7	38.0	22.4	4.1	58.9	10.8
WT-15000	33.5	22.2	—	67.2	—
AT-320	36.0	(23.0)	2.9	63.8	8.0
AT-343	(37.0)	(23.0)	3.3	62.2	8.9
AT-794	40.0	26.8	3.0	67.0	7.5
Scapula I	[40.0]	(25.0)	3.3	62.5	8.2
SH Mean ($n=4$)	38.2 ± 1.8	24.4 ± 1.6	3.1 ± 0.2	63.8 ± 1.9	8.1 ± 0.5
Neandertals ($n=12$)	37.0 ± 4.7	24.5 ± 3.7	2.9 ± 0.9	66.0 ± 3.0	7.7 ± 1.8
Coimbra total ($n=158$)	35.6 ± 3.3	25.8 ± 2.6	3.6 ± 0.8	72.6 ± 4.2	11.5 ± 2.3
Euroamericans* ($n=99$)	33.9 ± 3.1	24.9 ± 2.2	3.9 ± 0.7	73.4 ± 3.5	12.0 ± 1.6
Modern humans†					
Mean of means‡	33.5 ± 2.3	26.0 ± 1.9	3.6 ± 0.6	77.6 ± 3.0	10.9 ± 1.5
Range of means	28.9–38.4	22.0–28.7	2.6–4.9	68.8–81.8	8.3–13.6
Individual range			2.0–6.0	62.0–92.3	5.5–21.9

Parentheses () indicate estimated values. Brackets [] indicate highly estimated measurements.

Neandertal sample=La Ferrassie 1 (both sides), Krapina 125, 127, 129, 130, 131, 132, 133, Neandertal 1, Vindija 209 and Tabun C1 (by the authors), Amud 1 (Endo & Kimura, 1970), Shanidar 4 (Stewart, 1962).

*Data from Churchill & Trinkaus (1990).

†Data from Vallois (1928–1946).

#Mean of means calculated by the author with the raw data reported by Vallois (1928–1946). The sample sizes are: for the glenoid height, glenoid breadth and glenoid index, 23 modern human samples with a total of 1040 scapulae (both sides). For the glenoid depth and depth index 19 modern human samples with a total of 545 individuals (1090 scapulae).

(1) Glenoid fossa height (M12). Maximum craniocaudal distance in a coronal plane between the outer most edges of the line of attachment area of the labrum [similar to Vallois, 1929–1946; Olivier, 1960; Senut, 1981; Churchill & Trinkaus, 1990; Figure 10(b)1].

(2) Glenoid fossa breadth (M13). Maximum anteroposterior distance in a coronal plane between the outer most edges of the line of attachment area of the labrum [similar to Vallois, 1929–1946; Olivier, 1960; Senut, 1981; Churchill & Trinkaus, 1990; Figure 10(b)2].

(3) Glenoid fossa depth. Distance between the deepest point of the glenoid cavity and the line connecting the most laterally projecting points across the long axis of the cavity (Churchill & Trinkaus, 1990). (Not illustrated).

(4) Glenoid index = (glenoid breadth/glenoid height) × 100.

(5) Depth index = (glenoid depth/glenoid height) × 100.

Tableau 33. Comparaison et dimensions de la cavité glénoïde. Tableau tiré de CARRETERO J.M., ARSUAGA J.L., et LORENZO C., 1997. Clavicles, scapulae and humeri from the Sima de los Huesos Site (Sierra de Atapuerca, Spain), *Journal of Human Evolution*, 33, p. 380.

Specimen number	Year	Preservation	Age at death	Figure
VC3 ¹	1995	Complete vertebra	Adult	2a,b,c
VC7 ²	2000	Complete vertebra	Adult	2d,e,f
VC16 ³	1994, 1997	Masses and posterior arch	Adult	2g,h
VC17 ⁴	1995, 2000	Anterior arch and left mass	Adolescent (?)	3a
AT-269	1989	Left mass	Subadult	3b
AT-326	1990	Left mass		3c
AT-1818	1996	Left mass	Adult	3d
AT-2078	1997	Left mass	Subadult	3e
AT-2130	1997	Anterior arch		3l
AT-2264	1997	Posterior arch	>5 years	3p
AT-2584	1998	Left mass, posterior arch		3f
AT-2852	1998	Anterior arch		3m
AT-3003	1999	Left mass		3g
AT-3013	1999	Right mass, posterior arch fragment	Adult	3h
AT-3687	2000	Posterior arch	Subadult (?)	3q
AT-3691	2000	Posterior arch	Subadult (?)	3r
AT-3693	2000	Anterior arch		3n
AT-3694	2000	Right mass	Subadult	3i
AT-3971	1994	Right mass	Subadult	3j
AT-3985	?	Right mass	Adult	3k
AT-3992	1992	Posterior arch		3s
AT-4037	2000	Anterior arch fragment		3o

¹ VC3 = AT-1554.

² VC7 = AT-3339 + AT-3340 + AT-3341 + AT-3688.

³ VC16 = AT-1140 + AT-2201.

⁴ VC17 = AT-3374 + AT-3973 + AT-3991.

Tableau 34. Inventaire des atlas découverts à Sima de los Huesos, pendant la saison de fouille de 2004. Tableau tiré de GOMEZ-OLIVENCIA A., CARRETERO J.M., et ARSUAGA J.L. (et al.), 2007. Metric and Morphological Study of The Upper Cervical Spine from the Sima de los Huesos Site (Sierra de Atapuerca, Burgos, Spain), *Journal of Human Evolution*, 53, p. 10.

Specimen number	Year	Preservation	Age at death	Figure
VC2 ¹	1998	Complete vertebra	>25	4a,b,c
VC4 ²	1995	Complete vertebra	17–25 (21–25)?	4d,e,f
VC8 ³	2000, 2001	Complete vertebra	>25	4g,h,i
VC28 ⁴	2003	Complete except right transverse process	17–25 (17–20)?	5a
AT-150	1988	Right lamina, spinous process	>25	5d
AT-1573	1995	Dens, body, right art. facet, frag. upper left art. facet	12–16	5b
AT-2289	1997	Dens, frag. body, frag. upper right facet	12–16	5c
AT-2883	1998	Dens	>12	5f
AT-3696	2000	Dens	>12	5g
AT-3741	2000	Left superior art. facet	>6	5k
AT-3979	1998	Dens	>12	5h
AT-4046	1994	Frag. laminae, spinous process	4–25	5j
AT-4051	1998	Frag. right lamina, right lower art. facet	>4	5l
AT-4187	2003	Frag. body, right upper art. facet	6–16	5m
AT-4314	2003	Dens	>12	5i
AT-4662	1995	Tip of the spinous process	<25 (16–25)?	5e

¹ VC2 = AT-2465.

² VC4 = AT-1555.

³ VC8 = AT-3680 + AT-3840.

⁴ VC28 = AT-4634 + AT-4643.

Tableau 35. Inventaire des axis découverts à Sima de los Huesos, pendant la saison de fouille de 2004. Tableau tiré de GOMEZ-OLIVENCIA A., CARRETERO J.M., et ARSUAGA J.L. (et al.), 2007. Metric and Morphological Study of The Upper Cervical Spine from the Sima de los Huesos Site (Sierra de Atapuerca, Burgos, Spain), *Journal of Human Evolution*, 53, p. 10.

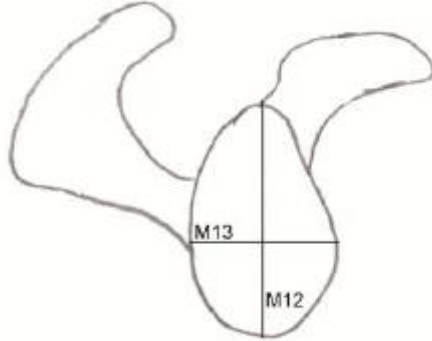


Fig. 110. Mesures prises dans les ossements du membre supérieur. Scapula droite en vue latérale. Image tirée de ARSUAGA J. L., CARRETERO J.M., et LORENZO C. (et al.), 2015. Postcranial morphology of the middle Pleistocene humans from Sima de los Huesos, Spain, PNAS, 112, annexe, p. 34. Image incomplète.

Anatomical region	Variable	Pooled-sex			Males			Females		
		Mean	SD	n	Mean	SD	n	Mean	SD	n
Scapula	Glenoid index	64.3	4.9	10	-	-	-	-	-	-
Clavicle	Robusticity index	22.6	0.5	3	22.2	-	1	22.9	0.4	2
Humerus	Humeral head shape	93.0	2.8	5	93.3	3.1	4	92.1	-	1
	Olecranon fossa index(*)	47.9	1.7	8	47.4	0.9	7	51.7	-	1
	Pillar index	29.0	3.9	8	29.7	4.0	6	26.9	3.3	2
Ulna	Trochlear notch orientation	80.7	4.6	10	82.4	5.4	5	81.6	3.6	2
	Radial fossa shape	82.0	12.0	12	75.4	14.7	4	95.6	11.2	2
	Robusticity index	15.9	1.9	3	17.8	-	1	13.9	-	1
	Diaphyseal index at <i>pronator teres</i>	75.5	4.1	3	71.7	-	1	79.8	-	1
Radius	Neck length index (*)	11.0	0.9	8	11.0	1.0	6	10.8	0.1	2
	Curvature index	4.1	0.8	8	4.2	0.9	6	3.7	0.8	2

SD = standard deviation; n = sample size. “Trochlear notch orientation” in degrees.

Definition of the variables from Martin-M (3), Senut-S (69), Trinkaus (29), Carretero et al.-C (11), Maia Neto-F (70) and McHenry-McH (12) (see Figure S6 for further details).

Scapula: Glenoid index: M13/M12×100; **Clavicle:** Robusticity index: M6/M1×100

Humerus: Humeral head index: C3/C4×100; Olecranon fossa index C16/C5×100; Pillar index: C18/C16×100. **Ulna:** Trochlear notch orientation: McH8/McH9; Radial fossa shape: S13/S12; Robusticity index: Midshaft circumference(MSC)/M1×100; Diaphyseal index at *pronator teres*: (Min/Max diameter)×100. **Radius:** Neck length index: F1b/M1×100; Curvature index: M6.1/M6×100.

Sexual diagnosis of SH upper limb bones following Carretero et al. (2).

Tableau 36. Mesure de la ceinture de l'épaule et des ossements des membres supérieurs chez les adultes de Sima de los Huesos. Tableau tiré de ARSUAGA J. L., CARRETERO J.M., et LORENZO C. (et al.), 2015. Postcranial morphology of the middle Pleistocene humans from Sima de los Huesos, Spain, PNAS, 112, annexe, p. 30.

Anatomical region	Variable	Juvenile I			Juvenile II		
		Mean	SD	n	Mean	SD	n
Scapula	Glenoid index	63.9	5.2	7	61.5	2.8	3
Clavicle	Robusticity index	23.9	0.1	2	-	-	-
Humerus	Humeral head shape	-	-	-	-	-	-
	Olecranon fossa index (*)	48.9	-	1	49.6	2.8	2
	Pillar index	32.2	-	1	23.6	3.3	2
Ulna	Trochlear notch orientation	-	-	-	80.1	-	1
	Radial fossa shape	72.6	-	1	81.6	10.6	2
	Robusticity index	-	-	-	-	-	-
	Diaphyseal index at <i>pronator teres</i>	79.5	-	1	79.3	-	1
Radius	Neck length index (*)	12.1	-	1	11.5	0.01	2
	Curvature index	3.2	-	1	4.2	1.2	2

See Table S13 for further details.

Juveniles I: traces of epiphyseal fusion in their extremities. Juveniles II: epiphyses are fusing or already fused.

(*) "Neck length" in juvenile individuals was measured as the length from proximal metaphysis to the upper limit of the radial tuberosity. "Olecreanon fossa index" in juveniles (Fossa breadth/Distal metaphysis medio-lateral diameter)×100.

Tableau 37. Mesure de la ceinture de l'épaule et des ossements des membres supérieurs chez les immatures de Sima de los Huesos. Tableau tiré de ARSUAGA J. L., CARRETERO J.M., et LORENZO C. (et al.), 2015. Postcranial morphology of the middle Pleistocene humans from Sima de los Huesos, Spain, PNAS, 112, annexe, p. 31.

Anatomical region	Variable	Pooled-sex			Males			Females		
		Mean	SD	n	Mean	SD	n	Mean	SD	n
Scapula	Glenoid index	66.1	3.2	15	67.7	2.7	5	67.7	0.1	2
Clavicle	Robusticity index	23.6	2.1	5	23.8	2.4	4	23.0	-	1
Humerus	Humeral head shape	98.4	4.4	6	99.6	3.8	5	92.7	-	1
	Olecranon fossa index	29.1	2.3	23	31.2	1.2	8	26.3	3.0	2
	Pillar index	26.7	5.5	23	25.3	6.5	8	21.1	0.02	2
Ulna	Trochlear notch orientation	82.4	6.9	11	82.4	5.0	8	78.2	13.7	2
	Radial fossa shape	91.6	25.0	16	67.0	15.0	6	110.1	38.1	2
	Robusticity index	-			-			14.8	-	1
	Diaphyseal index at <i>pronator teres</i>	70.1	7.1	3	66.3	3.9	2	77.7	-	1
Radius	Neck length index	9.9	0.5	4	9.8	0.3	3	10.5	-	1
	Curvature index	4.9	1.2	5	5.9	0.6	2	3.7	1.0	2

See Table S13 for further details.

Neandertal sample for:

Scapula: Amud 1; La Ferrassie 1 and 2; Neandertal 1; Shanidar 1 and 4; Tabun C1.

Clavicle: Kebara 2; Krapina 142, 143, 144, 145, 149, 153, 154, 155 and 156; La Chapelle-aux-Saints 1; La Ferrassie 1; Neandertal 1; Regourdou 1; Shanidar 1 and 3.

Humerus: Combe-Grenal; Hortus; Kebara 2; La Chapelle-aux-Saints 1; La Ferrassie 1; Lezetxiki; Krapina 159, 160, 161, 162, 164, 166, 169, 170, 171, 172 and 174; La Quina H5; Neandertal 1; Regourdou 1; Spy 1 and 3; Tabun C1; Vilafamés 1. **Ulna:** Amud 1; Krapina 179, 181, 182, 183, 184 and 185; La Chapelle-aux-Saints 1; La Ferrassie 1 and 2; La Quina H5. Neandertal 1; Regourdou 1; Shanidar 1, 3, 4, 5 and 6; Spy 1 and 2; Tabun C1. **Radius:** Amud 1; Kebara 2; La Chapelle-aux-Saints 1; La Ferrassie 1 and 2; Neandertal 1; Regourdou 1; Shanidar 1, 4, 5, 6, and 8; Spy 1; Tabun C1.

Tableau 38. Mesure de la ceinture de l'épaule et des ossements des membres supérieurs chez les échantillons d'*H. neandertaliensis*. Tableau tiré de ARSUAGA J. L., CARRETERO J.M., et LORENZO C. (et al.), 2015. Postcranial morphology of the middle Pleistocene humans from Sima de los Huesos, Spain, PNAS, 112, annexe, p. 32. Le “table S13” correspond au tableau 33.

Anatomical region	Variable	Pooled-sex			Males			Females		
		Mean	SD	n	Mean	SD	n	Mean	SD	n
Scapula	Glenoid index	71.5	6.2	111	73.1	6.2	79	67.3	4.5	29
Clavicle	Robusticity index	25.4	3.1	262	26.6	2.9	132	24.1	2.8	130
Humerus	Humeral head shape	108.2	4.3	234	108.1	4.4	129	108.3	4.3	105
	Olecranon fossa index	24.2	2.8	261	25.2	2.8	148	22.9	2.3	113
	Pillar index	44.2	10.1	258	45.8	9.6	147	41.9	10.5	111
Ulna	Trochlear notch orientation	68.9	7.2	336	69.2	7.3	170	68.6	7.2	165
	Radial fossa shape	66.9	11.0	330	67.6	11.7	169	66.0	10.2	169
	Robusticity index	18.0	1.6	310	18.4	1.6	156	17.6	1.6	152
	Diaphyseal index at <i>pronator teres</i>	85.3	7.6	336	84.5	8.5	163	86.3	6.5	173
Radius	Neck length index	9.3	0.8	456	9.5	0.8	243	9.1	0.8	213
	Curvature index	3.2	0.7	462	3.2	0.7	248	3.1	0.6	214

Tableau 39. Mesure de la ceinture de l'épaule et des ossements des membres supérieurs chez les hommes modernes. Tableau tiré de ARSUAGA J. L., CARRETERO J.M., et LORENZO C. (et al.), 2015. Postcranial morphology of the middle Pleistocene humans from Sima de los Huesos, Spain, *PNAS*, 112, annexe, p. 33.

Homo neanderthalensis

Figure 1. Kiik-Koba. Section of the settlement area with the adult burial (I) and the burial of the child (II).

Note: 1—outline of the grave-pit with a part of the adult burial; 2—bottom of the grave-pit; 3—outline of secondary interference with the adult burial; 4—area of the secondary interference; 5—finger and toe phalanges scattered in the upper Mousterian cultural horizon; 6—tooth found in the upper Mousterian cultural horizon.

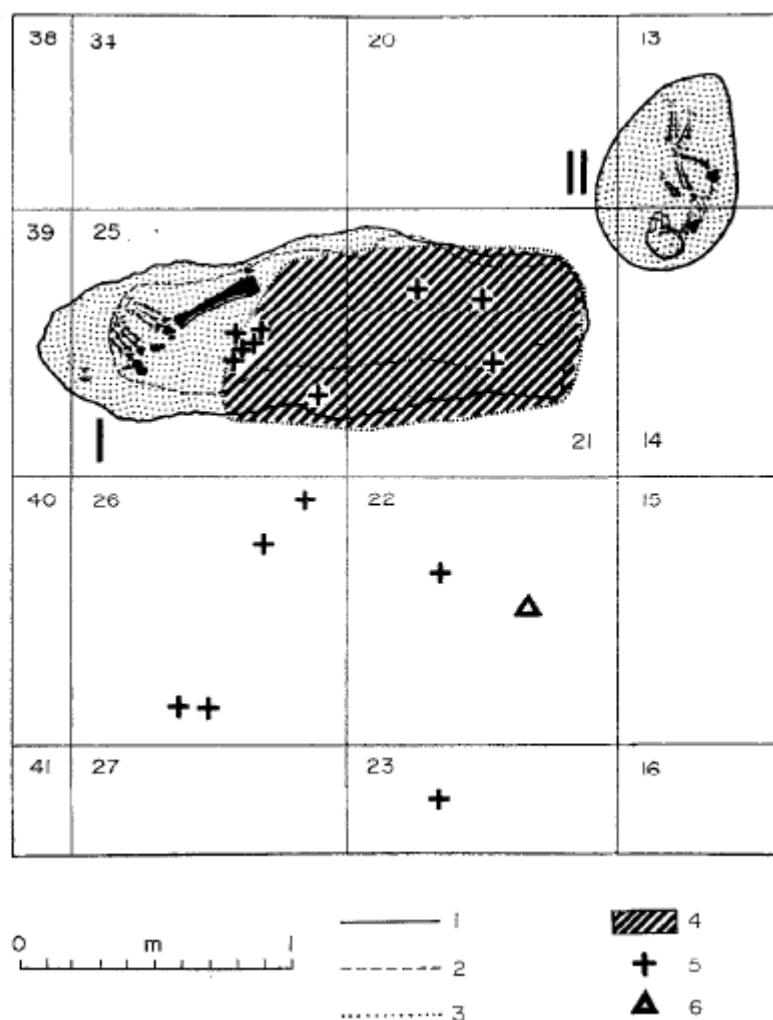


Fig. 111. Secteur de découverte des squelettes Kiik – Koba 1 et Kiik – Koba 2. Image et légende tirées de VLČEK E., 1972. Postcranial Skeleton of a Neandertal Child from Kiik – Koba, U.S.S.R., *Journal of Human Evolution*, 2, p. 538.

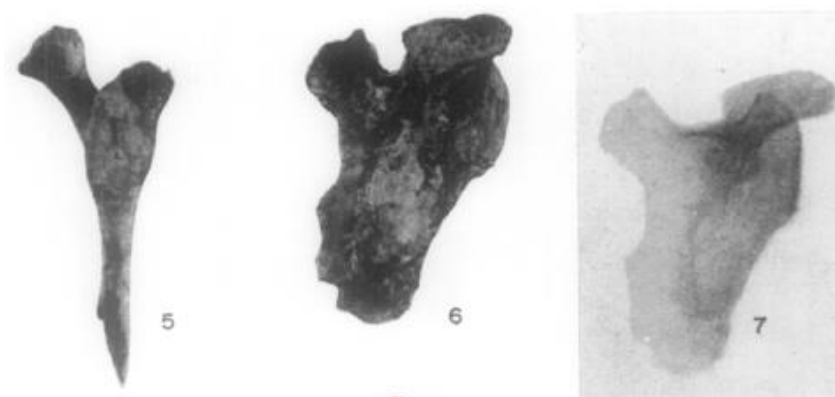


Fig. 112. Scapula droite de Kiik – Koba 2, vue latérale (5), vue dorsale (6), et radiographie (7). Photos tirées de VLČEK E., 1972. Postcranial Skeleton of a Neandertal Child from Kiik – Koba, U.S.S.R., *Journal of Human Evolution*, 2, p. 540.

Table 5**Angles of the scapula**

	Kiik-Koba infant	Recent infant
Axillo-glenoid	150°	134°
Spino-axillary	63°	45°

Tableau 40. Angles de la scapula de Kiik – Koba 2 et d'un enfant actuel. Tableau tiré de VLČEK E., 1972. Postcranial Skeleton of a Neandertal Child from Kiik – Koba, U.S.S.R., *Journal of Human Evolution*, 2, p. 543.



Figure 2 : Scapula droite : vue ventrale (photographie J.P. PARNAUDEAU)

Fig. 113. Vue ventrale de la scapula droite de KMH2, Kebara. Photo tirée de VANDERMEERSCH B., 1991. La ceinture scapulaire et les membres supérieurs, dans BAR-YOSEF O. et VANDERMEERSCH B. (éds.), 1991. *Le squelette moustérien de Kebara 2*, Paris, annexe, p. 2.



Fig. 114. Vue dorsale de la scapula droite de KMH 2, Kebara. Photo tirée de VANDERMEERSCH B., 1991. La ceinture scapulaire et les membres supérieurs, dans BAR-YOSEF O. et VANDERMEERSCH B. (éds.), 1991. *Le squelette moustérien de Kebara 2*, Paris, annexe, p. 1.

	Kébara		Shanidar				
	D	G	1G	2G	3D	4D	4G
Largeur anatomique (M ₁)	(167)						
Longueur anatomique (M ₂)	107	(115,5)	110	(116)	(115)	(115)	
Longueur du bord axillaire (M ₃)	(131)	130			(125)		
Largeur anatomique de la fosse sous-épineuse (M _{5a})	133,3	(140)			(127)		
Largeur maximale de l'acromion (M ₉)		28,9	28			(28,2)	(28,8)
Longueur de l'acromion (M ₁₀)		50,5					
Epaisseur bord axillaire à 30 mm sous-cavité glénoïde	15,6	14,5					

Tableau 41. Mesures des scapulas (d'après TRINKAUS E., 1983). Tableau tiré de VANDERMEERSCH B., 1991. La ceinture scapulaire et les membres supérieurs, dans BAR-YOSEF O. et VANDERMEERSCH B. (éds.), 1991. *Le squelette moustérien de Kebara 2*, Paris, p. 159.

	Kébara		Shanidar			Amud I	Tabun I
	D	G	1G	2G	4D	G	G
Longueur cavité glénoïde (M_{12})	(35,5)	(45)	(37)	(38,1)	(37,1)	(37)	29
Largeur cavité glénoïde (M_{13})	(22,7)	(27,7)	25,6		25,5	(25)	19
Indice glénoïdien	(63,9)	(61,5)	69,1		(68,7)	67,5	65,5

Tableau 42. Mesures de la cavité glénoïde de la scapula (d'après ENDO B., 1970. McCOWN T. D. et KEITH A., 1939 ; TRINKAUS E., 1983). Tableau tiré de VANDERMEERSCH B., 1991. La ceinture scapulaire et les membres supérieurs, dans BAR-YOSEF O. et VANDERMEERSCH B. (éds.), 1991. *Le squelette moustérien de Kébara 2*, Paris, p. 159.

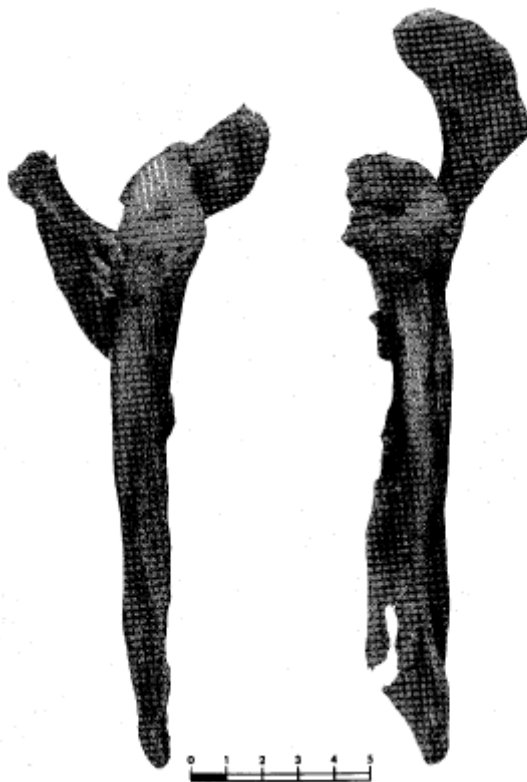


Fig. 115. Bord axillaire des scapulas droite et gauche de KMH 2, Kébara. Photo tirée de VANDERMEERSCH B., 1991. La ceinture scapulaire et les membres supérieurs, dans BAR-YOSEF O. et VANDERMEERSCH B. (éds.), 1991. *Le squelette moustérien de Kébara 2*, Paris, annexe, p. 3.

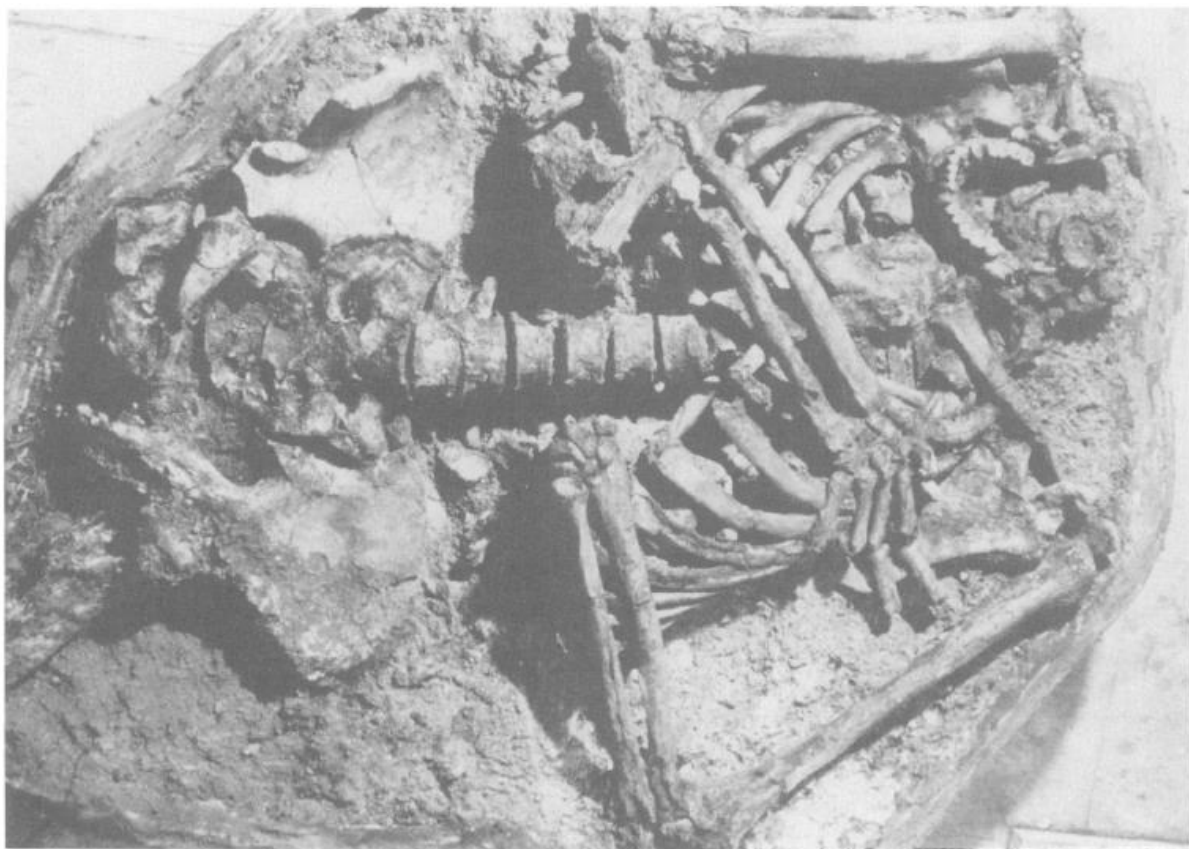


FIG. 14. The burial as exposed in the laboratory (photo: Kebara archives).

Fig. 116. Squelette KMH2, Kebara, tel qu'exposé dans le laboratoire. Photo tirée de BAR-YOSEF O., VANDERMEERSCH B., et ARENSBURG B. (et al.), 1992. The Excavations in Kebara Cave, Mt. Carmel, *Current Anthropology*, 33, p. 529.

Fig. 11.8 Mean and range of variation of the scapula neck index in West Europe, Central Europe, and Near-East Neanderthals

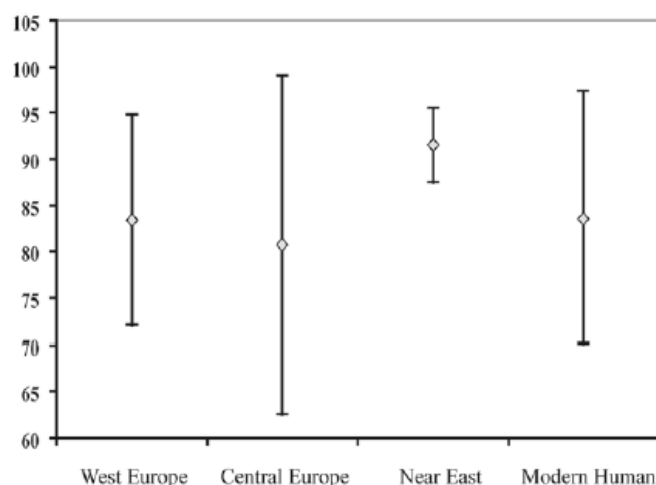


Fig. 117. Valeurs et rang de variation de l'index du col scapulaire des *H. neandertaliensis* en Europe de l'Ouest, Europe centrale et Proche-Orient. Image tirée de VOISIN J.L., 2006. A Preliminary Approach to the Neanderthal Speciation by Distance Hypothesis : A View from the Shoulder Complex, dans CONDEMI S. et WENIGER G.C. (éds.), 2006. Continuity and Discontinuity in the Peopling of Europe. One Hundred Fifty years of Neanderthal Study, *Vertebrate Paleobiology and Paleoanthropology Series*, Dordrecht, p. 134.

Fig. 11.9 Mean and range of variation of the angle between glenoid axis and the ventral bar, or angle A in West Europe, Central Europe, and Near-East Neanderthals and in modern humans

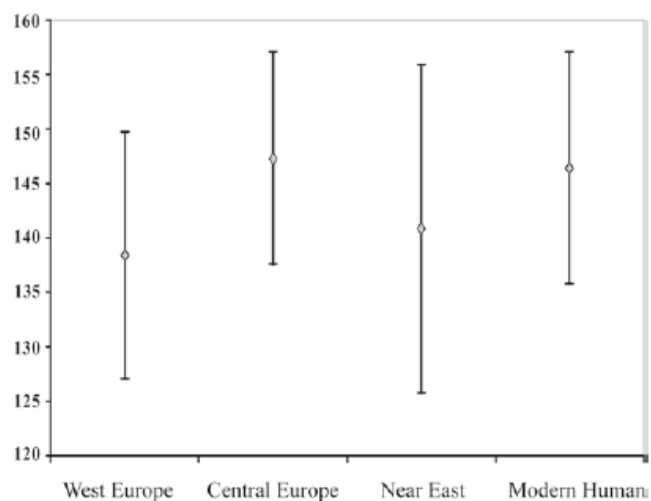


Fig. 118. Valeurs et rang de variation de l'angle A des *H. neandertaliensis* en Europe de l'Ouest, Europe centrale et Proche-Orient. Image tirée de VOISIN J.L., 2006. A Preliminary Approach to the Neanderthal Speciation by Distance Hypothesis : A View from the Shoulder Complex, dans CONDEMI S. et WENIGER G.C. (éds.), 2006. Continuity and Discontinuity in the Peopling of Europe. One Hundred Fifty years of Neanderthal Study, *Vertebrate Paleobiology and Paleoanthropology Series*, Dordrecht, p. 134.

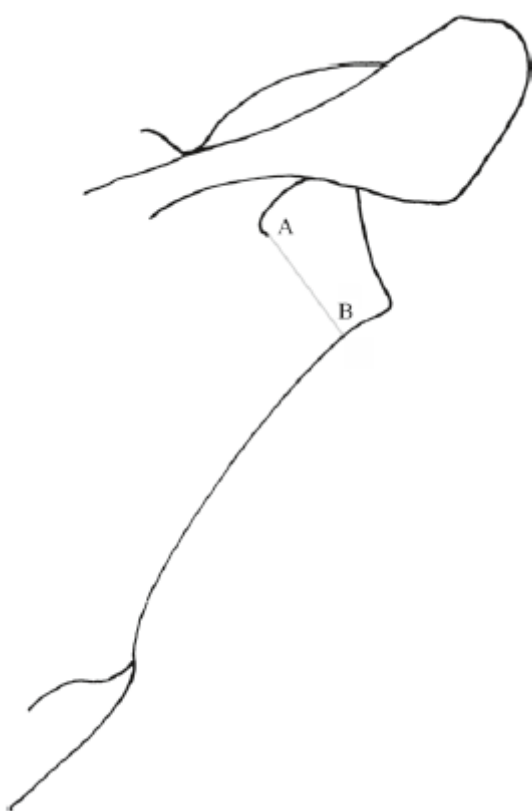


Fig. 119. Longueur du col scapulaire ou largeur minimale de la fosse infraépineuse (de A à B) (d'après Larson, 1995). Image tirée de VOISIN J.L., 2006. A Preliminary Approach to the Neanderthal Speciation by Distance Hypothesis : A View from the Shoulder Complex, dans CONDEMI S. et WENIGER G.C. (éds.), 2006. Continuity and Discontinuity in the Peopling of Europe. One Hundred Fifty years of Neanderthal Study, *Vertebrate Paleobiology and Paleoanthropology Series*, Dordrecht, p. 130.

Ventral	Bisulcate	Dorsal	Percent (%) ^a
	Shanidar 3 (R)		37.5
		Shanidar 1 (L)	
		Shanidar 2 (L)	
		Shanidar 4 (R)	
		Tabun 1 (L)	
		Amud 1	
	Kebara (L)		
	Kebara (R)		
	Krapina 125 (L)		20
Krapina 127 (R)			
		Krapina 128 (R)	
		Krapina 129 (R)	
		Krapina 130 (L)	
		Krapina 131 (L)	
		Krapina 132 (R)	
		Krapina 134 (R)	
		Krapina 135 (R)	
		Vindija 209 (L)	
		La Ferrassie 1 (R)	0
		La Ferrassie 1 (L)	
		La Ferrassie 2 (R)	
		Neanderthal (R)	
		Spy (R)	
		Spy (L)	

^aFrequencies, in percentage of non dorsal axillary sulcus

Tableau 43. Position du sulcus axillaire sur les scapulas néandertaliennes. Certaines données morphologiques sont prises de Boule (1911–1913), Fraipont (1927), Trinkaus (1982, 1983, 2006), Vandermeersch (1991), Frayer (1992) and Odwak (2006). Tableau tiré de VOISIN J.L., 2006. A Preliminary Approach to the Neanderthal Speciation by Distance Hypothesis : A View from the Shoulder Complex, dans CONDEMI S. et WENIGER G.C. (éds.), 2006. Continuity and Discontinuity in the Peopling of Europe. One Hundred Fifty years of Neanderthal Study, *Vertebrate Paleobiology and Paleoanthropology Series*, Dordrecht, p. 135.

Table 11.7 Data for the glenoid and scapula neck index as well as for angle A (angle between glenoid axis and ventral bar). Some glenoid index values are taken from Vandermeersch (1981, 1991) and Trinkaus (2006)

Individual	Glenoid index	Scapula neck index	Angle A
Kebara (R)	63.9	91.6	148.0
Kebara (L)	61.5	93.5	133.0
Shanidar 1 (L)	65.8		
Tabun 1 (L)	65.5	89.5	141.5
Amud 1	67.5		
Mean	64.8	91.5	140.8
Krapina 127 (R)	65.4	75.2	155.0
Krapina 129 (R)	61.5	67.1	147.0
Krapina 125 (L)	68.0	81.4	148.0
Krapina 132 (R)	67.1	73.7	146.5
Krapina 130 (L)	77.3	86.2	147.0
Krapina 131 (L)	63.3	91.3	149.0
Krapina 133 (R)	69.1	90.2	
Vindija 209 (L)	77.0		138.5
Mean	68.6	80.7	147.3
Ferrassie I (R)	68.1	77.1	132.5
Ferrassie I (L)	65.2	80.8	141.0
Spy (L)	75.0	93.8	
Spy (R)	72.3	83.2	135.0
Neanderthal (R)	63.2	81.1	145.0
Mean	68.8	83.2	138.4
Modern human (standard deviation/mean)	4.0/80.3	6.8/83.6	5.3/146.4

Tableau 44. Données pour l'index de la cavité glénoïde et l'index du col scapulaire ainsi que l'angle A. Certaines valeurs de l'index de la cavité glénoïde sont prises de Vandermeersch (1981, 1991) et Trinkaus (2006). Tableau tiré de VOISIN J.L., 2006. A Preliminary Approach to the Neanderthal Speciation by Distance Hypothesis : A View from the Shoulder Complex, dans CONDEMI S. et WENIGER G.C. (éds.), 2006. Continuity and Discontinuity in the Peopling of Europe. One Hundred Fifty years of Neanderthal Study, *Vertebrate Paleobiology and Paleoanthropology Series*, Dordrecht, p. 133.



Fig. 120. Scapula droite de Muierii 1 en vue latérale (gauche) et la scapula droite de Sunghir 1 en vue dorsale (droite). L'échelle est différente. Photo tirée de TRINKAUS E., 2006. Late Neandertals and Early Modern Humans in Europe, Population Dynamics and Paleobiology, dans CONDEMI S. et WENIGER G.C. (éds.), 2006. Continuity and Discontinuity in the Peopling of Europe. One Hundred Fifty years of Neanderthal Study, *Vertebrate Paleobiology and Paleoanthropology Series*, Dordrecht, p. 323.

Axillary Border Pattern ¹	Ventral sulcus (%)	Bisulcate (%)	Dorsal sulcus (%)	n
Gorillas ²	100	0.0	0.0	30
Chimpanzees ²	100	0.0	0.0	30
<i>Australopithecus</i> ³	100	0.0	0.0	3
Early <i>Homo</i> ⁴	100	0.0	0.0	2
European Middle Pleistocene ⁵	0.0	0.0	100	4
Western Eurasia OIS 6/5 ⁶	2.9	32.4	64.7	17
Neandertals OIS 4/3	0.0	25.0	75.0	10
Qafzeh-Skhul OIS 5	20.0	80.0	0.0	5
Earlier Upper Paleolithic ⁷	11.6	67.0	21.4	28

Samples for the early *Homo*, OIS 6/5, and Late Pleistocene scapulae include late juvenile and adolescent specimens, as well as mature scapulae. The other samples contain only adults. Data from personal observation unless otherwise referenced.

¹ The axillary border morphology is divided into three general categories following Eickstedt (1925) so as to include as many comparative samples as possible. The more detailed systems of Eickstedt (1925) and the seven-part system of Churchill (1994) better characterize the continuous variation of the region, but their finer distinctions are sometimes difficult to make on fragmentary scapulae.

² Data from Carretero et al. (1997).

³ Sts-7, Stw 431, AL 288-1 (Senut, 1981; Johanson et al., 1982).

⁴ KNM-WT 15000, Dmanisi 4166 (Walker and Leakey, 1993; Jashashvili, 2005). I (Trinkaus, 1995) previously noted that KNM-ER 1808 had a dorsal sulcus, based on a personal communication (see also Carretero et al., 1997); however, this has not been confirmed, and the inventory of the specimen (Leakey et al., 1978) does not mention a scapula.

⁵ Sima de los Huesos (Atapuerca) (Carretero et al., 1997).

⁶ Krapina (Trinkaus, 2006b), Bourgeois-Delaunay 2 (Condeuri, 2001), and Tabun 1.

⁷ European and southwestern Asian earlier Upper Paleolithic, plus Minatogawa (Baba and Endo, 1982).

Tableau 45. Comparaison des fréquences de la morphologie du bord axillaire chez échantillons des grands singes et des lignées humaines pré-Holocène. Tableau et légende tirés de TRINKAUS E., 2008. Kiik-Koba 2 and Neandertal axillary border ontogeny, *Anthropological Science*, 116, p. 232.



Fig. 121. Scapula de Kiik-Koba 2, en vue dorsale (gauche), latérale du bord axillaire (milieu) et dorsolatérale (droite). L'échelle pour la vue dorsale est en cm, et elle est approximativement exacte pour les autres vues. Photo tirée de TRINKAUS E., 2008. Kiik-Koba 2 and Neandertal axillary border ontogeny, *Anthropological Science*, 116, p. 234.

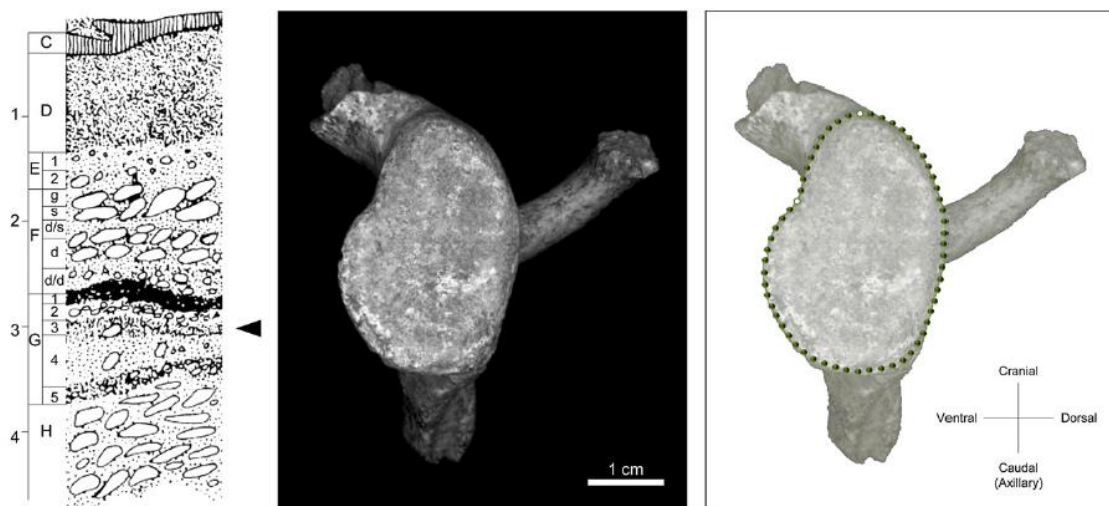


Fig. 122. Fragment scapulaire Vi – 209 et sa position stratigraphique (flèche) au sein des couches moustériennes de Vindija Cave, Croatie (selon Malez et al., 1980.). Sur la droite, la configuration des 60 points de repères utilisés pour les analyses. Image et photo tirées de DI VINCEZO F., CHURCHILL S. E., et MANZI G., 2012. The Vindija Neanderthal scapular glenoid fossa: Comparative shape analysis suggests evo-devo changes among Neanderthals, *Journal of Human Evolution*, 62, p. 275.

Table 1

List of OTUs and specimens included in the analysis.

OTU	Site	Specimen	Side	Label	Source	Age	
<i>Australopithecus africanus</i> ($N = 1$)	Sterkfontein (South Africa)	STS 7	R	STR	Original	Pliocene/Pleistocene	
<i>Australopithecus sediba</i> ($N = 1$)	Malapa (South Africa)	MH 2	R	MLP	CT-scan	Early Pleistocene	
<i>Homo georgicus</i> ($N = 1$)	Dmanisi (Georgia)	D 4166	R	DMS	CT-scan	Early Pleistocene	
<i>Homo floresiensis</i> ($N = 1$)	Liang Bua (Flores, Indonesia)	LB 6/4	R	LNG	Original	Late Pleistocene	
<i>Homo heidelbergensis</i> ($N = 5$)	Atapuerca	AT-320	L	SH1	Original	Middle Pleistocene	
		Sima de los Huesos (Spain)	AT-343	L	SH2	Original	Middle Pleistocene
			AT-794	R	SH3	Original	Middle Pleistocene
			AT-1256	R	SH4	Original	Middle Pleistocene
		Atapuerca Scapula 1	R	SH5	Original	Middle Pleistocene	
<i>Homo neanderthalensis</i> from Krapina ($N = 5$)	Krapina (Croatia)	Krapina 127	R	KR1	Cast	Late Pleistocene	
		Krapina 129	R	KR2	Original	Late Pleistocene	
		Krapina 130	L	KR3	Cast	Late Pleistocene	
		Krapina 131	L	KR4	Original	Late Pleistocene	
		Krapina 133	R	KR5	Original	Late Pleistocene	
<i>Homo neanderthalensis</i> ($N = 6$) Late European and Near-Eastern samples	Kebara (Israel)	Kebara 2	R	KBR	Cast	Late Pleistocene	
	La Ferrassie (France)	La Ferrassie 1	R	LP1	Cast	Late Pleistocene	
		La Ferrassie 2	R	LP2	Cast	Late Pleistocene	
	Feldhofer Grotto (Germany)	Neandertal 1	R	NND	Cast	Late Pleistocene	
	Shanidar (Iraq)	Shanidar 4	R	SHN	Original	Late Pleistocene	
	Tabun (Israel)	Tabun C 1	L	TBN	Cast	Late Pleistocene	
	Vindija Cave (Croatia)	Vi-209	L	VND	Original	Late Pleistocene	
<i>Homo neanderthalensis</i> from Vindija ($N = 1$)	Abri Pataud (France)	Abri Pataud 26 230 A	R	AP	Original	Late Pleistocene	
Late Pleistocene <i>Homo sapiens</i> ($N = 11$)	Dolni Věstonice (Czech Republic)	Dolní Věstonice 3	R	D1	Original	Late Pleistocene	
		Dolní Věstonice 13	R, L	D2r, l	Original	Late Pleistocene	
		Dolní Věstonice 14	R, L	D3r, l	Original	Late Pleistocene	
		Dolní Věstonice 16	L	D4	Original	Late Pleistocene	
	Monte Circeo (Italy)	Bosellone 2	L	PS	Original	Late Pleistocene	
	Gough's Cave (England)	Gough's Cave 1 118	L	GC	Original	Pleistocene/Holocene	
	Bonn-Oberkassel (Germany)	Oberkassel 1	L	O1	Cast	Late Pleistocene	
		Oberkassel 2	R	O2	Cast	Late Pleistocene	
Recent <i>Homo sapiens</i> Puegians ($N = 14$)	Strait of Magellan (Chile)	Ruegian 4	R, L	F1 r, l	Original	Holocene	
		Ruegian 5	R, L	F2 r, l	Original	Holocene	
		Ruegian 6	R, L	F3 r, l	Original	Holocene	
		Ruegian 7	R, L	F4 r, l	Original	Holocene	
		Ruegian 8	R, L	F5 r, l	Original	Holocene	
		Ruegian 9	R, L	F6 r, l	Original	Holocene	
		Ruegian 13	R, L	F7 r, l	Original	Holocene	
		Alfedena 126	R, L	A1 r, l	Original	Holocene	
		Alfedena 128	L	A2	Original	Holocene	
		Alfedena 130	R, L	A3 r, l	Original	Holocene	
		Alfedena 132	R, L	A4 r, l	Original	Holocene	
Recent <i>Homo sapiens</i> Iron Age Italians ($N = 7$)	Alfedena (Italy)	Iezzan 3333	L	G1	Original	Holocene	
		Iezzan 3334	R, L	G2 r, l	Original	Holocene	
		Iezzan 3337	R	G3	Original	Holocene	
		Iezzan 3338	L	G4	Original	Holocene	
		Iezzan 3347	R	G5	Original	Holocene	
Recent <i>Homo sapiens</i> Garamantes ($N = 6$)	Iezzan (Libya)	SLV 90 5	R, L	L1 r, l	Original	Holocene	
		SLV T-84 3	R, L	L2 r, l	Original	Holocene	
		SLV T-86 17	R, L	L3 r, l	Original	Holocene	
		SLV T-89 8	R, L	L4 r, l	Original	Holocene	

Tableau 46. Liste des spécimens inclus dans l'analyse. Tableau tiré de DI VINCEZO F., CHURCHILL S. E., et MANZI G., 2012. The Vindija Neanderthal scapular glenoid fossa: Comparative shape analysis suggests evo-devo changes among Neanderthals, *Journal of Human Evolution*, 62, p. 276.

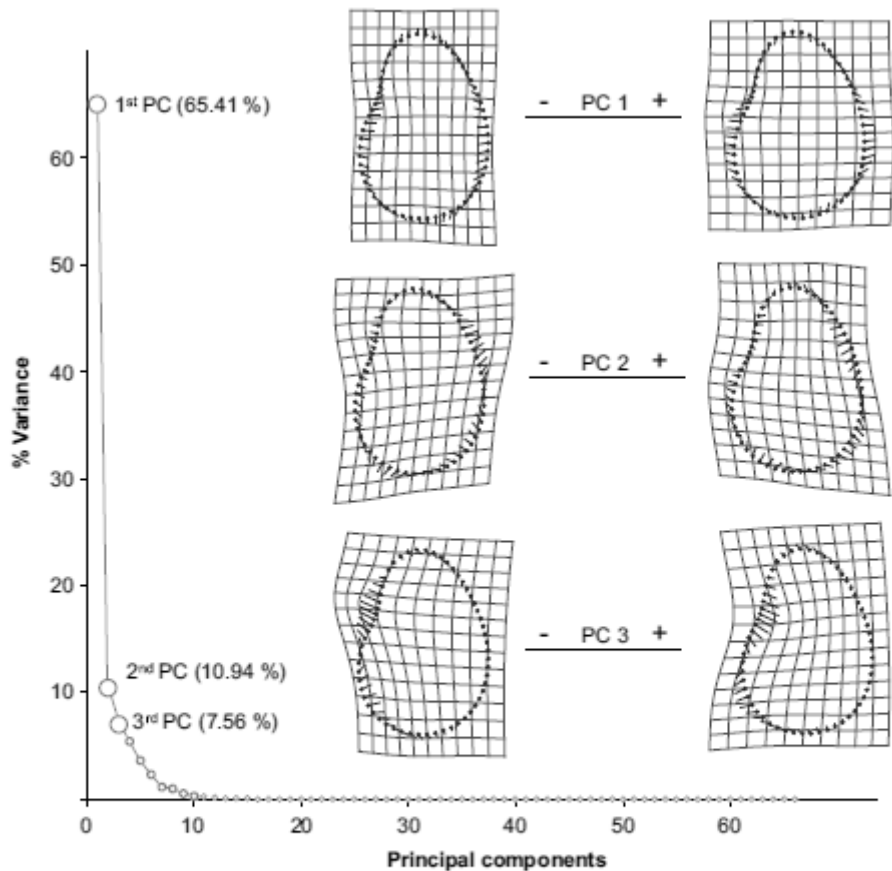


Figure 2. Variance explained by each principal component of the PCA. For the first three principal components, the extreme shape variations are visualized by thin-plate-spline deformation grids and vectors of change from the consensus configuration (dotted outlines).

Fig. 123. La variance expliquée par chaque composant principal de la PCA. Image et légende tirées de DI VINCEZO F., CHURCHILL S. E., et MANZI G., 2012. The Vindija Neanderthal scapular glenoid fossa: Comparative shape analysis suggests evo-devo changes among Neanderthals, *Journal of Human Evolution*, 62, p. 277.

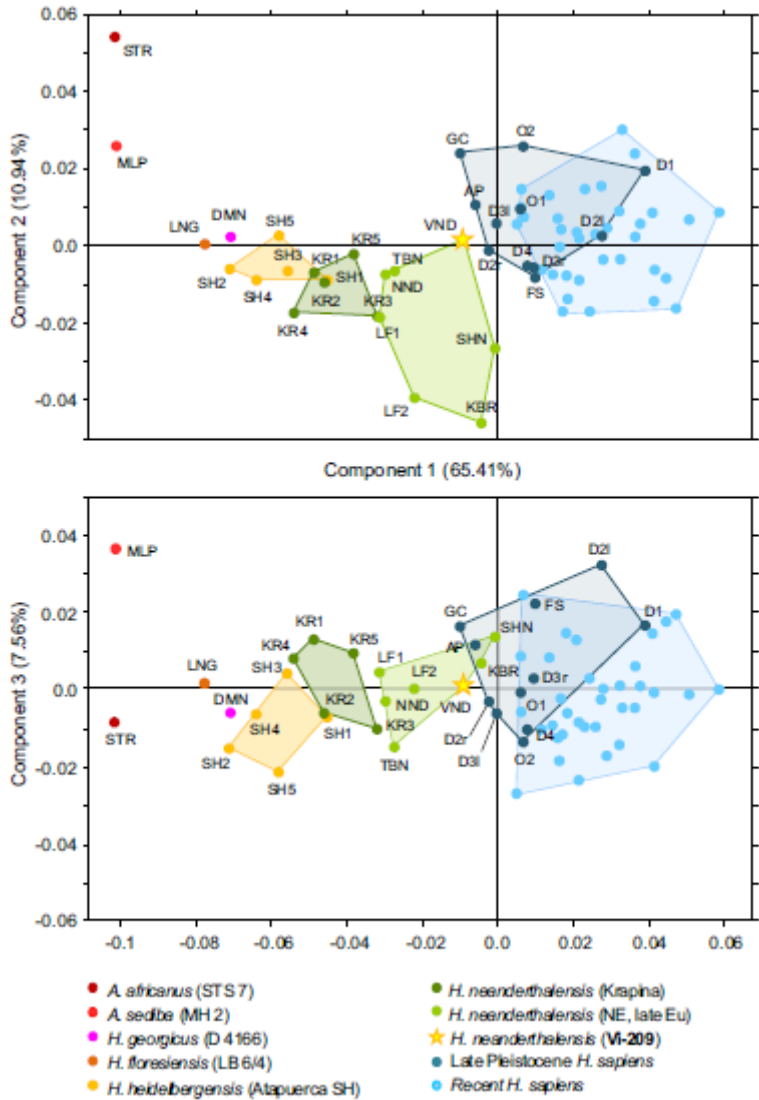


Fig. 124. Résultats de la PCA, avec PC1 vs. PC2 (au-dessus) et PC1 vs. PC3 (en-dessous). Image tirée de DI VINCEZO F., CHURCHILL S. E., et MANZI G., 2012. The Vindija Neanderthal scapular glenoid fossa: Comparative shape analysis suggests evo-devo changes among Neanderthals, *Journal of Human Evolution*, 62, p. 278.

Specimen		8 OTUs ^a		4 OTUs ^b
Vi-209	LP <i>H. sapiens</i>	(71.0%)	LP <i>H. sapiens</i>	(91.9%)
Krapina 127	Atapuerca SH	(67.2%)	<i>H. heidelbergensis</i>	(88.5%)
Krapina 129	Atapuerca SH	(67.2%)	<i>H. heidelbergensis</i>	(88.5%)
Krapina 130	LEuNE Neanderthals	(68.9%)	<i>H. neanderthalensis</i>	(93.4%)
Krapina 131	Atapuerca SH	(72.1%)	<i>H. neanderthalensis</i>	(91.8%)
Krapina 133	LEuNE Neanderthals	(85.2%)	<i>H. neanderthalensis</i>	(91.8%)
La Ferrassie 1	LEuNE Neanderthals	(67.2%)	<i>H. neanderthalensis</i>	(91.8%)
La Ferrassie 2	LEuNE Neanderthals	(70.5%)	<i>H. neanderthalensis</i>	(91.8%)
Neandertal 1	Krapina Neanderthals	(72.1%)	<i>H. neanderthalensis</i>	(91.8%)
Kebara 2	LEuNE Neanderthals	(68.9%)	<i>H. neanderthalensis</i>	(91.8%)
Tabun C1	Krapina Neanderthals	(70.5%)	<i>H. neanderthalensis</i>	(91.8%)
Shanidar 4	LEuNE Neanderthals	(70.5%)	<i>H. neanderthalensis</i>	(91.8%)

Reported data summarize the classification of each Neanderthal specimen when it was not assigned a priori to any OTU. Number in parentheses (%) indicate how many specimens of each group are correctly classified. Each analysis was performed twice using the following a priori groups.

^a 8 OTUs: Atapuerca Sima de los Huesos (SH); Krapina Neanderthals; Late European and Near-Eastern Neanderthals; Late Pleistocene *H. sapiens*; Fuegians; Iron Age Italians; Garamantes; Lombards.

^b 4 OTUs: *H. heidelbergensis*; *H. neanderthalensis*; Late Pleistocene *H. sapiens*; recent *H. sapiens*.

Tableau 47. Analyse discriminante (DA) identifiant tous les *H. neandertaliensis*. Tableau tiré de DI VINCEZO F., CHURCHILL S. E., et MANZI G., 2012. The Vindija Neanderthal scapular glenoid fossa: Comparative shape analysis suggests evo-devo changes among Neanderthals, *Journal of Human Evolution*, 62, p. 279.

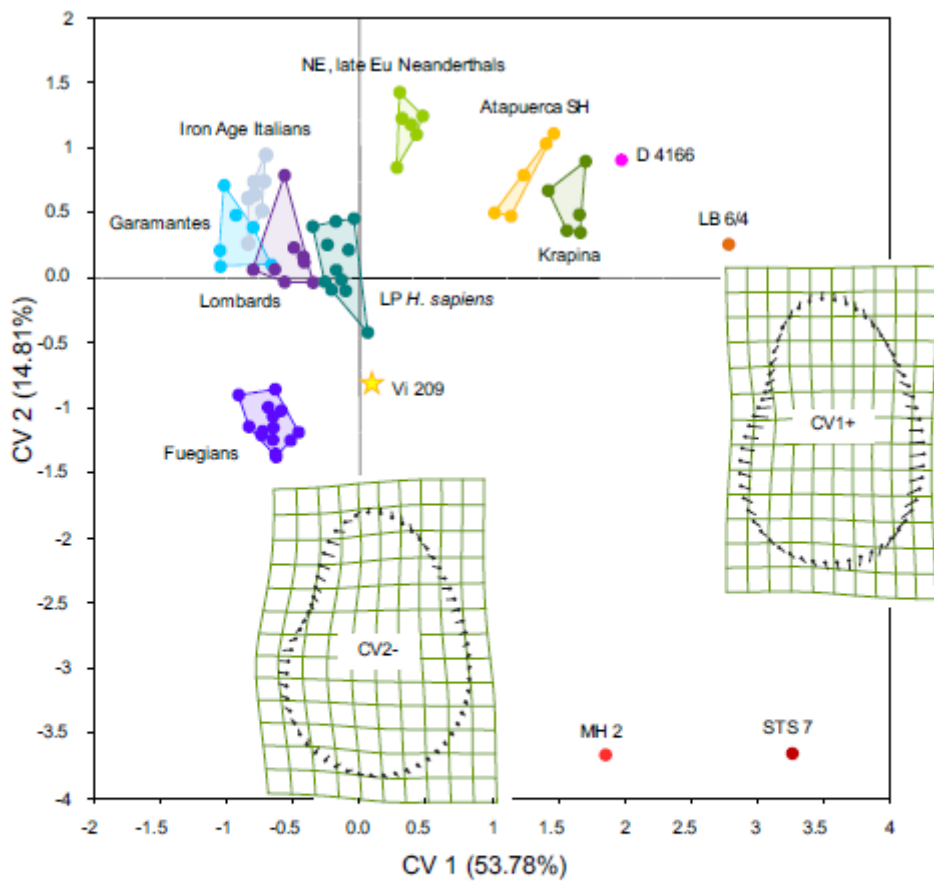
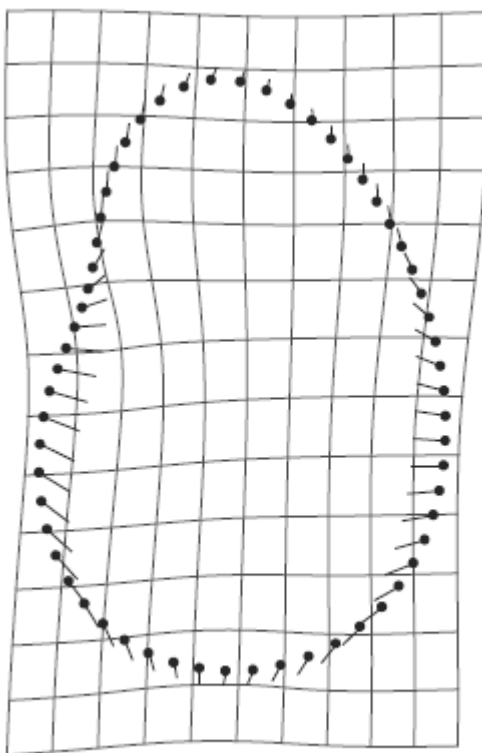
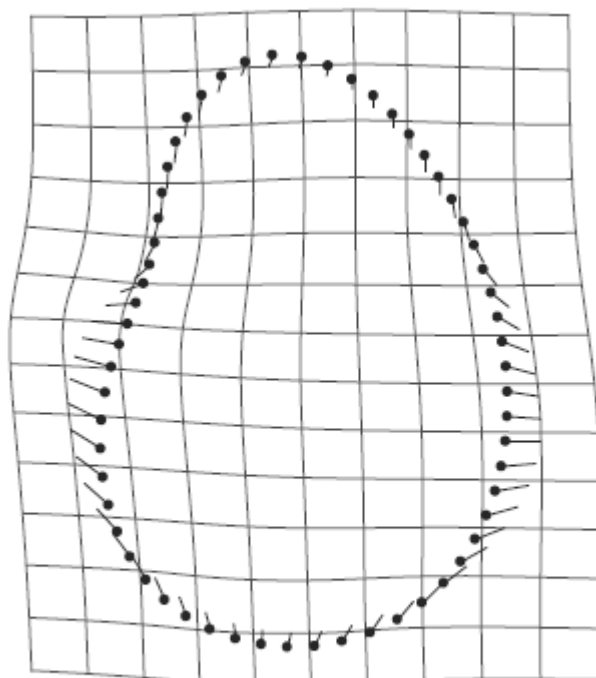


Figure 4. Plot of the entire SGF sample grouped into a priori OTUs within the space of the first two canonical variates (74.25% of the total variance explained). Thin-plate-spline deformation grids and shape transformation vectors show shape changes moving from the consensus (origin of axes) to positive and negative extremes of CV1 and CV2 respectively. Symbols as in Fig. 3.

Fig. 125. Résultats de la CVA de l'ensemble des échantillons des cavités glénoïdales analysées. Image et légende tirées de DI VINCEZO F., CHURCHILL S. E., et MANZI G., 2012. The Vindija Neanderthal scapular glenoid fossa: Comparative shape analysis suggests evo-devo changes among Neanderthals, *Journal of Human Evolution*, 62, p. 279.



CS = 2.53



CS = 2.67

Fig. 126. Comparaison entre la cavité glénoïde néandertalienne (gauche) et modern (droite) vs. consensus général (origine des axes de la PCA). La configuration des points de repère représente le consensus, tandis que les vecteurs et la grille décrivent le schéma de variation respectif. Image tirée de DI VINCEZO F., CHURCHILL S. E., et MANZI G., 2012. The Vindija Neanderthal scapular glenoid fossa: Comparative shape analysis suggests evo-devo changes among Neanderthals, *Journal of Human Evolution*, 62, p. 280.

First Cervical Vertebra

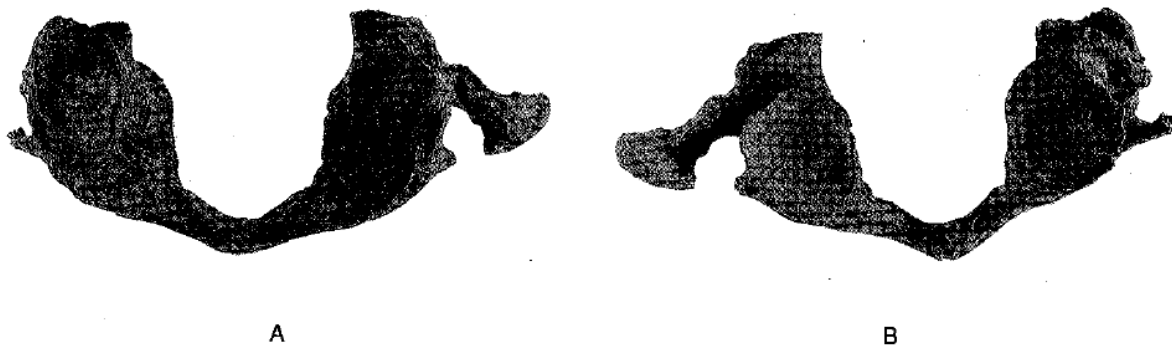


Fig. 127. Atlas de KMH 2, Kebara. Photo tirée d'ARENSBURG B., 1991. The vertebral column, thoracic cage and hyoid bone, dans BAR-YOSEF O. et VANDERMEERSCH B. (éds.), 1991. *Le squelette moustérien de Kebara 2*, Paris, annexe, p. 1.

Second Cervical Vertebra

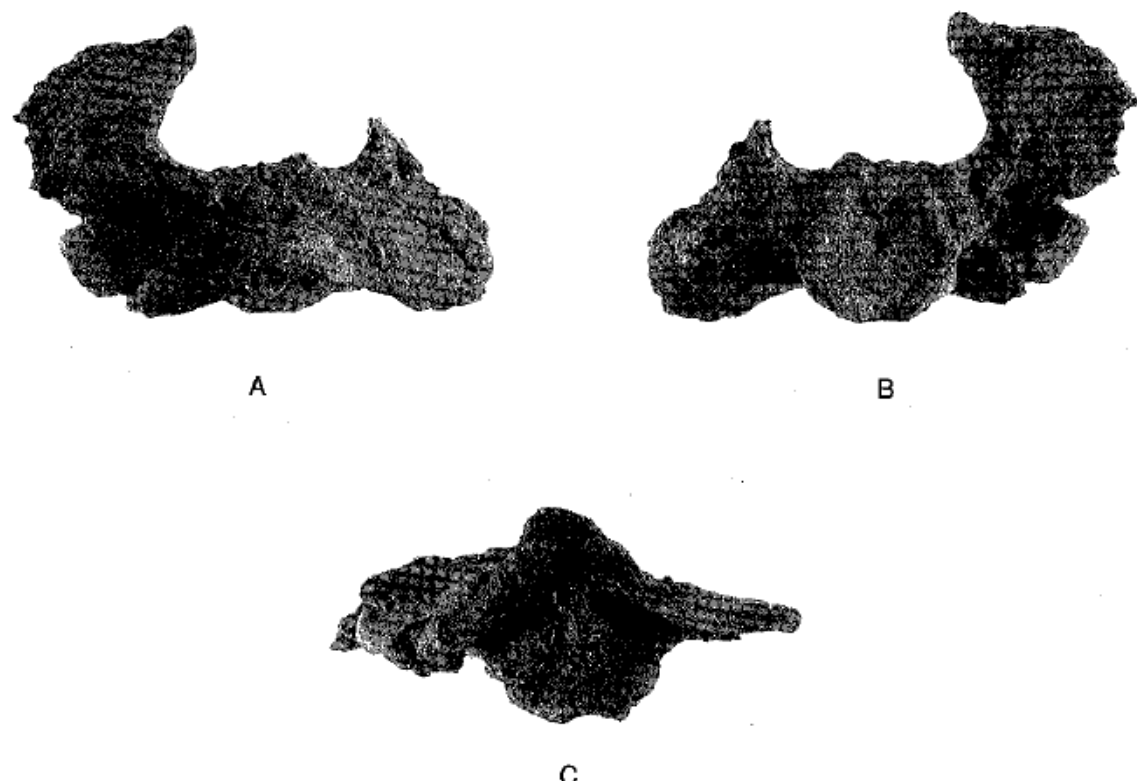


Fig. 128. Axis de KMH 2, Kebara. Photo tirée d'ARENSBURG B., 1991. The vertebral column, thoracic cage and hyoid bone, dans BAR-YOSEF O. et VANDERMEERSCH B. (éds.), 1991. *Le squelette moustérien de Kebara 2*, Paris, annexe, p. 1.

Diameter (mm)	Kebara** (Israel)	Mousterian Shanidar II (Trinkaus, 1983)	Skhul V (McCown and Keith, 1939)	Natufians**	Modern Males (Stewart, 1962)	Modern Euro- american males (Lanier, 1939)
Transverse, diameter maximum	82.0*	—	—	69.0-77.0	—	72.0-93.0
Transverse, between sup. articular processes	50.0	(51.0)	46.0 (?)**	43.0-45.0	—	—
Transverse, between inf. articular processes	47.5	(58.4)	47.0**	40.0-43.5	—	—
Vertebral canal, diameter transverse	27.5	ca. 34.0	30.0 (31.0)	24.0-28.0	26.0-32.5	23.5-39.0
Vertebral canal diameter dorso-ventral	ca. 32.0-35.0	ca. 36.5 (43.0)	38.0 (33.5)	29.0-33.0	31.0-36.0	15.4-28.0
Anterior arc length between sup. articular facets	20.0	—	ca. 24.0**	14.0-15.0	—	—
Anterior arc length in midline	10.8	—	11.0**	10.0-12.0	—	8.8-14.0
Anterior arc dorso-ventral in midline	4.5	—	ca. 6.5**	5.2-6.2	—	—
Atlanto-odontoid facet height	9.5	—	10.0**	10.0-11.0	—	—
Atlanto-odontoid facet transverse	12.5	—	11.0**	11.0	—	—
Major axis superior artic facets	22.0	ca. (25.0)	28.3 (21.0)	22.5-24.0	18.0-27.0	—
Major axis 90° of above	12.0	(10.0)	10.5**	12.0-13.0	9.0-17.0	—
Major axis inf. articular facet transverse	15.0	15.0-17.0***	14.0	14.0-15.0***	15.0-20.0***	—
Major axis inf. articular facet dorso-ventral	17.4	18.0-19.0***	(16.5-19.0)***	18.0-19.0***	14.5-20.5**	—

* Calculated from left complete side.

() Corrected from original by Stewart, 1962.

** Measured by present author.

*** Range between right and left sides.

Tableau 48. Comparaison de l'atlas de Kebara avec ceux des autres sites et périodes. Tableau tiré d'ARENDSBURG B., 1991. The vertebral column, thoracic cage and hyoid bone, dans BAR-YOSEF O. et VANDERMEERSCH B. (éd.), 1991. *Le squelette moustérien de Kebara 2*, Paris, p. 116.

Diameter (mm)	Kebara	Shanidar III (Trinkaus, 1983)	Skhul V (McCown and Keith, 1939)	Qafzeh 3 (Vander- meersch 1981)	Regour- dou I (Piveteau 1966)	La Ferras- sic I (Piveteau, 1966)	Natufians	Modern males (Stewart 1962)	Modern Eurame- rican males (Lanier, 1939)
Transverse diameter between sup. articular processes	ca. 50.0	51.2	44.5**	—	—	—	41.5-42.5	—	—
Transverse diameter vertebral foramen	25.0	27.5 (?)	26.0 (26.5)	—	—	—	22.0-24.0	20.0-26.0	19.0-27.6
Body ventral height	15.0	20.6	18.0**	ca. 18.0	20.5	24.5	15.0-17.0	—	—
Body dorsal height	13.0	15.7	13.0 (?)**	—	—	—	18.0-20.0	—	—
Body inferior dorso-ventral diameter	17.0	16.0	(16.0)	ca. 12.5	17.5	19.5	14.0	14.0-19.5	13.5-19.2
Body inferior transverse diameter	18.0	19.5	20.5 (19.0)	17.5	18.5	22.0	19.0-20.0	17.5-20.5	16.0-21.7

The sources for the data are the same as noted in Table I.

Tableau 49. Comparaison et mesures (en mm) de l'axis de Kebara. Tableau tiré d'ARENDSBURG B., 1991. The vertebral column, thoracic cage and hyoid bone, dans BAR-YOSEF O. et VANDERMEERSCH B. (éd.), 1991. *Le squelette moustérien de Kebara 2*, Paris, p. 117.

Site	C2	
	Dorsal	Ventral
Kebara**	13.5	15.0
Shanidar I (Trinkaus, 1983)	—	—
Shanidar II (Trinkaus, 1983)	15.7	20.6
Shanidar IV (Trinkaus, 1983)	—	—
Skhul V (McCown, and Keith 1939)	13.0	18.0
Regourdou I (Piveteau, 1966)	—	—
Krapina (Trinkaus, 1983)	—	—
Natufians	18.0-20.0	15.0-17.0
Modern males (Stewart, 1962)	—	—
Modern males (Lanier, 1939)	—	—

Tableau 50. Tableau partiel de comparaison de la hauteur du corps vertébral, dorsal et ventral, de la vertèbre cervicale C2 de Kebara avec celles d'autres sites et périodes. Tableau tiré d'ARENSBURG B., 1991. The vertebral column, thoracic cage and hyoid bone, dans BAR-YOSEF O. et VANDERMEERSCH B. (éds.), 1991. *Le squelette moustérien de Kebara 2*, Paris, p. 127.

Site or period	Total height (mm) C2 = C7				
	Dorsal	Ventral	Dens included	Height (mm.) C4-C6	Height (mm.) C5-C7
Kebara	67.5	70.8	85.8	31.8	33.8
Shanidar I	—	—	—	—	32.9
Shanidar II	80.2	78.0	108.0**	34.0	36.0
Shanidar IV	—	—	—	29.8	—
Skhul V	ca. 68.5	ca. 68.5	86.5	28.0	32.0
La Chapelle	—	—	—	—	34.0
Regourdou I	—	—	—	32.0	32.9
La Ferrassie	—	—	—	33.6	—
Natufians	—	71.0	87.0-92.0	30.5	32.0
Recent	78.0	—	98.0-121.0	33.5-40.6	35.5-40.2

* All measurements except Kebara and Natufians are according to Trinkaus, 1983.

** In Trinkaus, 1983 (Tables 25 and 26) the vertebral body height of C2 in Shanidar II is 20.6 mm, and of the dens 18 mm, giving to the axis a total height of 38.6 mm and to the whole cervical column (C2-C7) 103.1, not 108.0 as given. It must be noted that this latter figure is reached by combining the highest dorsal and ventral measurements of the vertebral bodies. It may also be noted that the values given by McCown (1939), Stewart, (1962) and Trinkaus (1983) on the same individuals differ significantly, probably due to the methods used by each author.

Tableau 51. Hauteurs complètes et partielles de la colonne cervicale parmi les Moustériens et autres groupes. Tableau tiré d'ARENNSBURG B., 1991. The vertebral column, thoracic cage and hyoid bone, dans BAR-YOSEF O. et VANDERMEERSCH B. (éds.), 1991. *Le squelette moustérien de Kebara 2*, Paris, p. 128.

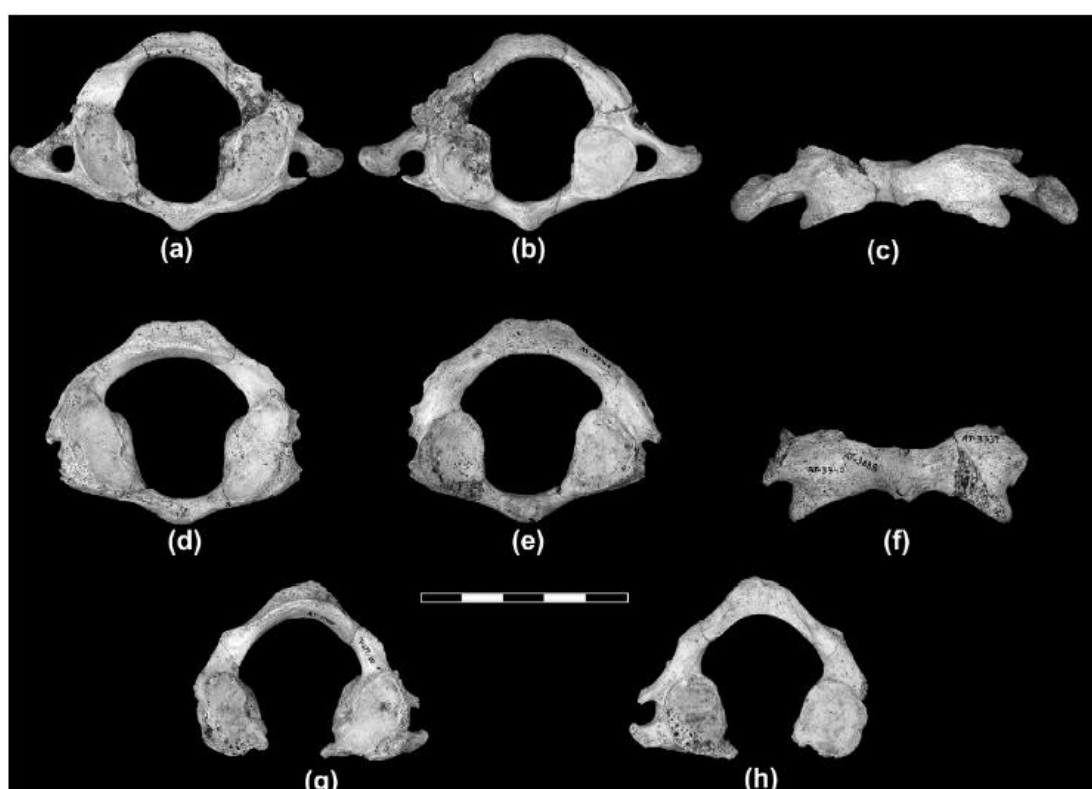


Fig. 129. Atlas complets ou quasi complets de Sima de los Huesos. Vues crâniale (a), caudale (b) et ventrale (c) de VC3. Vues crâniale (d), caudale (e) et ventrale (f) de VC7. Vues crâniale (g) et caudale (h) de VC16. L'échelle représente 5cm. Photo tirée de GOMEZ-OLIVENCIA A., CARRETERO J.M., et ARSUAGA J.L. (et al.), 2007. Metric and Morphological Study of The Upper Cervical Spine from the Sima de los Huesos Site (Sierra de Atapuerca, Burgos, Spain), *Journal of Human Evolution*, 53, p. 11.

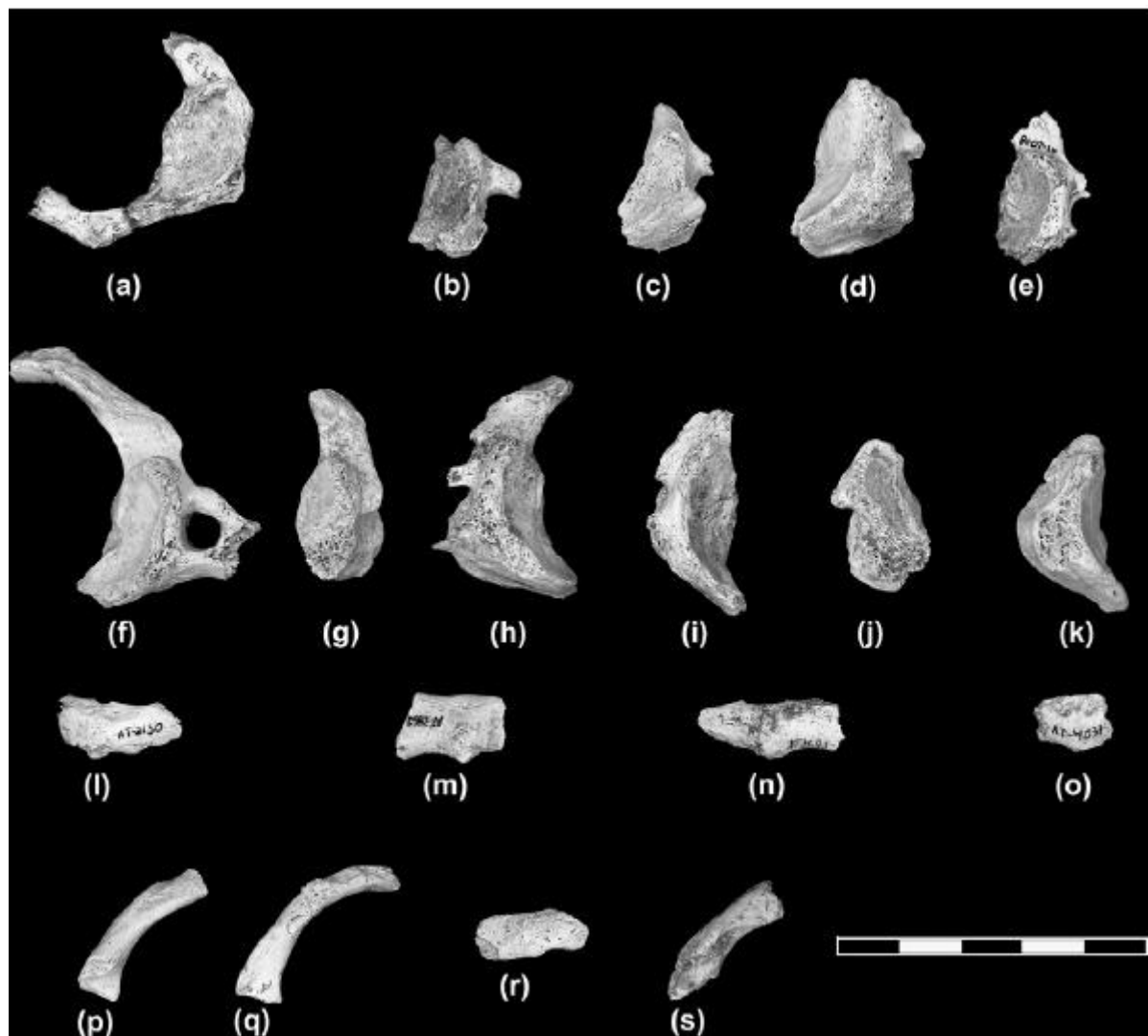


Fig. 130. Atlas fragmentaires de Sima de los Huesos. Vues crâniales de VC17 (a), AT – 269 (b), AT – 326 (c), AT – 1818 (d), AT – 2078 (e), AT – 2584 (f), AT – 3003 (g), AT – 3013 (h), AT – 3694 (i), AT – 3971 (j), et AT – 3985 (k). Vues dorsalis d'AT – 2130 (l), AT – 2852 (m), AT – 3693 (n), et AT – 4037 (o). Vues crâniales d'AT – 2264 (p), AT – 3687 (q), AT – 3691 (r), et AT – 3992 (s). L'échelle représente 5cm. Photo tirée de GOMEZ-OLIVENCIA A., CARRETERO J.M., et ARSUAGA J.L. (et al.), 2007. Metric and Morphological Study of The Upper Cervical Spine from the Sima de los Huesos Site (Sierra de Atapuerca, Burgos, Spain), *Journal of Human Evolution*, 53, p. 12.

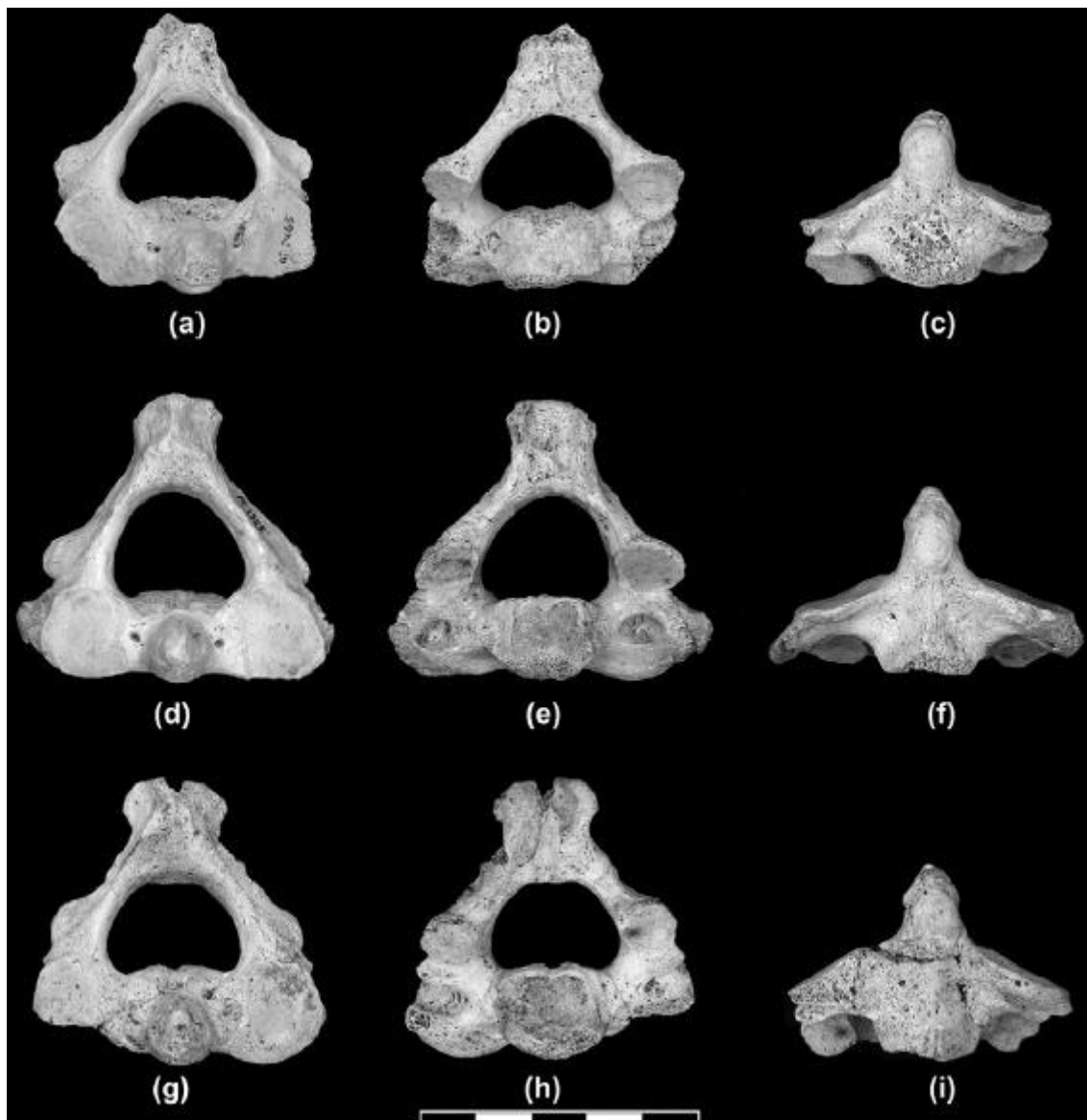


Fig. 131. Axis adultes complets de Sima de los Huesos. Vues crâniale (a), caudale (b) et ventrale (c) de VC2. Vues crâniale (d), caudale (e), et ventrale (f) de VC4. Vues crâniale (g), caudale (h), et ventrale (i) de VC8. L'échelle représente 5cm. Photo tirée de GOMEZ-OLIVENCIA A., CARRETERO J.M., et ARSUAGA J.L. (et al.), 2007. Metric and Morphological Study of The Upper Cervical Spine from the Sima de los Huesos Site (Sierra de Atapuerca, Burgos, Spain), *Journal of Human Evolution*, 53, p. 13.

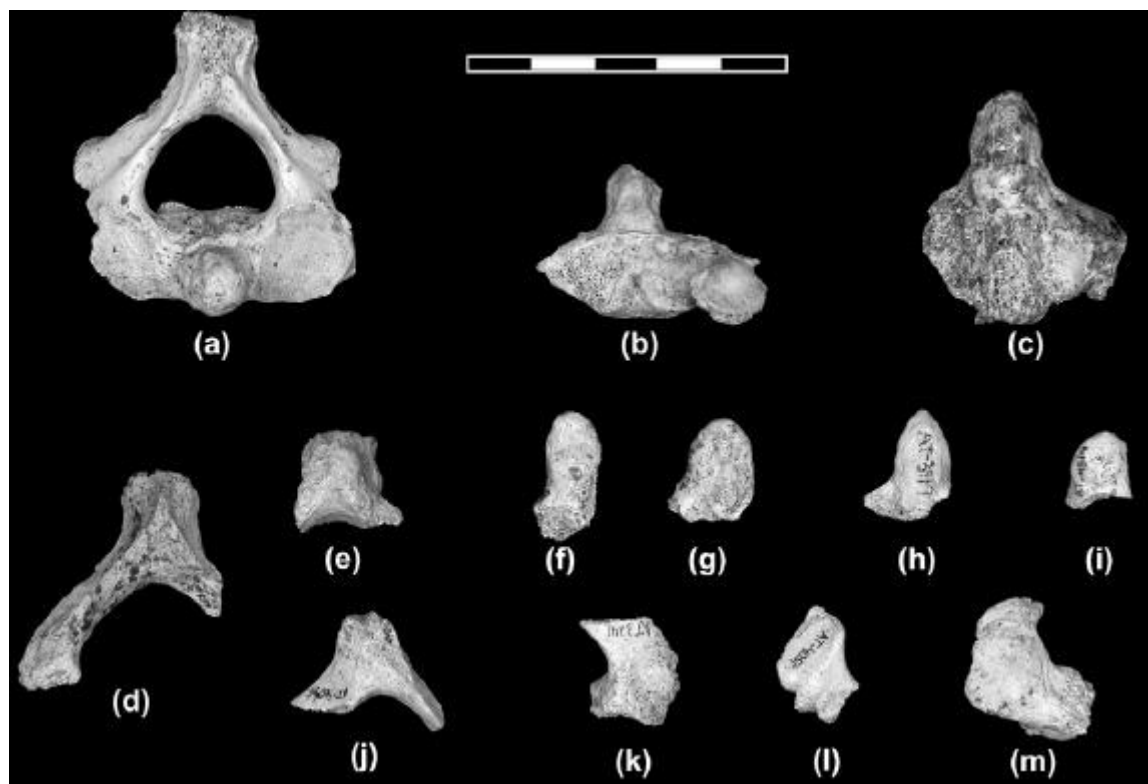


Fig. 132. Axis incomplets ou immatures de Sima de los Huesos. Vue crâniale de VC28 (a), vues dorsale d'AT – 1573 (b) et AT – 2289 (c). Vues crâniale d'AT – 150 (d), et AT – 4662 (e). Vues ventrale d'AT – 2883 (f), AT – 3696 (g), AT – 3979 (h), et AT – 4314 (i). Vues crâniale d'AT – 4046 (j) et AT – 4187 (k). L'échelle représente 5cm. Photo tirée de GOMEZ-OLIVENCIA A., CARRETERO J.M., et ARSUAGA J.L. (et al.), 2007. Metric and Morphological Study of The Upper Cervical Spine from the Sima de los Huesos Site (Sierra de Atapuerca, Burgos, Spain), *Journal of Human Evolution*, 53, p. 14.

Specimen/sample	Species	Sex	Original/cast	Location
ATD6-90 (C1) Krapina (C1, n = 3; C2, n = 3)	<i>H. antecessor</i> <i>H. neanderthalensis</i>	Female ?	Original Original	Museo de Burgos, Burgos (Spain) Croatian Natural History Museum, Zagreb (Croatia)
La Chapelle-aux-Saints (C1 and C2)	<i>H. neanderthalensis</i>	Male	Original	Musée de l'Homme, Paris (France)
La Ferrassie 1 (C1 and C2)	<i>H. neanderthalensis</i>	Male	Original	Musée de l'Homme, Paris (France)
Shanidar 2 (C1 and C2)	<i>H. neanderthalensis</i>	Male	Cast	Musée de l'Homme, Paris (France)
Skhul V (C1 and C2)	<i>H. sapiens</i>	Male	Original	Peabody Museum of Archaeology and Ethnology, Cambridge (MA, USA)
Arcy-sur-Cure, Grotte des Fées (C1 and C2)	<i>H. sapiens</i> (?) ¹	?	Original (C1) Cast (C2)	Musée de l'Homme, Paris (France) (C1) Institut de Paléontologie Humaine, Paris (France) (C2)
Cro-Magnon (C1)	<i>H. sapiens</i>	Male	Original	Musée de l'Homme, Paris (France)
Carolingian ² (C2, n = 4)	<i>H. sapiens</i>	?	Original	Musée de l'Homme, Paris (France)
Neolithic ³ (C2, n = 2)	<i>H. sapiens</i>	?	Original	Musée de l'Homme, Paris (France)
Afalou-Bou-Rhummel ⁴ (C1, n = 12; C2, n = 10)	<i>H. sapiens</i>	?	Original	Institut de Paléontologie Humaine, Paris (France)
Taforalt ⁵ (C1, n = 8; C2, n = 9)	<i>H. sapiens</i>	?	Original	Institut de Paléontologie Humaine, Paris (France)
Burgos ⁶ (n = 40)	<i>H. sapiens</i>	Males	Original	Laboratorio de Evolución Humana-University of Burgos, Burgos (Spain)
Hamman-Todd ⁷ (n = 101)	<i>H. sapiens</i>	50 males/51 females	Original	Cleveland Museum of Natural History, Cleveland (OH, USA)

¹ The Arcy-sur-Cure atlas was found in 1860 in the lower level of the Grotte des Fées, (Yonne, France). The axis was found in 1898 in the clearings of older excavations (Leroi-Gourhan, 1958). Leroi-Gourhan (1958) identified both specimens as Neandertal. In the case of the axis, the taxonomic assignment was based on the surface color of the fossil; Leroi-Gourhan pointed out that this specimen is within the modern human range of variation but that it resembles Neandertals in its weak cervical curvature. In the case of the atlas, he did not find any trait to distinguish it from modern humans. Due to the problematic provenience of both specimens and the fact that these fossils are morphologically more similar to our modern human comparative samples than to Neandertals, they should be cautiously considered as representing *H. sapiens*.

² The Carolingian sample comes from the Saint-Germain-des-Prés cemetery (Paris, France).

³ The Neolithic sample comes from a cave site in the Petit Morin Valley (France).

⁴ The Afalou-Bou-Rhummel sample was recovered from the homonymous rock-shelter in Algeria. This sample and the Taforalt sample are dated to >10,000 BP (see Irish, 2000, and references therein).

⁵ The Taforalt sample was recovered from the homonymous cave site in Morocco.

⁶ The Burgos sample comprises 40 contemporary adult (estimated age at death is 20–45 years) male individuals from Burgos, Spain.

⁷ The Hamann-Todd sample comprises 100 North American adults (50 Euro-Americans and 50 Afro-Americans, with equal sexual representation) from the Hamann-Todd Osteological Collection.

Tableau 52. Atlas et axis utilisés pour les mesures de GOMEZ-OLIVENCIA et al. Tableau et légende tirés de GOMEZ-OLIVENCIA A., CARRETERO J.M., et ARSUAGA J.L. (et al.), 2007. Metric and Morphological Study of The Upper Cervical Spine from the Sima de los Huesos Site (Sierra de Atapuerca, Burgos, Spain), *Journal of Human Evolution*, 53, p. 8.

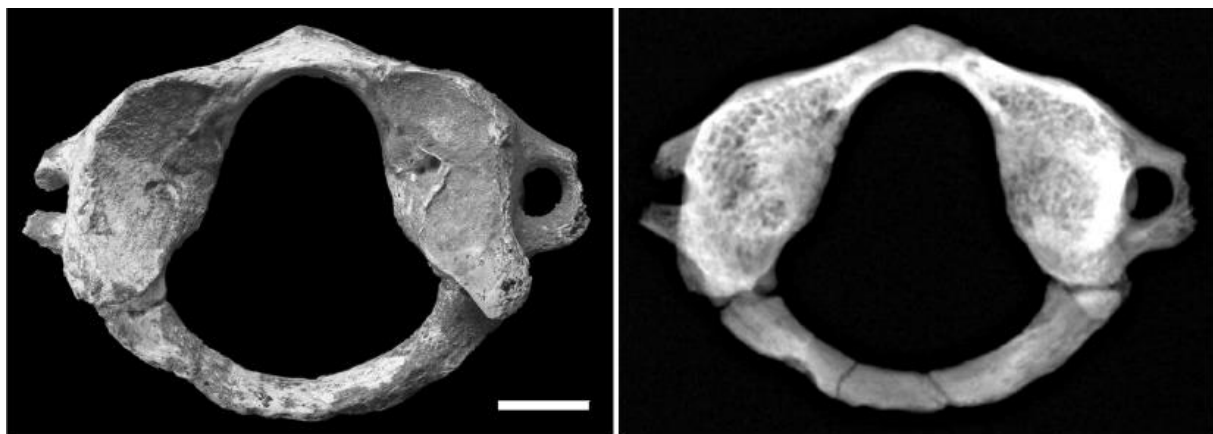


Fig. 133. Atlas SD – 1605/ 1595 d'El Sidron. Vue supérieure (gauche) et radiographie (droite). L'échelle représente 1cm. Photo tirée de RIOS L., ROSAS A., et ESTALRRICH A. (et al.), 2015. Possible Further Evidence of Low Genetic Diversity in the El Sidron (Asturias, Spain) Neandertal Group : Congenital Cleft of the Atlas, *PLoS One*, p. 5.

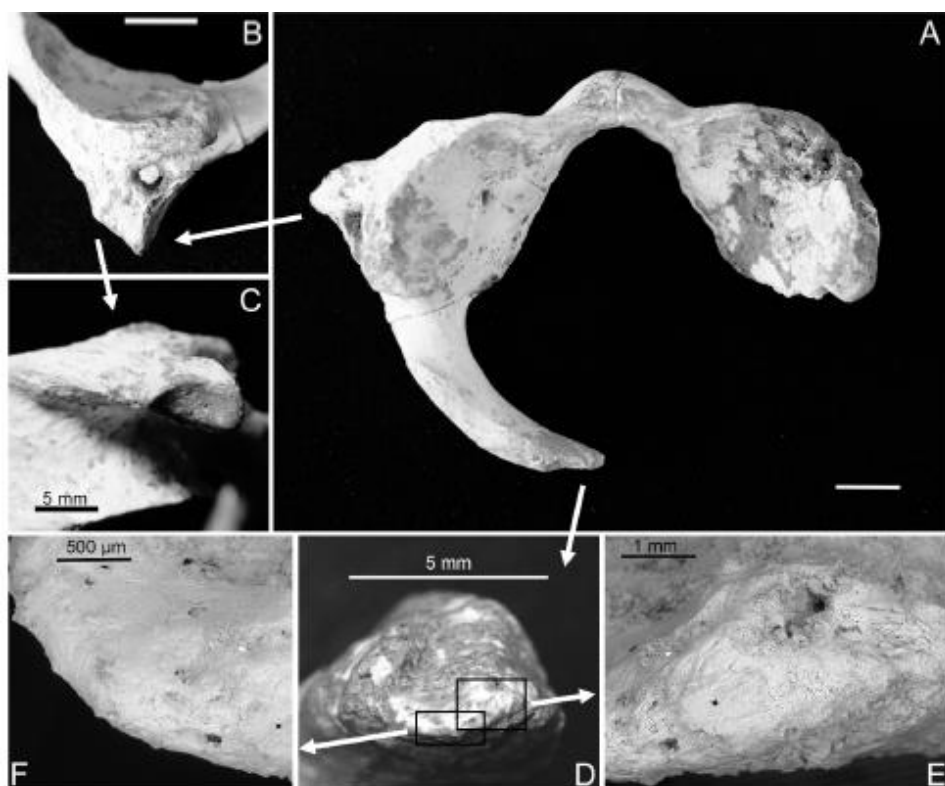


Fig. 134. Atlas SD – 1643 d'El Sidron. Vue supérieure (A), détail du foramen transverse gauche obstrué (B), et surface épiphyséale visible au sommet du processus transverse gauche (C). Vue médiale du sommet de la lamina gauche (pas de dommage et continuité de l'os cortical visibles, D). Image ESEM de l'os cortical (F), et image ESEM illustrant une autre surface du sommet avec continuité de l'os cortical (E). L'échelle représente 1cm. Photo tirée de RIOS L., ROSAS A., et ESTALRRICH A. (et al.), 2015. Possible Further Evidence of Low Genetic Diversity in the El Sidron (Asturias, Spain) Neandertal Group : Congenital Cleft of the Atlas, *PLoS One*, 10, p. 3.

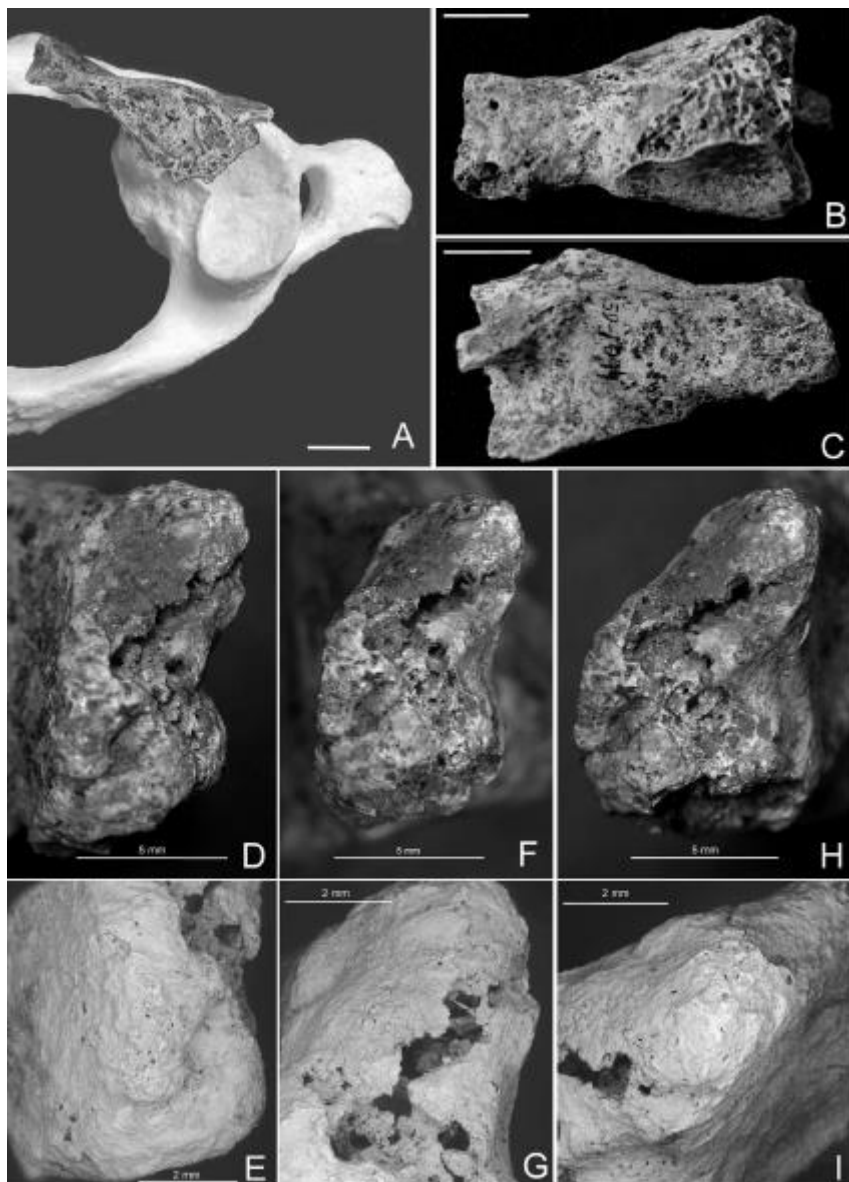


Fig 2. Atlas SD-1094. (A) Superior view of SD-1094, placed on its anatomical location within a modern human atlas, bar represents 1 cm. (B) Posterior view of SD-1094, the right superior and inferior articular surfaces can be observed. The facet for the dens of the axis can be observed in the anterior arch, bar represents 1 cm. (C) Anterior view of SD-1094, the beginning of the anterior tubercle of the transverse foramen can be observed on the left. (D) Medial anterior view of the midsagittal cleft, slightly tilted to superior in order to view its anterior inferior corner. Continuity of the cortical bone from the anterior to the sagittal surface can be observed. (E) ESEM image, with clearer view of the anterior inferior corner, with continuity of the cortical bone from the anterior to the sagittal surfaces. (F) Medial view of the anterior sagittal cleft. Cortical bone can be observed in the inferior and superior thirds. Bone breakage can be observed in the central third. (G) ESEM image, with clearer view of the cortical bone and the areas of bone breakage. (H) Medial posterior view with continuity of cortical bone from the posterior to the anterior surfaces of the posterior arch of the atlas. (I) ESEM image of the superior corner of the midsagittal cleft, with clearer view of the cortical continuity between the posterior and anterior surface along the sagittal cleft.

Fig. 135. Atlas SD – 1094 d'El Sidron. Photo et légende tirée de RIOS L., ROSAS A., et ESTALRRICH A. (et al.), 2015. Possible Further Evidence of Low Genetic Diversity in the El Sidron (Asturias, Spain) Neandertal Group : Congenital Cleft of the Atlas, *PLoS One*, 10, p. 4.

Homo sapiens ou les hommes anatomiquement modernes

Specimen	LuA-5228 Muierii 1 (scapula and tibia)	OxA-15529 Muierii 1 (cranium)	OxA-16252 Muierii 2 (temporal)	OxA-15554 <i>M. giganteus</i> molar (-0.9 m)	OxA-15530 <i>U. spelaeus</i> metapodial (-1.1/-1.2 m)
Radiocarbon age (^{14}C years BP)	30,150 ± 800	29,930 ± 170	29,110 ± 190	30,060 ± 280	40,850 ± 450
"Calendrical" age (cal years BP, based on CalPal 2005)	35,150 ± 908	35,257 ± 259	34,342 ± 457	35,367 ± 318	44,466 ± 677
$\delta^{13}\text{C}$	-20.0	-19.3	-19.3	-19.9	-20.3
C:N	-	3.4	3.3	3.5	3.3
Sample weight	437	420	240	520	640
Collagen weight (ultrafiltered gelatin yield)	-	56.0	26.8	13.1	52.2
Burnweight (gelatin combusted for graphitization)	-	6.0	5.4	5.6	5.3
%C (% carbon on combustion)	-	41.5%	41.7%	46.9%	43.4%
%N (% nitrogen on combustion)	-	13.3%	14.9%	16.1%	15.1%

LuA-5228 data are from Olariu et al. (8) and A. Olariu (personal communication). All weights are in milligrams. CalPal 2005: www.calpal.de.

Tableau 53. Résultats radiocarbone pour les restes humains et fauniques de Peștera Muierii, Baia de Fier, Roumanie. Tableau tiré de SOFICARU A., DOBOS A., et TRINKAUS E., 2006. Early modern humans from the Peștera Muierii, Baia de Fier, Romania, *PNAS*, 103, p. 17197.



Fig. 136. Scapula droite de Muierii 1. Vue latérale. La légère restauration du bord ventral de la cavité glénoïde est basée sur les contours de la cavité glénoïde et l'os situé sous la surface ventrale. L'échelle représente les mm/ cm. Photo tirée de SOFICARU A., DOBOS A., et TRINKAUS E., 2006. Early modern humans from the Peștera Muierii, Baia de Fier, Romania, *PNAS*, 103, p. 17200.

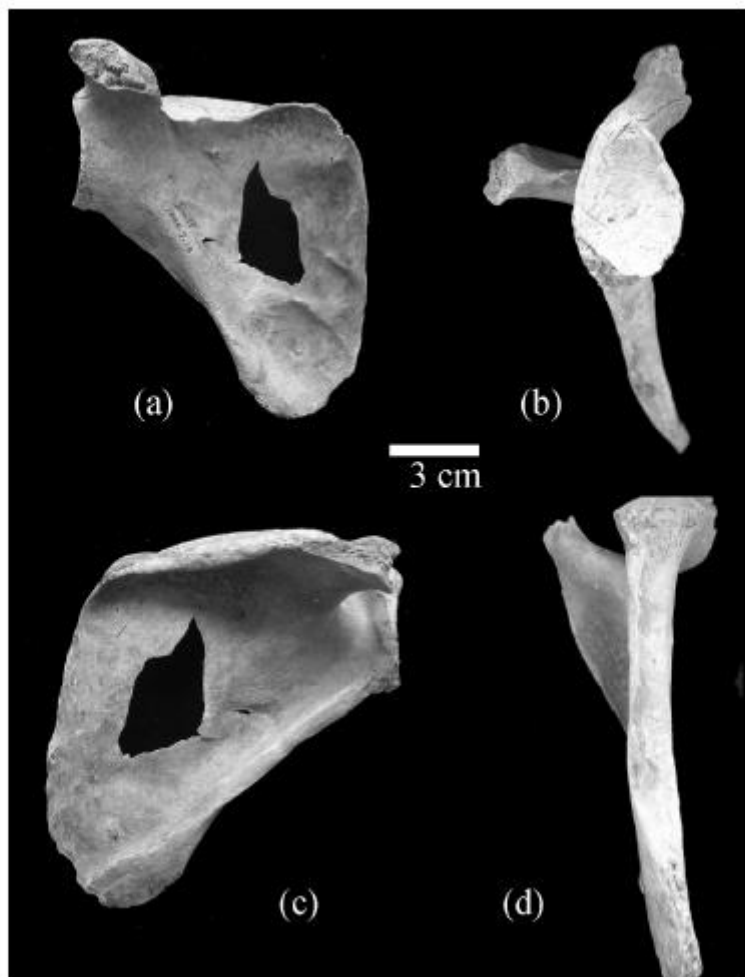


Fig. 137. Scapula droite de Salawusu, vue frontale (a), latérale avec la cavité glénoïde (b), occipitale (c), et vue latérale avec le bord axillaire (d). Photo tirée de SHANG H., LIU W., et WU X. (et al.), 2006. Upper Pleistocene human scapula from Salawusu, Inner Mongolia, China, *Chinese Science Bulletin*, 51, p. 2111.

Table 3 Glenoid fossa height (mm)

	Glenoid fossa height	SD	N	Sex
Salawusu s-11 ^{a)}	33		1	female
Neanderthals ^[23]	32.7—42.5		7	male
	30.5—33.1		2	female
Qafzeh 8 ^[23]	40.4		1	male
Qafzeh 9 ^[23]	36		1	female
European Early U.P. ^[23]	29.5—42.3		17	male
	33.2—38		6	female
European Late U.P. ^[23]	35.0—39.5		10	male
	32.0—34.0		8	female
Minatogawa I ^[19]	38		1	male
Minatogawa III ^[19]	33		1	female
Neolithic Japanese ^[19]	37.3	1.80	13	male
	31.6	2.94	15	female
Modern humans ^{[24]b)}	33.9	3.1	99	
Modern Chinese ^[20]	33.7		384	male
	33.48		308	female
Modern Chinese ^[22]	37.84	0.16	328	male
	33.64	0.2	159	female
Modern Chinese ^{a)}	34.6	1.7	65	
Modern Japanese ^[19]	35.1	1.80	30	male
	31.6	2.28	20	female

a) From the present authors; b) Euroamerican and Amerindian.

Tableau 54. Hauteur de la cavité glénoïde, comparatif. Tableau tiré de SHANG H., LIU W., et WU X. (et al.), 2006. Upper Pleistocene human scapula from Salawusu, Inner Mongolia, China, *Chinese Science Bulletin*, 51, p. 2113.

Table 4 Glenoid fossa breadth (mm)

	Glenoid fossa breadth	SD	N	Sex
Salawusu s-11 ^{a)}	22.3		1	female
Neanderthals ^[23]	21.8—30		8	male
	21—21.6		2	female
European Early U.P. ^[23]	21—29		17	male
	22.6—27		6	female
European Late U.P. ^[23]	24.2—28.9		8	male
	21.7—25.3		8	female
Minatogawa I ^[19]	26		1	male
Minatogawa III ^[19]	22		1	female
Neolithic Japanese ^[19]	26.2	1.34	12	male
	21.9	2.19	16	female
Modern humans ^{[24] b)}	24.9	2.2	99	
Modern Chinese ^[20]	26.83		384	male
	23.65		308	female
Modern Chinese ^[22]	27.6	0.12	328	male
	23.75	0.14	159	female
Modern Chinese ^{a)}	25.3	1.4	65	
Modern Japanese ^[19]	24.8	1.61	30	male
	21.1	1.21	20	female

a) From the present authors; b) Euroamerican and Amerindian.

Tableau 55. Largeur de la cavité glénoïde, comparatif. Tableau tiré de SHANG H., LIU W., et WU X. (et al.), 2006. Upper Pleistocene human scapula from Salawusu, Inner Mongolia, China, *Chinese Science Bulletin*, 51, p. 2113.

Table 5 Height - breadth index of glenoid fossa

	Indices (X or R)	SD	N	Sex
Salawusu s-11 ^{a)}	67.5		1	female
Neanderthals ^[24]	67.5	4.0	6	male
	65.4		2	female
Dolni Vestonic ^[18]	70.5—75.3		5	male
	84.3		1	female
Taforalt ^[25]	81(72.5—88.6)		24	male
Predmosti ^[23]	72.7	3.5	6	male
	71.1—77.1		4	female
Obercassel ^[25]	64		1	male
Minatogawa I ^[19]	68.4		1	male
Minatogawa III ^[19]	66.7		1	female
Neolithic Japanese ^[19]	70.5	1.87	11	male
	69.3	4.2	15	female
Modern humans ^{[24] b)}	73.1	3.4	46	male
	73.8	3.7	50	female
Modern Chinese ^[20]	74.41	0.6	84	male
	72.81	0.64	58	female
Modern Chinese ^[22]	72.56	0.36	337	male
	70.06	0.41	163	female
Modern Chinese ^{a)}	73.3	2.5	65	
Modern Japanese ^[19]	70.7	2.89	30	male
	67.1	4.85	20	female

a) From the present authors; b) Euroamerican and Amerindian.

Tableau 56. Indice hauteur/ largeur de la cavité glénoïde, comparatif. Tableau tiré de SHANG H., LIU W., et WU X. (et al.), 2006. Upper Pleistocene human scapula from Salawusu, Inner Mongolia, China, *Chinese Science Bulletin*, 51, p. 2114.

CERVICAL VERTEBRAE (C)							
	1011	B	504	5	2011	X7	Posterior arch.
C 1: Atlas	1013	B	504	5	2011	X7	Left articular mass.
	1042	B	504	5	2011	X7	Right articular mass.
	1014	B	504	5	2011	X7	Fragment of the body and odontoid process.
C 2: Axis	1002	B	504	5	2011	X8	Spinous process plus complete arch. Right lateral mass is missing.
	1611	D	504	6	2011	X7	Body and left articular facets.
C 5	1556	D	504	6	2011	X7	Right articular facets.
	1020	B	504	5	2010	X7	Articular facets and pedicle from the left side.
C 6	1022	B	504	5	2010	X7	Spinous process.
	1024	B	504	5	2010	X7	Vertebral body.
	1026	B	504	5	2010	X7	Right pedicle and articular facets.

SCAPULA							
	1636	D	504	6	2011	X7	Glenoid cavity + coracoid process + proximal axillary border.
	1673	D	504	6	2011	X7	Central portion of the spine.
Left side	1562	D	504	6	2011	X7	Vertebral (medial) portion of a left scapular spine.
	1563	C	504	6	2011	X7	Lateral (axilar) portion of a left scapular spine.
	1625	D	504	6	2011	X7	Small fragment a left scapular glenoid cavity.

Tableau 57. Inventaire des cervicales et scapulas découvertes à El Miron Cave, Espagne. Tableau tiré de CARRETERO . M., QUAM R. M., et GOMEZ-OLIVENCIA A. (et al.), 2015. The Magdalenian human remains from El Miron Cave, Cantabria (Spain), *Journal of Archaeological Science*, 60, annexe, pp. 4 et 7.

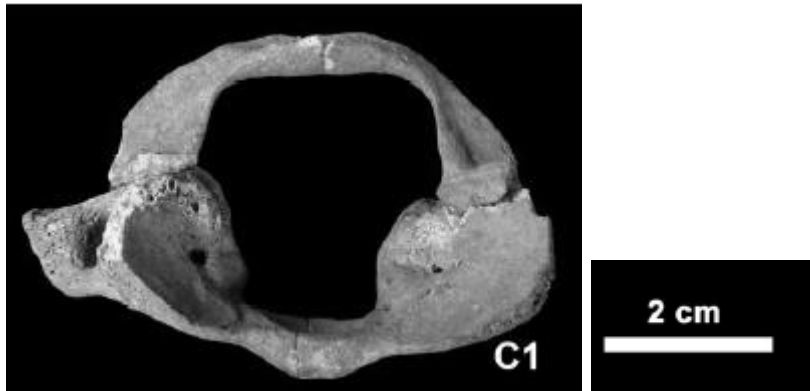


Fig. 138. Atlas d'El Miron 1, Cantabria. Photo tirée de CARRETERO . M., QUAM R. M., et GOMEZ-OLIVENCIA A. (et al.), 2015. The Magdalenian human remains from El Miron Cave, Cantabria (Spain), *Journal of Archaeological Science*, 60, annexe, p. 22.

Variable	El Mirón	Recent females				
		Mean	SD	Min	Max	n
Maximum dorso-ventral diameter (MaxDVDi)	39.6	43.1	2.5	38.2	50.2	34
Maximum transverse diameter (MaxTrDi)	(69.0)	71.9	3.9	62.7	79.4	30
Superior transverse diameter (SupTrDi)	(47.0)	46.8	2.4	41.8	52.3	34
Inferior transverse diameter (ITrDi)	42.1	44.1	2.6	37.7	50.6	34
Canal dorso-ventral diameter (M10)	28.3	30.2	2.0	27.4	34.2	34
Canal transverse diameter (M11)	27.9	28.4	2.2	25.6	34.6	34
Distance between the tuberosities for attachment of transverse ligament (DtTubTrLg)	15.3	16.2	2.9	12.7	28.5	34
Maximum crano-caudal diameter of the anterior tubercle (MaxCrCdDiAntA)	9.7	10.0	1.0	7.6	12.8	34
Maximum dorso-ventral diameter (thickness) of the anterior tubercle of the atlas (MaxDVDiAntTub)	6.6	6.0	0.6	5.0	7.8	34
Maximum transverse diameter for the facet for the dens (MaxTrDiFaDn)	<u>12.4*</u>	9.3	1.5	5.7	12.0	31
Maximum crano-caudal diameter (height) of lateral mass of the atlas (MaxCrCdDiLMa)	-/19.5	19.7	1.8	15.1	23.5	33
Maximum crano-caudal diameter of posterior tubercle of the atlas (MaxCrCdDiPTub)	9.7	9.1	1.4	5.8	12.9	32
Maximum dorso-ventral diameter of the posterior tubercle of the atlas (MaxDVDiPTub)	4.6	6.4	2.0	3.1	11.7	32
Cranio-caudal diameter of the groove for the vertebral artery (CrCdDiGr)	2.8/3.3	3.2	0.6	2.3	4.4	34
Diameters in major axis of upper articular facets (UFaSgDi)	-/20.0	21.9	1.9	17.0	24.6	33
Diameters in right angle to major axis of upper articular facets (UFaTrDi)	-/10.8	10.2	1.2	8.0	12.9	34
Lower articular facet: sagittal diameter (LwFaSgDi)	17.7/16.3	15.4	1.4	13.2	18.9	34
Lower articular facet transverse diameter (LwFaTrDi)	13.3/14.0	14.9	1.4	11.8	18.4	34

(a) Values in parentheses are estimated. Values underlined are outside the range of the recent modern human female comparative sample. For the z-score analysis values with a * or two ** are significantly different from the modern female comparative sample (* = $p < 0.05$; ** = $p < 0.01$). Cells that contain two entries are for the right and left sides (right/left) unless in modern humans in which only right side has been taken.

Variable	El Mirón 1	Recent females				
		Mean	SD	Min	Max	n
Maximum dorso-ventral diameter (MaxDVDi)	44.9	46.7	2.5	43.0	53.6	33
Inferior transverse diameter (ITrDi)	44.9	45.3	2.2	40.4	49.3	33
Canal dorso-ventral diameter (M10)	(17.1)	16.9	1.7	14.5	20.9	33
Canal transverse diameter (M11)	<u>25.4*</u>	23.0	1.2	20.7	25.7	33
Total vertebral ventral crano-caudal diameter (height) (M1a)	36.3	35.7	2.4	30.4	40.8	32
Height of the odontoid	13.5					
Minimum width odontoid	9.0					
Maximum width odontoid	10.4					
Min AP odontoid	10.3					
Max AP odontoid	11.9					
Upper articular facet: sagittal diameter (UFaSgDi)	-/(16.0)	16.8	1.4	13.2	19.5	33
Lower articular facet: sagittal diameter (LwFaSgDi)	<u>8.0*/7.9*</u>	9.4	1.1	6.8	11.5	33
Lower articular facet transverse diameter (LwFaTrDi)	9.8/10.2	10.5	0.9	8.8	12.1	33
Laminae: crano-caudal diameter (LamCrCdDi)	(9.9)/10.5	10.6	1.1	8.6	13.0	34
Laminae: thickness (LamTh)	5.4/3.4	5.2	1.1	2.5	7.6	34
Spinous process: maximum length (M13)	14.6	16.9	2.1	11.8	20.8	32
Spinous process: maximum transverse diameter of the tip (SpPrTrDiTp)	(12.3)	12.1	2.9	7.7	20.1	32

(a) Values in parentheses are estimated. Values underlined are outside the range of the recent modern human female comparative sample. For the z-score analysis values with a * or two ** are significantly different from the modern female comparative sample (* = $p < 0.05$; ** = $p < 0.01$). Cells that contain two entries are for the right and left sides (right/left) unless in modern humans in which only right side has been taken.

Tableau 58. Dimension de l'atlas (a) et de l'axis (b) d'El Miron (en mm) comparé à des échantillons plus récents (a). Tableaux tirés de CARRETERO . M., QUAM R. M., et GOMEZ-OLIVENCIA A. (et al.), 2015. The Magdalenian human remains from El Miron Cave, Cantabria (Spain), *Journal of Archaeological Science*, 60, annexe, pp. 21 et 24.

Table S17.
Summary statistics (mm) of the recent female comparative sample^a

Vertebra	T1	T2	T3?	T5?	T7?	T9	T11
	n = 32	n = 32	n = 32	n = 32	n = 32	n = 32	n = 32
Maximum dorso-ventral diameter (MaxDVDi)	57.2 ± 2.5		59.7 ± 2.8 (29)				
Maximum transverse diameter (MaxTrDi)			59.6 ± 3.3		58.7 ± 3.8		48.5 ± 3.8
Superior transverse diameter (SupTrDi)	45.9 ± 2.4		33.3 ± 1.9 (31)	30.3 ± 1.8	29.7 ± 2.3	31.7 ± 2.5	
Inferior transverse diameter (ITrDi)				30.4 ± 2.2			32.6 ± 3.0
Canal dorso-ventral diameter (M10)	14.4 ± 0.8		14.9 ± 0.9	15.4 ± 0.9	15.7 ± 1.1	14.9 ± 1.1	15.8 ± 1.2
Canal transverse diameter (M11)	20.6 ± 1.3		16.4 ± 1.0	15.8 ± 1.3	16.0 ± 1.4	16.6 ± 1.5	
Body ventral crano-caudal diameter (height) (M1)	14.7 ± 1.1		17.1 ± 1.1	17.5 ± 1.0 (30)	18.1 ± 1.0	19.9 ± 0.9 (30)	
Body dorsal crano-caudal diameter (height) (M2)			17.1 ± 1.0	18.2 ± 1.2	19.6 ± 1.1	20.3 ± 1.1	
Body superior dorso-ventral diameter (M4)		15.7 ± 1.1	17.0 ± 1.1	20.6 ± 1.2	23.6 ± 1.2	25.5 ± 1.3	
Body inferior dorso-ventral diameter (M5)	15.2 ± 1.1	16.7 ± 0.9	18.6 ± 1.2 (31)	21.5 ± 1.2 (31)	24.4 ± 1.4 (31)	25.7 ± 1.5 (31)	
Body superior transverse diameter (M7)			24.6 ± 1.7	24.3 ± 1.6 (30)	26.7 ± 1.4	29.1 ± 1.5	
Body inferior transverse diameter (M8)			26.2 ± 1.9	26.1 ± 1.8	28.7 ± 1.8	31.5 ± 1.9	
Body median transverse diameter (M9)			24.1 ± 1.4	22.9 ± 1.7	25.0 ± 1.8 (31)	27.5 ± 2.1	
Wedging of the vertebral body (WVerB) ^b			-0.04 ± 1.9 (30)	2.0 ± 2.3	3.3 ± 1.8	0.9 ± 2.1	
Pedicles: crano-caudal diameter (PedCrCdDi)	7.9 ± 0.8	10.3 ± 1.0	10.6 ± 0.9	10.5 ± 0.9 (30)	10.6 ± 0.9	11.9 ± 0.9	
Pedicles: transverse diameter (PedTrDi)	7.3 ± 0.9	5.9 ± 1.0	4.6 ± 0.9	3.7 ± 0.9	3.9 ± 0.9	4.5 ± 1.0	
Bi-articular diameter (BiArtDi)	27.0 ± 2.0		29.7 ± 1.4	31.0 ± 1.7			
Transverse process: maximum length (TrPrMaxLe)	25.9 ± 1.8		25.1 ± 1.7	25.3 ± 1.9 (31)	25.8 ± 1.9		
Laminae: crano-caudal diameter (LamCrCdDi)	15.0 ± 1.3	15.2 ± 1.5	15.6 ± 1.4				
Laminae: thickness (LamTh)	5.3 ± 0.8	5.3 ± 0.7	5.4 ± 0.7	5.5 ± 0.8 (31)	5.5 ± 0.8		
Spinous process: maximum length (M13)	33.4 ± 2.4	35.1 ± 3.5	35.6 ± 4.1 (28)				29.3 ± 3.4 (27)
Spinous process: length (SpPrLe)	31.9 ± 2.1		32.9 ± 3.3 (29)				27.1 ± 3.6 (27)
Spinous process: angle (M12)	37.3 ± 8.0 (31)		44.4 ± 7.8 (31)				

(a) Including the results of the z-score with our modern human sample. Measurements in mm except M12 in °.

(b) Following DiGiovanni et al. (1989).

Tableau 59. Sommaire des statistiques (en mm) du comparative des échantillons des vertèbres féminines récents. Tableau tiré de CARRETERO . M., QUAM R. M., et GOMEZ-OLIVENCIA A. (et al.), 2015. The Magdalenian human remains from El Miron Cave, Cantabria (Spain), *Journal of Archaeological Science*, 60, annexe, p. 31.



Fig. 139. Ceinture scapulaire d'El Miron 1. Clavicule droite en vue supérieure (a), scapula gauche en vue ventrale (b), scapula gauche en vue glénoïdale (c), et scapula gauche en vue axillaire (d). L'échelle est de 5cm. Photo tirée de CARRETERO . M., QUAM R. M., et GOMEZ-OLIVENCIA A. (et al.), 2015. The Magdalenian human remains from El Miron Cave, Cantabria (Spain), *Journal of Archaeological Science*, 60, annexe, p. 36.

Table 5

Metric comparisons (mm) of El Mirón 1 scapular glenoid fossa.

	Glenoid height	Glenoid breadth	Glenoid index ^a
El Mirón	32.1	24.6	76.6
SH mean (n = 4) ^b	32.8 ± 1.8	24.2 ± 1.6	63.8 ± 1.9
Neandertals (n = 12) ^b	37.0 ± 4.7	24.5 ± 3.7	66.0 ± 3.0
E/MUP (n = 21) ^c			72.8 ± 5.4
LUP (n = 14) ^c			71.2 ± 4.3
Europe MUP (n = 16) ^d			73.1 ± 5.3
Coimbra (n = 158) ^b	35.6 ± 3.3	25.8 ± 2.6	72.6 ± 4.2
Euroamericans (n = 99) ^e	33.9 ± 3.1	24.9 ± 2.2	73.4 ± 3.5
Modern humans mean of 23 sample means ^c	33.5 ± 2.3	26.0 ± 1.9	77.6 ± 3.0

^a Glenoid index = (Glenoid breadth/Glenoid height)*100.^b Carretero et al. (1997).^c Trinkaus (2014).^d Soficaru et al. (2006).^e Churchill and Trinkaus (1990).

Tableau 60. Comparaison des mesures de cavités glénoïdales. Tableau tiré de CARRETERO . M., QUAM R. M., et GOMEZ-OLIVENCIA A. (et al.), 2015. The Magdalenian human remains from El Miron Cave, Cantabria (Spain), *Journal of Archaeological Science*, 60, p. 17.

Différents types d'architecture de l'épaule à partir de 0,78 Ma

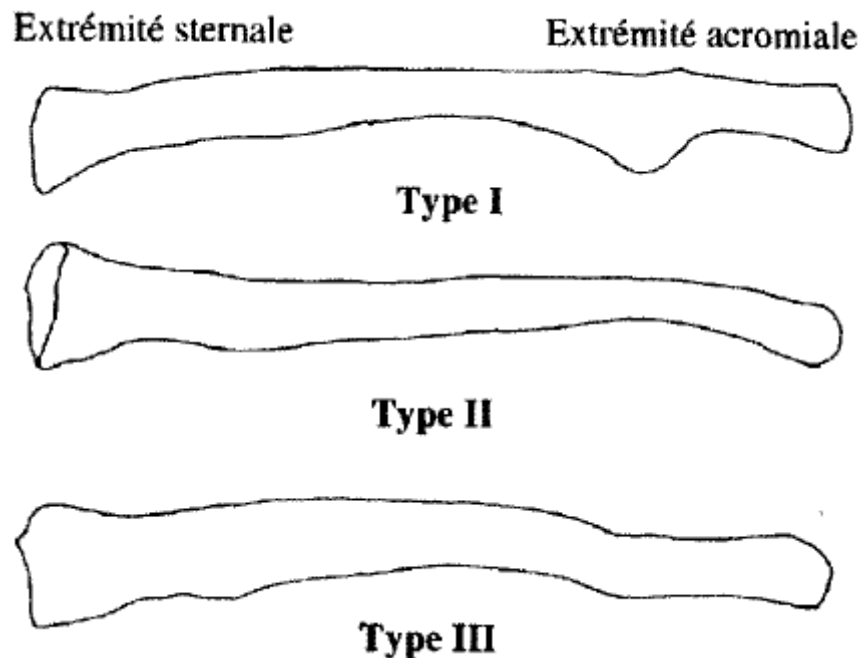


Fig. 140. Les trois types de clavicules chez l'homme moderne. Image tirée de VOISIN J.L., 2001. Évolution de la morphologie claviculaire au sein du genre Homo. Conséquences architecturales et fonctionnelles sur la ceinture scapulaire, *L'Anthropologie*, 105, p. 460.

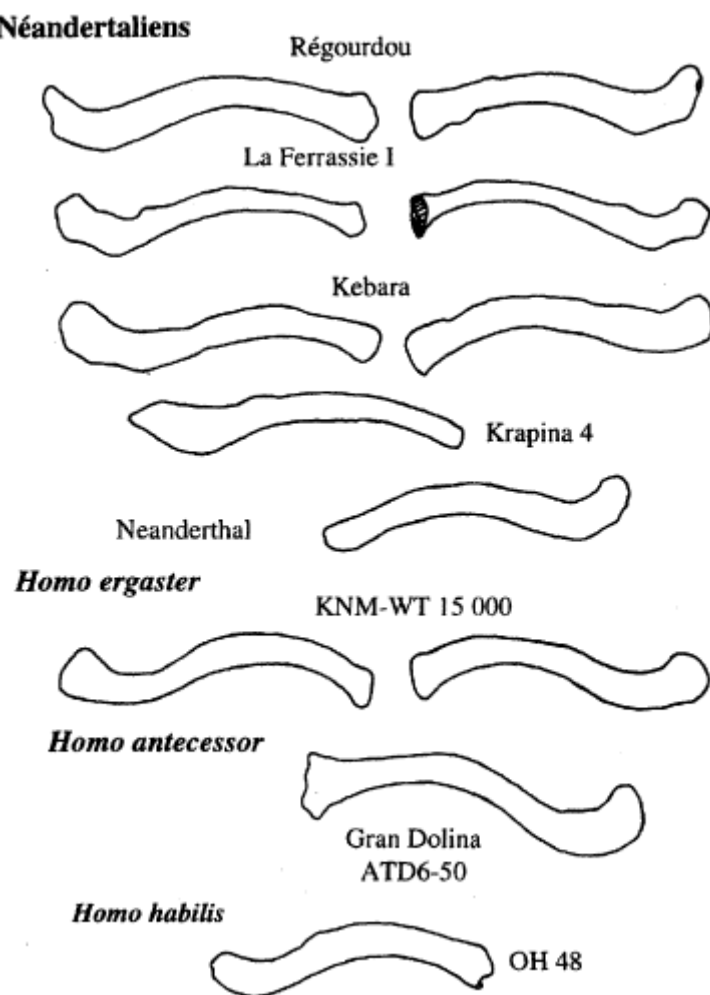


Fig. 141. Clavicules de *H. neandertaliensis*, *H. antecessor*, *H. ergaster* et *H. habilis* en vue supérieure. Les échelles ne sont pas respectées. Image tirée de VOISIN J.L., 2001. Évolution de la morphologie claviculaire au sein du genre *Homo*. Conséquences architecturales et fonctionnelles sur la ceinture scapulaire, *L'Anthropologie*, 105, p. 455.

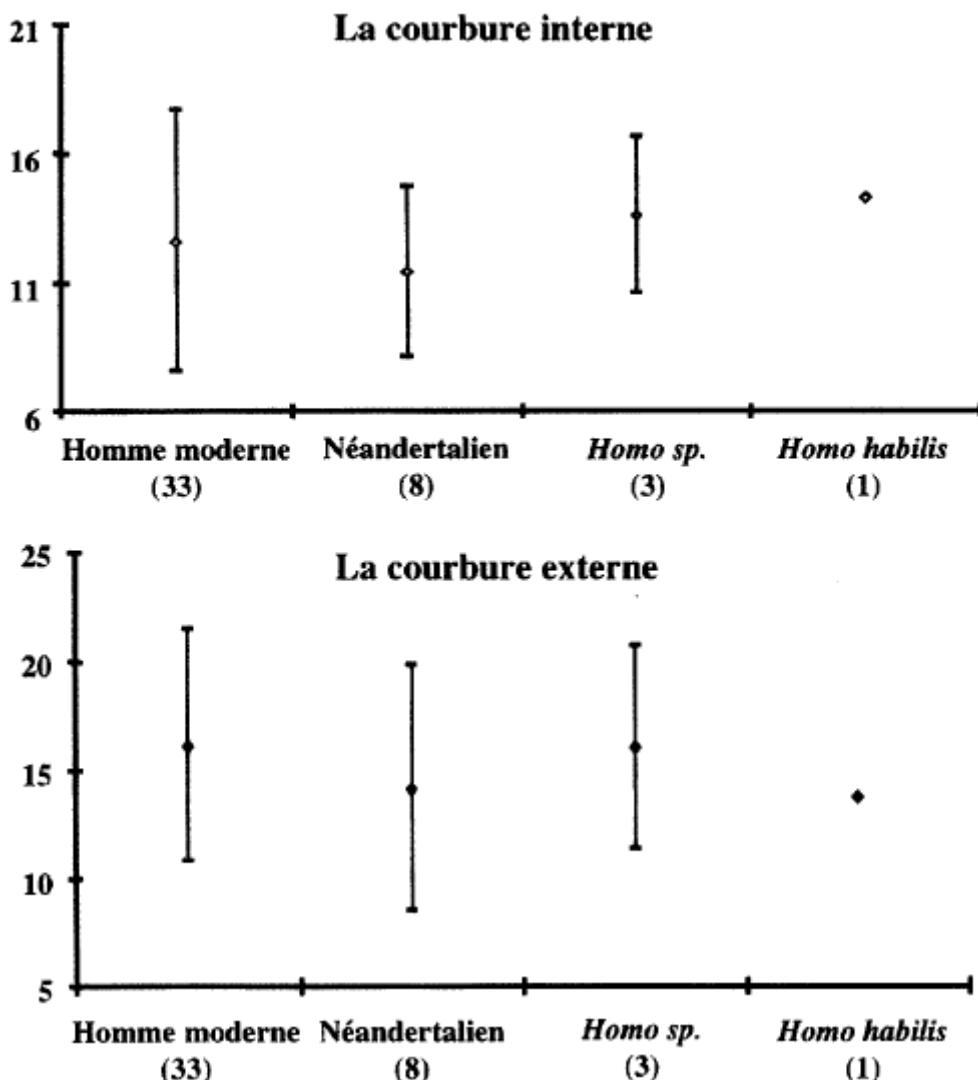


Fig. 142. Valeurs moyennes et amplitudes de variation des courbures en vue supérieure chez l'homme moderne et différents groupes fossiles. *Homo sp.* regroupe *H. ergaster* et *H. antecessor*. Les chiffres entre parenthèse rappellent les effectifs. Image tirée de VOISIN J.L., 2001. Évolution de la morphologie claviculaire au sein du genre *Homo*. Conséquences architecturales et fonctionnelles sur la ceinture scapulaire, *L'Anthropologie*, 105, p. 456.

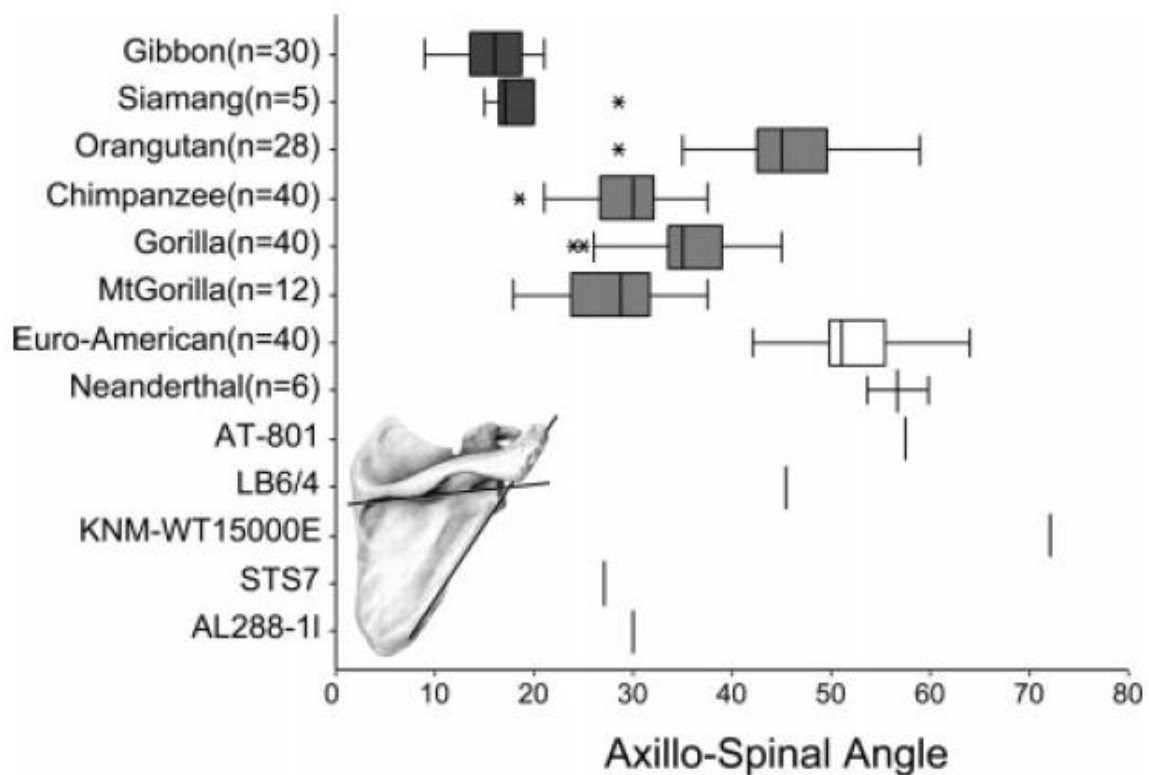


Fig. 143. Angle axillo-épineux chez les gibbons, siamang, orang-outans, chimpanzés, gorilles et gorilles de montagne, Euro-Américains, *H. neandertaliensis*, *H. neandertaliensis* AT – 801, *H. florensis* LB6/4, *H. erectus* KNM – WT 15 000, *Austra. STS 7 et AL 288 – 1*. Image tirée de LARSON S. G., 2007. Evolutionary Transformation of the Hominin Shoulder, *Evolutionary Anthropology*, 16, p. 176.